Sediment Yields from Ungaged Tributaries to the Middle Rio Grande between Bernardo and Elephant Butte Reservoir

Submitted to:

New Mexico Interstate Stream Commission
121 Tijeras NE, Suite 2000
Albuquerque, New Mexico 87102

Submitted by:

Mussetter Engineering, Inc.
1730 S. College Avenue, Suite 100
Fort Collins, Colorado   80525
Project: 04-33

November 2004

EXECUTIVE SUMMARY

A comprehensive sediment-transport model of the Middle Rio Grande (MRG) from Cochiti Dam to Elephant Butte Reservoir is needed to aid in understanding the sediment-transport dynamics of the river. The first phase of the modeling will likely consider the reach between the San Acacia Diversion Dam and Elephant Butte Reservoir (San Acacia Reach). The sediment-transport model of this reach will depend on quantification of both the sediment inflow from upstream and from tributaries within the reach. In order to develop a sediment-mass balance of the San Acacia reach, it is necessary to quantify the sediment inflow from upstream of San Acacia and from the tributaries within the reach. Quantification of the sediment inflow from upstream of San Acacia can be achieved by combining information from the Bernardo, Rio Puerco, and Rio Salado gages (MEI, 2004), and the ungaged tributaries between the Bernardo gage at US 60 bridge and San Acacia. Prior to this study there has been no quantification of sediment input from ungaged tributaries between the Bernardo gage and San Acacia, nor from ungaged tributaries within the San Acacia reach.

The specific objectives of this study, which was conducted by Mussetter Engineering, Inc. (MEI) for the New Mexico Interstate Stream Commission (NMISC), were to develop single event and mean annual estimates of ungaged tributary sediment delivery to the MRG between Bernardo and Elephant Butte Reservoir. With the exception of Brown Arroyo, the west side tributaries to the MRG have been truncated by the Low Flow Conveyance Channel (LFCC) and the west bank levee, and sediment delivery to the Rio Grande has been essentially eliminated. Therefore, this study involved field data collection (sediment sampling and topographic surveys of the channels) and hydrologic and hydraulic analyses of ten drainage basins, ranging in size between 2.6 and 47.3 square miles. The high frequency of tributaries on the east side of the river is geologically controlled, and the tributary basins drain the southern extension of the Los Pinos Mountains and the Chupadera Mesa (MEI, 2002). Since flow in all of the tributary basins is ephemeral, and ungaged, an HEC-HMS hydrologic model was developed for each of the basins to provide hydrographs at the downstream boundaries of the basins for the 2-, 5-, 10-, 25-, 50- and 100-year recurrence interval events. Topographic surveys of a representative reach of each channel near the downstream boundary of the basin were conducted for the purpose of developing one-dimensional normal-depth HEC-RAS hydraulic models. Output from the individual basin models was used with sediment gradations derived from samples collected in each of the tributaries to develop estimates of total sediment yields for the 2-, 5-, 10-, 25-, 50- and 100-year recurrence interval events, as well as the mean annual sediment yield. The wash-load fraction of the sediment yield for each basin was developed using the MUSLE equation. The bed-material fraction of the sediment yield was estimated using the MPM-Einstein equation. Field reconnaissance of the lower reaches of the arroyos determined the degree of integration of the arroyos and the Rio Grande, and this information was used to develop estimates of the sediment delivery ratio for each basin.

Results obtained for the 10 basins were used to develop regression relations between basin drainage area and sediment yield for the 2-, 5-, 10-, 25-, 50- and 100-year return period events, as well as for the mean annual sediment yield (Figure 6.2). Coefficients of determination (R^2) for the 5-, 10-, 25-, 50-, and 100-year return period events and the mean annual yield regression relations are high (>0.9). However, the R^2 value for the 2-year event is very low (0.01) when all 10 basins are included in the regression. If the three largest basins are removed from the data set (drainage areas > 40 mi^2), the R^2 value increases to 0.9. The data indicate, therefore, that for basins larger than 26 mi^2, where there is very little runoff during the 2-year storm, there are very low sediment yields for the 2-year return period event.

Mussetter Engineering, Inc.

Mean annual unit sediment yields from the 10 basins are inversely related to basin size (Figure 6.3), and this finding is similar to that reported by other investigators (Schumm and Hadley, 1961; Strand, 1975). Values determined from this investigation are about an order of magnitude lower than those determined by RTI (1994) for a basin that was common to both studies. The differences are due in part to the way the MUSLE calculations were done by RTI, differences in assumptions on infiltration rates used in the hydrologic modeling, and an overestimation of the bed-material load. Comparison of the methods and assumptions used in the two investigations indicates that the lower values derived from this study are more realistic and supportable. On average, the unit bed-material load for the basins represents about 20 percent of the total unit sediment load (Table 6.6).

Sediment delivery ratios (SDR) were estimated on the basis of the inverse relationship between SDR and basin size (Boyce, 1975; Schumm, 1977), the degree of integration of the arroyo and the Rio Grande, and the aggradational or degradational status of the lower reaches of the arroyos. SDR values were assumed to vary from about 0.2 where the arroyos were not directly connected to the river to >1 where the arroyo was both connected to the river and was incised or actively widening as a result of previous incision. The SDR values were applied to the estimated mean annual sediment yields for the individual arroyos to provide an estimate of the amount of sediment actually delivered to the river on an annual basis. About 75 percent (37,000 tons) of the estimated annual total sediment yield from the 10 arroyos (50,000 tons) is probably delivered to the Rio Grande, and about 7,400 tons is composed of bed material. Comparison of conditions at the mouths of the arroyos in 1935 with present conditions indicates that SDR values have changed with time, both as a result of the presence of increased non-native vegetation and channelization-induced baselevel lowering for the tributaries.

The regression relations developed for the 10 basins were applied to a further 12 basins of similar size that drain areas of similar lithology and topography between Bernardo and San Antonio. Application of estimated SDR values to the resulting mean annual values (Table 6.7) produced an estimated delivery of about 36,300 tons per year, of which about 7,300 tons are composed of the bed material. In combination, the mean annual sediment yield for the 22 basins along the east side of the Rio Grande between Bernardo and San Antonio is about 73,300 tons, and about 14,700 tons is bed material.

The eastside tributaries between Bernardo and San Acacia deliver about 3,500 tons of bed material to the Rio Grande on an annual basis, and this represents about 2.6 percent of the combined annual bed-material load from the Rio Puerco and Rio Salado (136,000 tons), MEI, 2004). The combined upstream inflows of the bed material to San Acacia is on the order of 420,000 tons per year (MEI, 2004). The eastside tributaries between San Acacia and San Antonio deliver about 8,200 tons of bed material per year, and this represents approximately 2 percent of the inflowing load at San Acacia. The preceding discussion has focused on the mean annual bed-material sediment yield, since it is the bed material that has the greatest influence on the channel morphologic characteristics (Schumm, 1977). The bed material represents about 20 percent of the total sediment yield, and the remaining 80 percent of the total yield is composed of silts and clay-size particles that have little direct effect on channel morphology. However, deposition of cohesive silts and clay on sandbars in the San Acacia reach appears to be important with respect to stabilizing the bars and encouraging growth of riparian vegetation (MEI, 2002), which indirectly affects the channel morphology.

Emphasis was placed on the mean annual sediment yields because of the need to place the tributary sediment yields in the context of the sediment mass balance that was conducted for the URGWOPS EIS alternatives evaluation (MEI, 2004). However, in arid and semi-arid region

Mussetter Engineering, Inc.

arroyos, the use of mean annual estimates does not represent the true sediment dynamics because of the episodic nature of flow and sediment-transporting events (Graff, 1988). The data in Table 6.3 (bed-material yield) and Table 6.4 (total yield) demonstrate that the single-event sediment yields from the modeled tributaries are likely to deliver significantly larger amounts of sediment to the Rio Grande. Because of the limited spatial distribution of thunderstorms that are likely to produce sediment-transporting events in the tributaries, the effects of the storm events are generally local. In other words, a large magnitude, but infrequent event, in the tributaries is likely to have spatially limited local effect on the Rio Grande. The longer-term legacy of large infrequent events is the accumulation of coarser sediments in the bed of the Rio Grande at the tributary confluence. The accumulation of coarse sediment at the tributary confluences creates local grade controls in the Rio Grande.

Mussetter Engineering, Inc.

Mussetter Engineering, Inc.

TABLE OF CONTENTS

LIST OF FIGURES

Mussetter Engineering, Inc.

Mussetter Engineering, Inc.

Mussetter Engineering, Inc.

Mussetter Engineering, Inc.

LIST OF TABLES

Mussetter Engineering, Inc.

Mussetter Engineering, Inc.

LIST OF PHOTOGRAPHS

Mussetter Engineering, Inc.

Mussetter Engineering, Inc.

Mussetter Engineering, Inc.

Mussetter Engineering, Inc.

1. INTRODUCTION

A comprehensive sediment-transport model of the Middle Rio Grande (MRG) from Cochiti Dam to Elephant Butte Reservoir is needed to aid in understanding the sediment-transport dynamics of the river. The sediment-transport model of this reach will be a valuable tool for understanding the dynamics of the river, the relationships between the morphology and dynamics of the river and restoration of habitat for the Rio Grande Silvery Minnow, and how sediment-driven changes in channel morphology can affect downstream water delivery. The first phase of the modeling would likely consider the reach between San Acacia Diversion Dam and Elephant Butte Reservoir (San Acacia Reach).

In order to develop a sediment mass balance of the San Acacia reach, it is necessary to quantify the sediment inflow from upstream of San Acacia and from the tributaries within the San Acacia reach. Quantification of the sediment inflow from upstream of San Acacia can be achieved by combining information from the USGS Bernardo, Rio Puerco, and Rio Salado stream gages and estimates of sediment yield from the ungaged tributaries between the Bernardo gage and San Acacia. To date, there has been no quantification of sediment yield from ungaged tributaries between the Bernardo gage and San Acacia. With the exception of Coyote Arroyo [Resource Technology Inc. (RTI), 1994], there has been no quantification of sediment yield from ungaged tributaries within the San Acacia reach. The primary goal of this study was to develop estimates of the tributary sediment inflow from the ungaged tributaries located between Bernardo and the head of Elephant Butte Reservoir at San Marcial.

The specific objectives of this study were to develop single event and average annual estimates of ungaged tributary sediment delivery to the MRG between Bernardo and Elephant Butte Reservoir. With the exception of Brown Arroyo, the west side tributaries to the MRG have been truncated by the Low Flow Conveyance Channel (LFCC) and the west bank levee, and sediment delivery to the Rio Grande has been essentially eliminated. Therefore, this study involved field data collection (sediment sampling and topographic surveys of the channels) and hydrologic and hydraulic analyses of 10 drainage basins, ranging in size between 2.6 and 47.3 square miles, located on the east side of the Rio Grande between San Acacia and San Antonio (**Figure 1.1**). Since all of the tributary basins are ephemeral and ungaged, HEC-HMS models were developed for each of the basins in order to provide hydrographs at the downstream boundaries of the basins for the 2-, 5-, 10-, 25-, 50- and 100-year recurrence interval events. Topographic surveys (cross sections and longitudinal profiles) of a representative reach of each channel near the downstream boundary of the basin were completed for the purpose of developing one-dimensional normal-depth HEC-RAS hydraulic models, the outputs from which were used to develop estimates of total sediment yields for the 2-, 5-, 10-, 25-, 50- and 100-year recurrence interval events, as well as the average annual sediment yield. Regression relations developed from the 10 modeled basins were used to predict single event and average annual sediment yields on the basis of their drainage basin areas from 12 additional ungaged tributaries that are located between Bernardo and San Antonio.

1.1. Project Authorization

This study of tributary sediment delivery between Bernardo and Elephant Butte Reservoir was conducted for the New Mexico Interstate Stream Commission (NMISC) by Mussetter Engineering, Inc. (MEI) under a subcontract to S.S. Papadopulos and Associates (SSP&A) under Work Order SSPA #33. Ms. Page Pegram was the NMISC project manager, and Dr.

Mike Harvey, P.G. was the MEI project manager. Dr. Bob Mussetter, P.E. provided quality assurance for the project, and Mr. Dai Thomas, P.E. was the project engineer.
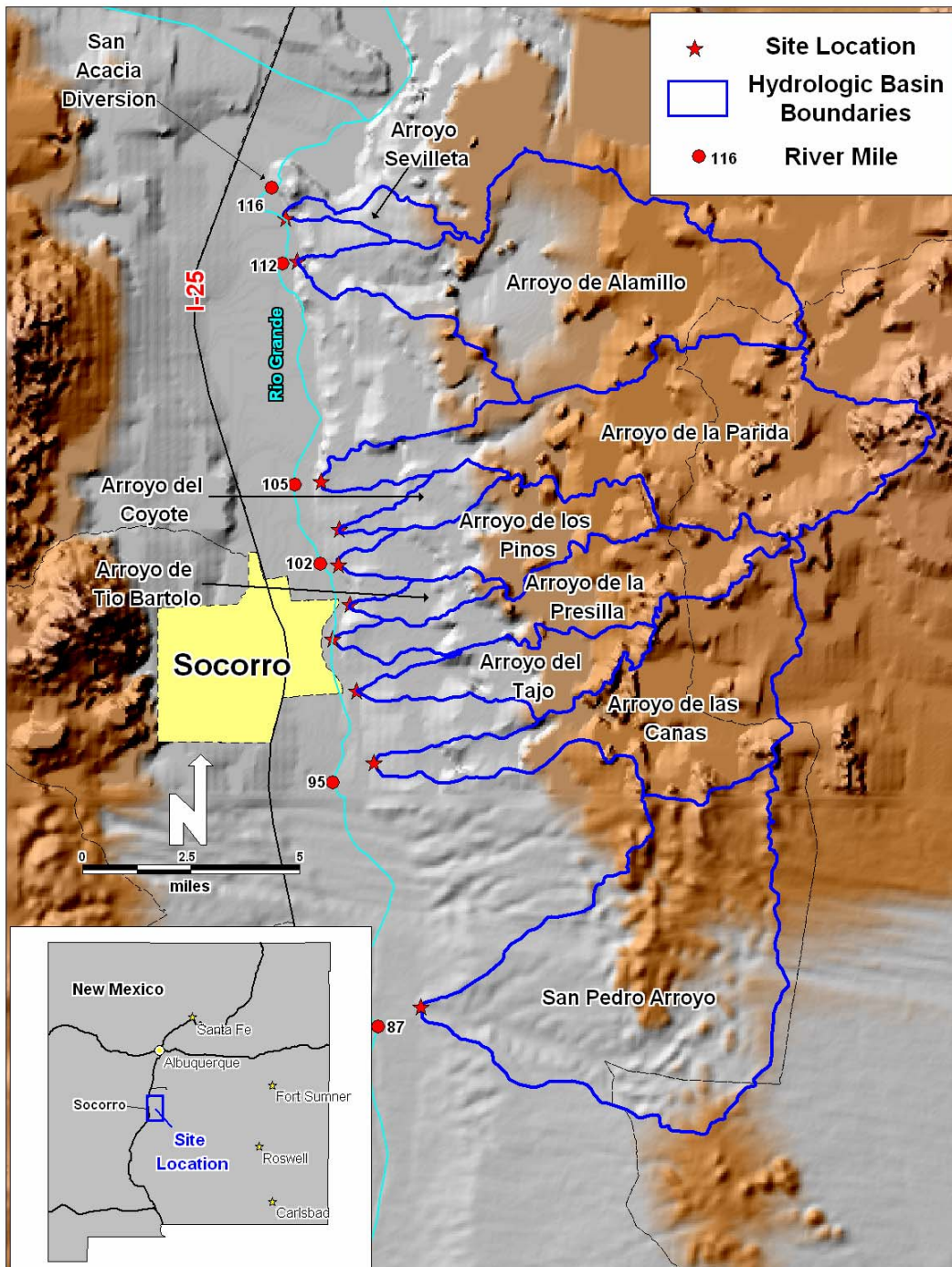
Figure 1.1. Map showing the locations of the 10 studied drainage basins on the east side of the Rio Grande between San Acacia and San Antonio.

2. GEOLOGY AND GEOMORPHOLOGY

The geologic and geomorphological characteristics of the Middle Rio Grande valley between Bernardo and San Antonio, the reach with the highest density of tributaries to the Rio Grande, control sediment production and delivery to the Rio Grande within the San Acacia reach (MEI, 2002).

2.1. Geology

The Rio Grande valley in New Mexico is composed of a sequence of connected basins and constrictions that are bordered by tilted fault blocks of the Basin and Range physiographic province. It has a complex geologic and geomorphic history (Smith et al., 2001; Belcher, 1975) with periods of mountain formation (Sangre de Christo, Sandia, San Cristobal, Calballo), faulting, volcanism and sediment deposition (Santa Fe Formation). A recent aeromagnetic survey of two areas of the Albuquerque basin revealed many faults in the valley alluvium that were not detected by traditional mapping methods (Grauch, 2001; Kelley, 1977, p. 43).

The Joyita Uplift, located on the east side of the Rio Grande affects both the topography and geology of the Rio Grande valley between Bernardo and San Antonio (**Figure 2.1**). The uplift, bounded on the west by the West Joyita Fault, causes a higher elevation complex of highly faulted sedimentary, volcanic, metamorphic and igneous rocks to be present on the east side of the river (Kelley, 1977). The primary lithologies are sedimentary, and include Pennsylvanian and Permian limestones, sandstones and shales (**Figure 2.2**). Precambrian granite crops out in the headwaters of the larger drainage basins. The exposed rocks are the source of both sediment and runoff that are able to traverse the much-narrowed belt of Santa Fe Formation that exists between the margin of the uplifted rocks and the Rio Grande. The reduced width of the Santa Fe Formation outcrop and the increased slope of the channels permit flood flows in the east-side tributaries to deliver sediment to the river. This is in contrast to the situation upstream of Bernardo where the Santa Fe Formation outcrop is wide and very few tributaries are present because of flow infiltration into the permeable Santa Fe sediments (Chronic, 1987). The local geological setting, therefore, is very important with respect to sediment delivery to the Rio Grande in the project reach.

2.2. Geomorphology

Between the uplifted mountain fronts to the east of the Rio Grande and the modern Rio Grande alluvium, there are a number of surfaces composed of terraces and pediments that form the lower portions of the studied basins. The Canada Mariana surface is about 50 feet above the Rio Grande, the Valle de Parida surface is about 150 feet above the river, and the Tio Bartolo surface is about 250 feet above the river (Chronic, 1987). The terraces are composed of both Rio Grande and tributary sediments that range in size from silts and clays to gravels, and the bedrock pediments are capped with coarse gravel deposits of varying thickness. Local erosion of the terraces and pediments provides a source of both fine and coarse sediment to the tributaries. The upper reaches of the more northerly of the tributaries head in the southern extension of the Los Pinos Mountains. The upper reaches of the more southerly of the tributaries head in the Chupadera Mesa. Intensive livestock grazing that commenced in the 1880's, significantly reduced plant cover over much of the rangelands to the east of the river (Crawford et al., 1993), and much of the original grass and forb vegetation has been converted to mesquite, creosotebush and sage brush with large amounts of bare ground between the individual plants (Chronic, 1987). The intensive grazing and reduced ground cover led to
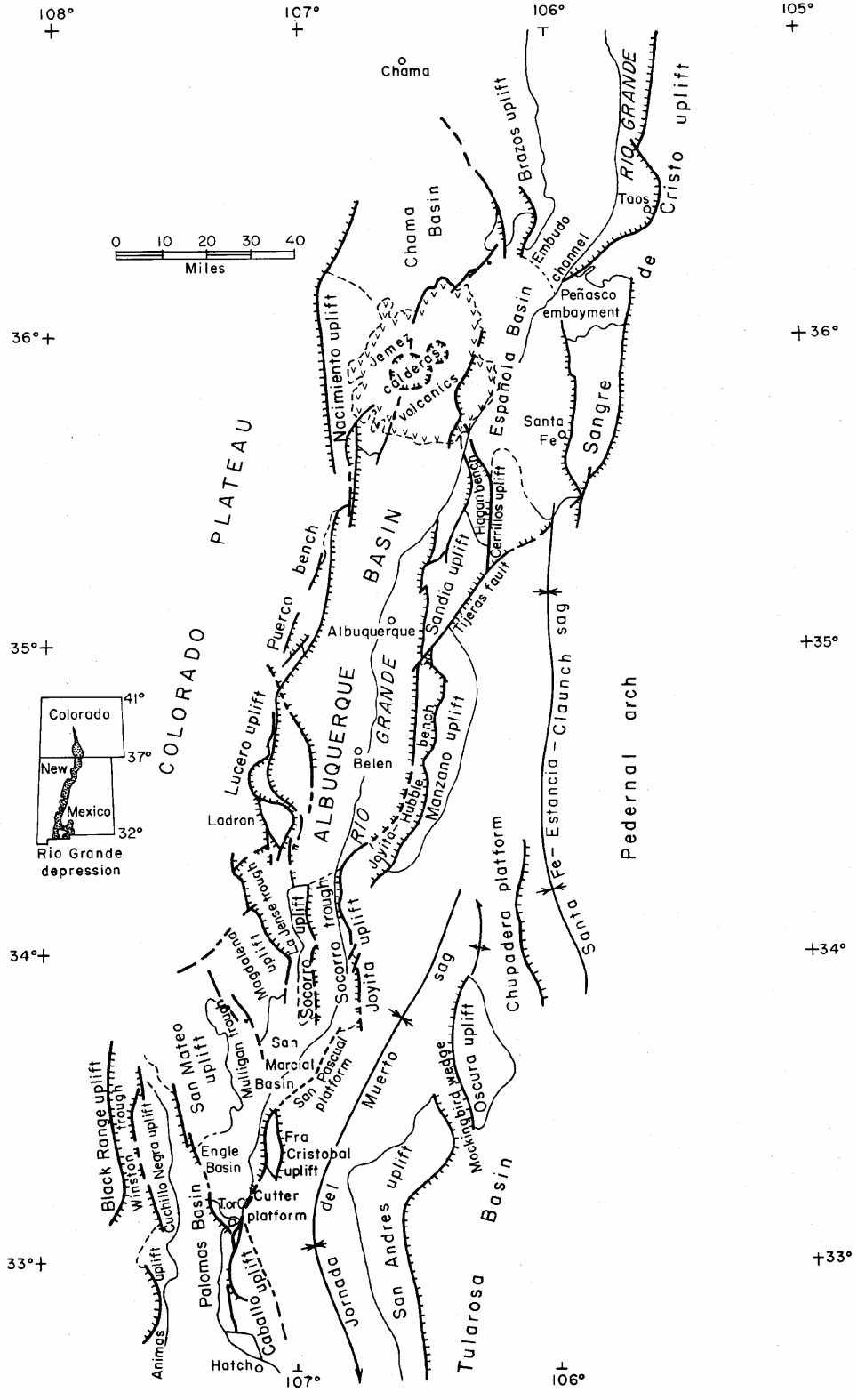
Figure 2.1. Tectonic map of the Rio Grande Rift system in New Mexico showing the locations of the structural basins and associated zones of uplift (Kelley, 1977).
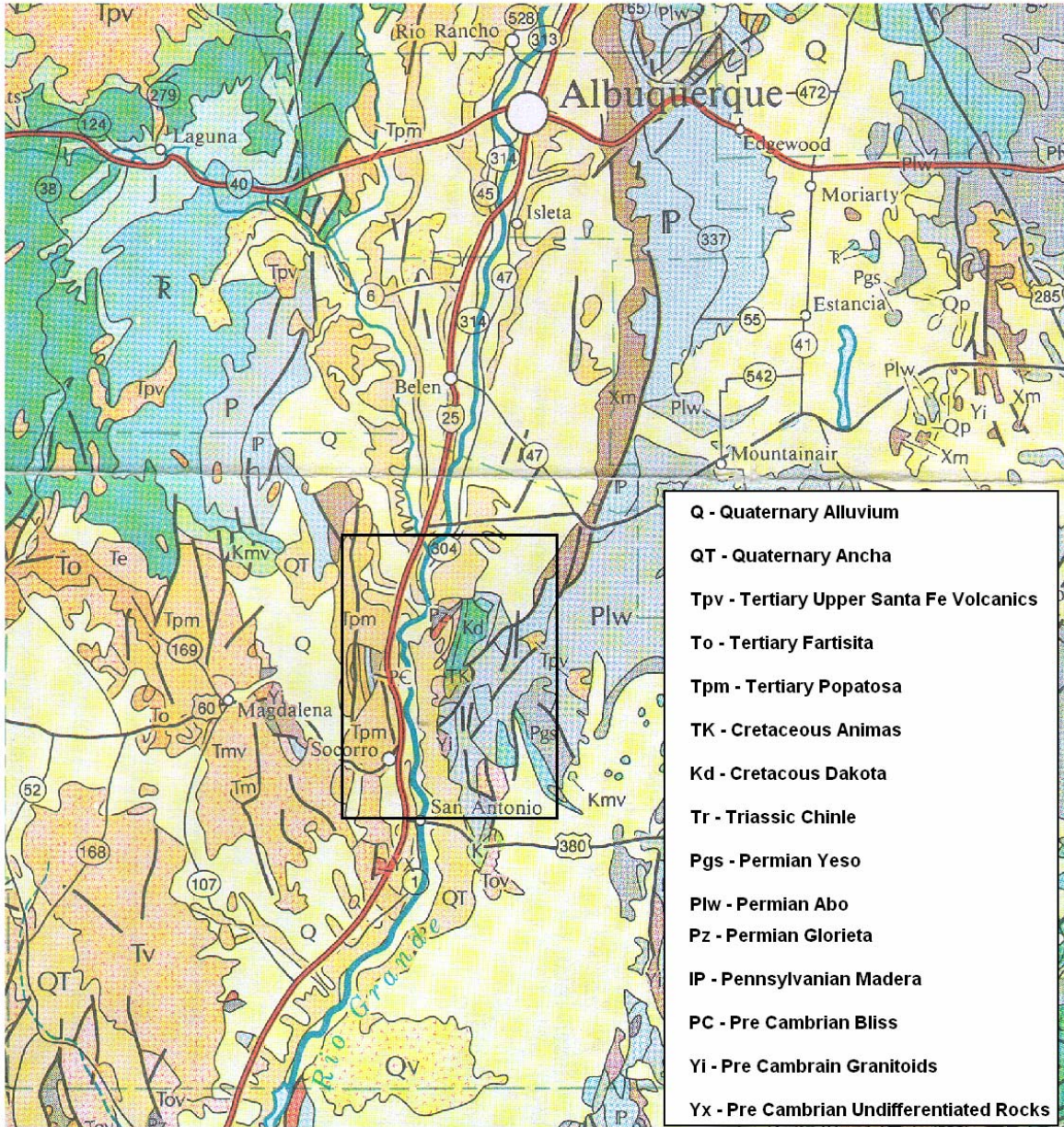
Figure 2.2. Geologic map of portion of the Middle Rio Grande Valley showing the bedrock geology and structure of the project reach between Bernardo and San Antonio that are controlled by the Joyita Uplift (from Bennison, 1990).

Mussetter Engineering, Inc.

increased rates of soil erosion and gullying (Scurlock, 1998). Based on the USDA SCS (1974) sediment yields map for the western U.S., expected sediment yields are on the order of 0.2 to 1 ac-ft/mi^2/year (440 to 2,178 tons/year).

Based on Lane's (1957) threshold relationships between mean annual discharge and channel slope, and using the pre-Cochiti mean annual discharge, the Rio Grande between San Acacia and Elephant Butte Reservoir plots in the transitional zone between braided and meandering planforms (MEI, 2000). The 1917/1918 survey indicated that the river planform was braided, but the 1935 aerial photography of the reach showed evidence of a meandering planform that had been abandoned as a result of the very large floods in the late 1920s and early 1930s. The observed changes in channel planform appear to have been driven by the combined effects of increases in sediment supply and reduced caliber of supplied sediments, probably as a result of incision of the Rio Puerco (Happ, 1948), and the high frequency of large floods (MEI, 2000). As a result of the aggradation, the MRGCD constructed drains and levees during the 1930s. Following large destructive floods in 1941 and 1942, the Corps of Engineers and the Bureau of Reclamation developed the Rio Grande Comprehensive Plan (Lagasse, 1980). Beginning in the 1950's in the San Acacia reach a leveed floodway was reconstructed, the Low Flow Conveyance Channel (LFCC) was constructed and the river was relocated in places and channelized (Crawford et al., 1993). Effectively, the west side tributaries were disconnected from the river. The combined effects of the flood- and erosion-control practices and the changes in hydrology caused by the upstream dams, resulted in channel incision in the reach between San Acacia and about San Antonio. No as-built surveys were conducted following the channeling action in the 1950s, so the first survey data on the new channel alignment were provided by the 1962 USBR photogrammetric surveys. The amount of degradation, as indicated by the changes in mean bed elevation, between 1962 and 1999 varied between about 8 feet near the San Acacia Diversion to about 2 feet near San Antonio (MEI, 2002). The riverbed continues to aggrade downstream of San Antonio.

The degradation of the Rio Grande between San Acacia and San Antonio has lowered baselevel for the tributaries within the affected reach. This in turn has caused incision of some of the tributaries, thereby increasing the sediment delivery from the tributaries to the Rio Grande during sediment transporting events in the tributaries. However, the 1950s channelization-induced baselevel lowering is not the only potential cause of tributary incision. Schumm and Hadley (1957), Patton and Schumm (1981), Wells (1988) and Balling and Wells (1990) have reported the widespread occurrence throughout the arid and semi-arid areas of the southwestern U.S. of prehistoric cycles of arroyo cutting and filling that appear to be related to changes in precipitation patterns and the exceedence of geomorphic thresholds. It is also likely that the pervasive arroyo cutting throughout the southwest was also related to overgrazing (Cooke and Reeves, 1976; Crawford et al., 1993). The widespread arroyo incision caused increased sediment delivery to the main stem rivers (Happ, 1948; Gellis et al., 1991) but eventually the sediment delivery from the arroyos was reduced due to arroyo evolution processes that ultimately lead to backfilling and sediment storage rather than sediment delivery from the incised drainages (Schumm et al., 1984; Gellis et al 1991; Gellis and Elliott, 2001). Review of the 1935 aerial photography of the San Acacia reach suggests that Arroyo de Tio Bartolo and Arroyo de las Canas were both incised prior to any incision of the Rio Grande.

The historical and present-day geomorphic characteristics of the 10 studied basins are discussed individually in the following sections. Topographic maps of the individual basins, and the sub-basin delineations within each of the basins that were used in the hydrologic modeling, are provided in **Appendix A**. Gradation curves for the sediment samples that were collected in the arroyos, and were used in the sediment-transport analyses, are provided in **Appendix B**.

Mussetter Engineering, Inc.

The surveyed cross sections and longitudinal profiles for the individual basins as well as the locations of the individual cross sections are provided in **Appendix G**.

2.2.1. Arroyo Sevilleta

 Arroyo Sevilleta (informally named) is located on the left (east) bank of the Rio Grande about 1 mile downstream of the San Acacia Diversion Dam (RM 114) (Figure 1.1). The basin area is about 2.6 mi^2, and the average basin slope is 2.3 percent (126 ft/mi). The details of the basin topography can be seen in **Figure A.1**. The fan boundaries can be clearly seen on the 1935 aerial photograph (**Figure 2.3**), and it is apparent that the fan was building onto the vegetated floodplain of the Rio Grande. The basic dimensions of the fan have not changed since 1935, but the downstream margin has become heavily vegetated with primarily tamarisk (**Photograph 1**). Because of recent (post-1950s) incision of the Rio Grande (MEI, 2002), the fan is now prograding onto a terrace, and it is highly unlikely that any sediment derived from the Arroyo Sevilleta basin is delivered to the Rio Grande.

The basin upstream of the fan heads in the Los Pinos Mountains, but the bulk of the watershed is composed of a large, relatively flat pediment surface that extends to the base of the mountains. The apex of the fan is located at an escarpment formed in Cenozoic-age basalt that extends south from the San Acacia Narrows to Arroyo Sevilleta (**Photograph 2**). The bulk of the sediment being delivered to the fan from the upstream watershed is sand-sized and finer, but erosion of a Rio Grande terrace on the right bank of the arroyo at about Cross Section 3 (**Figure G.1a**) is delivering both sands and gravels to the fan (**Photograph 3**). The median (D_{50}) size of the bed material of the active channels on the fan surface is about 1.2 mm, but clasts up to 90 mm are present (**Photograph 4**).

2.2.2. Arroyo de Alamillo

Arroyo de Alamillo is located on the left (east) bank of the Rio Grande about 2 miles downstream of the San Acacia Diversion Dam (RM 112) (Figure 1.1). The basin area is about 40.5 mi^2, and the average basin slope is 2.3 percent (126 ft/mi). The details of the basin topography can be seen in **Figure A.8**. On the 1935 aerial photograph (**Figure 2.3**), it is clear that the arroyo was discharging directly to the Rio Grande, but it does not appear that the channel was incised. Because of recent (post-1950s) incision of the Rio Grande (MEI, 2002) that lowered the baselevel, the channel has incised about 5 feet into its modern fan (**Photograph 5**). The incision has been halted at the apex of the fan by outcrop of erosion-resistant sandstone in the underlying Santa Fe Formation (**Photograph 6**). The modern incised fan is bounded by the Pleistocene-age Rio Grande terrace and the Canada Mariana surface (**Photograph 7**).

The basin upstream of the fan heads in the Los Pinos Mountains and the Chupadera Mesa. The bulk of the sediment being delivered to the incised fan from the upstream watershed is sand-sized and finer, but erosion of the modern terrace on the left bank of the arroyo is locally delivering both sands and gravels to the fan. The median (D_{50}) size of the bed material of the active channels on the fan surface is about 1.4 mm, but clasts up to 120 mm are present (**Photograph 8**).   The base level-lowering induced incision of the fan has increased the sediment loading from the arroyo since the 1950s (**Photograph 9**). Cobbles and small boulders derived from the arroyo are present in the bed of the Rio Grande at the confluence (MEI, 2002).

Figure 2.3.   1935 aerial photograph showing the lower reaches of Arroyo Sevilleta and Arroyo
de Alamillo and their confluences with the Rio Grande.

Mussetter Engineering, Inc.

Photograph 1.   View downstream of fan formed at the mouth of Arroyo Sevilleta. The margin of the fan is at the line of dense tamarisk trees that are located at the interface with the Rio Grande floodplain. No sediment is delivered to the river (08/20/2003).

Photograph 2.   View downstream of Arroyo Sevilleta at head of fan where the channel overflows the outcrop of Cenozoic age basalt that forms an escarpment (08/20/2003).

Mussetter Engineering, Inc.

Photograph 3.   Pleistocene-age Rio Grande terrace sediments exposed in eroding bank on right bank of Arroyo Sevilleta at surveyed Cross Section 3. Erosion of the base of the terrace is providing a fine and coarse supply of sediment to the fan (08/20/2003).

Photograph 4.   View of bed material in the active portion of the channel on the Arroyo Sevilleta fan. The D_{50} of the sample (S3) is 1.2 mm and the D_{84} is 8.5 mm (see Figure B.1) (08/20/2003).

Mussetter Engineering, Inc.

Photograph 5.   View downstream of the incised lower reaches of Arroyo de Alamillo with the Rio Grande in the background. The abandoned portion of the modern fan can be seen on the left side of the photograph (08/20/2003).

Photograph 6.   View of sandstone outcrop in the bed of Arroyo de Alamillo at the incised fan apex.   The gravel-capped Canada Mariana surface confines the arroyo (08/20/2003).

Mussetter Engineering, Inc.

Photograph 7.   View across the incised channel of Arroyo de Alamillo. The channel has incised about 5 feet into the modern fan. The Pleistocene-age Rio Grande terrace is inset below the Canada Mariana surface in the background (08/20/2003).

Photograph 8.   View of bed material in the incised channel of Arroyo de Alamillo. The D_{50} of the sample (S6) is 1.4 mm and the D_{84} is 12.7 mm (see Figure B.8) (08/20/2003).

Mussetter Engineering, Inc.

Photograph 9. View upstream of Arroyo Alamillo at the confluence with the Rio Grande. Note the active fan that has prograded into the river, and the incised fan surface along the left side of the photograph (08/20/2003).

2.2.3. Arroyo de la Parida

Arroyo de la Parida is located on the left (east) bank of the Rio Grande about 0.2 miles upstream of the Escondida Bridge (RM 105) (Figure 1.1). The basin area is about 42.1 mi^2, and the average basin slope is 3.2 percent (168 ft/mi). The details of the basin topography can be seen in **Figure A.9**. On the 1935 aerial photograph (**Figure 2.4**), it is clear that the arroyo was discharging directly to the Rio Grande, but it does not appear that the channel was incised. Because of recent (post-1950s) baselevel-lowering incision of the Rio Grande (MEI, 2002), the arroyo channel has incised about 5 feet into its modern fan (**Photograph 10**).

The upper reaches of the basin extend into the Los Pinos Mountains and the Chupadera Mesa. The lower reaches of the arroyo are confined by the gravel-capped Valle de Parida surface. The bulk of the sediment being delivered to the incised fan from the upstream watershed is sand-sized and finer, but erosion of the modern terrace is locally delivering both sands and gravels to the fan. The median (D_{50}) size of the bed material of the active channels on the fan surface is about 10 mm, but clasts up to 120 mm are present (**Photograph 11**). The baselevel-lowering induced incision of the fan has increased the sediment loading from the arroyo since the 1950s (**Photograph 12**). Cobbles and small boulders derived from the arroyo have formed a riffle in the bed of the Rio Grande at the confluence, and the D_{50} and D_{84} of the riffle sediments are 32 and 71 mm, respectively (MEI, 2002).

Mussetter Engineering, Inc.

Arroyo de la Parida

Figure 2.4.   1935 aerial photograph showing the lower reaches of Arroyo de la Parida and its
               confluences with the Rio Grande.

Mussetter Engineering, Inc.

Photograph 10.   View across the incised channel of Arroyo de la Parida, about 1,300 feet upstream of the confluence with the Rio Grande (08/22/2003).

Photograph 11.   View of bed material in the incised channel of Arroyo de la Parida. The D_{50} of the sample (S20) is 10 mm and the D_{84} is 36.4 mm (see Figure B.9) (08/22/2003).

2.13   Mussetter Engineering, Inc.

Photograph 12.　　　View upstream of Arroyo de la Parida at the confluence with the Rio Grande. The subaqueous portion of the fan that has prograded into the Rio Grande has formed a coarse gravel-cobble riffle in the Rio Grande (MEI, 2002) (11/24/2003).

2.2.4. Arroyo del Coyote

Arroyo del Coyote is located on the left (east) bank of the Rio Grande about 1 mile downstream of the Escondida Bridge (RM 103.8) (Figure 1.1). The basin area is about 3.2 mi^2, and the average basin slope is 3.4 percent (179 ft/mi). The details of the basin topography can be seen in **Figure A.3**. On the 1935 aerial photograph (**Figure 2.5**), it is clear that the arroyo was not discharging directly to the Rio Grande, but instead had formed a fan that prograded out onto the vegetated floodplain of the Rio Grande.

 The basin upstream of the fan heads in the Chupadera Mesa, but the lower reaches of the arroyo are confined by the gravel-capped Valle de Parida surface (**Photograph 13**). The bulk of the sediment being delivered to the modern fan from the upstream watershed is sand-sized and finer, but erosion of the Valle de Parida surface is locally delivering both sands and gravels to the fan. The median (D_{50}) size of the bed material in the arroyo is about 5 mm, but clasts up to 140 mm are present (**Photograph 14**). Because of the density of tamarisk on the Rio Grande floodplain and on the downstream margins of the fan, it is unlikely that there is significant sediment delivery from Arroyo del Coyote to the Rio Grande.

　　　　Mussetter Engineering, Inc.
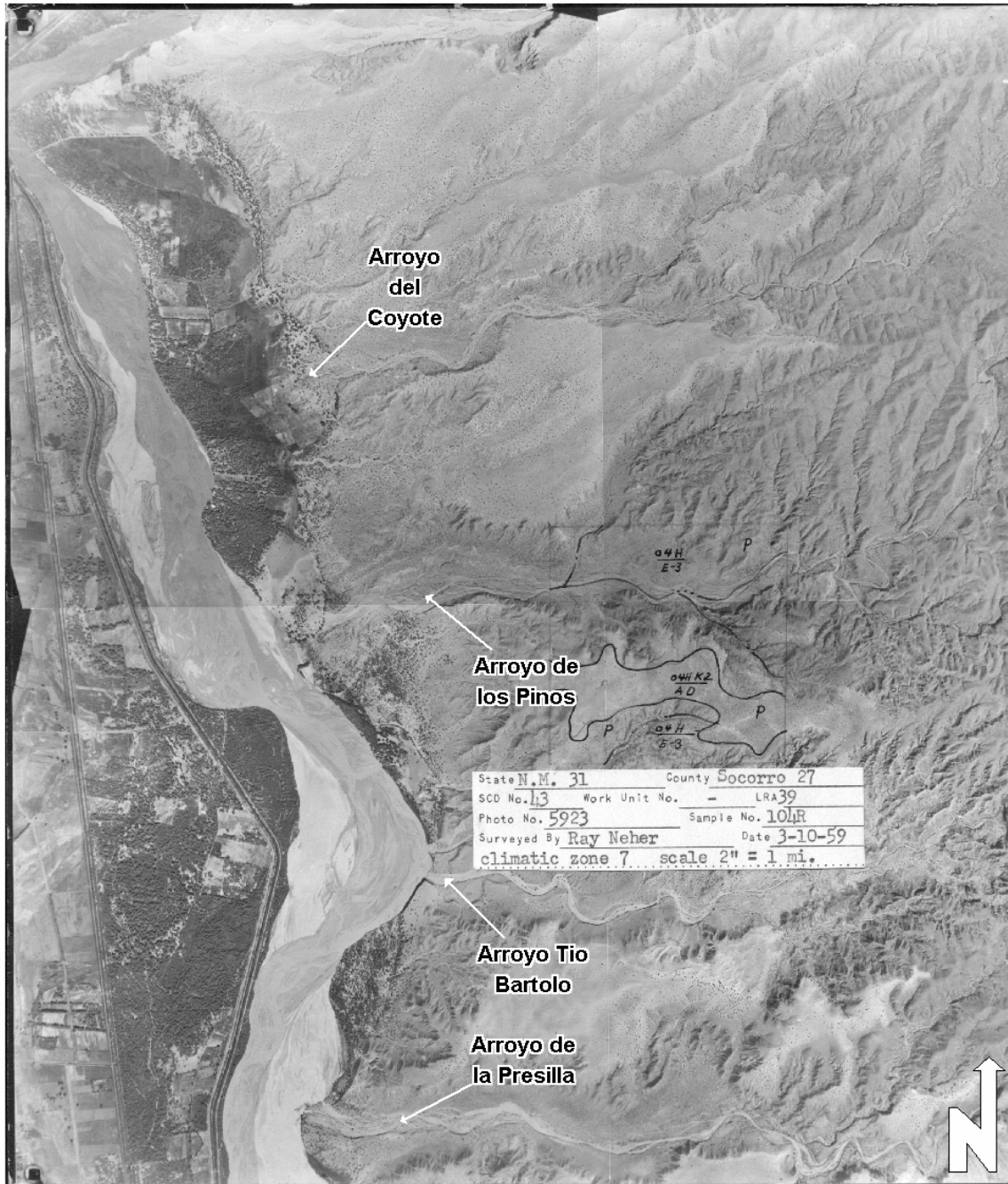
Figure 2.5.   1935 aerial photograph showing the lower reaches of Arroyo del Coyote, Arroyo de los Pinos, Arroyo Tio Bartolo and Arroyo de la Presilla.

Mussetter Engineering, Inc.

Photograph 13.   View north across Arroyo del Coyote. The vehicle is located on a higher level Arroyo del Coyote fan surface, and the ridge line is formed by the Valle de Parida surface (08/22/2003).

Photograph 14.   View of bed material in the incised channel of Arroyo del Coyote. The D_{50} of the sample (S18) is 5 mm and the D_{84} is 25.4 mm (see Figure B.2) (08/22/2003).

Mussetter Engineering, Inc.

2.2.5. Arroyo de los Pinos

Arroyo de los Pinos is located on the left (east) bank of the Rio Grande about 2.8 miles downstream of the Escondida Bridge (RM 102) (Figure 1.1). The basin area is about 12.1 mi^2, and the average basin slope is 3.5 percent (185 ft/mi). The details of the basin topography can be seen in **Figure A.7**. On the 1935 aerial photograph (Figure 2.5), it is clear that the arroyo was discharging directly to the Rio Grande, but there is no indication that the channel was incised.

The upper reaches of the basin extend into the Chupadera Mesa, but the lower reaches of the arroyo are confined by the gravel-capped Valle de Parida surface (**Photograph 15**). The bulk of the sediment being delivered to the modern fan from the upstream watershed is sand-sized and finer, but erosion of the Valle de Parida surface is locally delivering both sands and gravels to the fan. The median (D_{50}) size of the bed material in the arroyo is about 11 mm, but clasts up to 160 mm are present (**Photograph 16**). Channelization and leveeing of the lower reaches of the arroyo in order to cross the Escondida Drain (**Photograph 17**) has created a direct connection to the Rio Grande. At the confluence with the Rio Grande, the arroyo has incised into the floodplain of the Rio Grande and is eroding the floodplain sediments (**Photograph 18**).

2.2.6. Arroyo de Tio Bartolo

Arroyo de Tio Bartolo is located on the left (east) bank of the Rio Grande about 4.4 miles downstream of the Escondida Bridge (RM 100.4) (Figure 1.1). The basin area is about 2.6 mi^2, and the average basin slope is 3.3 percent (176 ft/mi). The details of the basin topography can be seen in **Figure A.2**. On the 1935 aerial photograph (Figure 2.5) it is clear that the arroyo was discharging directly to the Rio Grande.

The upper reaches of the basin extend into the Chupadera Mesa, but the lower reaches of the arroyo are confined by the Tio Bartolo surface (**Photograph 19**). The bulk of the sediment being delivered to the modern fan from the upstream watershed is sand-sized and finer, but erosion of the Tio Bartolo surface is locally delivering both sands and gravels to the fan. There has been recent incision of about 4 feet. The median (D_{50}) size of the bed material in the arroyo is about 0.8 mm, but clasts up to 80 mm are present (**Photograph 20**). The fan of the arroyo is prograding out onto the floodplain of the Rio Grande and onto lower elevation, vegetated bars (**Photograph 21**).

2.2.7. Arroyo de la Presilla

Arroyo de la Presilla is located on the left (east) bank of the Rio Grande about 5.6 miles downstream of the Escondida Bridge (RM 99.2) (Figure 1.1). The basin area is about 15.5 mi^2, and the average basin slope is 2.8 percent (145 ft/mi). The details of the basin topography can be seen in **Figure A.5**. On the 1935 aerial photograph (**Figure 2.6**), it is clear that the arroyo was discharging directly to the Rio Grande.

The upper reaches of the basin extend into the Chupadera Mesa, but the lower reaches of the arroyo are confined by the Tio Bartolo surface (**Photograph 22**). The channel is bordered on both sides by an 8-ft high terrace. The bulk of the sediment being delivered to the modern fan from the upstream watershed is sand-sized and finer, but erosion of the Tio Bartolo surface is locally delivering both sands and gravels to the fan. The median (D_{50}) size of the bed material in the arroyo is about 2.2 mm, but clasts up to 80 mm are present (**Photograph 23**).   The fan at the downstream end of the arroyo is prograding out onto the floodplain of the Rio Grande and onto lower elevation, vegetated bars (**Photograph 24**).

Mussetter Engineering, Inc.

Photograph 15.   View downstream of the lower reaches of Arroyo de los Pinos. The channel is incised into an older fan surface, and is bounded by the Valle de Parida surface (08/22/2003).

Photograph 16.   View of bed material in the channel of Arroyo de los Pinos. The D_{50} of the sample (S16) is 11 mm and the D_{84} is 39.5 mm (see Figure B.5) (08/22/2003).

Mussetter Engineering, Inc.

Photograph 17.   View downstream of the channelized and leveed lower reach of Arroyo de los Pinos where it crosses the Escondida Drain (11/24/2003).

Photograph 18.   View upstream of the downstream reach of Arroyo de los Pinos at the confluence with the Rio Grande. The channel has incised into the Rio Grande floodplain (11/24/2003).

Mussetter Engineering, Inc.
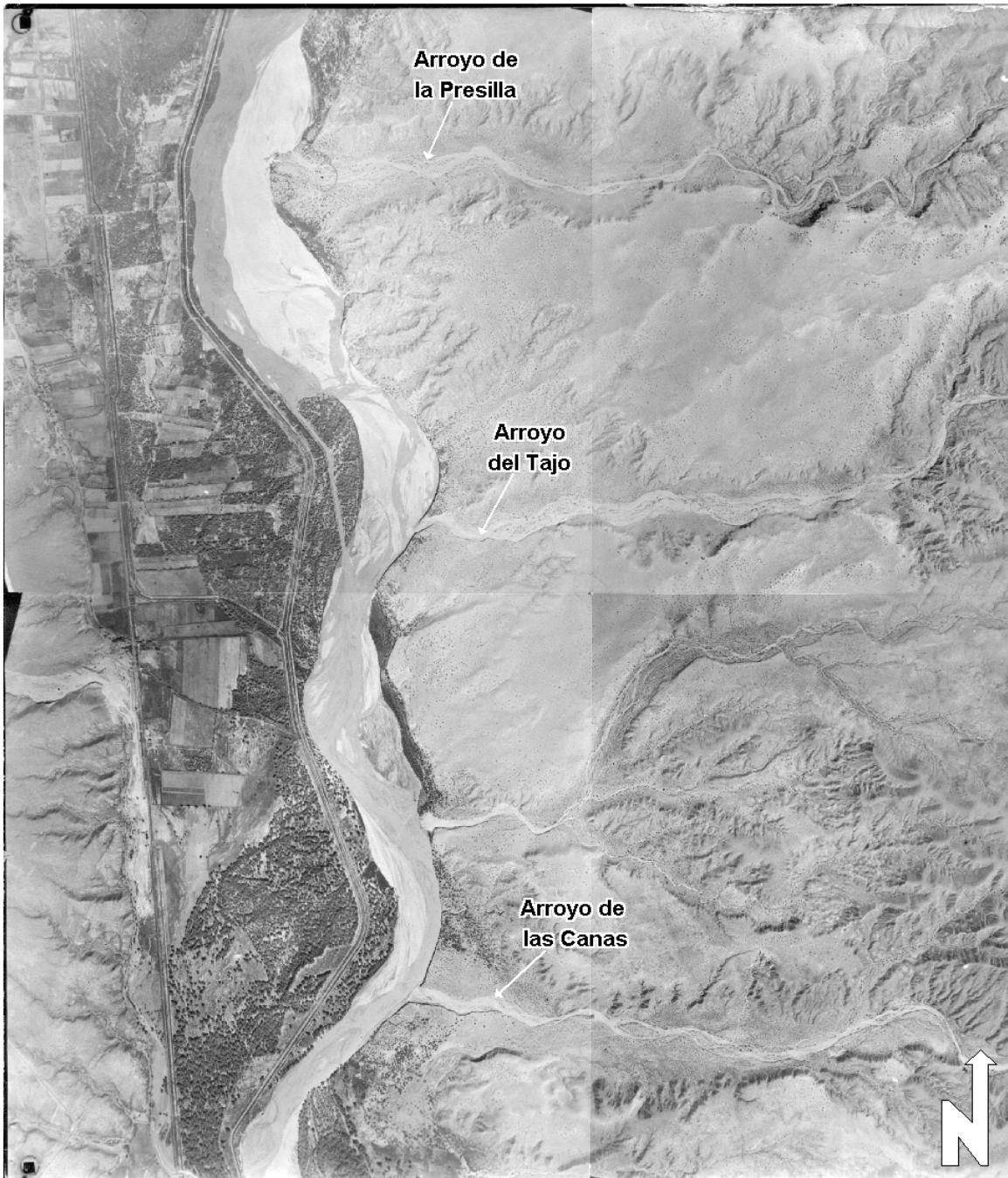
Figure 2.6.   1935 aerial photograph showing the lower reaches of Arroyo de la Presilla, Arroyo del Tajo and Arroyo de las Canas.

Mussetter Engineering, Inc.

Photograph 19.   View upstream of Arroyo Tio Bartolo within the surveyed reach. The channel has recently incised about 4 feet below its floodplain that is bounded by a terrace and the Tio Bartolo surface (08/22/2003).

Photograph 20.   View of bed material in the channel of Arroyo Tio Bartolo. The D_{50} of the sample (S14) is 0.8 mm and the D_{84} is 24 mm (see Figure B.3) (08/22/2003).

Mussetter Engineering, Inc.

Photograph 21.   View downstream of the confluence of Arroyo Tio Bartolo and the Rio Grande. The Tio Bartolo fan is prograding out onto the Rio Grande floodplain and lower elevation vegetated bars (11/24/2003).

Photograph 22.   View across Arroyo de la Presilla showing the 8-foot high terrace that borders the channel and the bounding Tio Bartolo surface (08/22/2003).

Mussetter Engineering, Inc.

Photograph 23.   View of bed material in the channel of Arroyo de la Presilla. The D_{50} of the sample (S12) is 2.2 mm and the D_{84} is 18.2 mm (see Figure B.6) (08/22/2003).

Photograph 24.   View upstream of the lower reach of Arroyo de la Presilla at the confluence with the Rio Grande. The fan is prograding out onto the Rio Grande floodplain and onto lower elevation, vegetated bars (11/24/2003).

Mussetter Engineering, Inc.

2.2.8. Arroyo del Tajo

Arroyo del Tajo is located on the left (east) bank of the Rio Grande about 8.6 miles downstream of the Escondida Bridge (RM 96.2) (Figure 1.1). The basin area is about 9 mi^2, and the average basin slope is 3.7 percent (194 ft/mi). The details of the basin topography can be seen in **Figure A.4**. On the 1935 aerial photograph (Figure 2.6), it is clear that the arroyo is discharging directly to the Rio Grande.

The upper reaches of the basin extend into the Chupadera Mesa, but the lower reaches of the arroyo are confined by the Tio Bartolo surface (**Photograph 25**). The channel is bordered on both sides by an 8-foot high terrace. The bulk of the sediment being delivered to the modern fan from the upstream watershed is sand-sized and finer, but erosion of the channel-bounding terrace is locally delivering both sands and gravels to the fan (**Photograph 26**). The median (D_{50}) size of the bed material in the arroyo is about 2.9 mm, but clasts up to 60 mm are present (**Photograph 27**).   The fan at the downstream end of the arroyo is prograding out onto the floodplain of the Rio Grande and onto lower elevation, vegetated bars (**Photograph 28**). The lower reaches of the fan were recently bulldozed to remove vegetation and connect the arroyo to the river.

2.2.9. Arroyo de las Canas

Arroyo de las Canas is located on the left (east) bank of the Rio Grande about 9.8 miles downstream of the Escondida Bridge (RM 95) (Figure 1.1). The basin area is about 26.3 mi^2, and the average basin slope is 3.1 percent (194 ft/mi). The details of the basin topography can be seen in **Figure A.6**. On the 1935 aerial photograph (Figure 2.6), it is clear that the arroyo was discharging directly to the Rio Grande, and it is highly likely that the arroyo was also incised.

The upper reaches of the basin extend into the Chupadera Mesa, but the lower reaches of the arroyo are confined by the Tio Bartolo surface. The channel is bordered on both sides by a 10-ft high terrace (**Photograph 29**). Locally within the channel there is evidence of debris flow deposits that contain boulder-sized materials (**Photograph 30**). The bulk of the sediment being delivered to the modern fan from the upstream watershed is sand-sized and finer, but erosion of the channel-bounding terrace is locally delivering considerable volumes of fine-grained sediments to the channel (**Photograph 31**). The median (D_{50}) size of the fine-grained bank material in the arroyo is about 0.2 mm, and the silt-clay content is about 25 percent. The median (D_{50}) size of the bed material in the arroyo is about 8.8 mm, but clasts up to 90 mm are present (**Photograph 32**).   The fan at the downstream end of the arroyo is prograding out onto the channel of the Rio Grande (**Photograph 33**), and the coarser sediments (**Photograph 34**) have formed a gravel-cobble riffle in the Rio Grande at the confluence.

2.2.10. Arroyo San Pedro

Arroyo San Pedro is located on the left (east) bank of the Rio Grande immediately upstream of the Highway 380 crossing at San Antonio (Figure 1.1). The basin area is about 47.3 mi^2, and the average basin slope is 2.7 percent (140 ft/mi). The details of the basin topography can be seen in **Figure A.10**. On the 1935 aerial photograph (**Figure 2.7**), it is clear that the arroyo was not discharging directly to the Rio Grande, but rather was forming a large fan on the floodplain of the Rio Grande. In about 1940, the highway was moved to the north, and it currently forms the southern boundary of the fan.

Mussetter Engineering, Inc.

Photograph 25.   View upstream of Arroyo del Tajo with the Tio Bartolo surface in the middle-ground and the Chupadera Mesa in the background (08/21/2003).

Photograph 26.   View of terrace fill on the right bank of Arroyo del Tajo showing the coarser grained channel deposits that are overlain by finer grained pre-incision overbank deposits (08/21/2003).

Mussetter Engineering, Inc.

Photograph 27.   View of bed material in the channel of Arroyo del Tajo. The D_{50} of the sample (S9) is 2.2 mm and the D_{84} is 13.4 mm (see Figure B.4) (08/21/2003).

Photograph 28.   View downstream of the eroding fan margin at the confluence of Arroyo del Tajo and the Rio Grande. Recent bulldozing of the lower reaches of the arroyo has been done to connect the arroyo and the river (08/21/2003).

Mussetter Engineering, Inc.

Photograph 29.   View downstream of the lower reaches of Arroyo de las Canas. The channel was probably incised in 1935 (08/19/2003).

Photograph 30.   View of debris flow deposits consisting of cobbles and boulders on the bed of Arroyo de las Canas (08/19/2003).

Mussetter Engineering, Inc.

Photograph 31.　　View of predominantly fine –grained terrace fill sediments along the right bank of Arroyo de las Canas. The D_{50} of the sample (S2) is 0.2 mm and the D_{84} is 0.27 mm (see Figure B.7). Silt-clay content of the fines is about 25 percent (08/19/2003).

　　　Mussetter Engineering, Inc.

Photograph 32.   View of bed material in the channel of Arroyo de las Canas. The D_{50} of the sample (S1) is 8.8 mm and the D_{84} is 29.9 mm (see Figure B.7) (08/19/2003).

Photograph 33.   View upstream of the mouth of Arroyo de las Canas at the confluence with the Rio Grande. The channel surface is covered with fine-grained mud deposits (11/24/2003).

Mussetter Engineering, Inc.

Photograph 34.   View of relatively coarse –grained sediments on toe of the fan of Arroyo de las Canas. The coarse grained sediments from the arroyo have formed a gravel-cobble riffle in the Rio Grande at the confluence (11/24/2003).

Mussetter Engineering, Inc.

Figure 2.7.   1935 aerial photograph showing the lower reaches of Arroyo San Pedro. The Highway 380 alignment was moved north to its present position closer to the channel in about 1941.

Mussetter Engineering, Inc.

The upper reaches of the basin extend into the Chupadera Mesa, but the lower reaches of the arroyo are confined by the Tio Bartolo surface. The channel is bordered on both sides by a 6-foot high terrace (**Photograph 35**). The bulk of the sediment being delivered to the active fan from the upstream watershed is sand-sized and finer. The median (D_{50}) size of the bed material in the arroyo is about 1.6 mm, but clasts up to 64 mm are present (**Photograph 36**). The fan at the downstream end of the arroyo is prograding out onto the heavily vegetated former floodplain of the Rio Grande, and it is highly unlikely that significant amounts of sediment are currently reaching the Rio Grande.

Mussetter Engineering, Inc.

Photograph 35.   View upstream of Arroyo San Pedro. The Chupadera Mesa can be seen in the background. The channel is confined between the Tio Bartolo surface to the north and Highway 380 to the south (08/21/2003).

Photograph 36.   View of bed material in the channel of Arroyo San Pedro. The D_{50} of the sample (S8) is 1.6 mm and the D_{84} is 16.6 mm (see Figure B.10) (08/21/2003).

Mussetter Engineering, Inc.

Mussetter Engineering, Inc.

3. FIELD DATA COLLECTION

A field data collection program to obtain channel topography, bed- and bank-material gradations, and other descriptive information for use in the study at the 10 selected basins (Figure 1.1) was conducted in August 2003.

3.1. Topographic Surveys

Topographic surveys of the channel and overbanks, including cross-section surveys and a detailed longitudinal profile were completed in August 2003 in the lower reaches of the 10 arroyos. The surveyed cross sections and longitudinal profiles provided the necessary geometric data to develop a one-dimensional (1-D) hydraulic model (HEC-RAS) of each study site (USCOE, 2002). The surveys were conducted using standard engineering survey techniques with a total station theodolite and electronic datalogger. The surveys at each site were referenced to a local, arbitrary coordinate system. The locations of the surveyed sites for each of the 10 basins are shown on Figures A.1 through A.10 (Appendix A).

At each site, five cross sections of the arroyo were surveyed with cross-section spacing between one and two channel widths. In addition, a detailed thalweg profile and supplemental bankline locations and elevations were also surveyed to better define the channel profile and alignment. The plotted cross sections and longitudinal profiles for the individual basins are provided in Appendix G.

3.2. Sediment Sampling

During the site surveys, two bulk sediment samples were collected at each site for subsequent laboratory sieve analysis. At the Arroyo de las Canas site, one bed-material sample and one bank-material sample were collected, and at the remaining nine sites, two bed- material samples were collected, one sample from finer material located within the most recently active part of the channel, and one coarser sample located on a channel bar. The coarser sample generally has higher gravel content, and both the coarse and fine samples had similar gradations in the sand-size fraction of the sediment-gradation curves. The computed average gradation of the two samples was used as the representative gradation for the sediment-transport calculations. The sediment- gradation curves and the representative gradations used in the sediment-transport calculations are provided in Appendix B. **Table 3.1** summarizes the median (D_{50}) and D_{84} parameters for the representative gradation at each site.

Table 3.1. Summary of D_{50} and D_{84} grain-size parameters for representative gradations.		
Arroyo	D_{50} (mm)	D_{84} (mm)
Arroyo Sevilleta	0.9	6.4
Arroyo de Tio Bartolo	0.9	14.5
Arroyo del Coyote	2.5	16.3
Arroyo del Tajo	4.3	22.6
Arroyo de los Pinos	5.1	22.3
Arroyo de la Presilla	2.9	17.6
Arroyo de las Canas	8.8	29.9
Arroyo de Alamillo	1.2	7.8
Arroyo de la Parida	5.4	23.6
San Pedro Arroyo	0.7	11.7

Mussetter Engineering, Inc.

The median grain size (D_{50}) of the bed material ranges from 0.7 mm at San Pedro Arroyo to 8.8 mm at Arroyo de las Canas, and the D_{84} values range from 6.4 mm at Arroyo Sevilleta to 29.9 mm at Arroyo de las Canas.

Although not sampled, coarser-grained deposits are located in all of the channels, but they are volumetrically limited and do not represent the bulk of the fluvially transported sediment. The coarser deposits were most likely transported and deposited by episodic mud and/or debris flows.

The gradation parameters for the tributaries, as summarized in Table 3.1, clearly indicate that the sediments that are being delivered to the Rio Grande by the tributaries are much coarser than the bed materials in the San Acacia reach where the median size of the bed material in on the order of 0.3 mm (MEI, 2002). However, review of the tributary sample gradation curves in Appendix B shows that depending on the individual tributary, the percentage of sand-size (<2 mm) material being delivered to the Rio Grande varies from about 23 to 70 percent. The coarser fractions (i.e., gravel and larger) delivered by the tributaries to the Rio Grande create locally coarser accumulations in the bed of the Rio Grande in the vicinity of the confluences. For example, at the mouth of the Arroyo de la Parida, the D_{50} of the bed material in the Rio Grande is about 33 mm (MEI, 2002).

Mussetter Engineering, Inc.

4. HYDROLOGY

Hydrologic models were developed for the 10 tributary basins to provide hydrographs, runoff volumes, and flood peak discharges for the individual subbasins within each of the basins. The modeling was conducted using the Hydrologic Modeling System (HEC-HMS) software, Version 2.2.2 (USACOE, 2003), and runoff hydrographs were developed for the 2-, 5-, 10-, 25-, 50-, and 100-year return period events. The HEC-HMS software is designed to simulate precipitation-runoff processes of dendritic watershed systems and supercedes HEC-1 software. The computed peak discharges and hydrograph volumes for subbasins within each watershed were used to compute the wash load in conjunction with the Modified Universal Soil Loss Equation (MUSLE, Section 6.2). The computed yield hydrographs were integrated with the sediment-rating curves (described in Section 6.3) to compute bedload volumes for 2-, 5-, 10-, 25-, 50-, and 100-year return period events, and for the mean annual condition.

4.1. Model Development

The boundaries of the 10 watersheds were delineated using the Watershed Modeling System (WMS) software developed by BOSS International (BOSS, 2003). WMS has the ability to compute the physical basin parameters from USGS Digital Elevation Models (DEMs), which have a 10-meter (approximately 33 feet) resolution. The watersheds were delineated into subbasins based on similar hydrologic properties, and the WMS-derived boundaries were verified with drainage basin boundaries delineated by hand on USGS 7½ minute quadrangle maps. **Table 4.1** summarizes the drainage areas of the 10 study sites and the number of subbasins in each basin. Basin areas range from 2.6 to 47.3 square miles.

Table 4.1. Summary of basin areas and number of subbasins.		
Arroyo	Area (mi^2)	Number of Subbasins
Arroyo Sevilleta	2.6	3
Arroyo de Tio Bartolo	2.6	3
Arroyo del Coyote	3.2	3
Arroyo del Tajo	9.0	8
Arroyo de los Pinos	12.1	11
Arroyo de la Presilla	15.5	4
Arroyo de las Canas	26.3	8
Arroyo de Alamillo	40.5	12
Arroyo de la Parida	42.1	13
San Pedro Arroyo	47.3	19

Physical parameters computed by WMS, including basin area, channel length, average basin slope and average channel slope, are used with the Synder synthetic unit hydrograph method for calculating the unit hydrograph.

Mussetter Engineering, Inc.

HEC-HMS requires the following parameters to compute the hydrograph for a given storm event:

1. rainfall hyetograph
2. rainfall loss rate
3. unit hydrograph transform method
4. channel routing parameters

4.1.1. Hyetograph

A 24-hour storm event hyetograph was developed for the 2- through 100-year return period events for each basin. These hyetographs were used as the precipitation input to the HEC-HMS model for developing the hydrographs that were used to compute the fine sediment yields and bedload yields.

The hyetographs were developed from equations and procedures outlined in Section 22.2, Hydrology of the Development Process Manual [Albuquerque Metropolitan Arroyo Flood Control Authority (AMAFCA), 1993]. AMAFCA developed this distribution pattern based on NOAA-2 atlas and the Federal Emergency Management Agency (FEMA) criteria. The resulting areal distribution pattern and length of the hyetograph are considered to be representative of the thunderstorm events that create the peak discharges in the Middle Rio Grande region (RTI, 1994).

The precipitation parameters required for use in the design storm equations are the 1-, 6- and 24-hour rainfall intensities for the 2-, 5-, 10-, 25-, 50-, and 100-year events. The 6- and 24-hour intensities were obtained from the NOAA Precipitation Frequency Data website which is based on NOAA-14 atlas for Arizona, Nevada, New Mexico, Utah, and southeastern California, and these values are very similar to those in the older NOAA-2 atlas. The point rainfall intensities for each basin were selected at the centroid of the basin and values vary between basins based on physiographic location.

Local experience in the Albuquerque area suggests that the NOAA-14 atlas overestimates values for the 1-hour rainfall intensities (C. Anderson, Anderson Hydro, personal communication, 2003). Based on Anderson's recommendation, the 10- and 15-minute values from the NOAA-14 atlas were used with the NOAA-2 equations to predict separate estimates of the 1-hour value. These results were then averaged with the NOAA-14 values to obtain a value for the 1-hour rainfall intensity.

An areal reduction factor for the precipitation-frequency values was applied based on depth-area-duration curves outlined in the "HYDRO 40" publication (NOAA, 1994). The areal reduction factor (**Figure 4.1**) is an inverse relationship between drainage area and rainfall depth and was derived to account for the non-uniformity of rainfall distributions over drainage basins of different sizes. In smaller basins, a thunderstorm cell can deliver an approximately uniform precipitation depth over the basin. However, over larger basins, the size of the thunderstorm cell is likely to be smaller than the basin area, and therefore, application of the areal reduction factor results in a rainfall depth less than the point precipitation value. **Table 4.2** summarizes the precipitation depths reflecting the areal adjustments for the 1-, 6-, and 24-hour duration storms. The resulting 2- through 100-year hyetographs are provided in Appendix C.

Mussetter Engineering, Inc.
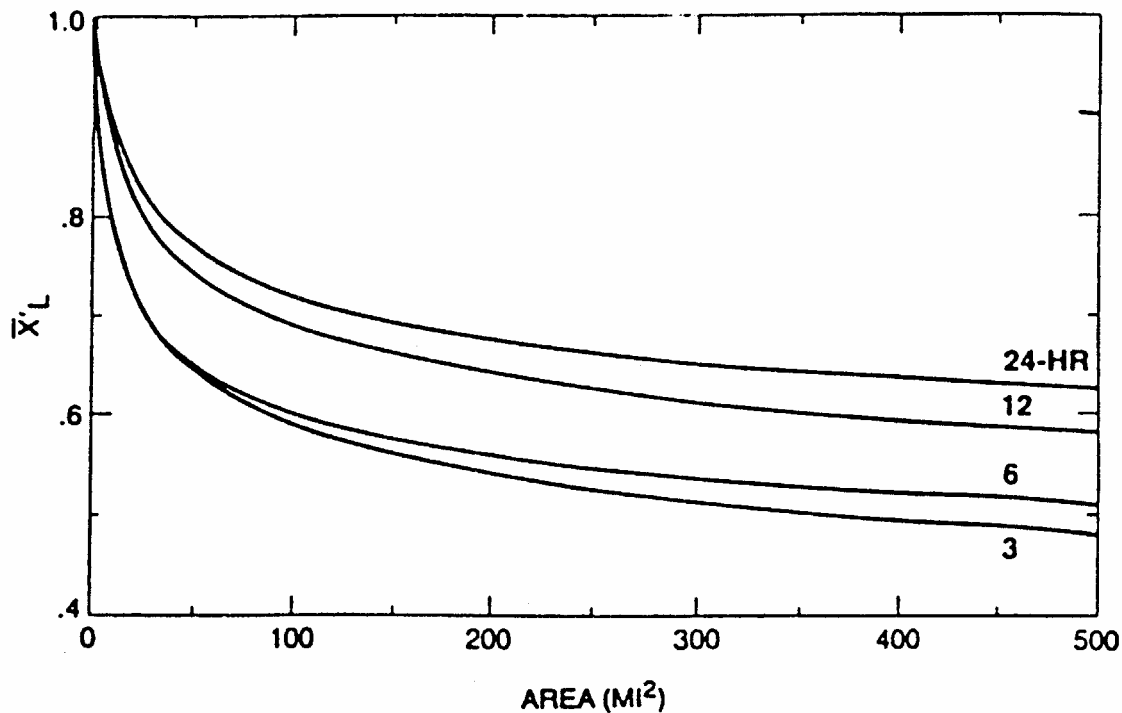
Figure 4.1.   Depth-area reduction curves for the 3-, 6-, 12-, and 24-hour events (HYDRO 40, NOAA, 1994).

4.1.2. Infiltration Rates

Soil infiltration losses were computed using the initial/constant loss method. The initial abstraction is the depth of precipitation which must be exceeded before runoff can occur, and it varies due to many factors, including vegetation interception, surface depressions, soil properties, and surface slope. After the initial abstraction, infiltration is treated as a constant loss rate.

The initial and constant loss parameters of 0.35 inches and 0.83 inches/hour, respectively, were selected for all frequency events and for all the watersheds based on guidelines outlined in the AMAFCA (1993) Design Manual for Land Treatment Area C, which *include soils with minimal vegetation, native grasses, weeds and shrub areas,* and soils with moderate slopes.

A sensitivity analysis was conducted to evaluate the effects of varying the initial/constant-loss parameters on runoff volume. The sensitivity analysis used the initial/constant loss parameters of 0.5 inches and 1.25 inches/hour for Land Treatment Area B (AMAFCA, 1993), which includes soils with *native grasses, weeds and shrubs, and soil uncompacted by human activity with slopes greater than 10 percent and less than 20 percent.* The results of the sensitivity analysis are discussed in Section 4.2.

Mussetter Engineering, Inc.

Arroyo	Rainfall Duration	Return Period (years)					
		2	5	10	25	50	100
Arroyo Sevilleta	1-hr	0.71	1.04	1.26	1.57	1.79	2.04
	6-hr	0.94	1.30	1.56	1.91	2.18	2.46
	24-hr	1.24	1.68	1.98	2.37	2.68	3.00
Arroyo de Tio Bartolo	1-hr	0.73	1.06	1.28	1.58	1.80	2.04
	6-hr	0.97	1.34	1.60	1.94	2.19	2.47
	24-hr	1.33	1.81	2.13	2.54	2.86	3.19
Arroyo del Coyote	1-hr	0.72	1.05	1.26	1.57	1.78	2.03
	6-hr	0.96	1.32	1.58	1.92	2.17	2.45
	24-hr	1.33	1.80	2.12	2.54	2.86	3.19
Arroyo del Tajo	1-hr	0.64	0.92	1.12	1.38	1.59	1.82
	6-hr	0.84	1.16	1.39	1.71	1.94	2.21
	24-hr	1.25	1.70	2.01	2.42	2.74	3.08
Arroyo de los Pinos	1-hr	0.61	0.88	1.06	1.32	1.51	1.71
	6-hr	0.81	1.11	1.34	1.63	1.84	2.09
	24-hr	1.21	1.64	1.94	2.32	2.62	2.93
Arroyo de la Presilla	1-hr	0.60	0.86	1.05	1.30	1.49	1.71
	6-hr	0.79	1.10	1.32	1.61	1.83	2.08
	24-hr	1.21	1.64	1.94	2.33	2.64	2.97
Arroyo de las Canas	1-hr	0.56	0.82	1.00	1.24	1.44	1.65
	6-hr	0.75	1.04	1.25	1.54	1.76	2.01
	24-hr	1.17	1.59	1.89	2.29	2.61	2.94
Arroyo de Alamillo	1-hr	0.60	0.88	1.07	1.32	1.52	1.74
	6-hr	0.67	0.94	1.13	1.37	1.57	1.78
	24-hr	0.87	1.18	1.40	1.67	1.90	2.12
Arroyo de la Parida	1-hr	0.52	0.76	0.93	1.14	1.32	1.51
	6-hr	0.70	0.96	1.16	1.42	1.62	1.84
	24-hr	1.09	1.49	1.76	2.12	2.41	2.70
San Pedro Arroyo	1-hr	0.51	0.75	0.93	1.18	1.39	1.64
	6-hr	0.67	0.95	1.16	1.45	1.69	1.97
	24-hr	1.04	1.44	1.72	2.10	2.43	2.78

Table 4.2.   Summary of precipitation frequency depth estimates for the 1-, 6-, and 24-hour duration storms (inches) after application of areal reduction factors.

Mussetter Engineering, Inc.

4.1.3. Unit Hydrograph

The unit hydrograph is a method for converting 1 inch of excess rainfall runoff volume generated over the drainage area at a constant rate into an instantaneous discharge at a given location. A modified version of the Synder synthetic unit hydrograph method was used to compute unit hydrographs for this study. This method is consistent with the method used by the U.S. Army Corps of Engineers and Resource Technology, Inc. (RTI) in this area. ["*The following modified equation was developed by the Albuquerque District of the COE and has been used with good results for basins in the Rio Grande watershed*" (RTI, 1994).

The modified Synder equation was used to determine the time to peak (t$_p$) for each subbasin. The equation is given by:

$$ t_p = 24 * Kn * \left(\frac{L * L_{CA}}{S^{0.5}} \right)^{0.36} \tag{4.1} $$

where   L   = length of the main channel to basin outlet in miles
         L$_{CA}$ = travel length to the centroid of the basin in miles
         S   = average channel slope in feet/mile
         Kn = Modified Manning's *n*-value for average channel flow

Manning's *n*-values (Kn) selected on the basis of observed field conditions and previous experience, range from 0.045 for developed flow paths to 0.065 for undeveloped flow paths, and length and slope parameters were calculated from the USGS DEMs using the WMS software. Selected Kn values are consistent with those used by RTI (1994).

The unit hydrograph C$_P$ coefficient was based on an optimization study for arroyos in the Rio Grande basin (RTI, 1994), and varies as a function of watershed slope as follows:

         C$_P$ = 0.70   Slope < 0.008 ft/ft
         C$_P$ = 0.84   Slope > 0.008 ft/ft

All subbasins considered in the study had watershed slopes greater than 0.008 ft/ft, and were therefore, assigned a value of C$_P$ = 0.84.

The Synder unit hydrograph parameters for the 10 study basins are summarized in **Table 4.3**.

4.1.4. Channel Routing

The kinematic wave-routing method was used to route channel flow between the subbasins. Estimates of the kinematic-routing parameters were based on field observations and maps of the study areas. Estimated Manning's *n*-values ranged from 0.045 to 0.065. Reach lengths and slopes were computed using WMS software, and channel bottom widths for the trapezoidal cross sections were estimated from 7½ minute quadrangle maps.

4.2.   Model Calibration

The hydrologic models were calibrated to the extent possible by comparing the HEC-HMS derived peak discharges to flood-frequency values reported by Thomas et al. (1997) who defined 16 hydrologic regions in the southwestern U.S., and report the flood-frequency values

Mussetter Engineering, Inc.

Study Site	Subbasin	D.A. (mi²)	L (mi)	L_CA (mi)	S (ft/mi)	24Kn	$t_{p \, (hrs)}$	C_p

Table 4.3. Summary table of basin parameters for Synder synthetic unit hydrographs.

Study Site	Subbasin	D.A. (mi²)	L (mi)	L_CA (mi)	S (ft/mi)	24Kn	$t_{p \, (hrs)}$	C_p
Arroyo Sevilletta	1	1.13	3.28	1.80	121.4	1.08	0.862	0.84
	2	0.76	2.58	1.54	121.4	1.08	0.748	0.84
	3	0.67	2.03	0.84	137.3	1.08	0.539	0.84
Arroyo de Tio Bartolo	1	0.94	2.87	1.27	200.6	1.08	0.662	0.84
	2	0.63	2.57	1.04	190.1	1.08	0.599	0.84
	3	1.03	2.64	1.25	137.3	1.08	0.684	0.84
Arroyo del Coyote	1	1.72	3.93	1.91	184.8	1.56	1.259	0.84
	2	1.17	3.55	1.82	179.5	1.56	1.200	0.84
	3	0.27	1.51	0.70	163.7	1.56	0.636	0.84
Arroyo del Tajo	1	0.93	1.64	0.55	332.6	1.56	0.527	0.84
	2	1.34	2.00	0.78	322.1	1.56	0.646	0.84
	3	0.99	2.02	0.87	147.8	1.56	0.776	0.84
	4	0.89	2.44	1.20	153.1	1.56	0.928	0.84
	5	1.04	2.24	1.03	137.3	1.56	0.868	0.84
	6	0.46	1.48	0.69	227.0	1.56	0.593	0.84
	7	1.18	2.14	1.07	211.2	1.56	0.801	0.84
	8	2.21	3.54	1.52	121.4	1.56	1.205	0.84
Arroyo de los Pinos	1	1.71	2.92	1.22	242.9	1.56	0.917	0.84
	2	0.58	1.68	0.76	301.0	1.56	0.610	0.84
	3	0.43	1.54	0.70	216.5	1.56	0.609	0.84
	4	1.15	2.06	0.94	105.6	1.56	0.854	0.84
	5	1.32	2.92	1.62	126.7	1.56	1.141	0.84
	6	1.59	2.87	1.48	110.9	1.56	1.124	0.84
	7	0.36	1.55	0.64	322.1	1.56	0.549	0.84
	8	0.47	1.90	0.80	279.8	1.56	0.659	0.84
	9	1.54	3.70	1.33	179.5	1.56	1.086	0.84
	10	1.07	2.14	1.13	158.4	1.56	0.862	0.84
	11	1.87	3.10	1.23	126.7	1.56	1.057	0.84
Arroyo de la Presilla	1	3.87	3.34	1.15	237.6	1.56	0.946	0.84
	2	4.31	4.51	1.65	137.3	1.56	1.325	0.84
	3	1.20	3.36	0.82	184.8	1.56	0.879	0.84
	4	6.13	8.01	4.43	95.0	1.56	2.483	0.84
Arroyo de las Canas	1	1.52	2.39	0.80	295.7	1.56	0.708	0.84
	2	1.63	3.52	1.07	211.2	1.56	0.958	0.84
	3	4.45	3.47	0.48	100.3	1.56	0.815	0.84
	4	1.21	2.23	1.25	163.7	1.56	0.900	0.84
	5	4.90	6.29	3.05	132.0	1.56	1.875	0.84
	6	3.46	3.72	1.70	137.3	1.56	1.251	0.84
	7	2.18	4.84	2.03	174.2	1.56	1.404	0.84
	8	0.83	2.04	0.87	290.4	1.56	0.690	0.84
	9	1.02	2.80	1.14	200.6	1.56	0.912	0.84
	10	5.12	7.66	3.82	116.2	1.56	2.234	0.84

Mussetter Engineering, Inc.

Study Site	Subbasin	D.A. (mi^2)	L (mi)	L$_{CA}$ (mi)	S (ft/mi)	24Kn	t$_{p\ (hrs)}$	C$_p$

Table 4.3.   Summary table of basin parameters for Synder synthetic unit hydrographs (continued).

Study Site	Subbasin	D.A. (mi^2)	L (mi)	L$_{CA}$ (mi)	S (ft/mi)	24Kn	t$_{p\ (hrs)}$	C$_p$
Arroyo de Alamillo	1	5.83	4.44	1.79	179.5	1.56	1.293	0.84
	2	2.84	4.7	1.98	110.9	1.56	1.492	0.84
	3	1.59	2.86	1.46	137.3	1.56	1.075	0.84
	4	1.91	2.52	0.99	190.1	1.56	0.844	0.84
	5	2.75	3.57	1.27	110.9	1.56	1.152	0.84
	6	1.75	3.88	1.68	147.8	1.56	1.246	0.84
	7	9.24	4.49	2.43	63.4	1.56	1.748	0.84
	8	3.05	5.9	2.11	95	1.56	1.703	0.84
	9	1.28	3.01	1.06	158.4	1.56	0.95	0.84
	10	3.35	3.23	1.19	137.3	1.56	1.045	0.84
	11	0.51	1.44	0.62	58.1	1.56	0.72	0.84
	12	6.42	6.39	3.22	105.6	1.56	2.003	0.84
Arroyo de la Parida	1	8.25	5	1.29	274.6	1.56	1.112	0.84
	2	3.14	4.73	2.58	205.9	1.56	1.471	0.84
	3	3.6	3.86	1.86	205.9	1.56	1.215	0.84
	4	4.86	5.41	2.48	142.6	1.56	1.627	0.84
	5	3.39	4.77	2.29	163.7	1.56	1.475	0.84
	6	3.91	4.89	2.22	200.6	1.56	1.418	0.84
	7	1.61	2.53	0.89	137.3	1.56	0.861	0.84
	8	1.59	3.28	1.62	200.6	1.56	1.097	0.84
	9	0.16	0.84	0.08	322.1	1.56	0.209	0.84
	10	4.69	1.89	1	52.8	1.56	0.961	0.84
	11	0.97	1.74	0.87	264	1.56	0.663	0.84
	12	1.22	2.03	0.9	89.8	1.56	0.862	0.84
	13	4.76	8.11	3.41	68.6	1.56	2.407	0.84
San Pedro Arroyo	1	3.11	3.32	1.32	169.0	1.56	1.056	0.84
	2	1.64	4.14	2.03	116.2	1.56	1.427	0.84
	3	4.44	4.70	2.01	205.9	1.56	1.341	0.84
	4	5.17	4.40	2.24	169.0	1.56	1.413	0.84
	5	5.02	4.47	1.03	63.4	1.56	1.282	0.84
	6	1.99	3.01	1.52	110.9	1.56	1.155	0.84
	7	2.92	4.35	2.37	105.6	1.56	1.561	0.84
	8	3.10	6.92	3.02	95.0	1.56	2.052	0.84
	9	2.96	4.77	1.70	163.7	1.56	1.323	0.84
	10	1.61	4.84	1.22	195.4	1.56	1.142	0.84
	11	0.14	0.80	0.12	153.1	1.56	0.273	0.84
	12	0.59	1.57	0.33	121.4	1.56	0.516	0.84
	13	2.79	4.25	2.50	174.2	1.56	1.443	0.84
	14	0.80	3.07	1.06	84.5	1.56	1.074	0.84
	15	4.09	3.73	1.42	174.2	1.56	1.123	0.84
	16	2.52	3.81	1.77	190.1	1.56	1.207	0.84
	17	1.16	3.44	2.12	184.8	1.56	1.246	0.84
	18	2.51	4.49	1.92	89.8	1.56	1.506	0.84
	19	0.70	2.35	0.48	105.6	1.56	0.705	0.84

Mussetter Engineering, Inc.

for the 2-, 5-, 10-, 25-, 50-, and 100-year events computed from stream gaging station measurements. Thomas et al (1997) used the flood-frequency values in conjunction with physical basin parameters (e.g. basin area, mean basin elevation and mean annual evaporation) to develop regional regression equations. **Figure 4.2** shows the locations of the 83 USGS gaging stations located in Region 16 in New Mexico and western Texas that were considered by Thomas et al. (1997) and which are considered to represent the study area. *The flood regions were delineated on the basis of the magnitudes of floods, meterologic cause of floods (snowmelt, summer thunderstorms or cyclonic rainfall), elevation of the sites and geographic patterns in residuals from the regression analysis (*Thomas et al., 1997).

Peak discharges computed with Land Treatment C values (initial/constant loss values of 0.35 inches and 0/83 inches/hour) from the hydrologic models and the regional flood-frequency values for the 5-, 10-, 25-, 50-, and 100-year events are in good agreement (**Figures 4.3 through** 4.**8)**. Computed peak values for the 2-year discharge for the four largest drainage basins appear to be low compared to the regional values (Figure 4.3).

The low values for the larger drainage basins can be explained by the areal reduction factor applied to the hyetographs, and further examination of the five closest gages to the study basins (**Figure 4.9**). Application of the areal reduction factor to the hyetographs reduces the rainfall intensity, and therefore, reduces the peak discharge and volume of runoff as the drainage basins increase in size. As the drainage basin-size increases, the decreasing rainfall intensity rate approaches the infiltration rate, and for the 2-year events, the rainfall intensity is only slightly greater than the infiltration rate, which produces low runoff and low peak discharges with increasing drainage area. At the higher return periods, the higher rainfall intensity is much greater than the infiltration rate, and therefore, produces greater peak discharges and runoff volumes as the drainage basin area increases.

The five closest gages to the study area are located in the mountains of the Cibola National Forest and on the Chupadera Mesa, which are different physiographically, and hydrologically from the 10 study basins, especially at the 2-year event. Observations of non- and lightly urbanized basins in the Albuquerque area indicate that runoff in response to the 2-year storm is very small or does not occur (MEI, 1996), which is consistent with the low 2-year peak-flow values obtained for the study basins.

A sensitivity analysis was conducted to evaluate effects of varying the initial and constant loss parameters by using Land Treatment Area B values of 0.5 and 1.25 inches/hour. Use of the higher values results in no runoff at the 10 study basins for the 2-year return period event (Figure 4.3). Peak discharges for the 5- and 10-year events are consistently in the lower range of reported USGS values and lie well below the best-fit line generated from the USGS data (Figures 4.4 and 4.5). Peak discharges for the 25-, 50- and 100-year events are generally lower than the best-fit line but lie within the spread of the USGS data points (Figures 4.6 through 4.8). The initial/constant loss parameters for Land Treatment Area C calibrate better with the USGS stream-gage data and were used, therefore, in the hydrologic analysis.

The estimated peak discharges and volumes of runoff for the 10 study basins using Land Treatment Area C values are summarized in **Table 4.4**, and values for the individual subbasins that were used to estimate average annual sediment loads for the basins are summarized in **Appendix D**. Plots of the hydrographs are provided in **Appendix E**.

Mussetter Engineering, Inc.
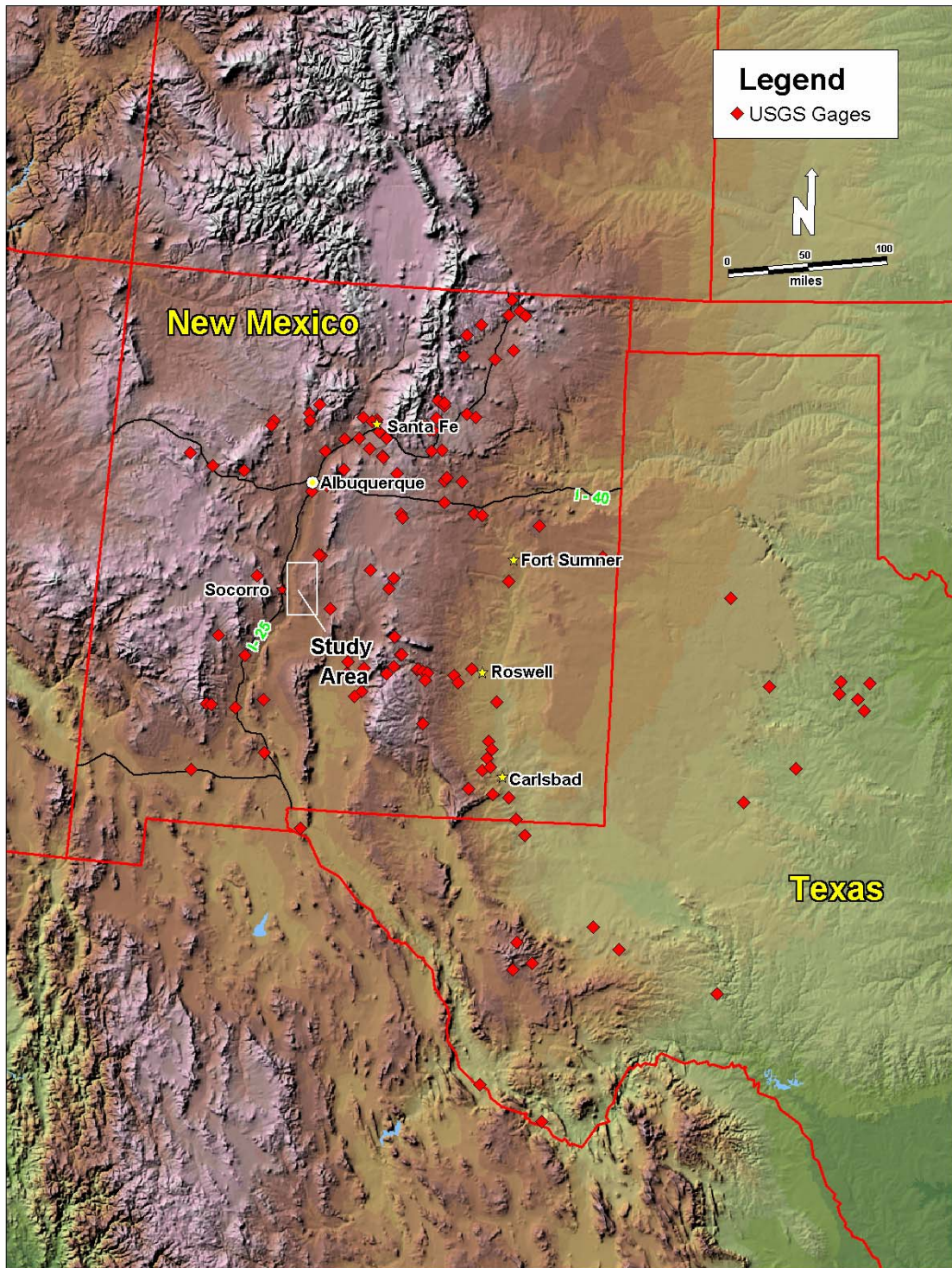
Figure 4.2.   USGS stream gage locations identified in Region 16 of "Methods for Estimating Magnitude and Frequency of Floods in the Southwestern United States" (Thomas et al., 1997).

Mussetter Engineering, Inc.
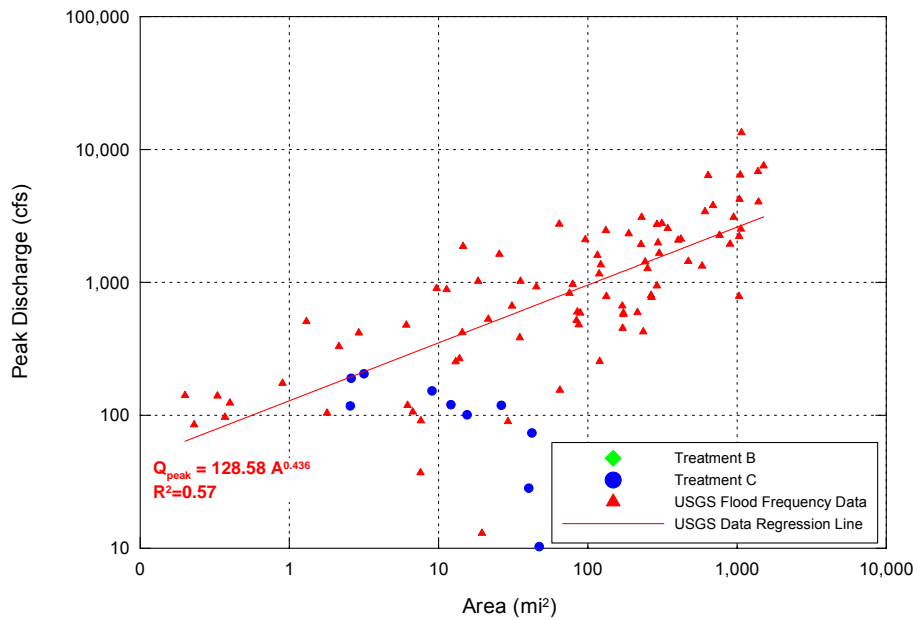
Figure 4.3. Comparison between 83 USGS 2-year flood-frequency discharge measurements reported for Region 16 by Thomas et al. (1997) and computed peak discharges of the 10 study basins from the HEC-HMS analysis using Treatment B and Treatment C infiltration rates (AMAFCA, 1993).
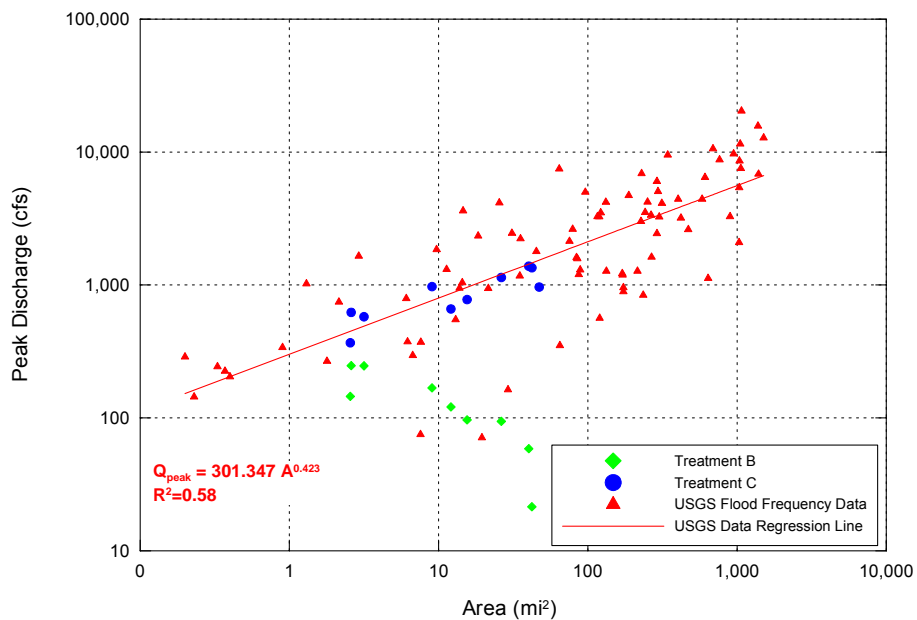
Figure 4.4. Comparison between 83 USGS 5-year flood-frequency discharge measurements reported for Region 16 by Thomas et al. (1997) and computed peak discharges of the 10 study basins from the HEC-HMS analysis using Treatment B and Treatment C infiltration rates (AMAFCA, 1993).

Mussetter Engineering, Inc.
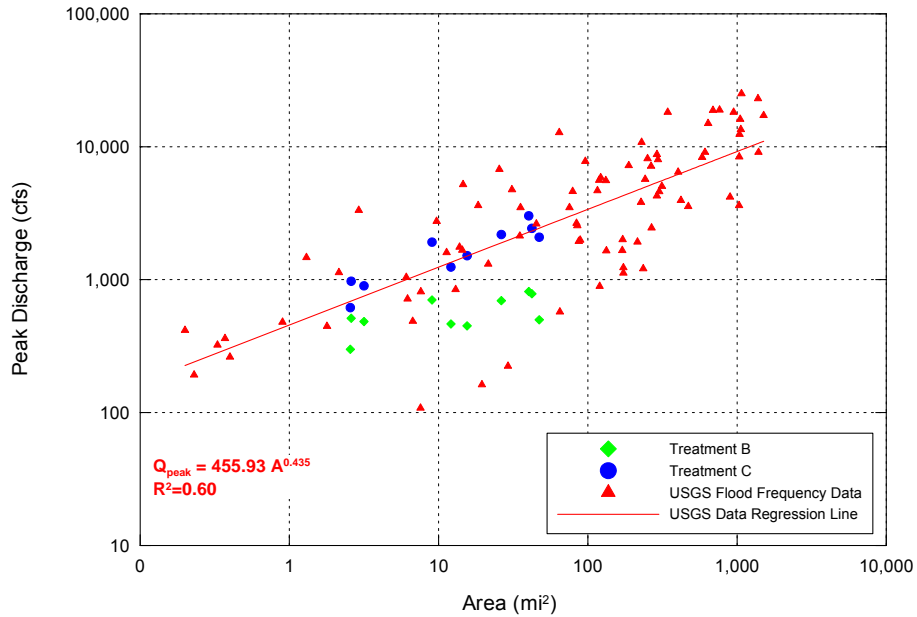
Figure 4.5.   Comparison between 83 USGS 10-year flood-frequency discharge measurements reported for Region 16 by Thomas et al. (1997) and computed peak discharges of the 10 study basins from the HEC-HMS analysis using Treatment B and Treatment C infiltration rates (AMAFCA, 1993).
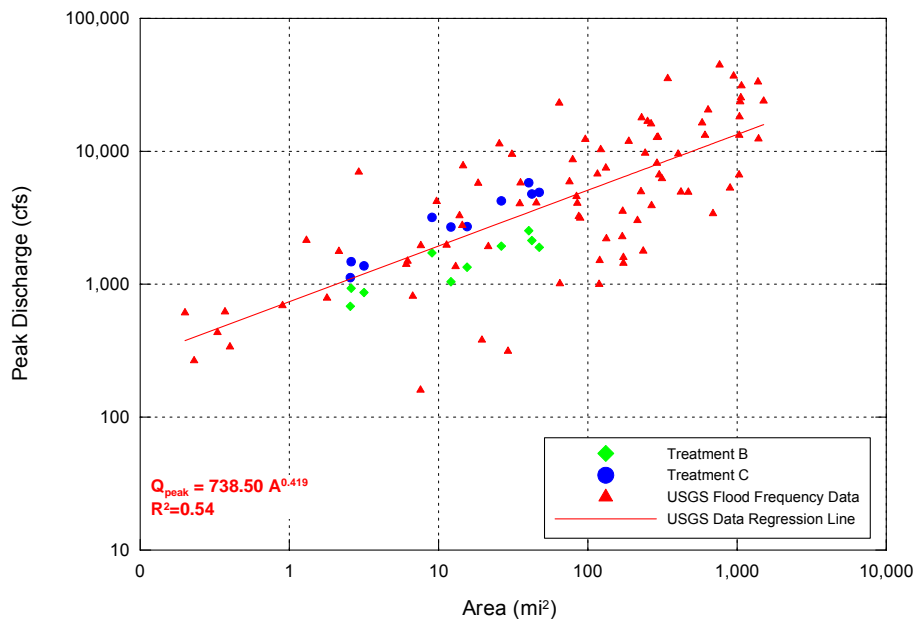
Figure 4.6.   Comparison between 83 USGS 25-year flood-frequency discharge measurements reported for Region 16 by Thomas et al. (1997) and computed peak discharges of the 10 study basins from the HEC-HMS analysis using Treatment B and Treatment C infiltration rates (AMAFCA, 1993).

Mussetter Engineering, Inc.
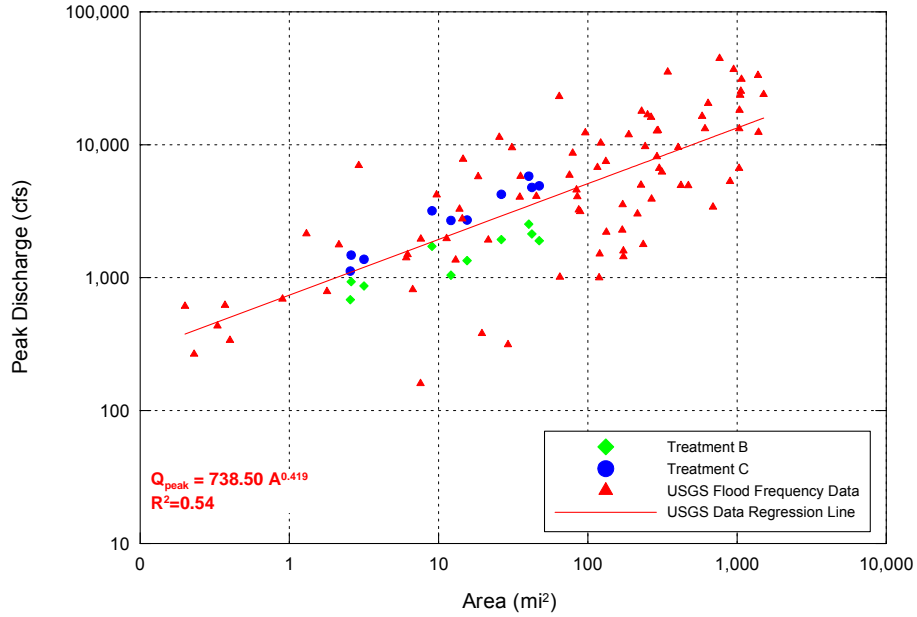
Figure 4.7.   Comparison between 83 USGS 50-year flood-frequency discharge measurements reported for Region 16 by Thomas et al. (1997) and computed peak discharges of the 10 study basins from the HEC-HMS analysis using Treatment B and Treatment C infiltration rates (AMAFCA, 1993).
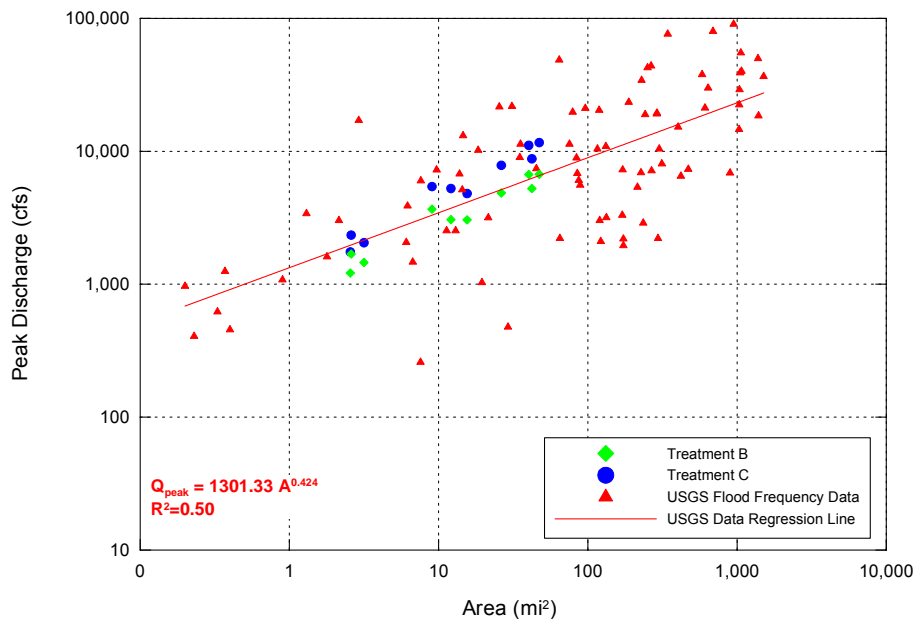
Figure 4.8.   Comparison between 83 USGS 100-year flood-frequency discharge measurements reported for Region 16 by Thomas et al. (1997) and computed peak discharges of the 10 study basins from the HEC-HMS analysis using Treatment B and Treatment C infiltration rates (AMAFCA, 1993).

Mussetter Engineering, Inc.
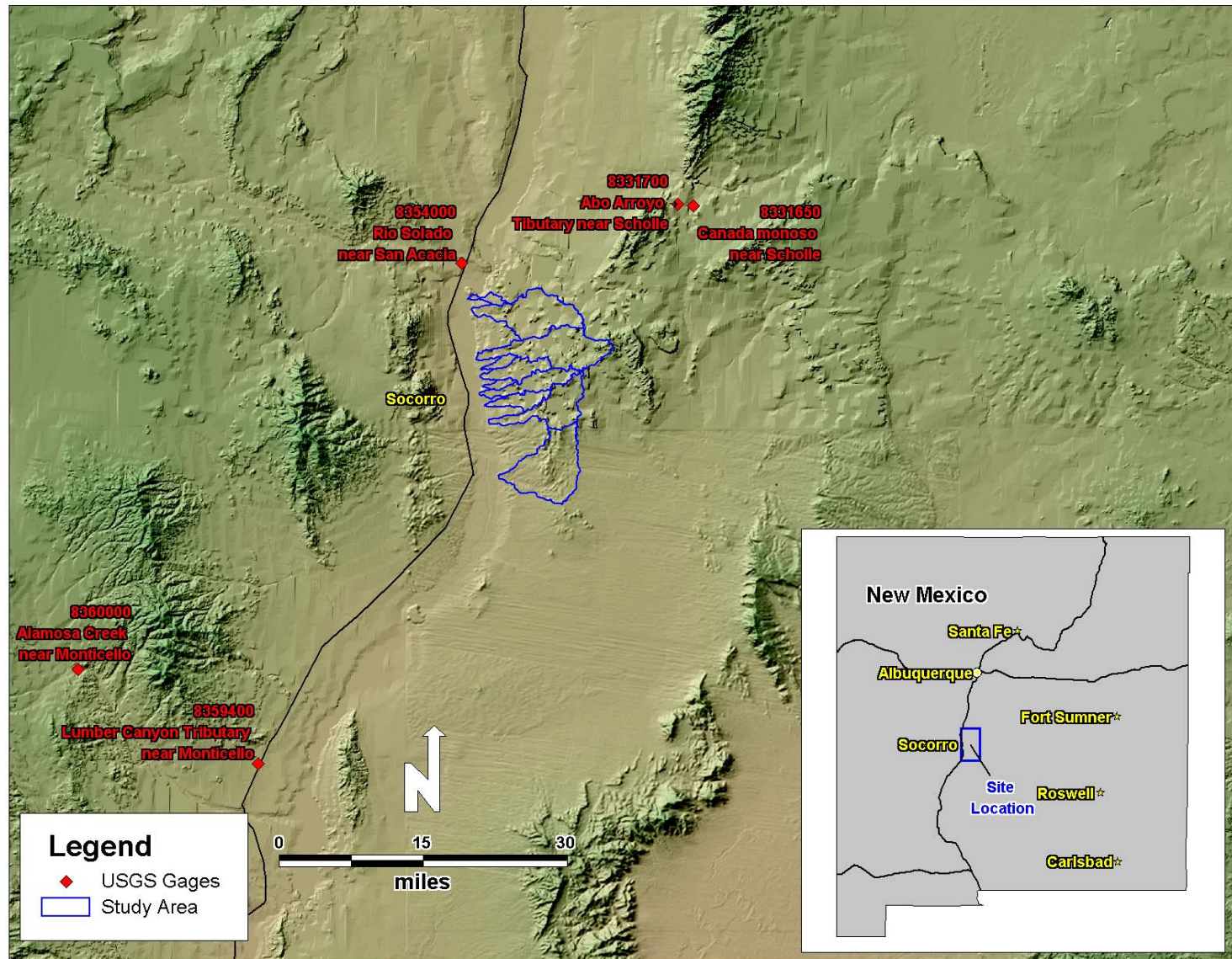
Figure 4.9.   Locations of the five closest USGS gaging stations reported by Thomas et al. (1997) to the study basins.

Mussetter Engineering, Inc.

Table 4.4. Summary of peak discharge and runoff volumes for the 2-, 5-, 10-, 25-, 50-, and 100-year events.												
	2-Year		5-Year		10-Year		25-Year		50-Year		100-Year	
Arroyo	Peak (cfs)	Volume (ac-ft)	Peak (cfs)	Volume (ac-ft)	Peak (cfs)	Volume (ac-ft)	Peak (cfs)	Volume (ac-ft)	Peak (cfs)	Volume (ac-ft)	Peak (cfs)	Volume (ac-ft)
Arroyo Sevilleta	118	14	367	41	616	64	1,121	99	1,470	129	1,748	162
Arroyo de Tio Bartolo	190	18	622	46	973	68	1,477	103	1,921	132	2,340	165
Arroyo del Coyote	206	19	576	52	898	81	1,374	124	1,752	157	2,052	197
Arroyo del Tajo	153	33	971	108	1,913	182	3,181	285	4,207	372	5,431	462
Arroyo de los Pinos	120	34	660	127	1,244	203	2,692	331	3,839	434	5,252	559
Arroyo de la Presilla	101	47	776	172	1,513	281	2,713	464	3,659	598	4,807	761
Arroyo de las Canas	119	43	1,138	281	2,185	475	4,230	719	5,915	1,014	7,848	1,291
Arroyo de Alamillo	28	13	1,385	309	3,020	561	5,797	964	8,244	1,316	11,079	1,738
Arroyo de la Parida	74	2	1,347	312	2,433	546	4,770	989	6,599	1,308	8,781	1,703
San Pedro Arroyo	10	4	964	292	2,086	538	4,906	988	7,910	1,408	11,620	1,960

Mussetter Engineering, Inc.

The five smallest drainage basins (Arroyo Sevilleta, Arroyo de Tio Bartolo, Arroyo del Coyote, Arroyo del Tajo and Arroyo del los Pinos) show similar hydrologic responses, with the peak discharges occurring approximately 4 hours after the beginning of the simulation (rainfall peak occurs at 1.4 hours). The peak flow in the larger basins (Arroyo de la Presilla, Arroyo de las Canas, Arroyo de Alamillo, Arroyo de la Parida, and San Pedro Arroyo) occurs at approximately 6 hours after the beginning of the simulation.

The computed hydrographs for Arroyo de la Parida shows two distinct peaks because of the unusual shape of the watershed (Figures A.9 and E.9). The majority of the watershed area is located in the upper elevation subbasins, which creates a significant lag time in routing the runoff from the upper part of the basin through the lower elevation subbasins. The hydrograph peak of Subbasin 13, which is located closest to the surveyed site near the mouth of the basin (**Figure G.9a**), occurs approximately two hours before the flows from the upper basins reach the study site, which creates the double peak in the hydrograph.

Mussetter Engineering, Inc.

Mussetter Engineering, Inc.

5.   HYDRAULIC ANALYSIS

One-dimensional (1-D) hydraulic analyses of the surveyed reaches (Appendix G) within each of the 10 basins were carried out to determine the hydraulic conditions (e.g., flow velocity, depth, topwidth and energy slope) at the individual sites for subsequent use in estimating the bed material transport capacities. The hydraulic analysis was performed using Version 3.1 of the U.S. Army Corps of Engineers HEC-RAS computer software (USCOE, 2002). HEC-RAS is a Windows-based computer modeling system for 1-D analysis of stream hydraulics, one component of which allows the user to compute steady-state water-surface profiles.

5.1.   Model Development

Geometric data used in the hydraulic models were developed from in-channel and overbank surveys within each of the 10 basins that were conducted by MEI in August 2003. Each model contains 5 cross sections that are based on surveyed transects across the channel (Appendix G).

The roughness and energy loss characteristics of the arroyo channels and overbanks are accounted for in the HEC-RAS software through the use of Manning's *n*-roughness coefficients and expansion and contraction losses. Manning's *n*-roughness coefficients for the main channel were set at 0.045 for all sites based on standard references (Chow, 1959; Barnes, 1967; Hicks and Mason, 1991), and past experience with similar channels.   Overbank Manning's *n*-values were selected to reflect roughness conditions in the overbanks and ranged from 0.06 to 0.07 to account for the presence of obstructions, vegetation, non-linearity and nonuniformity of the banks.

To perform the hydraulic calculations, a starting water-surface elevation is required at the downstream end of the model. The starting water-surface elevations were determined by assuming normal depth conditions where the energy slope is equal to the surveyed local bed slope. Calibration of the hydraulic models was not possible because the channels were dry at the time of the surveys, and high-water marks observed within the channels could not be related to known discharges.

Levees and encroachments were employed at appropriate locations in the models to block ineffective flow areas, to ensure that low areas in the overbanks would not convey flow until the banks were overtopped, and to ensure continuity of flow between the cross sections.

5.2.   Model Results

The HEC-RAS models for each of the basins were run for 28 discharges that ranged from 10 cfs up to the 100-year flood peak. Reach-averaged hydraulic parameters obtained from those runs for the 2-, 5- 10-, 25-, 50-, and 100-year discharges are summarized in **Table 5.1**.

Reach-averaged velocities range from 1.9 fps (Arroyo del la Parida) to 3.1 fps (Arroyo del Coyote) for the 2-year peak flow and range from 5.4 fps (Arroyo de las Canas) to 10.1 fps (Arroyo de la Parida) for the 100-year peak flow. Hydraulic depths for the 2-year peak flow range from 0.2 feet (Arroyo de la Parida) to 0.5 feet (Arroyo de la Presilla, Arroyo del Coyote and Arroyo de Tio Bartalo), and from 1.4 feet (Arroyo del Coyote) to 3.7 feet (Arroyo de la Parida) for the 100-year peak flow. Arroyo Sevilleta is the steepest of the channels with energy slope values ranging from 0.0224 ft/ft at the 2-year peak to 0.0197 (ft/ft) at the 100-year peak. Energy slopes for the different flows in the individual basins will depend on the energy losses

Table 5.1.				Reach-averaged hydraulic parameters for the 2-, 5-, 10-, 25-, 50-, and 100-year return period events at the study sites.		
Site	Return Interval (years)	Discharge (cfs)	Main Channel Velocity (fps)	Hydraulic Depth (ft)	Effective Width (ft)	Energy Slope (ft/ft)
Arroyo Sevilleta	2	118	2.8	0.4	95	0.0224
	5	367	4.3	0.8	102	0.0217
	10	616	5.3	1.1	103	0.0214
	25	1,121	6.6	1.6	105	0.0211
	50	1,470	7.2	1.9	106	0.0203
	100	1,748	7.6	2.1	107	0.0197
Arroyo de Tio Bartolo	2	190	2.6	0.5	161	0.0171
	5	622	3.7	0.8	214	0.0165
	10	973	4.3	1.0	222	0.0166
	25	1477	5.0	1.3	228	0.0166
	50	1921	5.6	1.5	231	0.0167
	100	2340	6.0	1.7	234	0.0167
Arroyo del Coyote	2	206	3.1	0.5	130	0.0210
	5	576	4.1	0.8	178	0.0216
	10	898	4.8	1.0	195	0.0216
	25	1,374	5.3	1.1	230	0.0214
	50	1,752	5.7	1.3	241	0.0219
	100	2,052	6.1	1.4	243	0.0220
Arroyo del Tajo	2	153	2.4	0.4	156	0.0174
	5	971	3.7	0.8	321	0.0170
	10	1,913	4.8	1.2	337	0.0173
	25	3,181	5.9	1.6	337	0.0171
	50	4,207	6.6	1.9	337	0.0170
	100	5,431	7.2	2.2	337	0.0169
Arroyo de los Pinos	2	118	2.8	0.4	95	0.0224
	5	367	4.3	0.8	102	0.0217
	10	616	5.3	1.1	103	0.0214
	25	1,121	6.6	1.6	105	0.0211
	50	1,470	7.2	1.9	106	0.0203
	100	1,748	7.6	2.1	107	0.0197

Mussetter Engineering, Inc.

Site	Return Interval (years)	Discharge (cfs)	Main Channel Velocity (fps)	Hydraulic Depth (ft)	Effective Width (ft)	Energy Slope (ft/ft)
Table 5.1. Reach-averaged hydraulic parameters for the 2-, 5-, 10-, 25-, 50-, and 100-year return period events at the study sites (continued).						
Arroyo de la Presilla	2	120	2.5	0.5	106	0.0157
	5	660	3.2	0.7	306	0.0164
	10	1,244	3.7	0.8	406	0.0159
	25	2,692	4.7	1.2	465	0.0152
	50	3,839	5.3	1.5	490	0.0152
	100	5,252	5.8	1.7	527	0.0153
Arroyo de las Canas	2	101	2.4	0.4	109	0.0181
	5	776	2.8	0.6	425	0.0132
	10	1,513	3.5	0.9	472	0.0131
	25	2,713	4.4	1.2	500	0.0130
	50	,3659	4.9	1.5	511	0.0130
	100	4,807	5.4	1.7	514	0.0130
Arroyo de Alamillo	2	119	2.4	0.4	125	0.0177
	5	1,138	4.0	0.9	325	0.0171
	10	2,185	4.9	1.2	364	0.0169
	25	4,230	6.1	1.8	390	0.0159
	50	5,915	6.6	2.1	424	0.0148
	100	7,848	7.4	2.5	427	0.0147
Arroyo de la Parida	2	28	1.9	0.2	67	0.0267
	5	1,385	5.5	1.3	164	0.0200
	10	3,020	7.1	1.9	170	0.0192
	25	5,797	8.6	2.7	173	0.0180
	50	8,244	9.4	3.2	174	0.0170
	100	11,079	10.1	3.7	175	0.0163
San Pedro Arroyo	2	74	2.5	0.4	69	0.0183
	5	1,347	3.3	0.9	461	0.0121
	10	2,433	3.8	1.1	553	0.0111
	25	4,770	5.0	1.7	567	0.0111
	50	6,599	5.6	2.1	567	0.0110
	100	8,781	6.3	2.4	567	0.0110

*M*ussetter *E*ngineering, *I*nc.

that in turn depend on local conditions in the channel and overbank areas. San Pedro Arroyo has the flattest channel with energy slopes ranging from 0.0121 ft/ft at the 2-year peak to 0.0110 ft/ft at the 100-year peak. The effective widths range from 107 feet at Arroyo del Coyote and Arroyo de los Pinos to 567 feet at Arroyo de la Parida at the 100-year peak. From a sediment-transport perspective, the higher the velocities, depths, and slopes, and the narrower the channel, the higher will be the sediment-transport rates.

Froude numbers approach 1.0 at Arroyo de Alamillo at discharges greater than 2,500 cfs (approximately 8-year return interval) at Cross Sections 2 through 5 indicating that critical discharge conditions may occur. The Froude number is the ratio of inertial to gravitational forces and is an important measure of the state of open channel flow and is defined by:

$$F = \frac{V}{\sqrt{gD}}$$

(5.1)

where F = Froude number
        V = average velocity at the cross section
        g = gravitational constant
        D = hydraulic depth

Depending on the magnitude of the Froude number, the state of flow is either "subcritical" (i.e. Fr<1, "critical" (Fr=1) or "supercritical" (Fr>1). When the flow becomes critical (i.e. Froude number equal or greater than 1.0), HEC-RAS computes the parameters associated with the critical discharge conditions (i.e. depth and velocity) which may vary from actual conditions, creating uncertainty in the hydraulics and hence predicted sediment-transport rates. Care must be taken, therefore, in interpreting sediment transport values at discharges greater than 2,500 cfs in Arroyo de Alamillo.

Mussetter Engineering, Inc.

6.   SEDIMENT YIELD

The sediment yield from a watershed is composed of the following components: (1) bed-material load, which is composed of material commonly found in the bed and is controlled by the composition of the sediment and the hydraulic properties of the channel, and (2) wash load, which is the fine sediment that originates from the erosion of the soil, gullies and channel bed and banks, and that this not commonly found in the bed. Bed-material load actively exchanges with the channel bed as it is transported downstream; whereas, wash load typically remains in suspension once it reaches a channel. In addition, bed material load is typically carried at the capacity of the stream; whereas, wash load is controlled by the upstream supply and is generally not carried at capacity.

A long-term analysis of erosion or sedimentation needs to account for the probability of occurrence of various flood events during any one year (Chang, 1988). For example, if Y_S is the sediment yield for a given flood and P is the probability of occurrence of that flood in one year, the Product $Y_S \cdot P$ represents the contribution of that one flood to the long-term mean annual yield. To account for the contribution of all possible flows, the integration

$$\overline{Y_S} = \int_0^1 Y_S dP$$

(6.1)

is required. For practical purposes, the integration can be accomplished by determining the area under the sediment yield frequency curve (Mussetter et al., 1994). The frequency curve for the sediment yield can be estimated by computing the sediment yield expected for each of several floods of known return periods. The area under the curve represents the mean annual sediment yield, and can be computed graphically or numerically. The numerical procedure involves summing the incremental trapezoidal areas established by calculation of Y_S for discrete return periods. Assuming this calculation is completed for the 2-, 5-, 10-, 25-, 50-, and 100-year events, the mean annual sediment yield can be approximated by the following relation:

$$Y_m = 0.015Y_{100} + 0.015Y_{50} + 0.04Y_{25} + 0.08Y_{10} + 0.2Y_5 + 0.4Y_2$$

(6.2)

The fine sediment yields (wash load) were estimated using the Modified Universal Soil Loss Equation (MUSLE), and bed-material loads were estimated by integrating the sediment-transport rating curves computed using the Meyer-Peter, Müller (MPM)-Einstein sediment-transport equation with the HEC-HMS hydrographs.

6.1.   Measured Sediment Load Data

There are few reports of measured suspended-sediment concentrations for arroyos in the vicinity of the study area that can be used to validate the estimates from this study. Copeland (1995) summarized the available measured suspended-sediment concentrations obtained from field measurements and reservoir sediment deposition data. Twenty six (26) suspended-sediment samples were collected between 1936 and 1947 from Tijeras Canyon, located near Albuquerque, which had an average concentration of 58,000 ppm at an average discharge of 300 cfs, with concentrations ranging between 20,000 and 300,000 ppm. Four suspended-sediment samples were taken at Embudo Arroyo, which is located in South East Albuquerque, during flash floods in 1953, with concentrations ranging from 9,000 to 29,000 ppm for

Mussetter Engineering, Inc.

discharges between 8 and 350 cfs. Thirteen suspended-sediment samples collected in Abo Arroyo located in the Manzano Mountains (approximately 35 miles North East of Arroyo Sevilleta) had an average sediment concentration of 16,000 ppm at an average discharge of 140 cfs. Additional estimates of sediment yields were based on reservoir sedimentation analyses that report average sediment inflow concentrations of 176,700 ppm at Bernalillo Reservoir, located 17 miles north of Albuquerque and 57,800 ppm at Tortugas Reservoir, located near Las Cruces. The 55 measured suspended-sediment values summarized by Copeland (1995) had an average concentration of 47,000 ppm with a large range of variability (9,000 to 300,000 ppm).

6.2. Fine Sediment Yield

The Modified Universal Soil loss Equation (MUSLE), as adapted for the Albuquerque area (Mussetter et al., 1994), was used to estimate the wash-load yield for the study basins. This equation is given by:

$$Y_S = \alpha \, (Vq_p)^\beta \, KLSCP \tag{6.3}$$

where
Y_S = sediment yield (tons)
V = storm clear-water runoff volume (ac-ft)
q_p = clear-water peak discharge (ft^3/s)
K = soil-erodibility factor
LS = topographic factor representing the combined effect of slope length and gradient
C = cover and management factor
P = erosion-control factor
α = 285
β = 0.56

The V and q_p values for the 2- through 100-year events were obtained from the results of the hydrologic analysis (Chapter 4) that are summarized in Appendix D.

A representative soil erodibility factor (K value) was computed by taking an area weighted average of the K-values in each watershed (summarized in Appendix F). Areas of the various soil types within each watershed were determined by digitizing soil maps from the "Soil Survey of Socorro County Area, New Mexico" (SCS, 1988) using MapInfo, a Geographic Information Systems (GIS) software package. Basin area-weighted average K-values were computed for each subbasin, and the values ranged from 0.10 at Arroyo del los Pinos to 0.19 at Arroyo de Alamillo.

A cropping factor (C) of 0.2 was used in the computations to represent relatively sparse vegetation conditions for the entire watershed. The erosion-control practice factor (P) accounts for the effect of conservation practices such as contouring, strip cropping, and terracing. The factor has no significance for the rangeland conditions of the undeveloped watersheds in this study, and hence, the value was set equal to 1.0.

LS factors were computed using the following relationship:

$$LS = \left(\frac{\lambda}{72.6}\right)^n (0.065 + 0.454S + 0.0065S^2) \tag{6.4}$$

Mussetter Engineering, Inc.

where   λ   =   slope length (feet)
         S   =   percent slope
         n   =   exponent that depends on slope as follows:

                 n = 0.3 for slope≤ 3 percent
                 n = 0.4 for 3 percent < slope < 5 percent
                 n = 0.5 for slope ≥ 5 percent

The slope values were computed using the WMS software, and overland slope lengths (λ) were measured from maps developed with the WMS software (Appendix F). The MUSLE equation represents total sediment yield including the silts and clays that comprise the wash load from the watershed portion of the basin

The wash-load component of the sediment load (silt and clay fraction, sediment finer than 0.074 mm) was estimated for each basin based on an area-weighted average of silt-clay content (percent finer than 0.074 mm) of each soil type in the watershed (Appendix F). The SCS soil survey (1988) provides a range of percentages of material finer than 0.074 mm for each soil type, and an average of the range was used as an estimate for each basin. The fine sediment yield estimates for each watershed for the 2- though 100-year events, and average annual yields are summarized in **Tables 6.1 and 6.2**. Computed values ranged from 3,500 ppm at Arroyo Sevilleta to 44,000 ppm at Arroyo de la Parida, with an average of 24,000 ppm.

The variation in sediment concentrations between the 10 basins occurs primarily because of the differences in basin slope and the percent silt/clay in the soil. The LS parameter in the MUSLE equation is a product of the slope-length factor and average basin slope. The slope-length factor is relatively constant for all basins in the study (basin length averages approximately 200 feet); however, the average basin slopes vary from 6 percent at Arroyo Sevilleta to 17 percent at Arroyo de los Pinos. The range of silt/clay percentage in the soil ranges from 10 percent at Arroyo Sevilleta, which has the lowest average annual fine sediment yield, to 35 percent at Arroyo de la Parida, which has the highest average annual fine sediment yield.

A sensitivity analysis was conducted to determine the effect of using different K- and silt/clay values for each subbasin, compared to using the same K- and silt/clay value for all of the subbasins within each watershed. Values for Arroyo de las Canas and Arroyo del Tajo were computed using both methods, and the results yielded less than 10 percent difference between the methods because of the homogeneity of the soil erodibility (K) values and silt/clay fraction within the watersheds. As a result, the values for the remaining 8 basins were estimated using a weighted K-value for the complete basin.

6.3. Bed Material Sediment Yield

To determine the average annual bed material sediment yield, sediment-rating curves (the relationship between the discharge and the amount of sediment transported) for each channel were developed using the Meyer-Peter, Müller-Einstein (MPM-Einstein) sediment-transport equation (Mussetter et al., 1994) (**Figures 6.1a and 6.1b**), and the Colby correction for fine sediment effects. The sediment rating curves were developed using hydraulic data (e.g. discharge, velocity and depth) from the HEC-RAS models and sediment gradations computed from sediment samples collected at the sites (Appendix B). The Colby correction factor (Colby, 1964) was applied to the sediment rating curves to account for the increase in the transport capacity of sands when high concentrations (Cs>10,000 ppm) of wash load are present. The rating curves were then integrated with the 2- through 100-year hydrographs to compute the

Mussetter Engineering, Inc.

Table 6.1.	Fine sediment yield (wash load) (tons) for the 2-, 5-, 10-, 25-, 50-, and 100-year return interval events and mean annual yield.						
Site	2-year	5-year	10-year	25-year	50-year	100-year	Mean Annual
Arroyo Sevilleta	56	184	304	524	693	888	128
Arroyo del Coyote	410	1,269	2,025	3,188	4,200	5,329	850
Arroyo de Tio Bartolo	337	1,061	1,725	2,772	3,620	4,462	717
Arroyo del Tajo	936	3,725	6,523	10,844	14,619	19,198	2,582
Arroyo de los Pinos	889	4,294	7,594	13,027	17,584	23,175	2,954
Arroyo de la Presilla	793	4,103	7,404	12,812	17,381	23,216	2,852
Arroyo de las Canas	1,355	10,260	18,814	34,185	47,460	63,615	7,133
Arroyo de Alamillo	175	6,488	13,186	23,997	33,827	45,991	4,580
Arroyo de la Parida	559	14,345	28,816	52,557	73,370	98,544	10,079
San Pedro Arroyo	90	6,695	13,969	27,450	40,473	58,226	5,071

Table 6.2. Mean annual fine sediment yield concentration (ppm).	
Study Site	Cs (ppm)
Arroyo Sevilleta	3,503
Arroyo de Tio Bartolo	21,762
Arroyo del Coyote	15,484
Arroyo del Tajo	27,732
Arroyo de los Pinos	27,344
Arroyo de la Presilla	21,369
Arroyo de las Canas	37,462
Arroyo de Alamillo	17,434
Arroyo de la Parida	44,295
San Pedro Arroyo	19,464

bed material yields for each event. The mean annual bed-material sediment yield was estimated using the probability weighting in Equation 6.2. The bed-material sediment-rating curves were developed using the hydraulic data for 28 discharges ranging from 10 cfs to greater than the 100-year event and the average sediment gradation curves for each site (Appendix B).

Bed material transport capacity is a function of hydraulic conditions and the characteristics of the sediment in the arroyo. The MPM-Einstein equation is appropriate when both the bed load and suspended load compose a significant portion of the total bed material load. Because of its formulation as an excess shear stress equation, this equation is well suited to modeling the transport of sand, as well as gravel- and cobble-sized material, and the suspended sediment-transport capacity is estimated using a solution developed by Einstein (1950).

Colby correction factors applied in the calculations were highest at Arroyo de la Parida, where they varied from 1.64 at 100 cfs to 2.00 at 10,500 cfs and were lowest at Arroyo Sevilleta where they had a value of 1.1 for all discharges.

Mussetter Engineering, Inc.
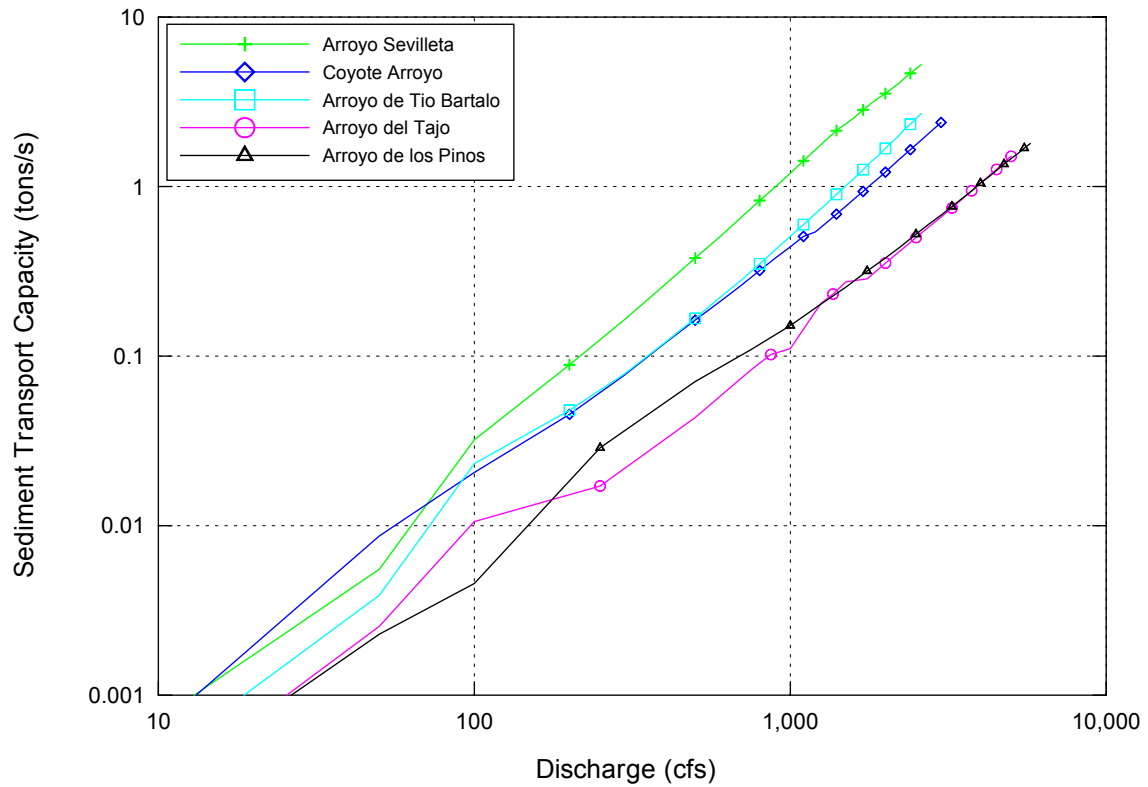
Figure 6.1a. Computed bed-material sediment rating curves with Colby correction factors applied.
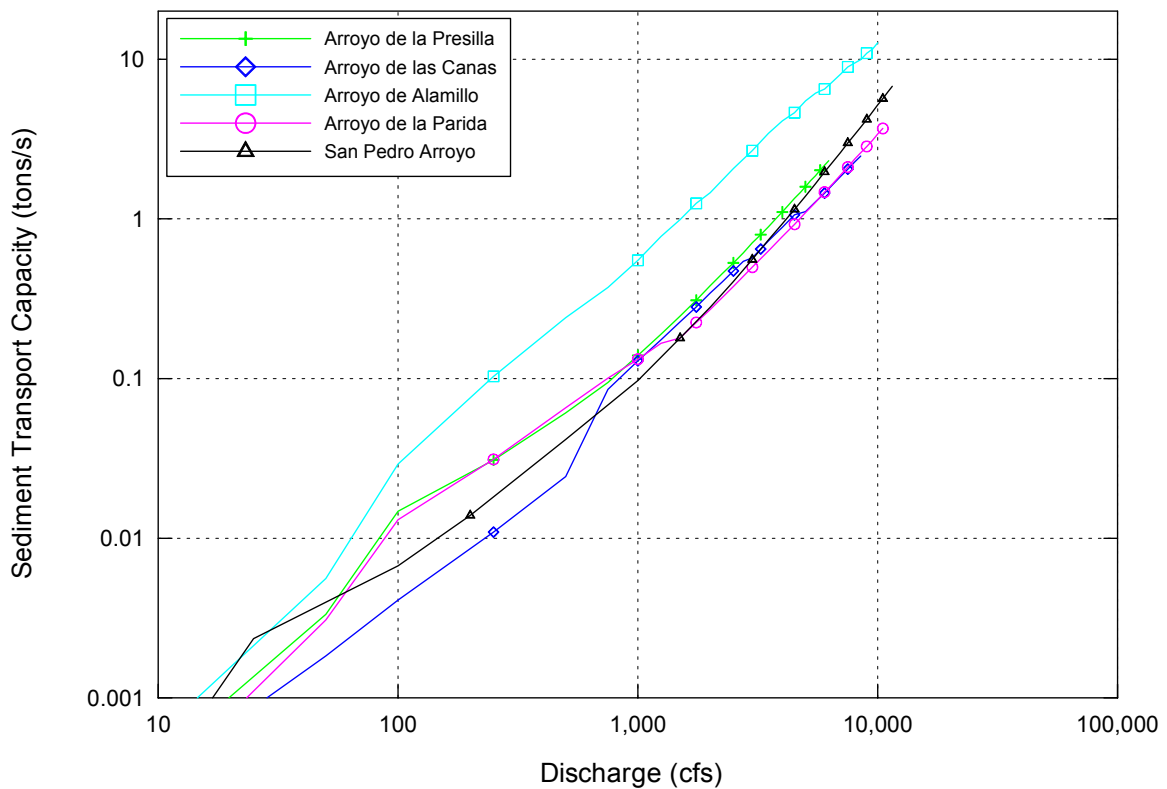
Figure 6.1b. Computed bed-material sediment-rating curves with Colby correction factors applied.

Mussetter Engineering, Inc.

Tables 6.3 and 6.4 summarize the bed material and total sediment yields (wash load and bed-material load) for the 10 basins for the 2- though 100-year recurrence interval events, as well as the mean annual yield. Mean annual bed material yields ranged from 361 tons (Arroyo del Tajo) to 5,933 tons (Arroyo de Alamillo). Mean annual total sediment yields ranged from 886 tons (Arroyo Sevilleta) to 11,362 tons (Arroyo de la Parida).

The ratio of mean annual wash load to bed-material load (**Table 6.5**) ranges from 0.2 (Arroyo Seviletta) to 8.3 (Arroyo de las Canas). Ratio values of less than 1.0 indicate that the bed-load sediment yield contributes more to the total sediment yield than the fine sediment yield. The contribution of bed-load is greater than the wash-load at Arroyo Seviletta and Arroyo de Alamillo. These are the two steepest channels and have the finest bed-material sediment gradations which create the conditions for the highest bed-load transport rates of the 10 study basins.

At Arroyo de las Canas and Arroyo de la Parida, the mean annual wash-load component is 8.3 and 7.9 times higher, respectively, than the bed-material load component. The sediment gradations (Table 3.1) indicate these channels transport the coarsest bed material loads and have lower than average bed-material transport rates and have the lowest mean annual unit sediment yields (**Table 6.6**). Arroyo de las Canas and Arroyo del la Parida have relatively high unit wash-loads compared with the other larger basins because of their relatively steep basins and higher percentage of silt/clay sized material in the fine-sediment yield (Appendix F).

The relationships between total sediment yield and drainage area for each recurrence interval event and the mean annual yield are shown in **Figure 6.2.** The power function best-fit curves show good agreement with the individual values for all events (R^2 >0.92) except the 2-year event.

Table 6.3. Bed-material sediment yield (tons) for the 2-, 5-, 10-, 25-, 50-, and 100-year return interval events and mean annual yield.							
Arroyo	2-year	5-year	10-year	25-year	50-year	100-year	Mean Annual
Arroyo Sevilleta	129	823	1,779	4,161	6,543	8,972	758
Arroyo del Coyote	130	540	1,030	2,089	3,448	4,826	450
Arroyo de Tio Bartolo	155	651	1,228	2,218	3,194	4,362	493
Arroyo del Tajo	90	404	943	1,949	3,042	2,975	361
Arroyo de los Pinos	65	581	1,117	2,295	3,484	5,187	453
Arroyo de la Presilla	161	907	1,601	3,246	4,808	7,128	683
Arroyo de las Canas	71	896	2,312	4,534	7,669	11,196	857
Arroyo de Alamillo	43	6,621	16,426	37,109	56,031	63,523	5,933
Arroyo de la Parida	5	1,767	3,115	6,860	10,571	16,336	1,283
San Pedro Arroyo	3	1,049	2,479	7,472	15,578	31,359	1,412

Table 6.4.	Total yield (tons) for the 2-, 5-, 10-, 25-, 50-, and 100-year return interval events and mean annual yield.						
Arroyo	2-year	5-year	10-year	25-year	50-year	100-year	Mean Annual
Arroyo Sevilleta	185	1,008	2,084	4,684	7,237	9,861	886
Arroyo del Coyote	540	1,809	3,056	5,277	7,647	10,156	1,300
Arroyo de Tio Bartolo	493	1,713	2,954	4,990	6,814	8,825	1,210
Arroyo del Tajo	1,026	4,129	7,466	12,792	17,661	22,173	2,943
Arroyo de los Pinos	954	4,875	8,711	15,323	21,068	28,362	3,408
Arroyo de la Presilla	954	5,010	9,005	16,057	22,188	30,343	3,534
Arroyo de las Canas	1,425	11,156	21,126	38,719	55,129	74,811	7,989
Arroyo de Alamillo	218	13,109	29,611	61,106	89,858	109,514	10,513
Arroyo de la Parida	564	16,113	31,931	59,417	83,941	114,880	11,362
San Pedro Arroyo	93	7,743	16,448	34,922	56,051	89,585	6,483

Table 6.5.	Ratio of wash-load yield to bed-material sediment yields for the 2-, 5-, 10-, 25-, 50-, and 100-year return interval events.						
Arroyo	2-year	5-year	10-year	25-year	50-year	100-year	Mean Annual
Arroyo Sevilleta	0.4	0.2	0.2	0.1	0.1	0.1	0.2
Arroyo del Coyote	3.2	2.4	2.0	1.5	1.2	1.1	1.9
Arroyo de Tio Bartolo	2.2	1.6	1.4	1.2	1.1	1.0	1.5
Arroyo del Tajo	10.3	9.2	6.9	5.6	4.8	6.5	7.2
Arroyo de los Pinos	13.7	7.4	6.8	5.7	5.0	4.5	6.5
Arroyo de la Presilla	4.9	4.5	4.6	3.9	3.6	3.3	4.2
Arroyo de las Canas	19.2	11.5	8.1	7.5	6.2	5.7	8.3
Arroyo de Alamillo	4.1	1.0	0.8	0.6	0.6	0.7	0.8
Arroyo de la Parida	107.0	8.1	9.2	7.7	6.9	6.0	7.9
San Pedro Arroyo	30.7	6.4	5.6	3.7	2.6	1.9	3.6

Table 6.6.	Mean annual unit sediment yield (tons/mi^2).						
Arroyo	Drainage Area (mi^2)	Mean Annual Sediment Yield (tons)			Mean Annual Unit Sediment Yield (tons/mi^2)		
		Wash Load	Bed Load	Total Load	Wash Load	Bed Load	Total Load
Arroyo Sevilleta	2.56	128	758	886	50	296	346
Arroyo de Tio Bartolo	2.59	850	450	1,300	328	173	501
Arroyo del Coyote	3.16	717	493	1,210	227	156	383
Arroyo del Tajo	9.03	2,582	361	2,943	286	40	326
Arroyo de los Pinos	12.10	2,954	453	3,408	244	37	282
Arroyo del la Presilla	15.51	2,852	683	3,534	184	44	228
Arroyo del las Canas	26.31	7,133	857	7,989	271	33	304
Arroyo de Alamillo	40.22	4,580	5,933	10,513	114	148	261
Arroyo del la Parida	42.13	10,079	1,283	11,362	239	30	270
San Pedro Arroyo	47.25	5,071	1,412	6,483	107	30	137

Mussetter Engineering, Inc.
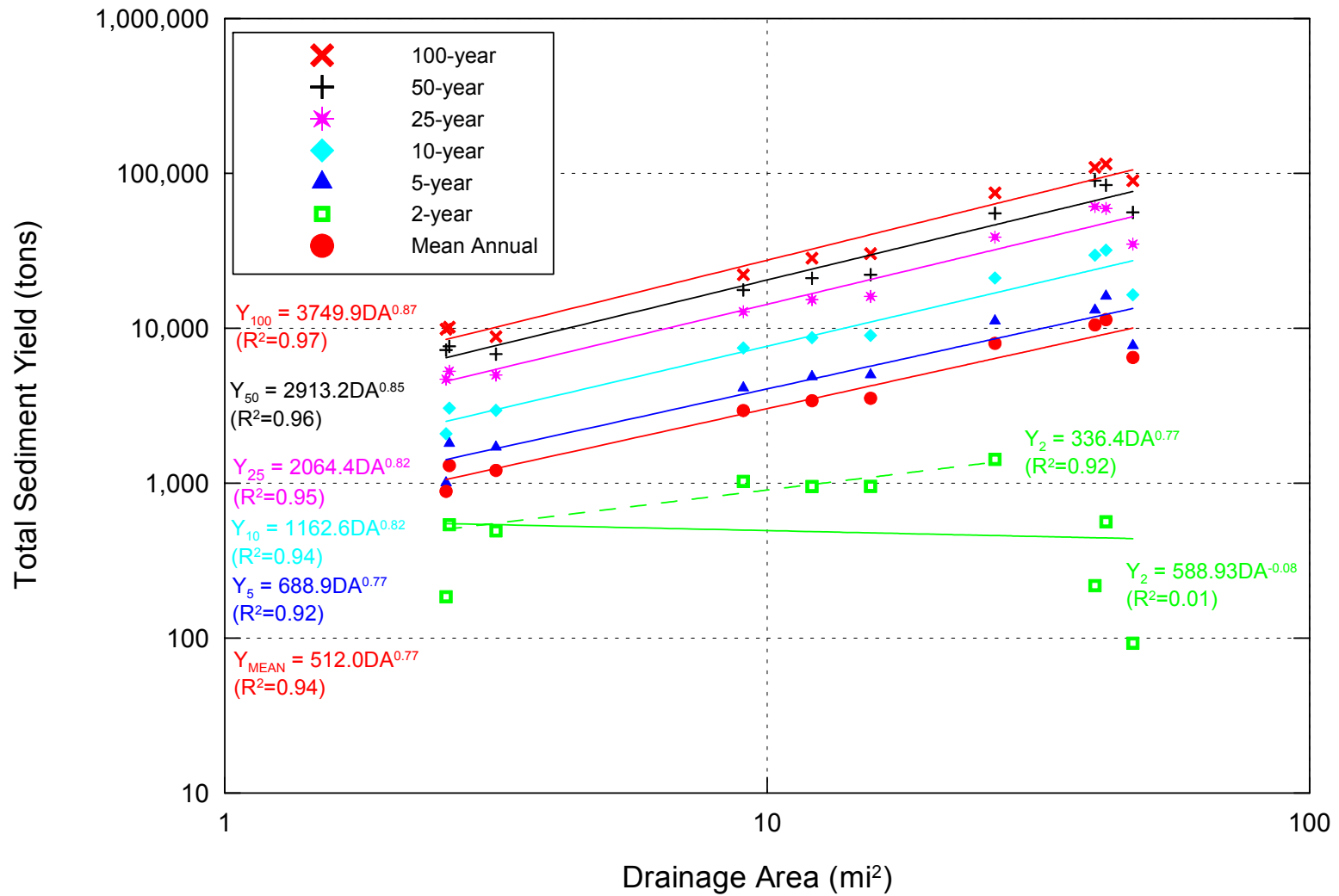
Figure 6.2. Relationship between total sediment yield and drainage area for the 2-, 5-, 10-, 25-, 50-, 100-year events and the mean annual event.

Mussetter Engineering, Inc.

The best-fit curve for the 10 basins for the 2-year event shows a weak relationship between sediment yield and drainage area (R^2 = 0.01) because of the low sediment yields of the three largest basins. There is a good relationship (R^2 = 0.92) between sediment yield and drainage area for the seven smaller study basins (study basins up to 26.3 mi^2). The estimated sediment yields show an inverse relationship between drainage area and mean annual unit sediment yield for the 10 basins (**Figure 6.3**). The relationship is similar in form to those developed by Schumm and Hadley (1961) and Strand (1975), and the strength of the relationship is quite high (R^2 = 0.66).

RTI (1994) also estimated a mean annual unit sediment yield for Arroyo del Coyote, but their estimate was an order of magnitude higher than that shown in Table 6.6. Review of the RTI methodology indicated that their estimate was based on (1) total sediment yield rather than wash-load yield derived from the MUSLE procedure, (2) uniform, but physically improbable infiltration rate assumptions, and (3) double counting of the bed-material load due to the use of both the MPM-Einstein equation and the Zeller-Fullerton equation.

6.4.   Sediment Delivery

The decline in unit sediment yield with increase in basin size has been recognized in numerous studies (Schumm and Hadley, 1961; Strand, 1975; Schumm, 1977), and has been encapsulated in the concept of the sediment delivery ratio (SDR). SDR is the ratio between annual sediment yield of a watershed and the annual gross erosion, with values reported in the literature between 1 and about 0.1 (Boyce, 1975; Walling, 1983; Maidment, 1992). The inverse relationship between SDR and the size of the basin has been attributed to the increased availability of potential sediment storage sites as drainage basins increase in size (Schumm, 1977). However, as pointed out by Graf (1988), in the long-term, the delivery ratio concept is untenable because all long-term delivery ratios must approximate 1, or the channels in the basin would be progressively aggrading. Therefore, a temporal component must be addressed in the context of sediment delivery from drainage basins. In arid and semi-arid regions where unit sediment yields are highest (Langbein and Schumm, 1959), sediment eroded from the hillslopes tends to be stored on the valley floors until it is episodically removed by channel incision when slope thresholds are exceeded (Schumm and Hadley, 1957; Schumm, 1968; Patton and Schumm, 1975; Schumm, 1977). Sediment delivery ratios in the arid and semi-arid areas can, therefore, range from 0 to >1, depending on whether the channel system in the drainage basin is storing sediment or is incising and exporting previously stored sediment from the basin (Gellis et al., 1991).

In the context of the 10 tributaries that are the subject of this investigation, the estimated total sediment yield is positively correlated with the drainage basin size for the various return period events and for the mean annual yield (Figure 6.2). The estimated mean annual unit sediment yield is, however, inversely correlated with drainage basin size (Figure 6.3). The amount of sediment that is actually delivered to the Rio Grande from the individual basins (i.e. the delivery ratio) has changed through time. Variation in the delivery ratio can be due to a number of factors, including whether the tributary channel is incised, and whether the tributary channel is physically integrated with the river. The 1935 aerial photography (Chapter 2) indicates that delivery ratios were probably very low (<0.2) for Arroyo Sevilleta, Arroyo del Coyote, and Arroyo San Pedro because the arroyos were not directly connected to the Rio Grande. In contrast, it appears from the 1935 photography that Arroyo de Alamillo, Arroyo de la Parida, Arroyo de los Pinos, and Arroyo de la Presilla were directly connected to the Rio Grande and, therefore, probably had delivery ratios that ranged from about 0.5 to 1.0, since alluvial fans were present at their mouths. The 1935 photography suggests that Arroyo de Tio Bartolo and Arroyo de las

Mussetter Engineering, Inc.
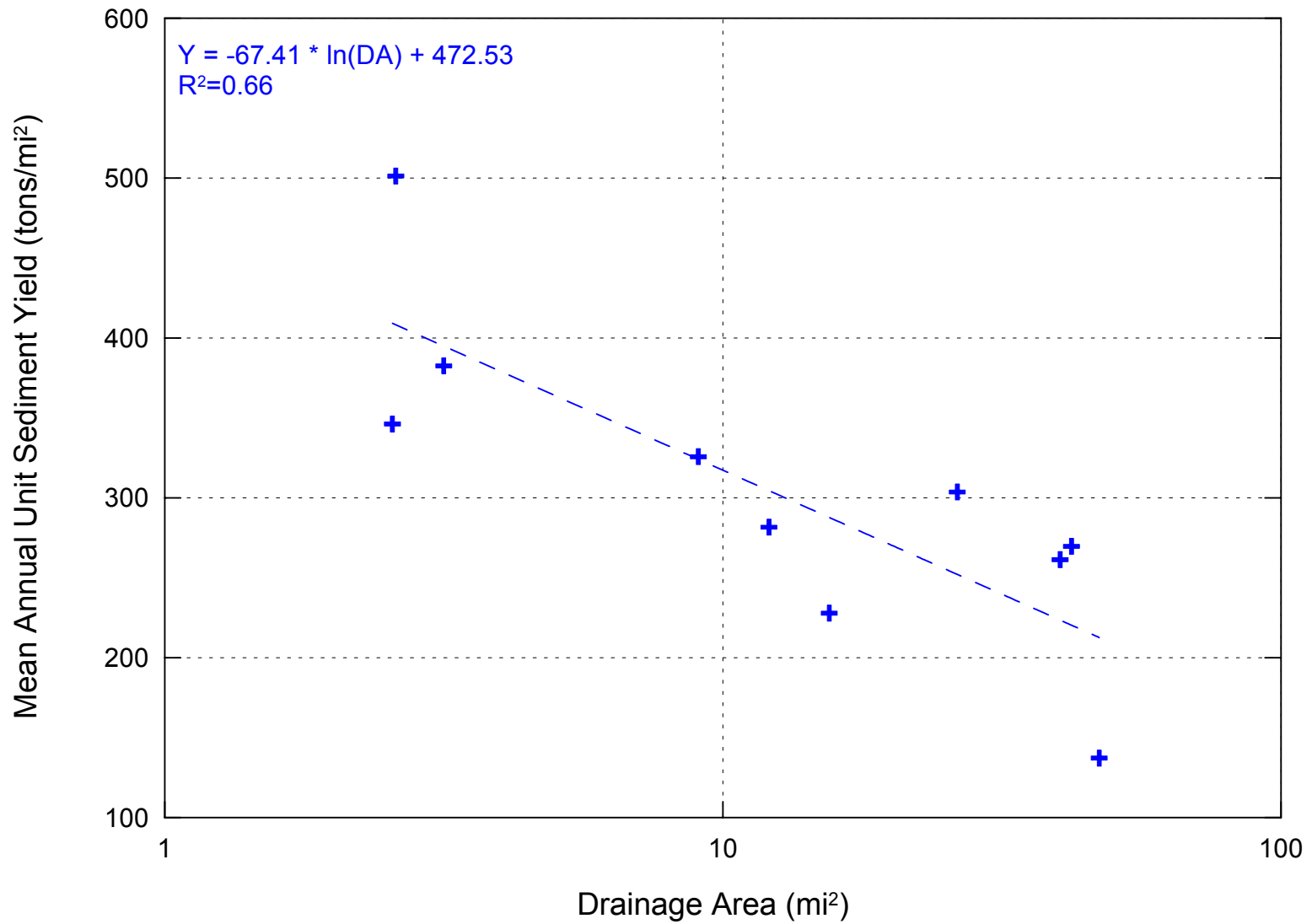
Figure 6.3.   Relationship between drainage area and mean annual unit sediment yield for the 10 basins.

Canas were both directly connected to the Rio Grande and incised, which suggests that the delivery ratios were probably higher than 1 at that time.

Under current conditions, the delivery ratios for Arroyo Sevilleta, Arroyo del Coyote and Arroyo San Pedro are still very low, and may in fact be lower than they were in 1935 because of the presence of very dense stands of tamarisk and other non-native species on the former floodplain of the Rio Grande. In this context, the two smallest basins in the study, with drainage areas of about 3 mi^2, have about the same delivery ratio as the largest basin in the study (about 47 mi^2), and it is very probable that little of the estimated sediment yield in the 3 basins is actually delivered to the Rio Grande.

Because of channelization-induced degradation of the Rio Grande since the 1950s, the base level for both Arroyo de Alamillo and Arroyo de la Parida has been lowered, and in response to the baselevel lowering, the arroyos have incised. Because of the incision, sediment delivery ratios for these two arroyos probably equal 1, and therefore, on a mean annual basis, these basins probably each deliver the estimated approximately 11,000 tons (Table 6.6) to the Rio Grande. Channelization of the lower reaches of Arroyo de los Pinos has integrated the tributary with the Rio Grande, and has caused some degradation of the lower reaches of the arroyo. However, there is significant sediment deposition taking place in the channel upstream of the channelized reach, and as a result, the sediment delivery ratio is probably about 0.5. If the SDR value is correct this means that the mean annual sediment yield from this basin is about 1,700 tons (Table 6.6).

The lower reaches of Arroyo de Tio Bartolo are not incised, and it appears that vegetation clearing on the distal end of the modern fan has integrated the basin with the Rio Grande. Because the basin is small (2.6 mi^2) and the channel is integrated with the Rio Grande, the SDR is probably moderately high (> 0.5), and the mean annual sediment yield to the Rio Grande is probably on the order of 600 tons (Table 6.6). The lower reaches of Arroyo de la Presilla are not incised and the modern fan is prograding out onto the floodplain of the Rio Grande. The SDR is probably moderately high (>0.5) because the basin is medium sized (about 15 mi^2) and integrated with the Rio Grande. The mean annual sediment yield to the Rio Grande is probably on the order of 1,700 tons (Table 6.6.). Until very recently when the dense vegetation on the fan was removed, SDR at Arroyo del Tajo was probably very low. A relatively large alluvial fan has formed where the arroyo prograded out onto the floodplain of the Rio Grande, and the distal margin of the fan is now being incised. Incision into the fan will increase the SDR to >1, and therefore in the future, the mean annual sediment yield from this relatively small (9 mi^2) basin will probably exceed the estimated yield of about 3,000 tons (Table 6.6).

Although Arroyo de las Canas was incised in 1935, there is little evidence that the arroyo is still in a degradational mode. However, it does appear that the arroyo is still widening in response to the earlier incision (Schumm et al., 1984; Harvey and Watson, 1986). The arroyo is integrated with the Rio Grande, and therefore, the SDR is likely to be at least 1, if not higher. The mean annual sediment yield from this arroyo is, therefore, likely to be at least 8,000 tons (Table 6.6).

Based on the estimates of the mean annual sediment yield alone, the 10 tributary basins could deliver about 50,000 tons per year of sediment to the Rio Grande. However, when other factors such as basin size, integration with the river and arroyo incision, are taken into account the mean annual sediment yield is more likely to be on the order of 37,000 tons. Based on the wash-load to bed-material load ratios presented in Table 6.5, an average value for the mean annual unit bed-material load is about 20 percent of the total load. Application of this ratio to the total load of 37,000 tons indicates that the mean annual bed-material yield from the 10

Mussetter Engineering, Inc.

tributaries is about 7, 400 tons. This value is about 5 percent of the combined annual bed-material yield from the Rio Puerco and Rio Salado (MEI, 2004).

6.5.   Projected Sediment Yields

Along the east side of the Rio Grande between Bernardo and San Antonio are 12 drainage basins that were not selected for direct analysis for a variety of reasons including accessibility, but they all have the potential to deliver sediment to the Rio Grande (**Figure 6.4**). Four of the basins are located downstream of San Acacia and the remainder (8) are located upstream of San Acacia. Estimates of the sediment yields for the 2-, 5-, 10-, 25-, 50-, and 100-year return period events and the mean annual sediment yield were developed for each of the basins using the regression equations on Figure 6.2 (**Table 6.7**). Because of the sizes of the two largest basins and the uncertainty associated with estimating sediment yields for the 2-year event at drainage basin areas in excess of 26 mi^2, 2-year estimates were not developed for these two arroyos. The areas of these two basins (Arroyo los Alamos at 59.8 mi^2, and Salas Arroyo at 63.9 mi^2) are larger than those encompassed in the 10 study basins (Arroyo San Pedro is the largest with an area of 47.3 mi^2), and therefore, strictly speaking the regression relations are being extrapolated beyond the database from which they were created.

Table 6.7.   Estimate of sediment yields for 12 unsurveyed basins for the 2-, 5-, 10-, 25-, 50-, and 100-year period events and average annual event (tons).

Basin	Area (mi^2)	Recurrence Interval (years)						Average Annual
		2	5	10	25	50	100	
Canoncito Colorado	1.79	528	1,080	1,877	3,334	4,788	6,235	803
Bernardo Arroyo	1.81	530	1,086	1,888	3,352	4,815	6,271	807
Canada Ancha	4.52	1,074	2,200	4,004	7,110	10,497	13,926	1,635
Poecual Arroyo	5.01	1,163	2,382	4,357	7,736	11,457	15,231	1,770
Unnamed-2	5.39	1,230	2,519	4,625	8,212	12,188	16,226	1,872
Arroyo Rosa de Castillo	5.52	1,254	2,567	4,719	8,380	12,448	16,580	1,908
Arroyo del Veranito	5.75	1,293	2,648	4,877	8,659	12,877	17,166	1,968
Unnamed-3	6.12	1,358	2,780	5,137	9,121	13,590	18,139	2,066
Unnamed-1	6.34	1,395	2,857	5,288	9,389	14,004	18,705	2,123
Maes Arroyo	10.91	2,118	4,338	8,250	14,649	22,209	29,987	3,224
Arroyo los Alamos	59.81	nc	16,079	33,295	59,122	94,325	131,769	11,950
Salas Arroyo	63.85	nc	16,909	35,129	62,377	99,714	139,479	12,567

nc (not computed)

Mussetter **E**ngineering, Inc.
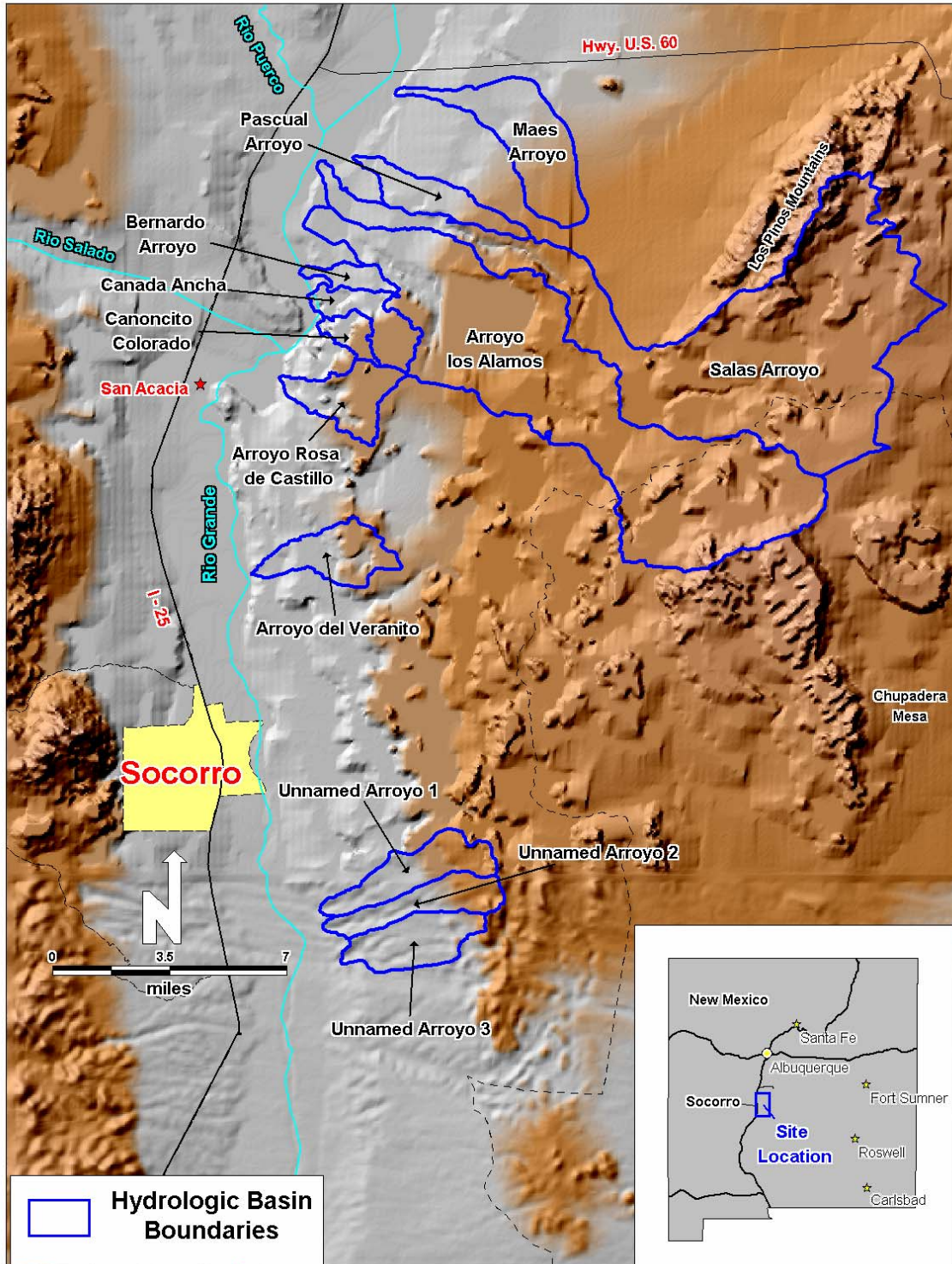
Figure 6.4.   Map showing the locations of the 12 unsurveyed drainage basins to which the developed sediment yield equations were applied.

Mussetter Engineering, Inc.

On a mean annual basis, the additional 12 basins could potentially deliver about 42,690 tons of sediment to the Rio Grande. However, based on review of recent aerial photographs it is apparent that the SDR values for the individual basins are variable. Very little, if any, sediment is being delivered to the Rio Grande from Bernardo Arroyo, Canoncito Colorado, Poecual Arroyo, and Unnamed 1, 2, 3 Arroyos. The SDR values for Arroyo del Veranito and Arroyo Rosa de Castillo are about 0.3 since they are not fully integrated with the Rio Grande and fans are building on the Rio Grande floodplain. Canada Ancha is directly connected to the Rio Grande, but a fan is also building near its mouth, so the SDR value is probably on the order of 0.5. Maes Arroyo, Arroyo los Alamos and Salas Arroyo are directly connected to the Rio Grande and the lower reaches of the arroyos have been channelized, and therefore, the SDR values are probably about 1. Application of the SDR estimates result in a mean annual sediment yield from the 12 basins of about 36,300 tons, which is about 85 percent of the estimated total. The bed-material load is about 7,300 tons per year.

In combination, the estimated and projected mean annual sediment yield for the 22 basins along the east side of the Rio Grande between the Rio Puerco confluence and San Antonio is about 73,300 tons, of which about 14, 700 tons is bed material.

6.6.   Contribution of Tributaries to Sediment Budget for San Acacia Reach

A sediment-continuity analysis was performed to develop a sediment budget for the URGWOPS EIS alternatives analysis (MEI, 2004). The continuity analysis was performed with estimates of the annual bed-material load. Based on the results of this analysis, the annual inflowing bed-material load upstream of the Rio Puerco confluence is about 287,000 tons. In combination, the inflowing annual bed-material loads from the Rio Puerco and Rio Salado is about 136,000 tons, and the inflowing annual bed-material load from the eastside tributaries between Bernardo and San Acacia is about 3,500 tons, or about 2.6 percent. The combined upstream annual inflow of bed-material load at San Acacia is about 420,000 tons. The combined annual bed-material yield from the 14 eastside tributaries between San Acacia and San Antonio is about 8,200 tons, which represents approximately 2 percent of the inflowing load a San Acacia. Downstream of San Antonio, there is effectively no tributary sediment inflow to the Rio Grande.

Mussetter Engineering, Inc.

7.   SUMMARY AND CONCLUSIONS

7.1.   Summary

A comprehensive sediment-transport model of the Middle Rio Grande (MRG) from Cochiti Dam to Elephant Butte Reservoir is needed to aid in understanding the sediment-transport dynamics of the river. The first phase of the modeling will likely consider the reach between the San Acacia Diversion Dam and Elephant Butte Reservoir (San Acacia Reach). The sediment-transport model of this reach will depend on quantification of both the sediment inflow from upstream and from tributaries within the reach. The primary goal of this study was to develop estimates of the tributary sediment inflow from the ungaged eastside tributaries located between Bernardo and Elephant Butte Reservoir.

In order to develop a sediment-mass balance of the San Acacia reach, it is necessary to quantify the sediment inflow from upstream of San Acacia and from the tributaries within the reach. Quantification of the sediment inflow from upstream of San Acacia can be achieved by combining information from the Bernardo, Rio Puerco, and Rio Salado gages, and the ungaged tributaries between the Bernardo gage at US 60 bridge and San Acacia. To date there has been no quantification of sediment input from ungaged tributaries between the Bernardo gage and San Acacia, nor from ungaged tributaries within the San Acacia reach.

The specific objectives of this study, which was conducted by Mussetter Engineering, Inc. (MEI) for the New Mexico Interstate Stream Commission (NMISC), were to develop single event and mean annual estimates of ungaged tributary sediment delivery to the MRG between Bernardo and Elephant Butte Reservoir. With the exception of Brown Arroyo, the west side tributaries to the MRG have been truncated by the Low Flow Conveyance Channel (LFCC) and the west bank levee, and sediment delivery to the Rio Grande has been essentially eliminated. Therefore, this study involved field data collection (sediment sampling and topographic surveys of the channels) and hydrologic and hydraulic analyses of ten drainage basins, ranging in size between 2.6 and 47.3 square miles. The high frequency of tributaries on the east side of the river is geologically controlled, and the tributary basins drain the southern extension of the Los Pinos Mountains and the Chupadera Mesa (MEI, 2002). Since flow in all of the tributary basins is ephemeral, and ungaged, an HEC-HMS hydrologic model was developed for each of the basins to provide hydrographs at the downstream boundaries of the basins for the 2-, 5-, 10-, 25-, 50- and 100-year recurrence interval events. Topographic surveys of a representative reach of each channel near the downstream boundary of the basin were conducted for the purpose of developing one-dimensional normal-depth HEC-RAS hydraulic models. Output from the individual basin models was used to develop estimates of total sediment yields for the 2-, 5-, 10-, 25-, 50- and 100-year recurrence interval events, as well as the mean annual sediment yield. The wash-load fraction of the sediment yield for each basin was developed using the MUSLE equation. The bed-material fraction of the sediment yield was estimated using the MPM-Einstein equation. Field reconnaissance of the lower reaches of the arroyos determined the degree of integration of the arroyos and the Rio Grande, and this information was used to develop estimates of the sediment delivery ratio for each basin.

Results obtained for the 10 basins were used to develop regression relations between basin drainage area and sediment yield for the 2-, 5-, 10-, 25-, 50- and 100-year return period events, as well as for the mean annual sediment yield (Figure 6.2). Coefficients of determination (R^2) for the 5-, 10-, 25-, 50-, and 100-year return period events and the mean annual yield regression relations are high (>0.9). However, the R^2 value for the 2-year event is very low

(0.01) when all 10 basins are included in the regression. If the three largest basins are removed from the data set (drainage areas > 40 mi^2), the R^2 value increases to 0.9. The data suggest, therefore, that, for basins larger than 26 mi^2, there is very little runoff during the 2-year storm, and this, therefore, translates into very low sediment yields for the 2-year return period event.

Mean annual unit sediment yields from the 10 basins are inversely related to basin size (Figure 6.3), and this finding is similar to that reported by other investigators (Schumm and Hadley, 1961; Strand, 1975). Values determined from this investigation are about an order of magnitude lower than those determined by RTI (1994) for a basin that was common to both studies. The differences are due in part to the way the MUSLE calculations were done by RTI, differences in assumptions on infiltration rates used in the hydrologic modeling, and an overestimation of the bed-material load. Comparison of the methods and assumptions used in the two investigations indicates that the lower values derived from this study are more realistic and supportable. On average, the unit bed-material load for the basins represents about 20 percent of the total unit sediment load (Table 6.6).

Sediment delivery ratios (SDR) were estimated on the basis of the inverse relationship between SDR and basin size (Boyce, 1975; Schumm, 1977), the degree of integration of the arroyo and the Rio Grande, and the aggradational or degradational status of the lower reaches of the arroyos. SDR values were assumed to vary from about 0.2 where the arroyos were not directly connected to the river to >1 where the arroyo was both connected to the river and was incised or actively widening as a result of previous incision. The SDR values were applied to the estimated mean annual sediment yields for the individual arroyos to provide an estimate of the amount of sediment actually delivered to the river on an annual basis. About 75 percent (37,000 tons) of the estimated annual total sediment yield for the 10 arroyos (50,000 tons) is probably delivered to the Rio Grande, and about 7,400 tons is composed of bed material. Comparison of conditions at the mouths of the arroyos in 1935 with present conditions indicates that SDR values have changed with time, both as a result of the presence of increased non-native vegetation and channelization-induced baselevel lowering for the tributaries.

The regression relations developed for the 10 basins were applied to a further 12 basins of similar size that drain areas of similar lithology and topography between Bernardo and San Antonio. Application of estimated SDR values to the resulting mean annual values (Table 6.7) produced an estimated delivery of about 36,300 tons per year, of which about 7,300 tons are composed of the bed material. In combination, the mean annual sediment yield for the 22 basins along the east side of the Rio Grande between Bernardo and San Antonio is about 73,300 tons, and about 14,700 tons is bed material.

The eastside tributaries between Bernardo and San Acacia deliver about 3,500 tons of bed material to the Rio Grande on an annual basis, and this represents about 2.6 percent of the combined annual bed-material load from the Rio Puerco and Rio Salado (136,000 tons), MEI, 2004). The combined upstream inflows of the bed material to San Acacia is on the order of 420,000 tons per year (MEI, 2004). The eastside tributaries between San Acacia and San Antonio deliver about 8,200 tons of bed material per year, and this represents approximately 2 percent of the inflowing load at San Acacia. The preceding discussion has focused on the mean annual bed-material sediment yield, since it is the bed material that has the greatest influence on the channel morphologic characteristics (Schumm, 1977). The bed material represents about 20 percent of the total sediment yield, and the remaining 80 percent of the total yield is composed of silts and clay-size particles that have little direct effect on channel morphology. However, deposition of cohesive silts and clay on sandbars in the San Acacia reach appears to be important with respect to stabilizing the bars and encouraging growth of riparian vegetation (MEI, 2002), which indirectly affects the channel morphology.

Mussetter Engineering, Inc.

Emphasis has been placed on the mean annual sediment yields because of the need to place the tributary sediment yields in the context of the sediment mass balance that was conducted for the URGWOPS EIS alternatives evaluation (MEI, 2004). However, in arid and semi-arid region arroyos, the use of mean annual estimates does not represent the true sediment dynamics because of the episodic nature of flow and sediment-transporting events (Graff, 1988). The data in Table 6.3 (bed-material yield) and Table 6.4 (total yield) demonstrate that the single-event sediment yields from the modeled tributaries are likely to deliver significantly larger amounts of sediment to the MRG. Because of the limited spatial distribution of thunderstorms that are likely to produce sediment-transporting events in the tributaries, the effects of the storm events are generally local. In other words, a large magnitude, but infrequent event, in the tributaries is likely to have spatially limited local effect on the MRG. The longer-term legacy of large infrequent events is the accumulation of coarser sediments in the bed of the Rio Grande at the tributary confluence.

7.2.   Conclusions

The analyses that were conducted for this investigation of sediment yields from ungaged tributaries on the east side of the Rio Grande between Bernardo and Elephant Butte Reservoir enabled the following to be concluded:

1. With the exception of the 2-year event in drainage basins larger than 26 mi^2, where there is little runoff from the 2-year storm, drainage basin area can be used to predict the total sediment yields for the 5-, 10-, 25-, 50-, and 100-year return period events (Figure 6.3), as well as the mean annual sediment yield with a reasonable degree of confidence ($R^2 > 0.9$).

2. Unit sediment yields are inversely related to drainage basin area, as is the sediment delivery ratio. However, sediment delivery ratios for the individual basins are determined not only by the size of the basin, but also by whether the channel is integrated with the Rio Grande and whether the channel is incised or widening. SDR values at any given time can range from 0 to >1.

3. Application of estimated SDR values to the computed estimates of sediment yield from the 10 basins involved in the study reduced the mean annual sediment delivery estimate to the Rio Grande from 50,000 to 37,000 tons. About 20 percent (7,400 tons) of the total yield is composed of bed material.

4. Regression equations developed from the 10 studied basins were used to develop estimates of sediment yield for the 2-, 5-, 10-, 25-, 50-, and 100-year return period events, and the mean annual yield for 12 other basins that have the potential to deliver sediment to the Rio Grande.

5. The combined estimated mean annual total sediment yield from the 22 eastside tributaries is on the order of 92,700 tons. However, when SDR values are applied to the individual basin yields, the more likely yield of sediment to the Rio Grande from the 22 tributaries is about 73,300 tons per year. This represents a mean annual bed-material yield of about 14,700 tons.

6. Approximately 20 percent of the total sediment yield from the tributaries is composed of bed-material load that is primarily responsible for morphologic characteristics of the MRG.

Mussetter Engineering, Inc.

7. The eastside tributaries between Bernardo and San Acacia deliver a mean annual bed-material yield of about 3,500 tons, which represents about 2.6 percent of the combined mean annual bed-material yield of the Rio Puerco and Rio Salado (136,000 tons).

8. The eastside tributaries between San Acacia and San Antonio deliver a mean annual bed-material yield of about 8,200 tons, which represents about 2 percent of the total inflowing bed-material load at San Acacia (420,000 tons).

9. The coarsest sediments moved by infrequent large-magnitude events on the tributaries create local areas of gravel, cobble, and boulder accumulations in the bed of the MRG at the tributary confluences. The coarser sections of the riverbed probably behave as local grade controls in the incised reach of the MRG between San Acacia and San Antonio.

Mussetter Engineering, Inc.

8.   REFERENCES

Albuquerque Metropolitan Arroyo Flood Control Authority, 1993. Section 22.2, Hydrology of the Development Process Manual, Volume 2, Design Criteria. Prepared for the City of Albuquerque, New Mexico, in cooperation with Bernalillo County, New Mexico and AMAFCA, January.

Barnes, H.H., 1967. Roughness characteristics of natural channels. U.S. Geological Survey Water-Supply Paper 1849.

Belcher, R.C., 1975. The geomorphic evolution of the Rio Grande. Baylor Geologic Studies, Bulletin no. 29, Baylor University, Waco, Texas, 64 p.

Bennison, A.P., 1990. Southern Rocky Mountain Region, Utah, Colorado, Arizona, New Mexico geological highway map. U.S. Geological Highway Map Series, Map Number 2.

BOSS International, 2002. Watershed Modeling System. Version 7.0.

Boyce, R.C., 1975. Sediment routing with sediment delivery ratios. Agr. Res. Service, ARS-S-40, pp. 61-65.

Chow, V.T., 1959. Open Channel Hydraulics. McGraw-Hill Book Co., New York, 680 p.

Chronic, H., 1987. Roadside Geology of New Mexico. Mountain Press Publishing Company, Missoula, Montana, 255 p.

Copeland, R.R., 1995. Albuquerque Arroyos Sedimentation Study: Numerical Model Investigation. Prepared for the U.S. Army Corps of Engineers, Albuquerque District, Technical Report HL-95-2, March.

Crawford, C.S., Cully, A.C., Leutheuser, R., Sifuentes, M.S., White, L.H., and Wilber, J.P., 1993. Middle Rio Grande Ecosystem: Bosque Biological Management Plan. Middle Rio Grande Biological Interagency Team, October.

Einstein, H.A., 1950. The bed-load function for sediment transportation in open channel flows. U.S. Department of Agriculture, Soil Conservation Service, Technical Bulletin No. 1026, 69 p.

Gellis, A., Hereford, R., Schumm, S.A., and Hayes, B.R., 1991. Channel Evolution and Hydrologic Variations in the Colorado River Basin: Factors Influencing Sediment and Salt Loads. Journal of Hydrology, v. 124, pp. 317-344.

Graf, W.L., 1988. Fluvial processes in dryland rivers. Berlin, Springer-Verlag.

Grauch, V.J.S., 2001. High-resolution aeromagnetic data, a new tool for mapping intrabasin faults: Examples from the Albuquerque basin, New Mexico. Geology, v. 29, p. 367-370.

Harvey, M.D. and Watson, C.C., 1986. Fluvial processes and morphological thresholds in incised channel restoration. Water Resources Bulletin, v. 22, no. 3, p. 359-368. Reprinted in Engineering Considerations in Small Stream Management, W.L. Jackson (ed.), AWRA Monograph Series, No. 5.

Hicks, D.M. and Mason, P.D., 1991. Roughness Characteristics of New Zealand Rivers. Water Resources Survey, DSIR Marine and Freshwater, Wellington, New Zealand.

Kelley, V.C., 1977. Geology of Albuquerque Basin, New Mexico. New Mexico Bureau of Mines and Mineral Resources, Mem. 33, p. 59.

Mussetter Engineering, Inc.

Langbein, W.B. and Schumm, S.A., 1959.   Yield of sediment in relation to mean annual precipitation: Am. Geophys, Union Trans., v. 39, p. 1076-1084.

Maidment, D. R., 1992. Handbook of Hydrology. McGraw-Hill, Inc., New York, NY.

Mussetter Engineering, Inc., 1996. Calabacillas Arroyo Prudent Line Study and Related Work: Hydraulic Capacity and Stability Analysis for Levees Between Coors Road and the Rio Grande. Prepared for Albuquerque Metropolitan Arroyo Flood Control Authority, April.

Mussetter Engineering, Inc., 2002.   Geomorphic And Sedimentologic Investigations of the Middle Rio Grande Between Cochiti Dam and Elephant Butte Reservoir. Prepared for the New Mexico Interstate Stream Commission, Albuquerque, New Mexico, June.

Mussetter Engineering, Inc., 2004. Sediment Continuity Analysis of the Rio Grande, Cochiti Dam to Elephant Butte Reservoir, prepared for the River Morphology, Sedimentation and River Mechanics Technical Team, URGWOPS Review, June

Patton, P.C. and Schumm, S.A., 1975.   Gully Erosion, Northern Colorado.   A Threshold Phenomenon: Geology, v. 3, pp. 88-90.

Resource Consultants & Engineers, Inc. 1994.   "Prudent Line Analysis, La Cueva Arroyo Tributary between Tennyson Street and Modesto Avenue," prepared for Albuquerque Metropolitan Arroyo Flood Control Authority, New Mexico.

Resource Technology, Inc., 1994.   Analysis of possible channel improvements to the Rio Grande from Albuquerque to Elephant Butte Lake, Phase IA, Sediment Yield Analysis from the Rio Grande Tributary Basins. Prepared for the U.S. Army Corps of Engineers, Albuquerque District, January.

Schumm, S. A. 1977. *The Fluvial System*, Wiley, New York.

Schumm, S.A., 1968.   Speculations concerning paleohydrologic controls of terrestrial sedimentation: Geol. Soc. America Bull, v. 79, p. 1572-1588.

Schumm, S.A. and Hadley, R.F., 1957. Arroyos and the Semiarid Cycle of Erosion. American Journal of Science, v. 255, pp. 161-174.

Schumm, S.A., and Hadley, R.F., 1961. Progress in the application of landform analysis in studies of semiarid erosion: U.S. Geol. Survey Circ. 437, 14 p.

Schumm, S.A., Harvey, M.D. and Watson, C.C., 1984. Incised Channels: Morphology dynamics and control: Water Resources Pub., Littleton, CO. 200 p.

Soil Conservation Service, 1988.   Soil Survey of Socorro County Area, New Mexico. A57.38.SO1. pp. 306-316.

Scurlock, D., 1998, From the Rio to the Sierra: An environmental history of the Middle Rio Grande Basin. USDA, Forest Service, Rocky Mountain Research Station, Fort Collins, Colorado, General Technical Report RMRS-GTR-5.

Smith, G.A., McIntosh, W., and Kuhle, A.J., 2001. Sedimentologic and geomorphic evidence for seesaw subsidence of the Santo Domingo accommodation-zone basin, Rio Grande Rift, New Mexico. Geol. Soc. America, v. 113, p. 561-574.

Strand, R.I., 1975.   Bureau of Reclamation procedures for predicting sediment yield. Agricultural Research Service, ARS-S-40, pp. 10-15.

Thomas, B.E., Hjalmarson, H.W., and Waltemeyer, S.D., 1997.   Methods for estimating magnitude and frequency of floods in the Southwestern United States. U.S. Geological Survey Open-File Report 93-419, 211 p.

Mussetter Engineering, Inc.

U.S. Army Corps of Engineers, 2002. HEC-HMS, Hydrologic Modeling System. Hydrologic Engineering Center, User's Manual, CPD-74C, Davis California, December.

U.S. Army Corps of Engineers, 2002. HEC-RAS, River Analysis System, Hydrologic Engineering Center, User's Manual, Davis California, Version 3.1, CPD-68.

U.S. Army Corps of Engineers. 1990. HEC-2, Water Surface Profiles, Version 4.6.0, Hydrologic Engineering Center, Davis, California.

U.S. Department of Commerce, National Oceanic and Atmospheric Administration, National Weather Service, NOAA, 1994. Technical Memorandum NWS HYDRO-40, Depth-Area rations in the Semi-Arid Southwest United States, Silver Spring, Maryland, August, Figure 14.

*M*ussetter *E*ngineering, *I*nc.

Mussetter Engineering, Inc.

APPENDIX A
Topographic Maps of the Tributary Basins

Figure A.1.   Watershed delineation of Arroyo Sevilleta used in the HEC-HMS hydrologic model.

Mussetter Engineering, Inc.

Figure A.2.   Watershed delineation of Arroyo de Tio Bartolo used in the HEC-HMS hydrologic model.

Mussetter Engineering, Inc.
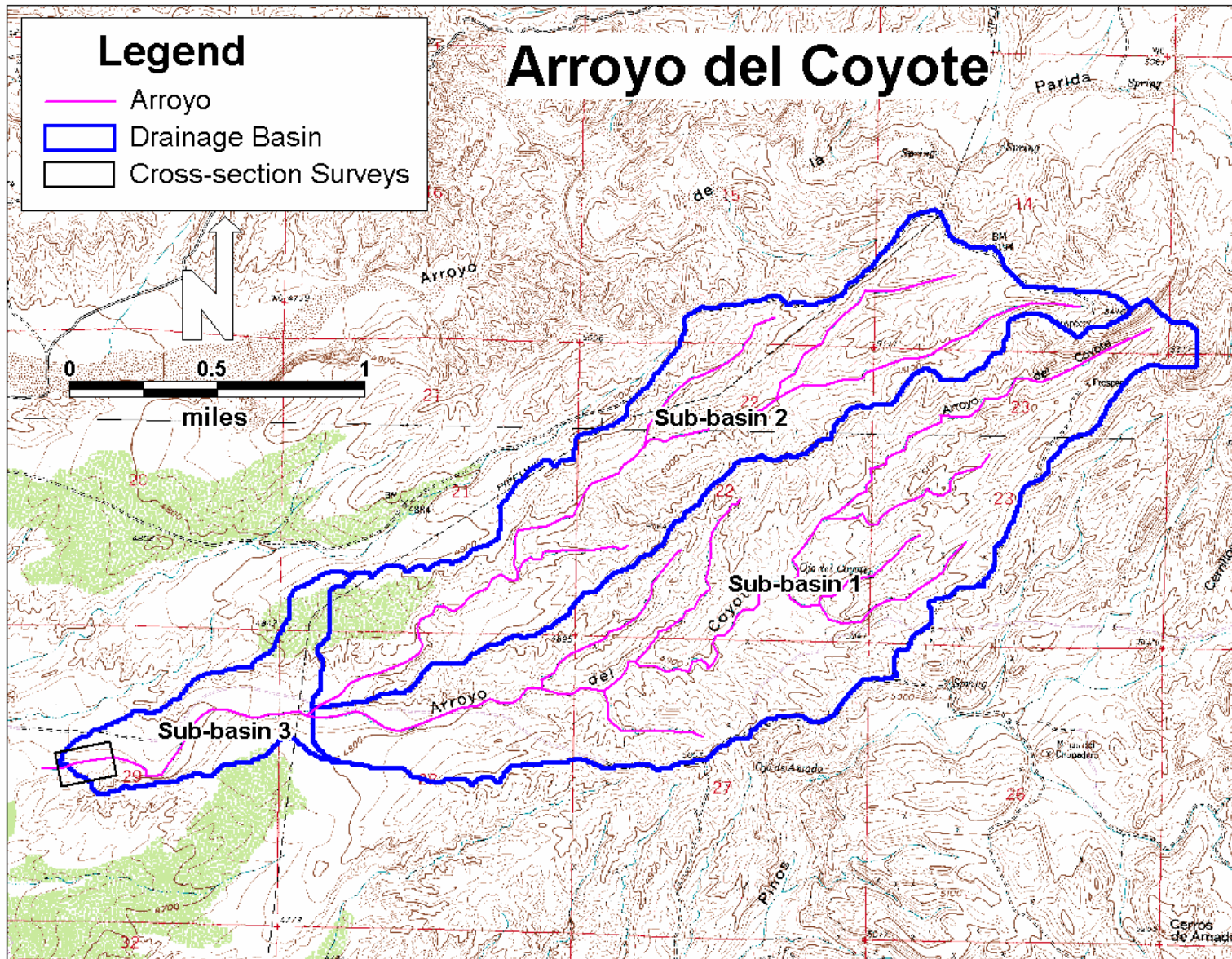
Figure A.3.   Watershed delineation of Arroyo del Coyote used in the HEC-HMS hydrologic model.

Mussetter Engineering, Inc.
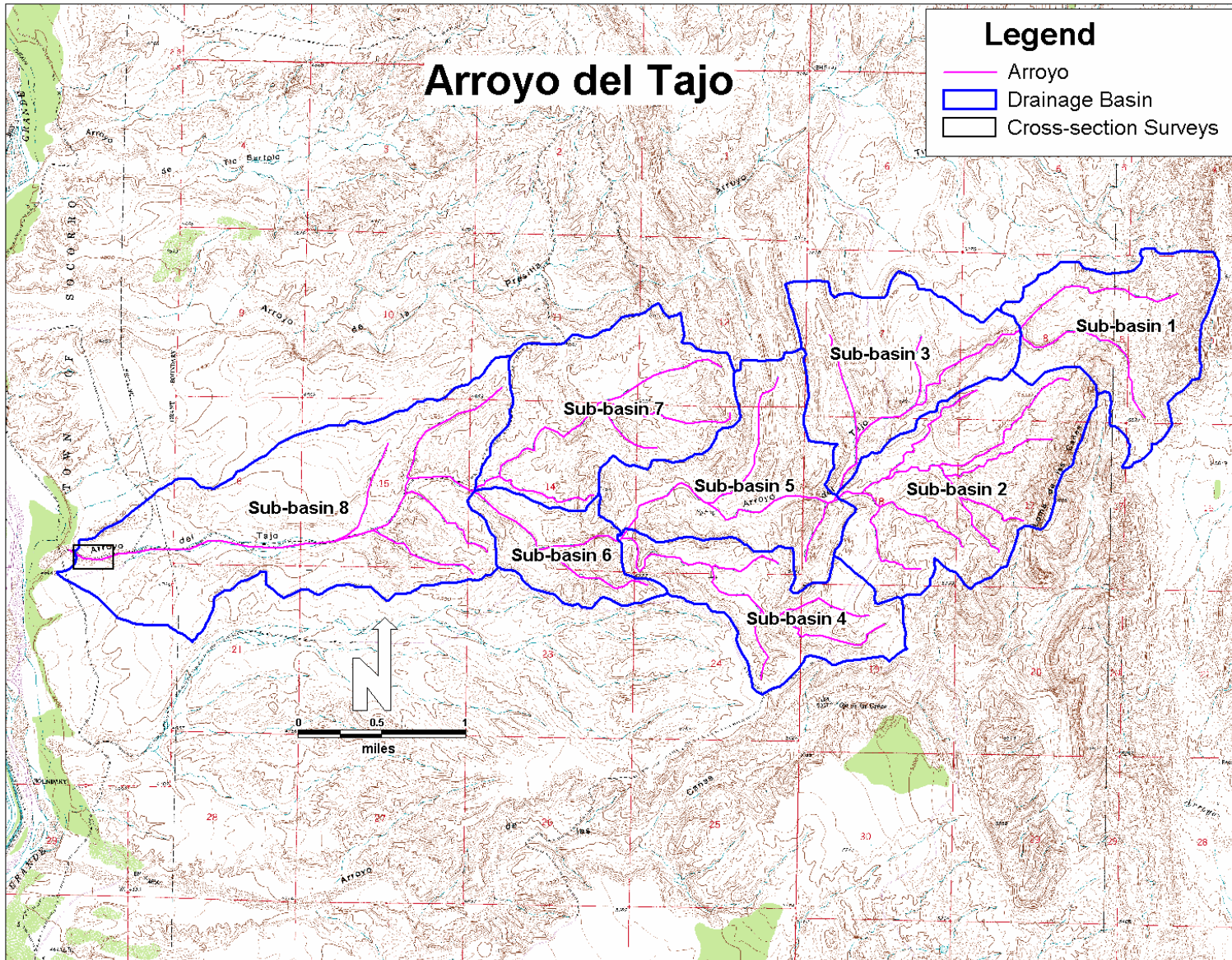
Figure A.4.   Watershed delineation of Arroyo del Tajo used in the HEC-HMS hydrologic model.

A.4
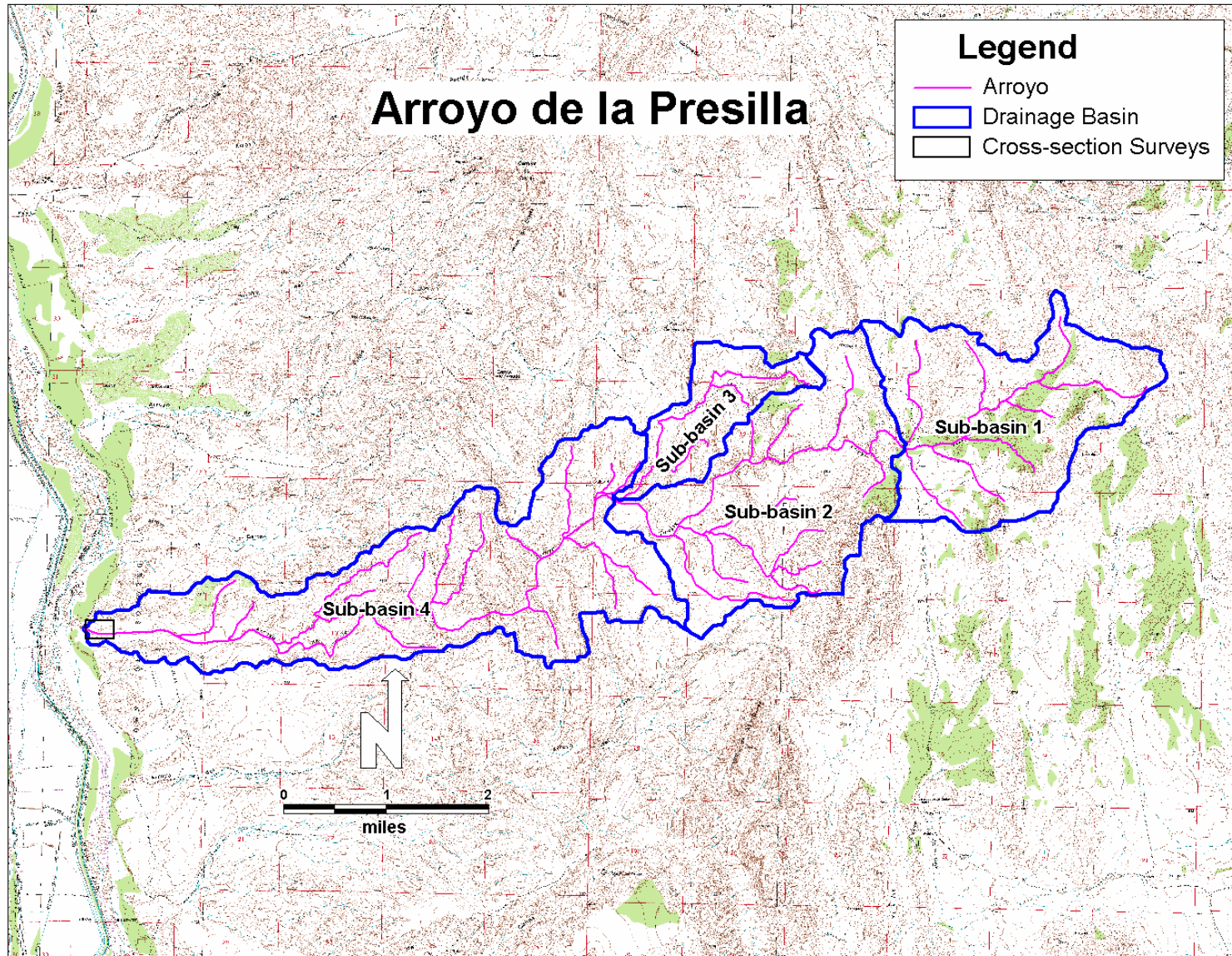
Figure A.5.   Watershed delineation of Arroyo de la Presilla used in the HEC-HMS hydrologic model.

Mussetter Engineering, Inc.
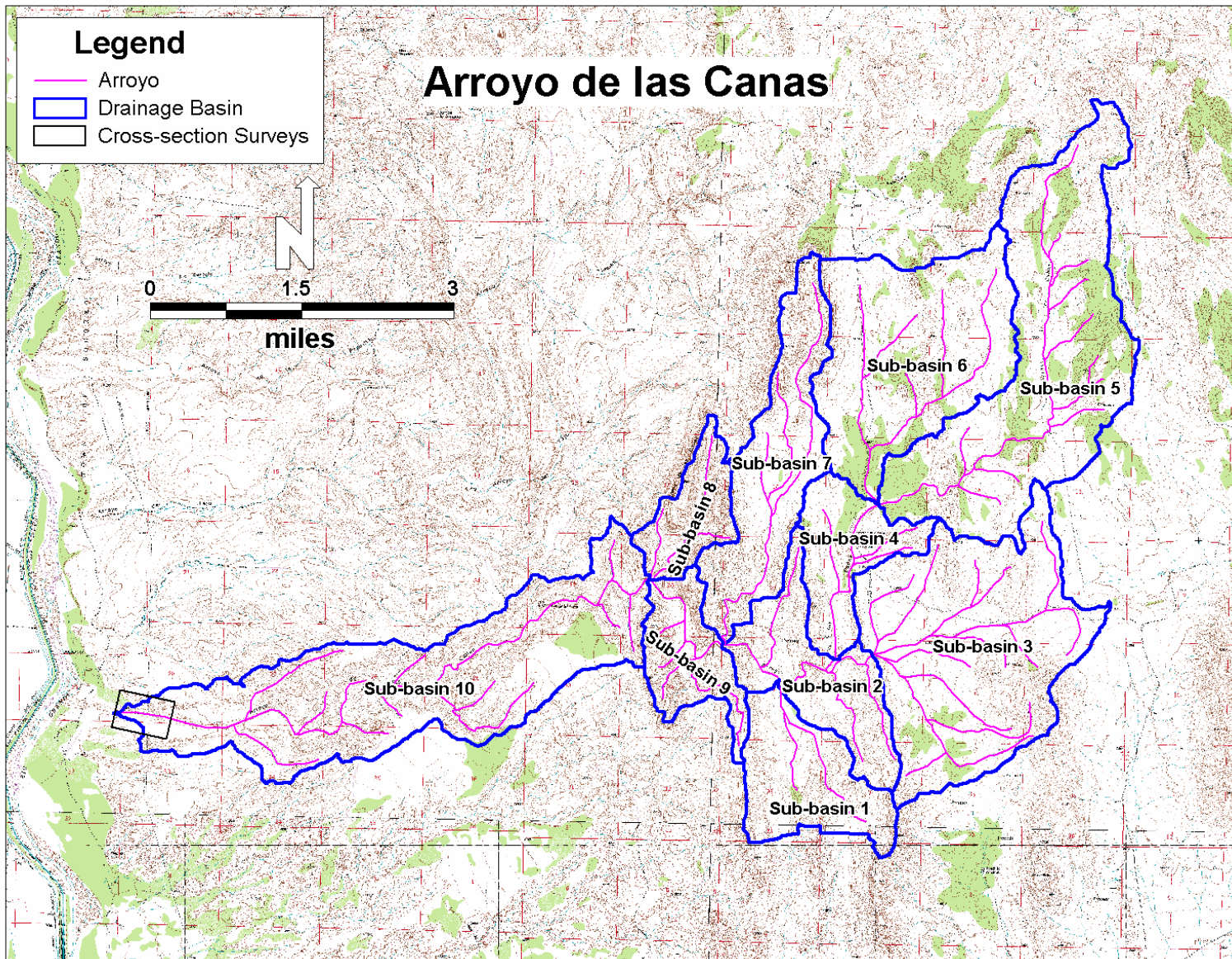
Figure A.6.   Watershed delineation of Arroyo de las Canas used in the HEC-HMS hydrologic model.

Mussetter Engineering, Inc.

Figure A.7. Watershed delineation of Arroyo de los Pinos used in the HEC-HMS hydrologic model.

A.7

Mussetter Engineering, Inc.
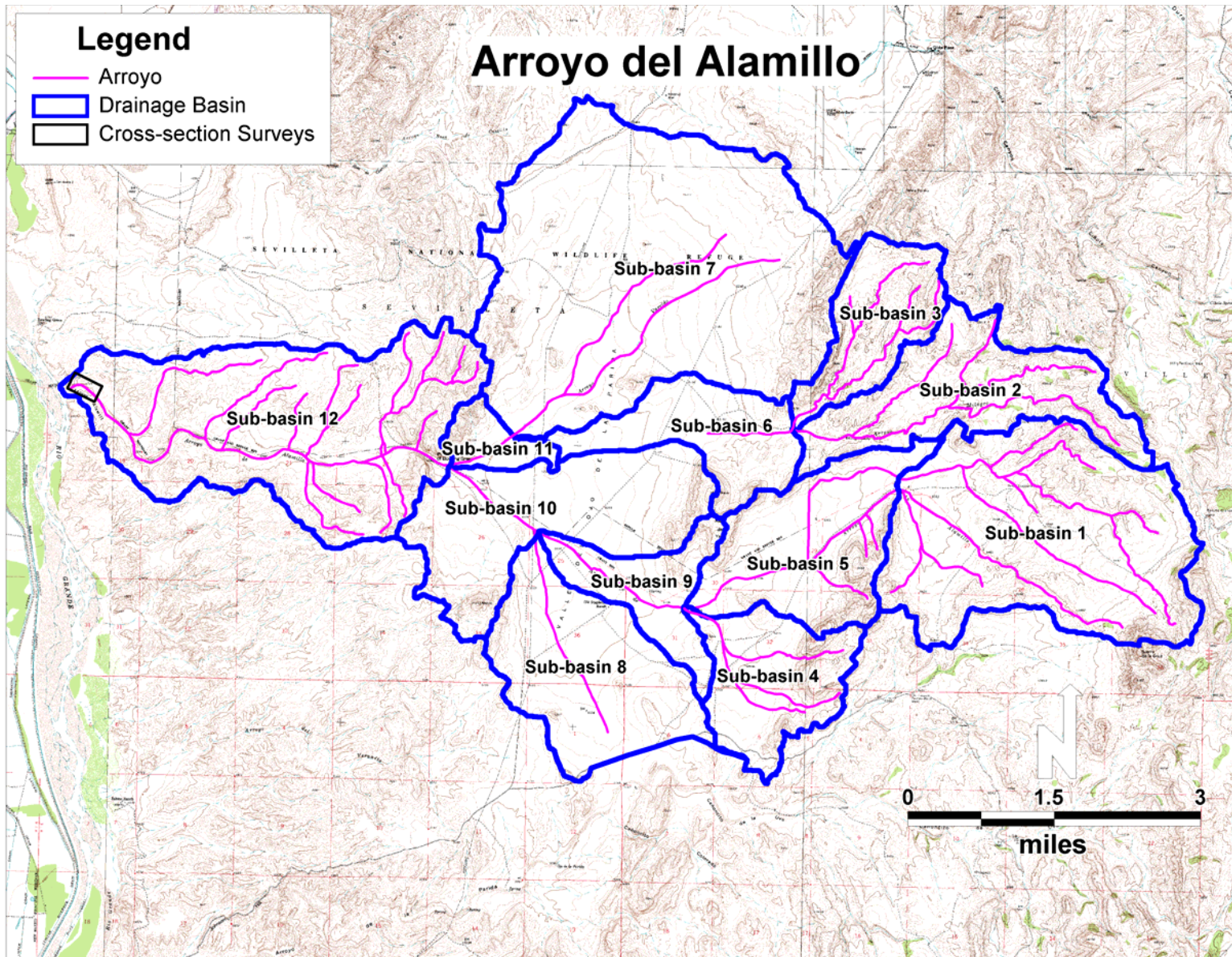
Figure A.8.   Watershed delineation of Arroyo de Alamillo used in the HEC-HMS hydrologic model.

Mussetter Engineering, Inc.
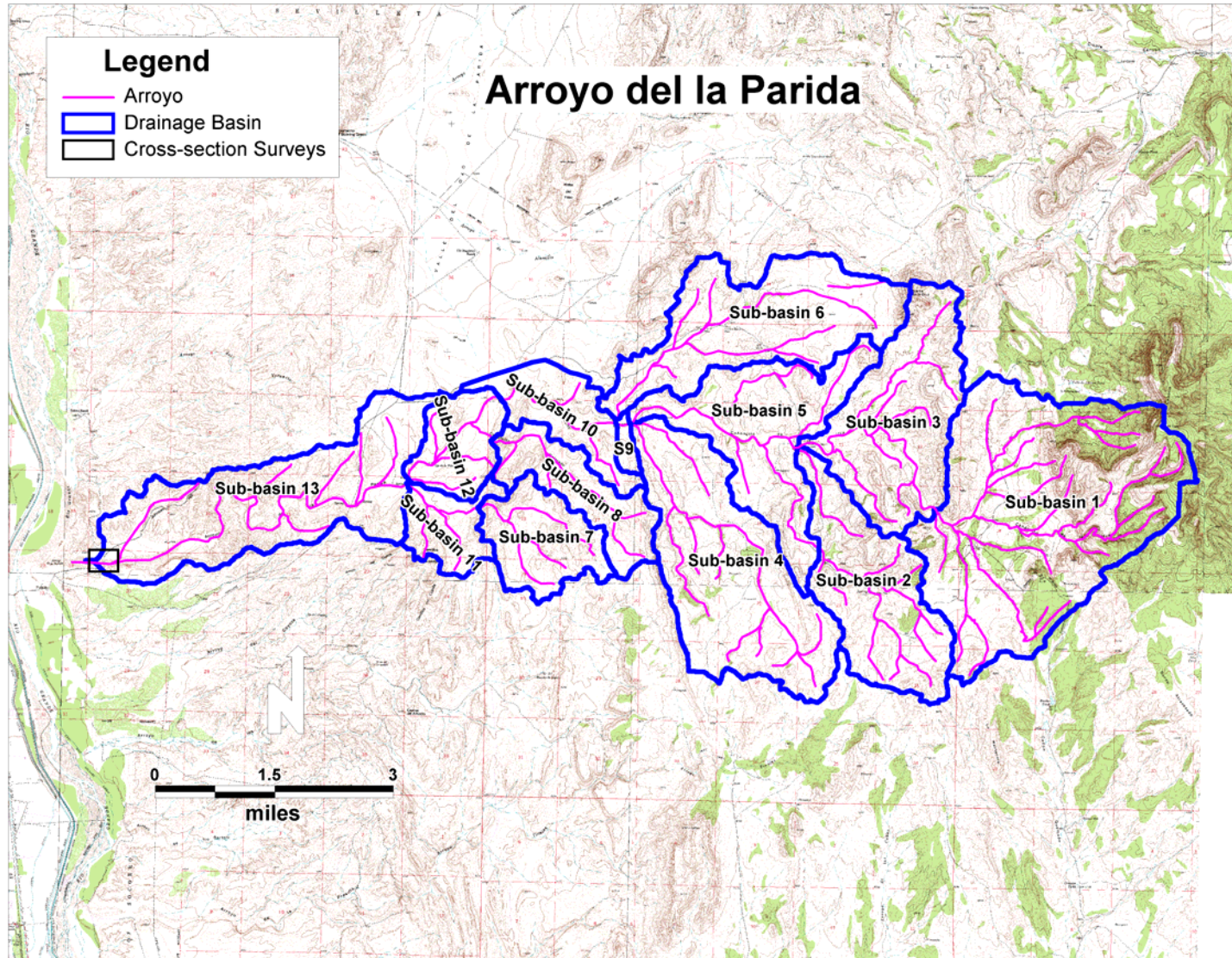
Figure A.9.   Watershed delineation of Arroyo de la Parida used in the HEC-HMS hydrologic model.

Mussetter Engineering, Inc.
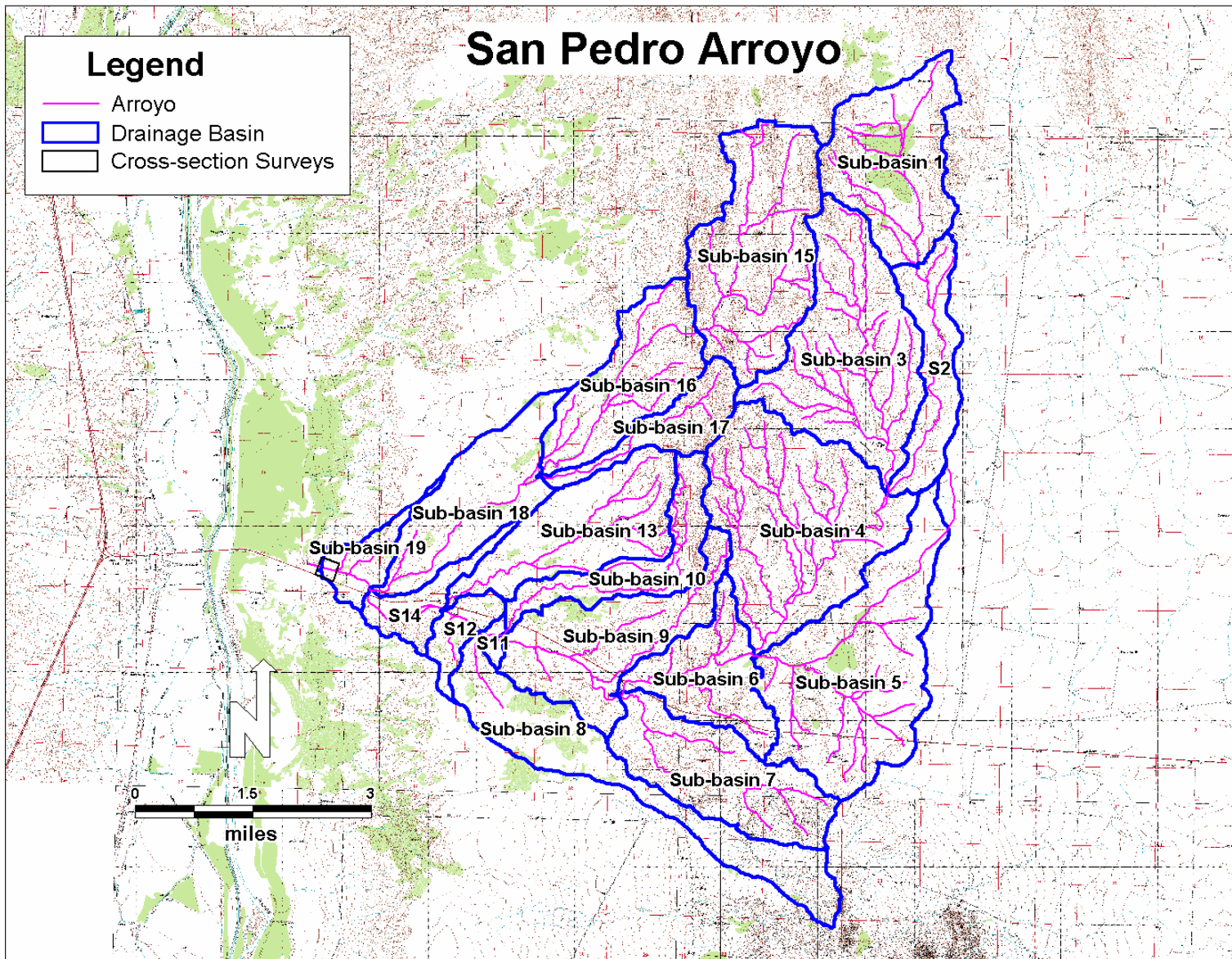
Figure A.10.   Watershed delineation of San Pedro Arroyo used in the HEC-HMS hydrologic model.

APPENDIX B
Sediment Gradation Curves for Tributary Basins
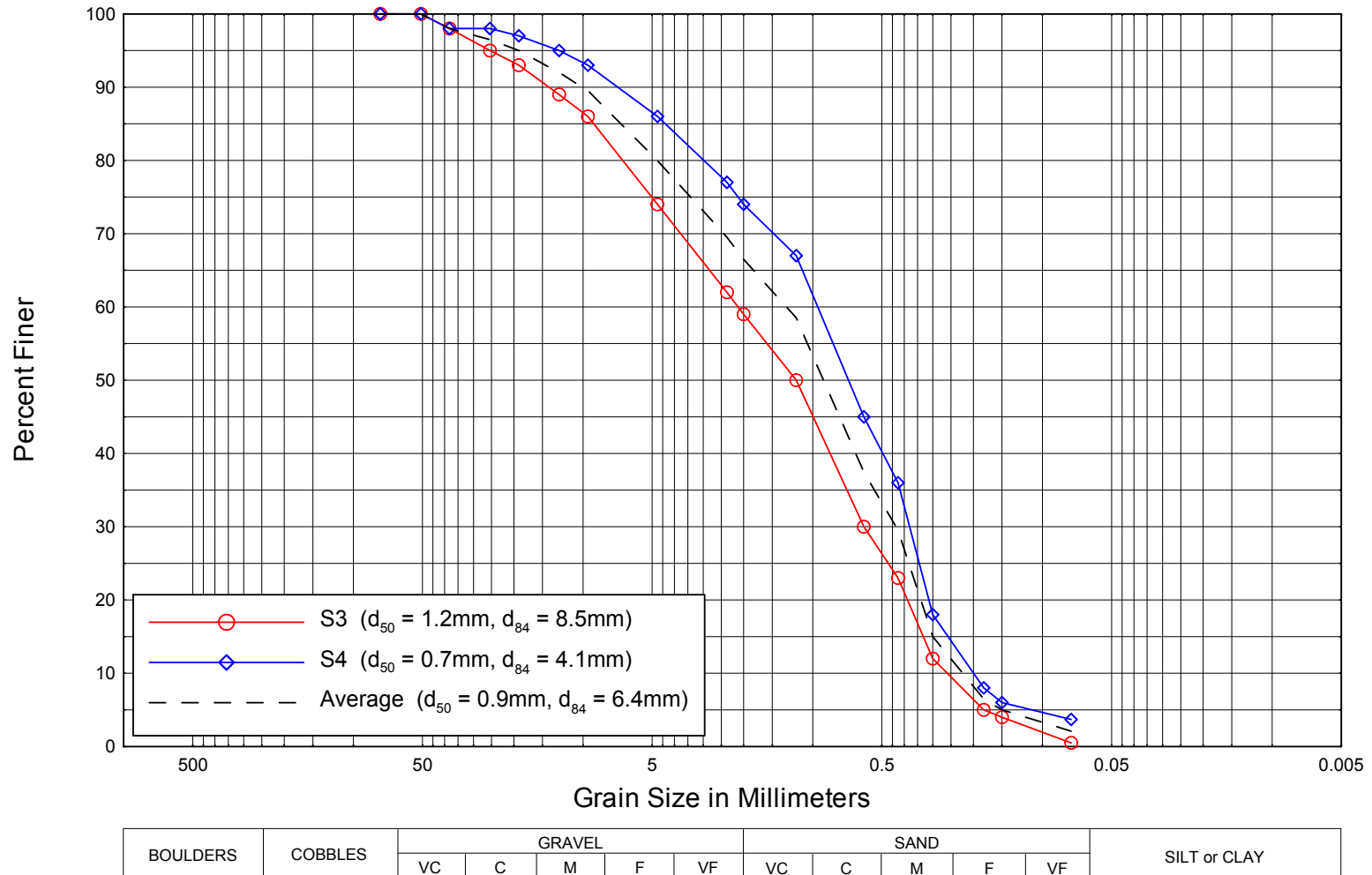
Figure B.1. Grain-size distribution curve for bed-material samples collected at the Arroyo Sevilleta study site.

Mussetter Engineering, Inc.
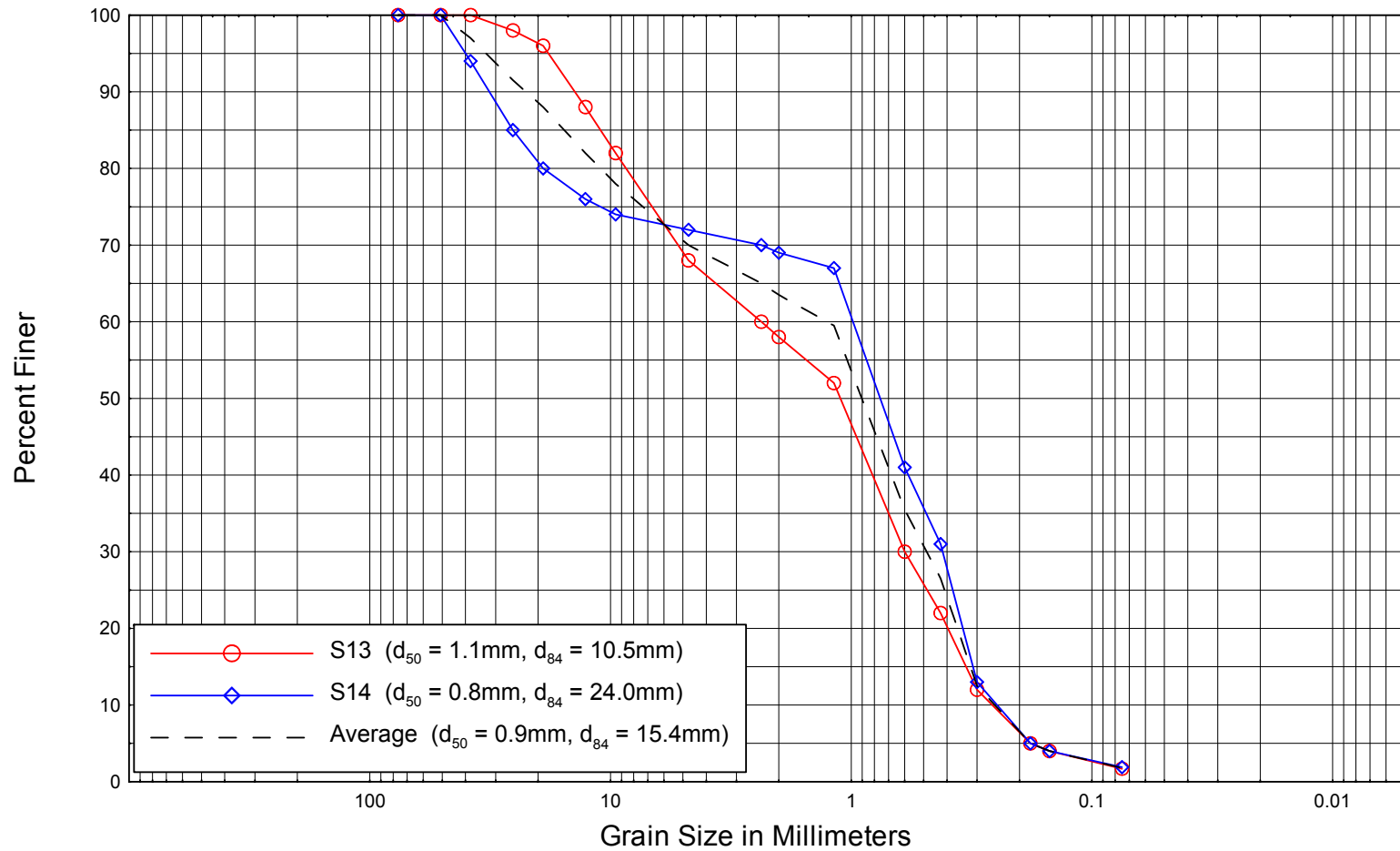
Figure B.2. Grain-size distribution curve for bed-material samples collected at the Arroyo del Coyote study site.

Mussetter Engineering, Inc.
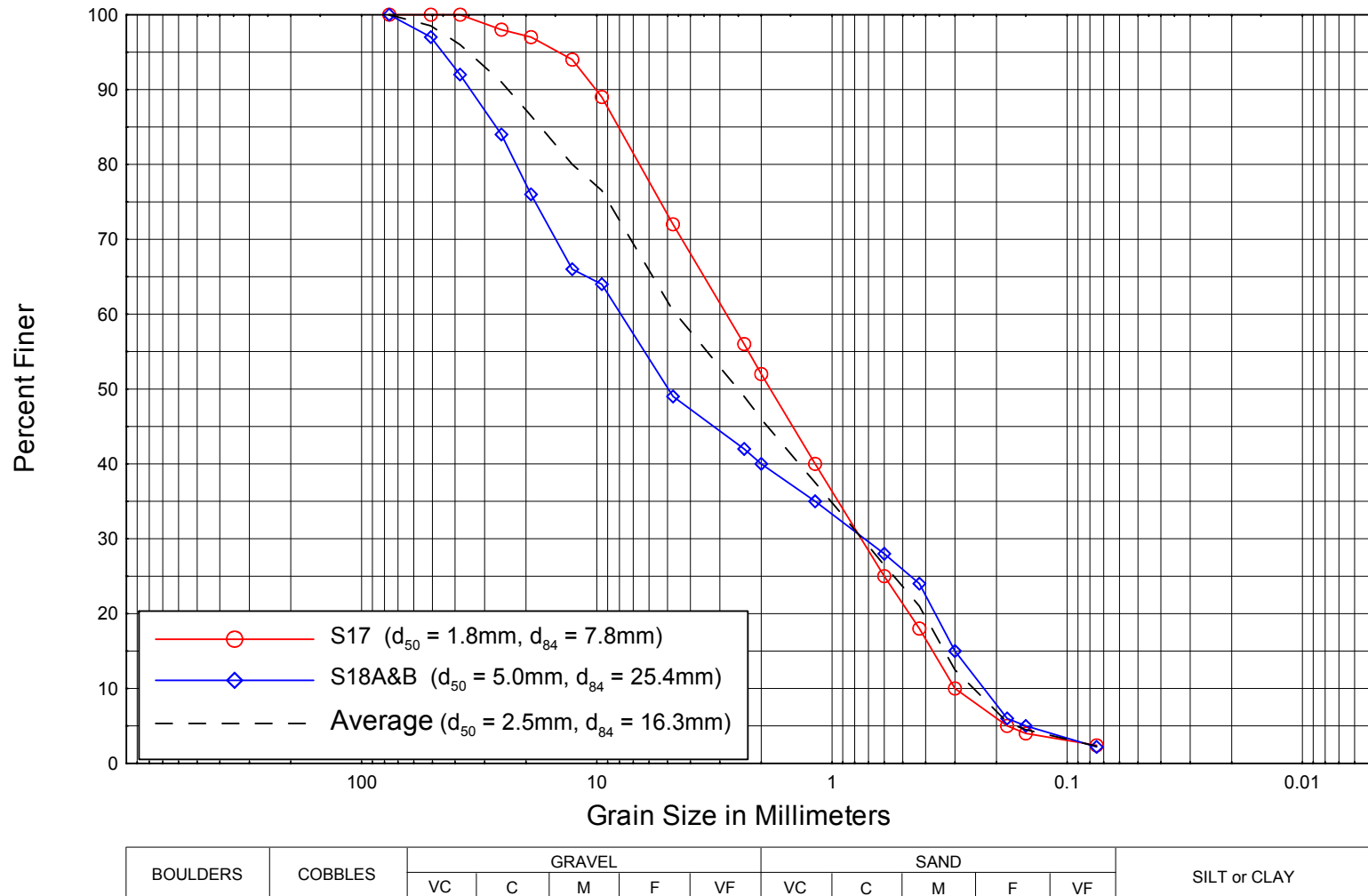
Figure B.3.   Grain-size distribution curve for bed-material samples collected at the Arroyo de Tio Bartolo study site.

Mussetter Engineering, Inc.
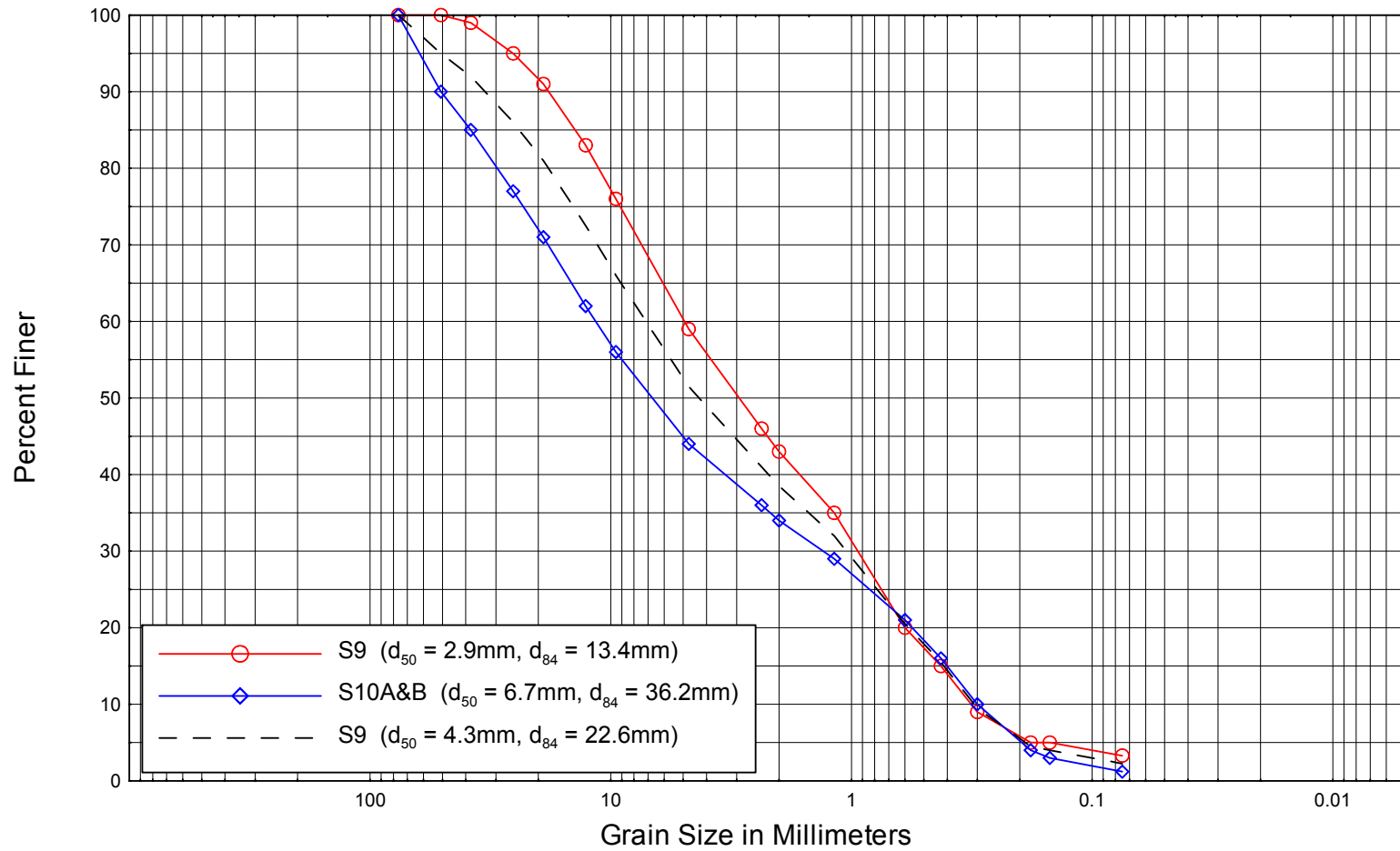
Figure B.4.   Grain-size distribution curve for bed-material samples collected at the Arroyo del Tajo study site.

B.4
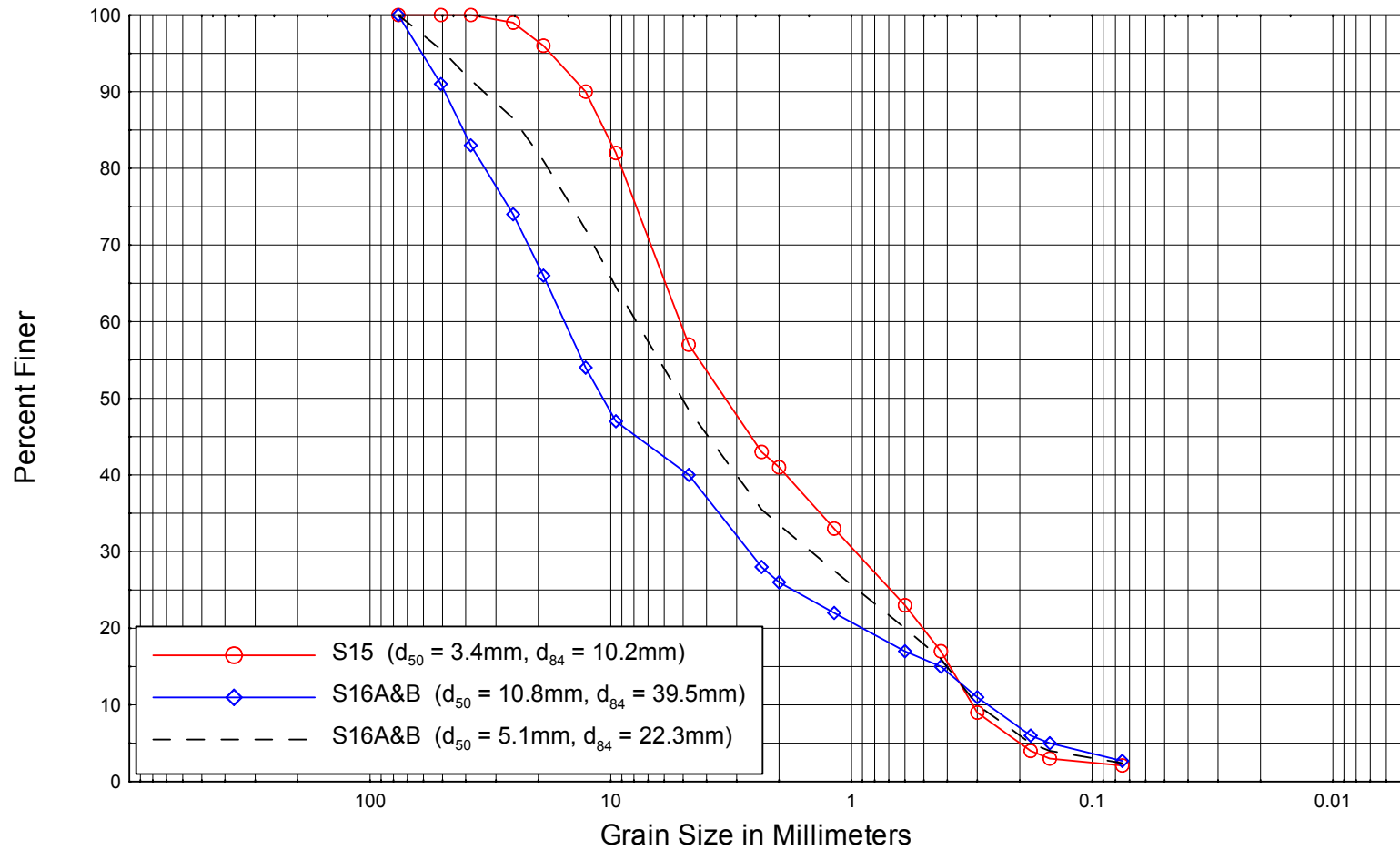
Figure B.5.   Grain-size distribution curve for bed-material samples collected at the Arroyo de los Pinos study site.
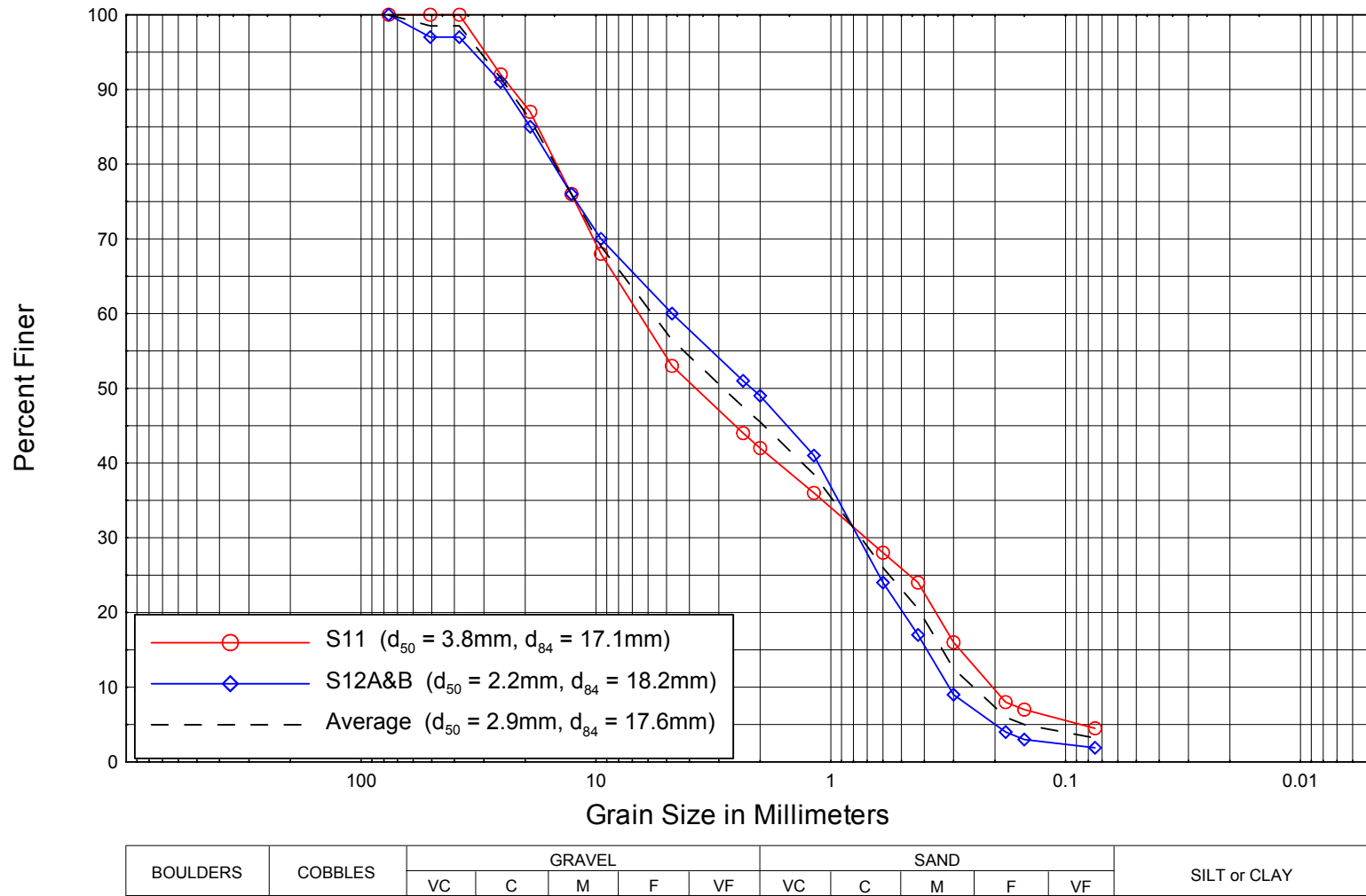
Figure B.6.   Grain-size distribution curve for bed-material samples collected at the Arroyo de la Presilla study site.

Mussetter Engineering, Inc.
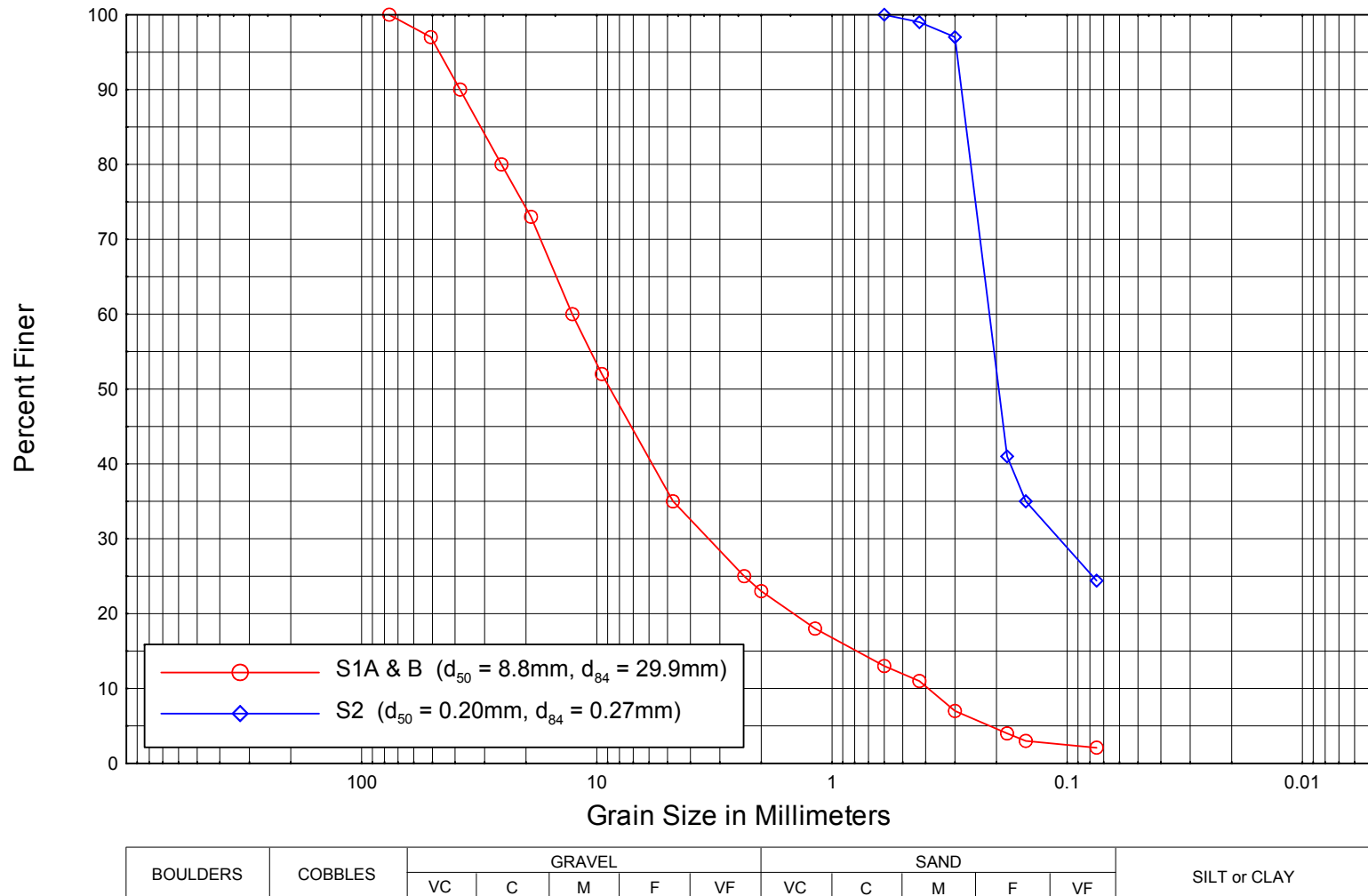
Figure B.7.   Grain-size distribution curve for bed-material sample (S1A & B) and bank sample (S2) collected at the Arroyo de las Canas study site.
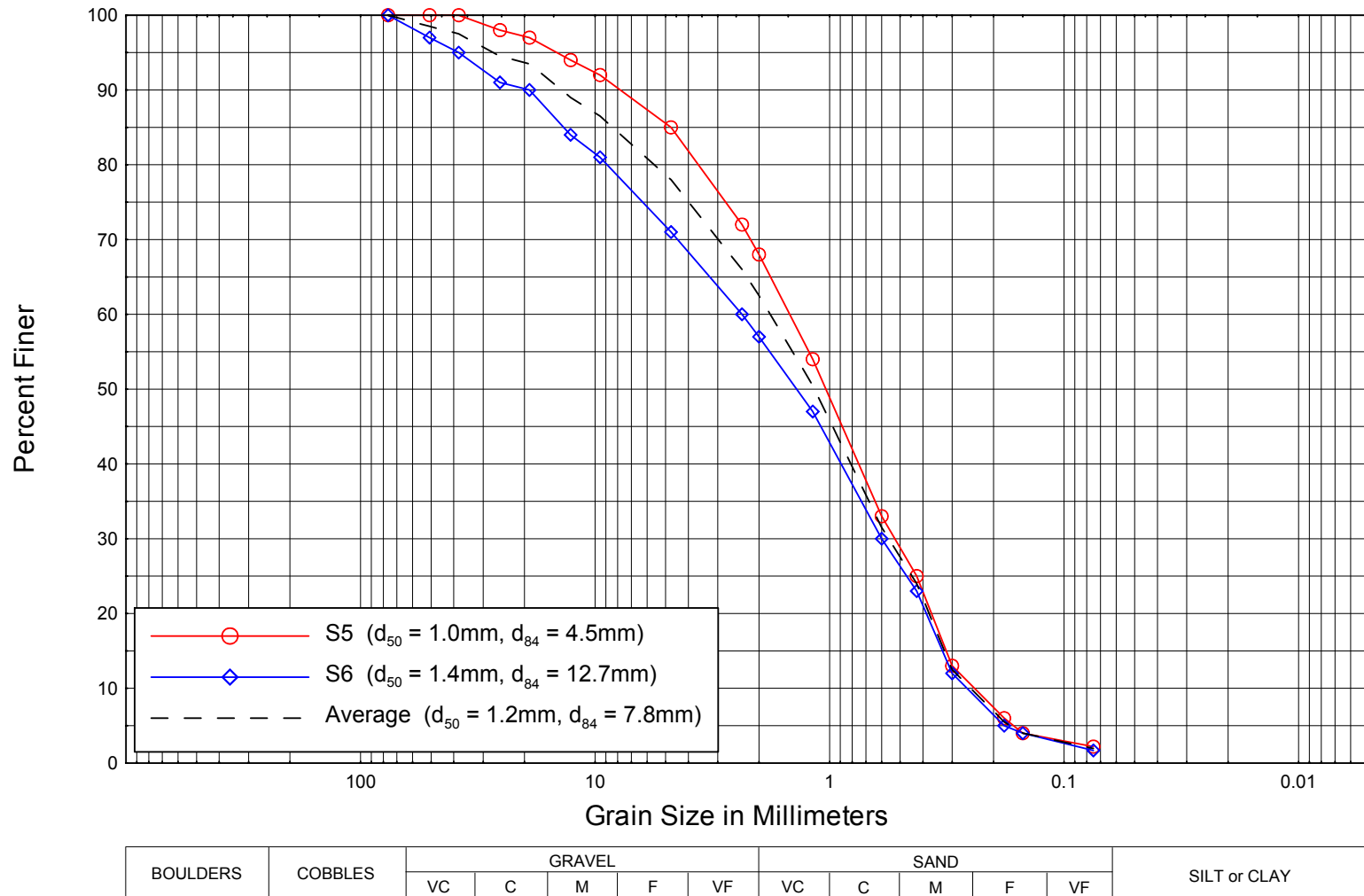
Figure B.8. Grain-size distribution curve for bed-material samples collected at the Arroyo de Alamillo study site.

Mussetter Engineering, Inc.
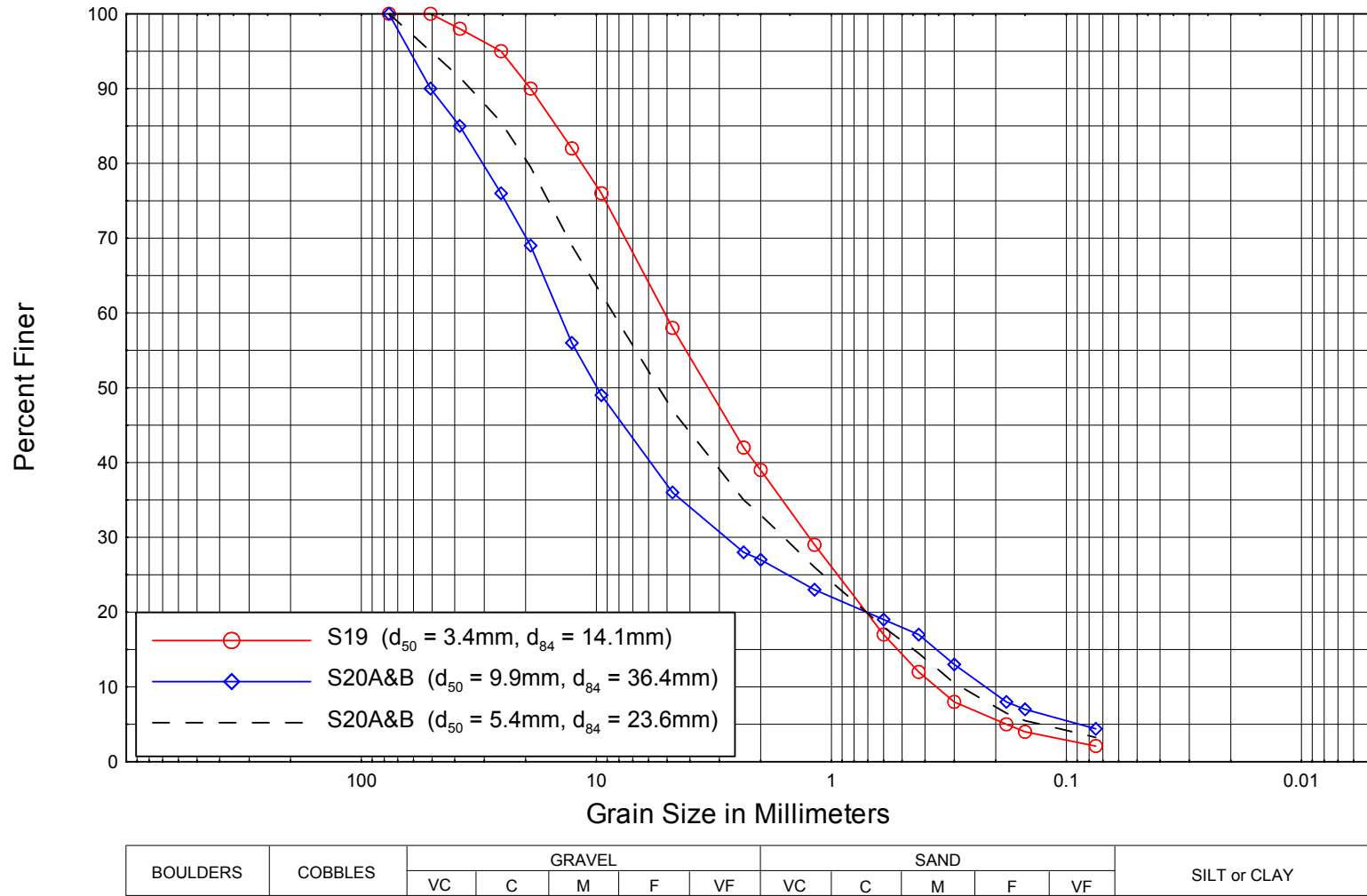
Figure B.9.   Grain-size distribution curve for bed-material samples collected at the Arroyo de la Parida study site.
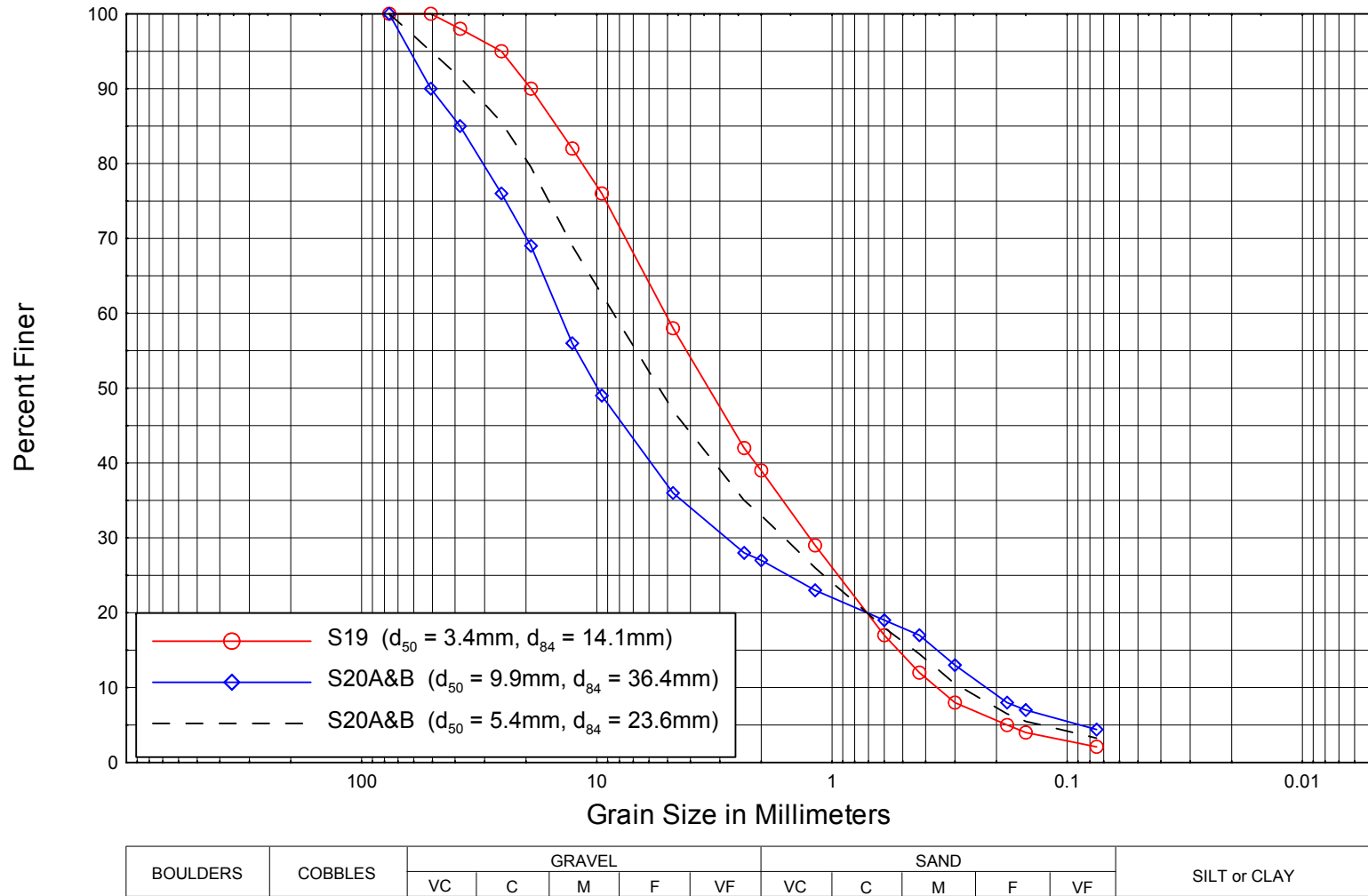
Figure B.10. Grain-size distribution curve for bed-material samples collected at the San Pedro Arroyo study site.

Mussetter Engineering, Inc.

APPENDIX C
Hyetographs for Tributary Basins

Mussetter Engineering, Inc.
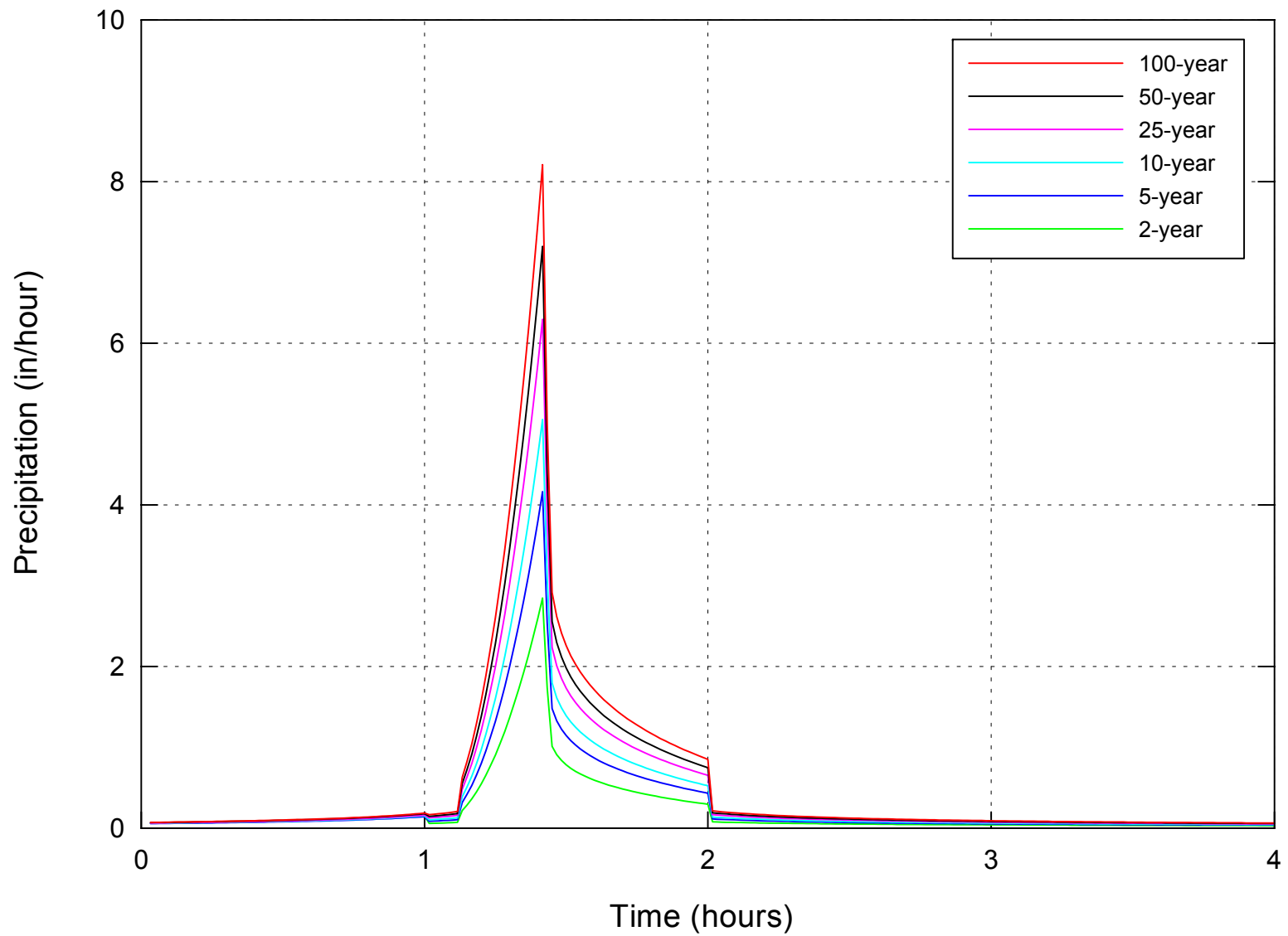
Figure C.1.   Hyetograph for Sevilleta Arroyo for the 2-, 5-, 10-, 25-, 50-, and 100-year events.

C.1
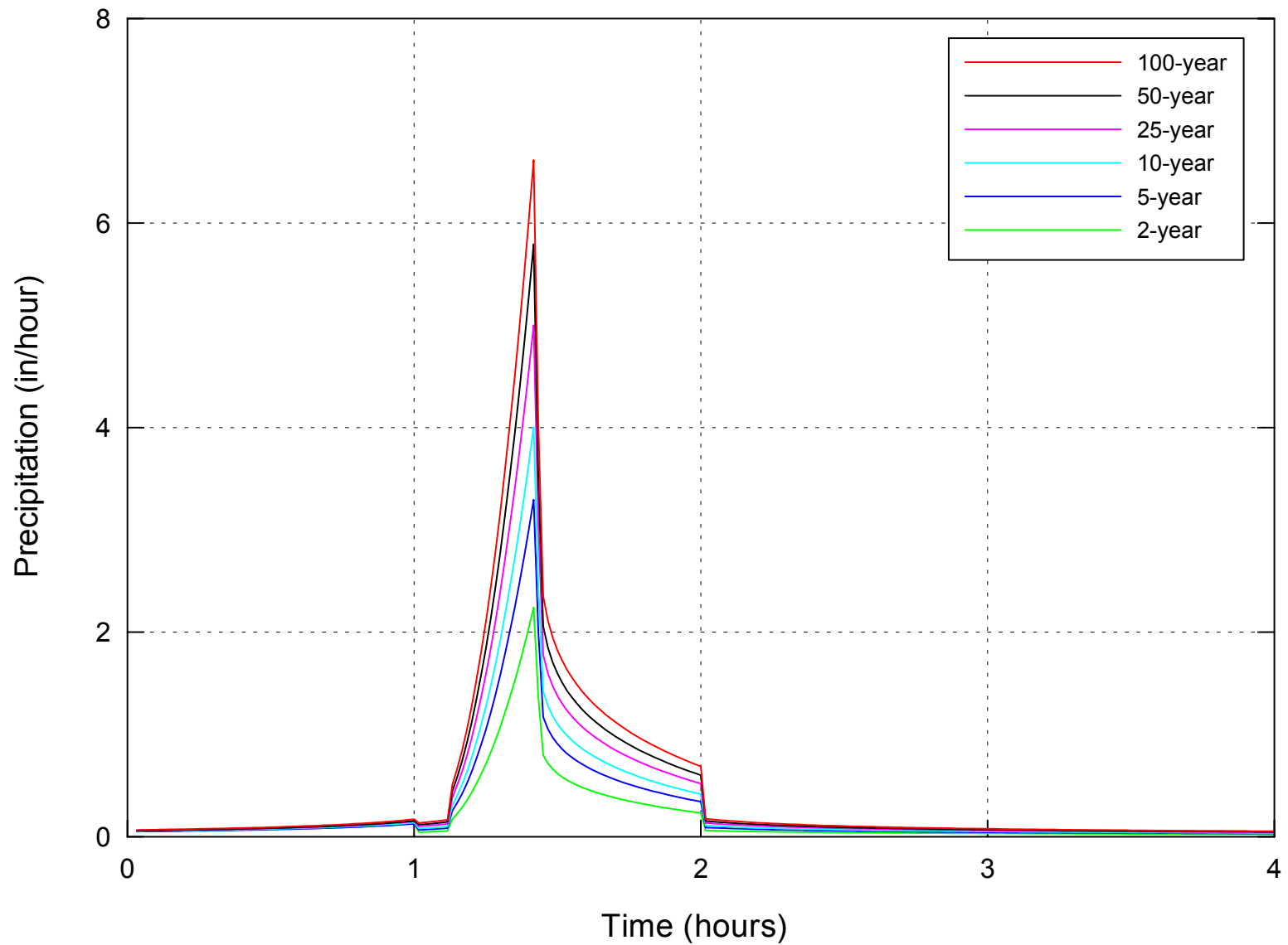
Figure C.2.   Hyetograph for Arroyo del Coyote for the 2-, 5-, 10-, 25-, 50-, and 100-year events.

Mussetter Engineering, Inc.
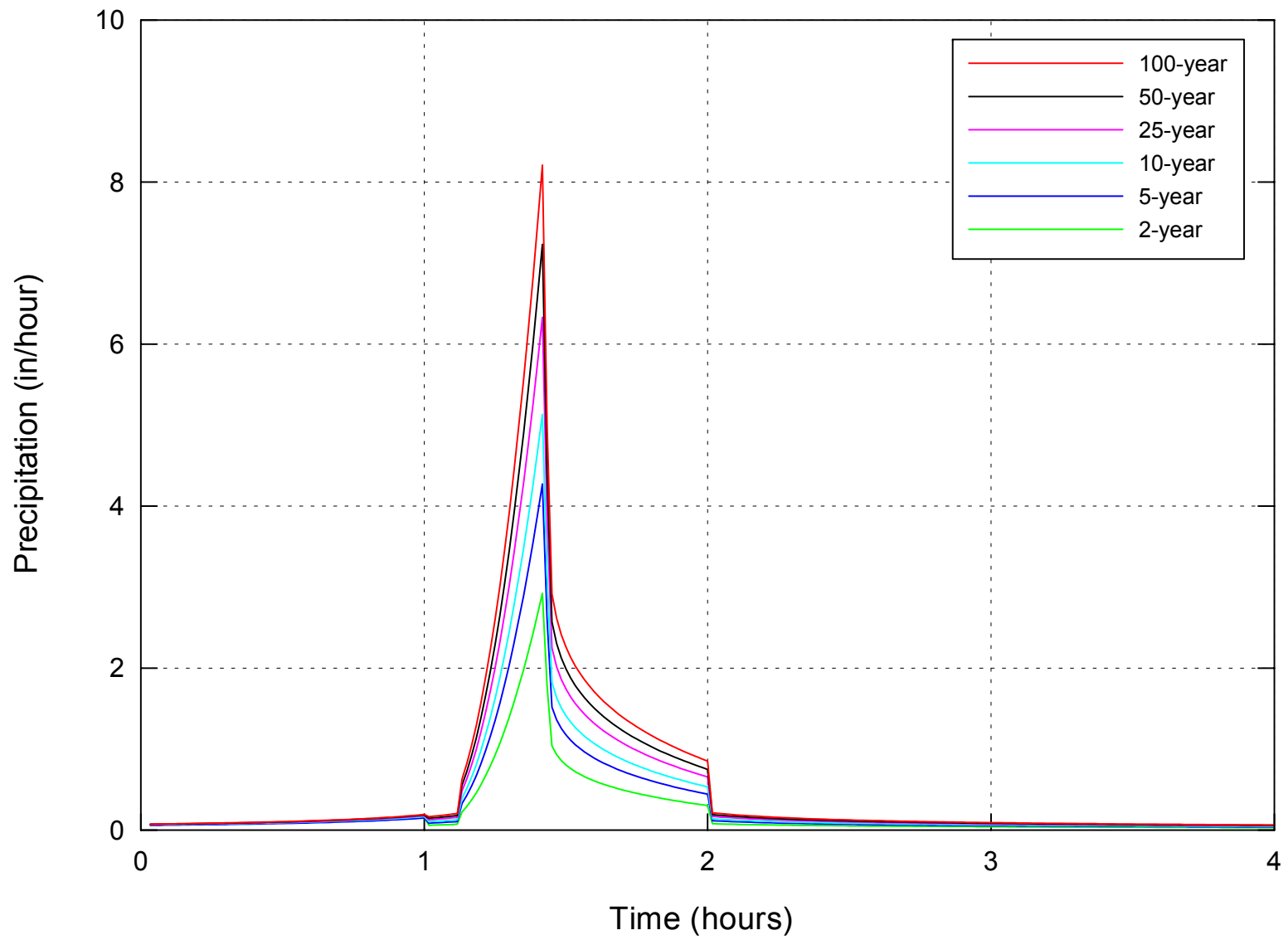
Figure C.3.   Hyetograph for Arroyo de Tio Bartolo for the 2-, 5-, 10-, 25-, 50-, and 100-year events.

Mussetter Engineering, Inc.
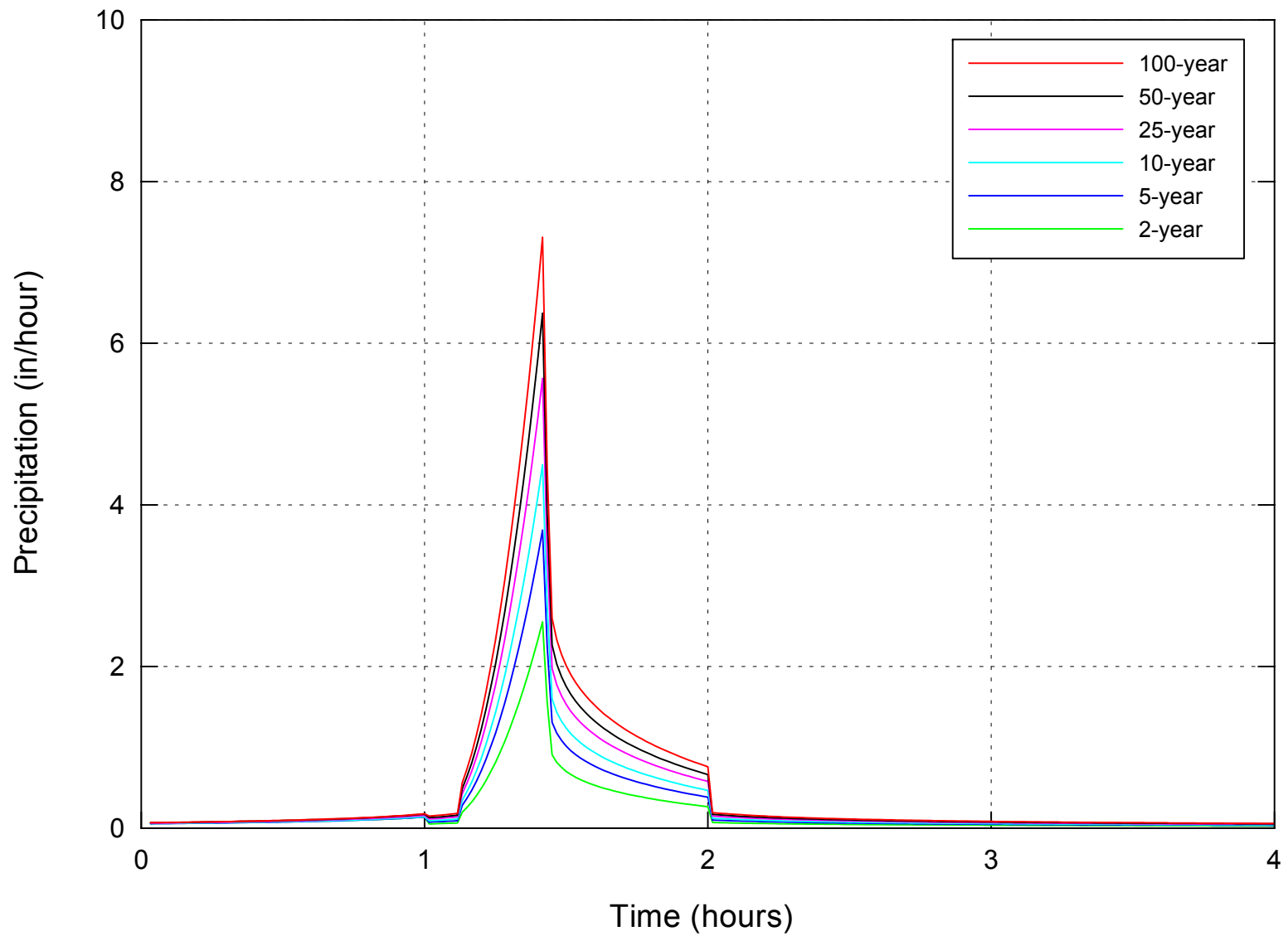
Figure C.4. Hyetograph for Arroyo del Tajo for the 2-, 5-, 10-, 25-, 50-, and 100-year events.

C.4

Mussetter Engineering, Inc.
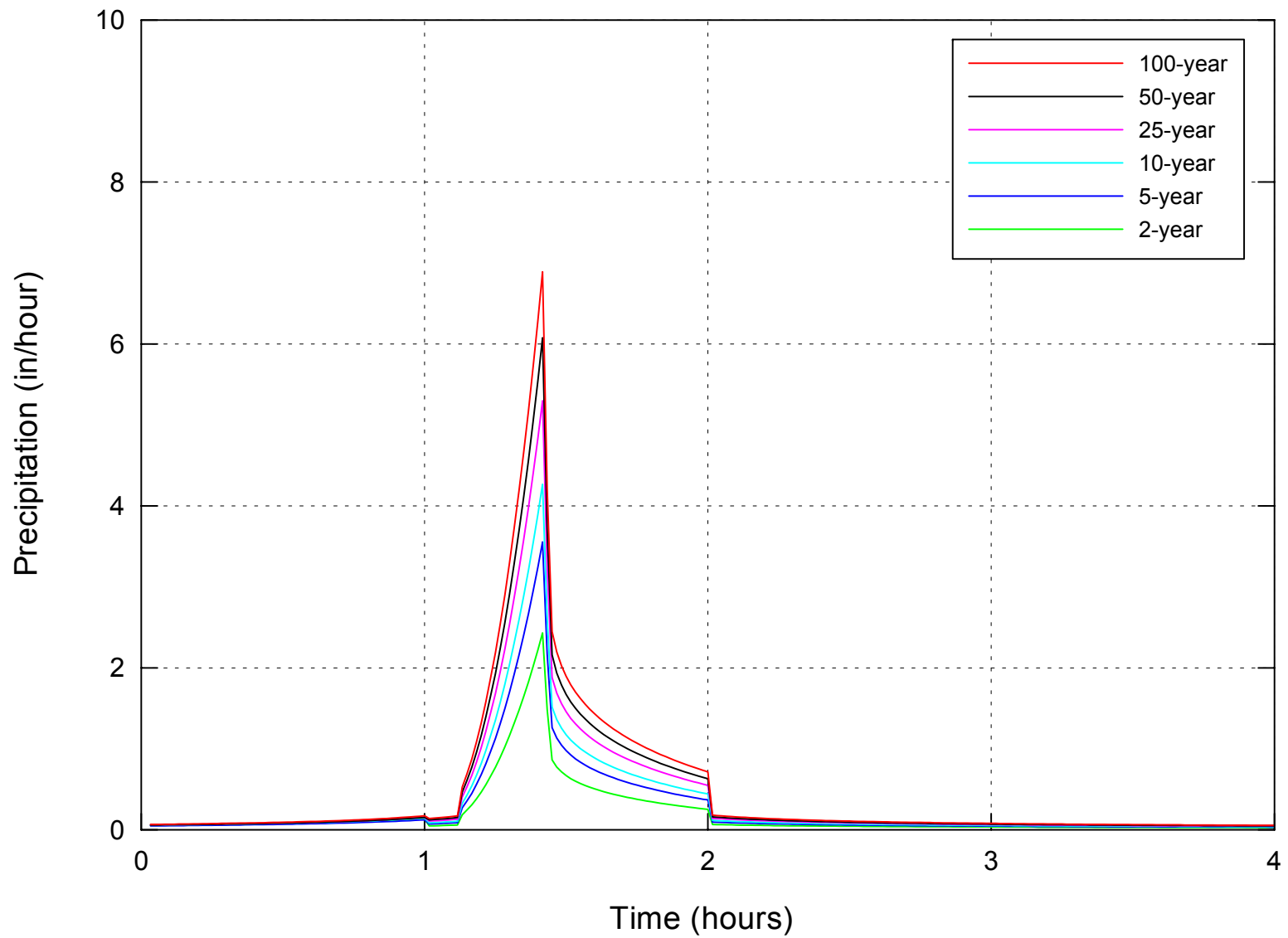
Figure C.5.   Hyetograph for Arroyo de los Pinos for the 2-, 5-, 10-, 25-, 50-, and 100-year events.

Mussetter Engineering, Inc.
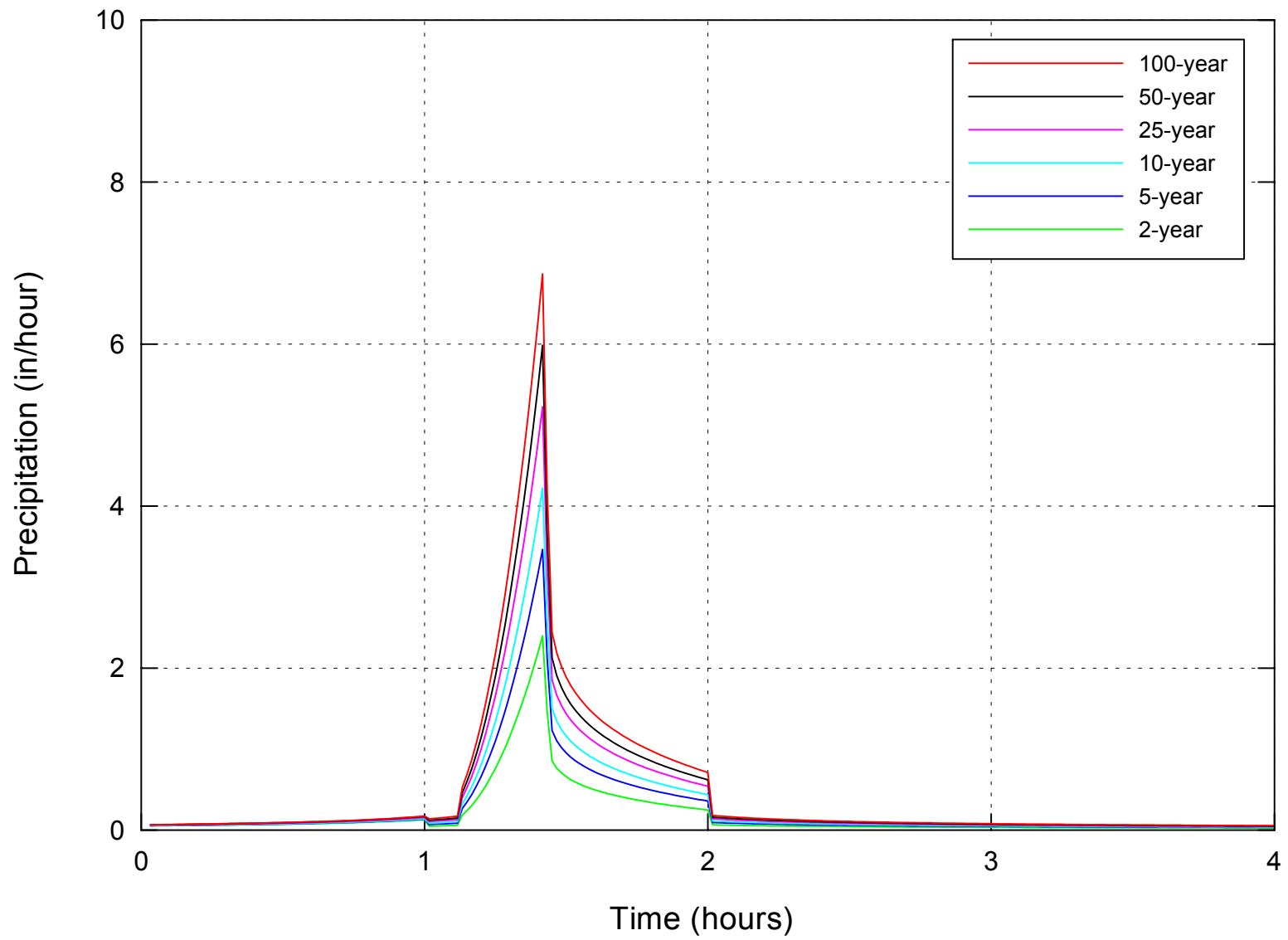
Figure C.6.   Hyetograph for Arroyo de la Presilla for the 2-, 5-, 10-, 25-, 50-, and 100-year events.

Mussetter Engineering, Inc.
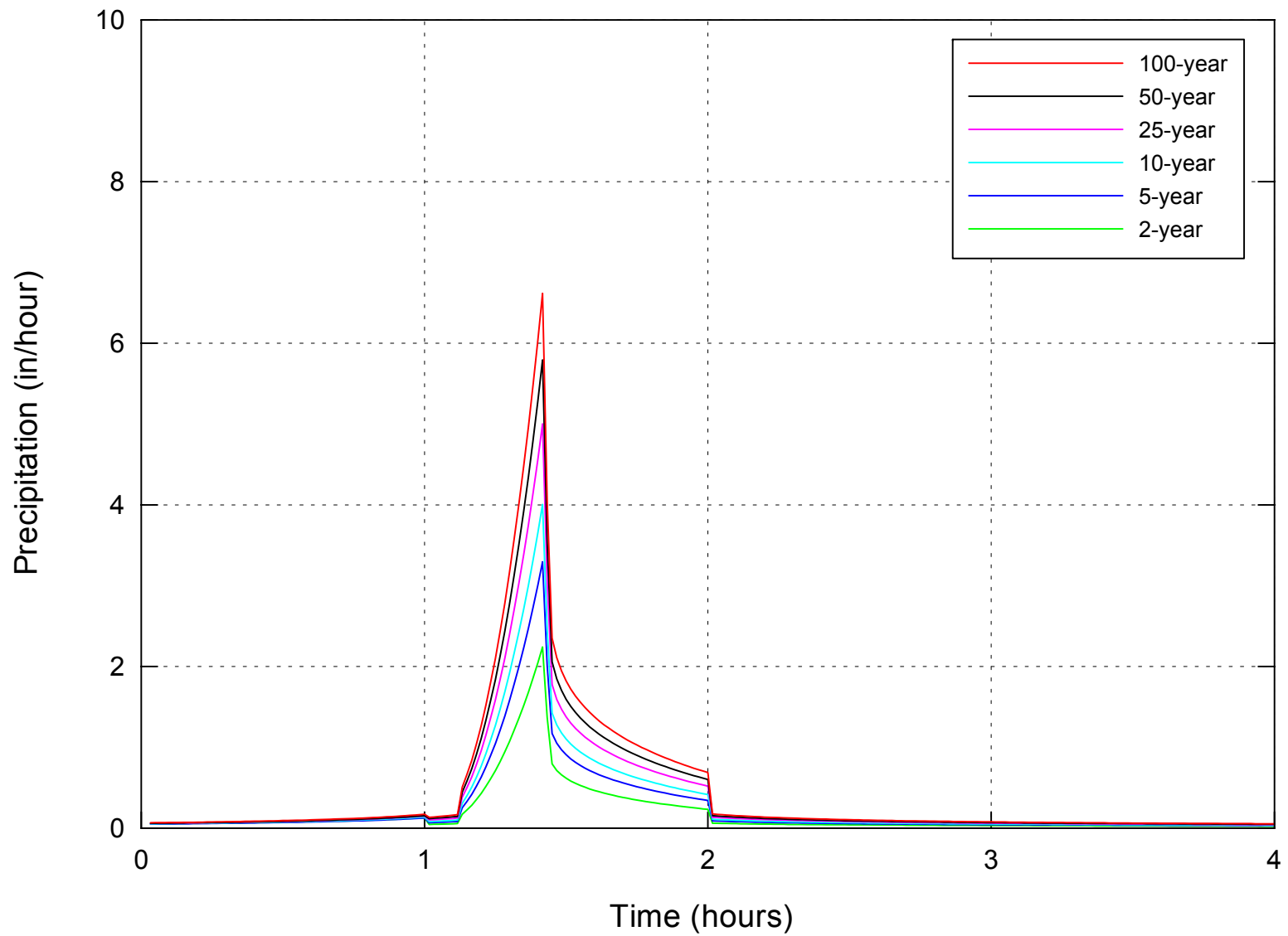
Figure C.7.   Hyetograph for Arroyo de las Canas for the 2-, 5-, 10-, 25-, 50-, and 100-year events.

Mussetter Engineering, Inc.
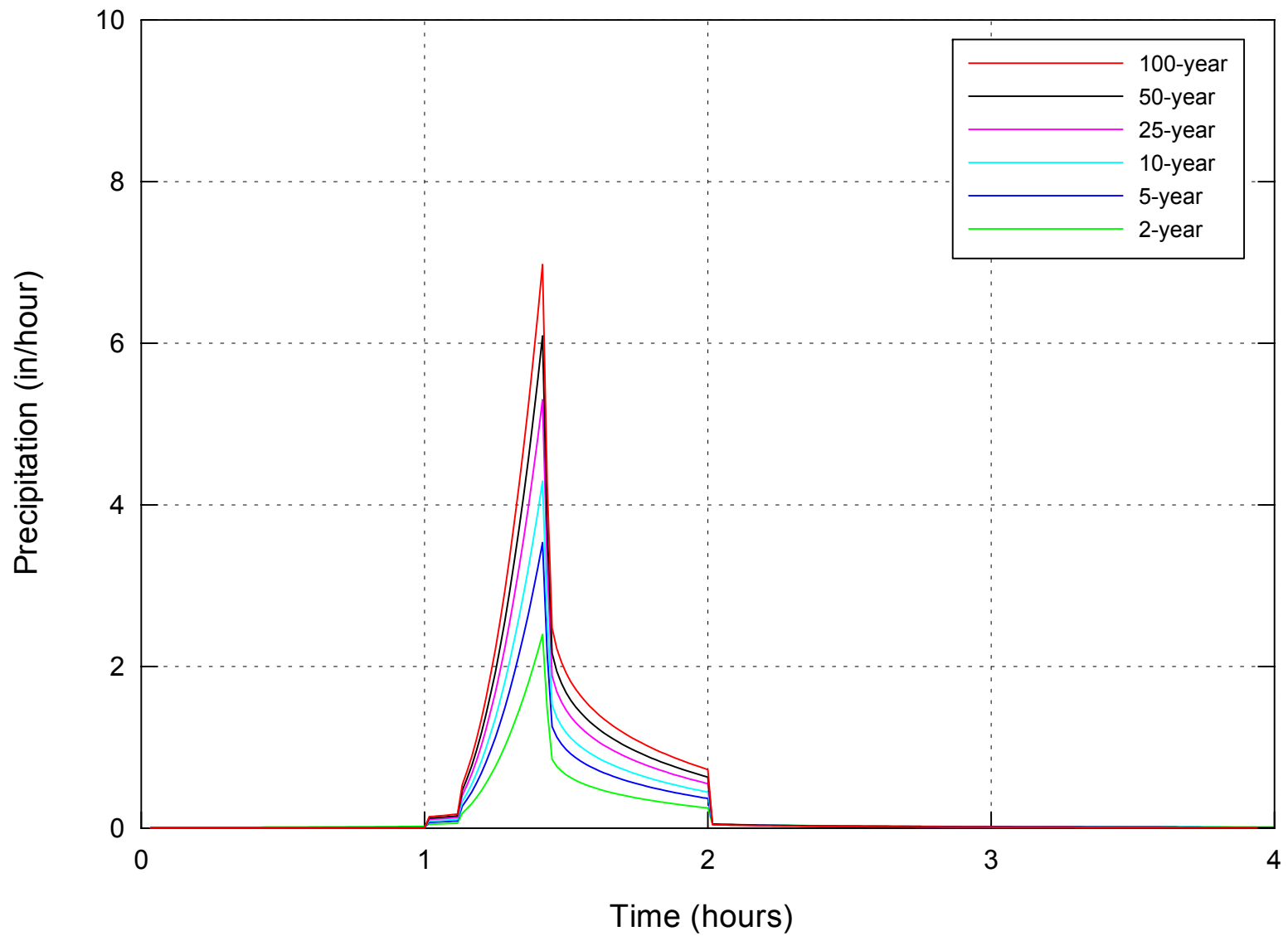
Figure C.8.   Hyetograph for Arroyo de Allamilo for the 2-, 5-, 10-, 25-, 50-, and 100-year events.

Mussetter Engineering, Inc.
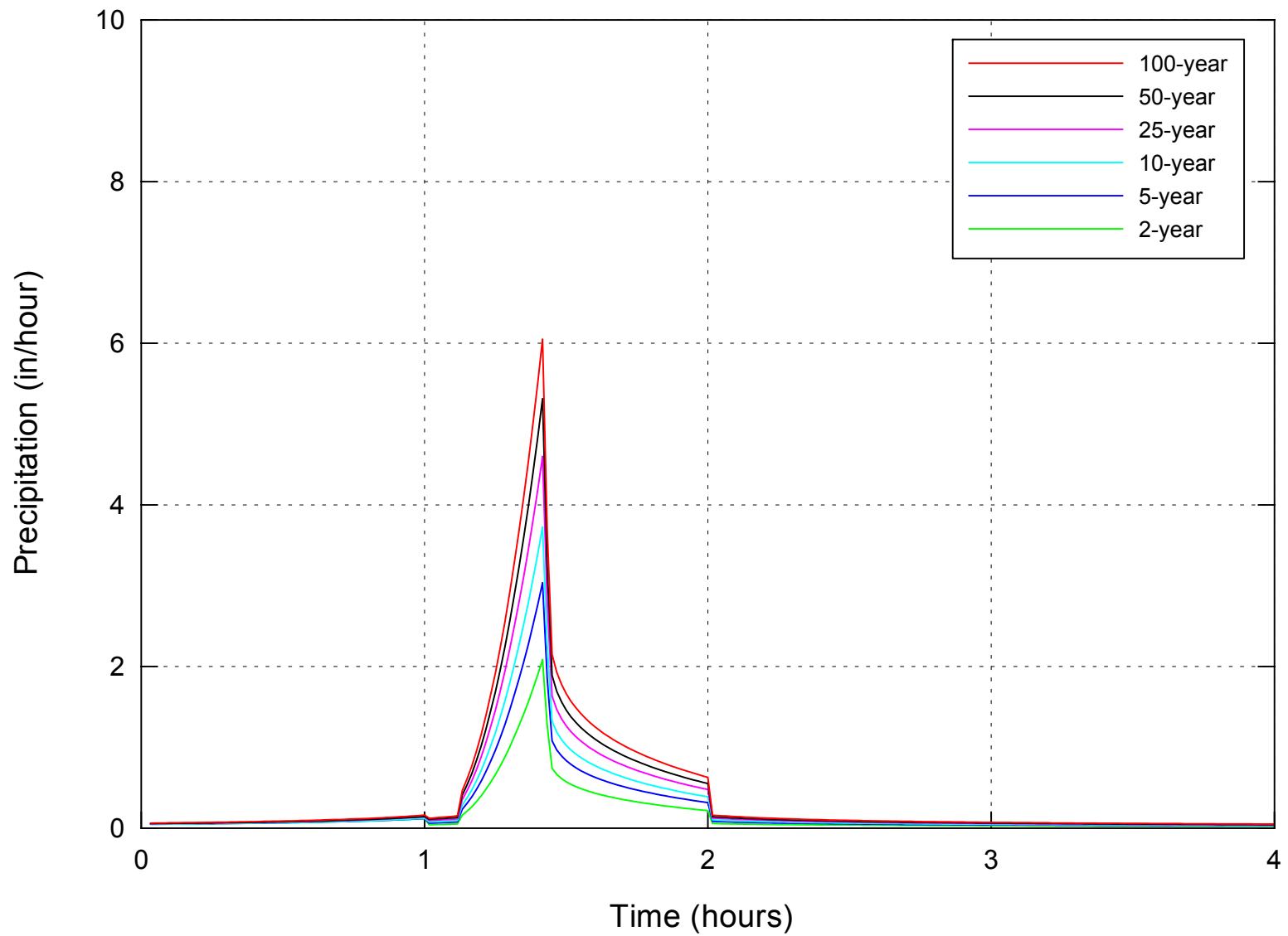
Figure C9.   Hyetograph for Arroyo de la Parida for the 2-, 5-, 10-, 25-, 50-, and 100-year events.

Mussetter Engineering, Inc.
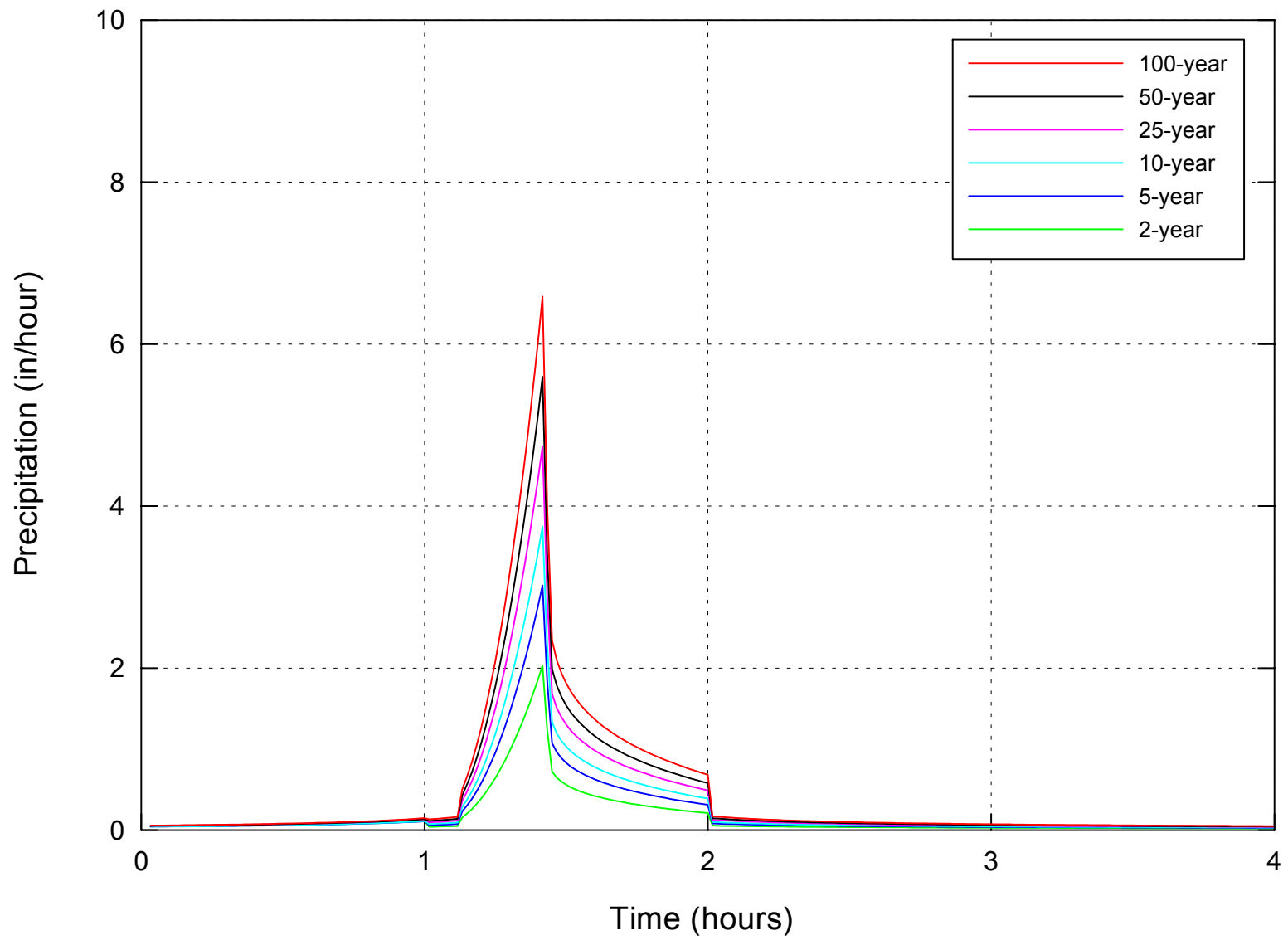
Figure C.10.   Hyetograph for San Pedro for the 2-, 5-, 10-, 25-, 50-, and 100-year events.

Mussetter Engineering, Inc.

APPENDIX D
HEC-HMS Output for Tributary Basins

Table D.1. Computed peak flows and runoff volumes for Arroyo Sevilleta for the 2-, 5-, 10-, 25-, 50- and 100-year return intervals.

Subbasin	2-Year		5-Year		10-Year		25-Year		50-Year		100-Year	
	Peak Discharge (cfs)	Runoff Volume (ac-ft)	Peak Discharge (cfs)	Runoff Volume (ac-ft)	Peak Discharge (cfs)	Runoff Volume (ac-ft)	Peak Discharge (cfs)	Runoff Volume (ac-ft)	Peak Discharge (cfs)	Runoff Volume (ac-ft)	Peak Discharge (cfs)	Runoff Volume (ac-ft)
1	66	6.1	189	17.8	295	28.0	509	43.6	652	56.4	812	70.9
2	51	4.2	147	12.0	230	18.9	389	29.4	497	38.1	617	47.9
3	63	3.7	180	10.6	279	16.6	463	25.9	586	33.5	722	42.1

Table D.2. Computed peak flows and runoff volumes for Arroyo de Tio Bartolo for the 2-, 5-, 10-, 25-, 50-, and 100-year return intervals.

Subbasin	2-Year		5-Year		10-Year		25-Year		50-Year		100-Year	
	Peak Discharge (cfs)	Runoff Volume (ac-ft)	Peak Discharge (cfs)	Runoff Volume (ac-ft)	Peak Discharge (cfs)	Runoff Volume (ac-ft)	Peak Discharge (cfs)	Runoff Volume (ac-ft)	Peak Discharge (cfs)	Runoff Volume (ac-ft)	Peak Discharge (cfs)	Runoff Volume (ac-ft)
1	90	5.8	246	15.9	372	24.3	553	36.8	703	47.4	863	59.1
2	67	3.9	182	10.7	274	16.4	406	24.8	515	31.9	630	39.8
3	94	6.4	258	17.5	389	26.7	579	40.4	736	52.1	904	65.0

Table D.3. Computed peak flows and runoff volumes for Arroyo del Coyote for the 2-, 5-, 10-, 25-, 50-, and 100-year return intervals.

Subbasin	2-Year		5-Year		10-Year		25-Year		50-Year		100-Year	
	Peak Discharge (cfs)	Runoff Volume (ac-ft)	Peak Discharge (cfs)	Runoff Volume (ac-ft)	Peak Discharge (cfs)	Runoff Volume (ac-ft)	Peak Discharge (cfs)	Runoff Volume (ac-ft)	Peak Discharge (cfs)	Runoff Volume (ac-ft)	Peak Discharge (cfs)	Runoff Volume (ac-ft)
1	120	10.1	333	28.2	512	43.6	778	67.0	983	85.4	1,099	106.9
2	85	6.9	235	19.1	361	29.6	549	45.5	693	58.1	857	72.6
3	30	1.6	83	4.4	126	6.9	189	10.6	237	13.5	268	16.9

Table D.4.	Computed peak flows and runoff volumes for Arroyo del Tajo for the 2-, 5-, 10-, 25-, 50-, and 100-year return intervals.											
	2-Year		5-Year		10-Year		25-Year		50-Year		100-Year	
Subbasin	Peak Discharge (cfs)	Runoff Volume (ac-ft)	Peak Discharge (cfs)	Runoff Volume (ac-ft)	Peak Discharge (cfs)	Runoff Volume (ac-ft)	Peak Discharge (cfs)	Runoff Volume (ac-ft)	Peak Discharge (cfs)	Runoff Volume (ac-ft)	Peak Discharge (cfs)	Runoff Volume (ac-ft)
1	59	3.1	202	10.7	330	17.8	513	28.2	661	37.0	832	47.5
2	71	4.5	244	15.6	400	25.7	625	40.8	810	53.5	1,026	68.7
3	44	3.3	149	11.5	246	19.0	385	30.1	501	39.5	636	50.7
4	30	2.7	104	9.4	171	15.5	269	24.6	351	32.3	447	41.4
5	42	3.5	143	12.1	235	20.0	370	31.7	482	41.6	614	53.4
6	27	1.5	91	5.3	149	8.8	232	13.9	299	18.3	378	23.4
7	51	4.0	174	13.7	286	22.6	448	35.9	582	47.1	741	60.4
8	64	7.4	219	25.6	362	42.3	570	67.1	746	88.1	952	113.0

Table D.5.	Computed peak flows and runoff volumes for Arroyo de los Pinos for the 2-, 5-, 10-, 25-, 50- and 100-year return intervals.											
	2-Year		5-Year		10-Year		25-Year		50-Year		100-Year	
Subbasin	Peak Discharge (cfs)	Runoff Volume (ac-ft)	Peak Discharge (cfs)	Runoff Volume (ac-ft)	Peak Discharge (cfs)	Runoff Volume (ac-ft)	Peak Discharge (cfs)	Runoff Volume (ac-ft)	Peak Discharge (cfs)	Runoff Volume (ac-ft)	Peak Discharge (cfs)	Runoff Volume (ac-ft)
1	59	4.2	239	17.3	396	28.8	637	46.7	827	61.3	1,051	78.8
2	15	1.4	62	5.9	102	9.8	165	15.9	216	20.8	276	26.7
3	12	1.1	49	4.3	82	7.2	132	11.7	173	15.4	220	19.8
4	36	2.8	148	11.6	245	19.4	395	31.5	514	41.4	654	53.2
5	31	3.3	128	13.3	212	22.2	343	36.2	448	47.4	572	60.9
6	51	3.9	209	16.1	347	26.8	560	43.6	728	57.1	926	73.4
7	11	0.9	44	3.7	74	6.1	119	10.0	154	13.1	197	16.8
8	14	1.2	56	4.7	94	7.9	151	12.8	197	16.8	251	21.6
9	38	3.8	154	15.6	256	26.0	414	42.2	540	55.4	690	71.2
10	27	2.6	112	10.8	186	18.0	300	29.3	392	38.4	500	49.4
11	51	4.6	210	18.9	348	31.5	563	51.3	733	67.3	935	86.4

Mussetter Engineering, Inc.

Table D.6.		Computed peak flows and runoff volumes for Arroyo de la Presilla for the 2-, 5-, 10-, 25-, 50- and 100-year return intervals.										
	2-Year		5-Year		10-Year		25-Year		50-Year		100-Year	
Subbasin	Peak Discharge (cfs)	Runoff Volume (ac-ft)	Peak Discharge (cfs)	Runoff Volume (ac-ft)	Peak Discharge (cfs)	Runoff Volume (ac-ft)	Peak Discharge (cfs)	Runoff Volume (ac-ft)	Peak Discharge (cfs)	Runoff Volume (ac-ft)	Peak Discharge (cfs)	Runoff Volume (ac-ft)
1	92	8.6	399	37.3	675	63.3	1,096	103.5	1,432	136.2	1,845	176.8
2	74	9.6	321	41.6	544	70.6	887	115.5	1,162	151.9	1,503	197.2
3	31	2.7	135	11.6	229	19.7	371	32.2	485	42.3	625	54.9
4	57	13.6	246	59.1	416	100.3	680	164.0	894	215.7	1,159	280.0

Table D.7.		Computed peak flows and runoff volumes for Arroyo de las Canas for the 2-, 5-, 10-, 25-, 50- and 100-year return intervals.										
	2-Year		5-Year		10-Year		25-Year		50-Year		100-Year	
Subbasin	Peak Discharge (cfs)	Runoff Volume (ac-ft)	Peak Discharge (cfs)	Runoff Volume (ac-ft)	Peak Discharge (cfs)	Runoff Volume (ac-ft)	Peak Discharge (cfs)	Runoff Volume (ac-ft)	Peak Discharge (cfs)	Runoff Volume (ac-ft)	Peak Discharge (cfs)	Runoff Volume (ac-ft)
1	30	2.1	183	12.6	314	21.6	530	37.0	706	49.7	910	64.8
2	24	2.2	144	13.5	247	23.3	420	39.8	561	53.5	726	69.7
3	76	6.0	465	36.8	797	63.4	1,351	108.4	1,804	145.6	2,330	189.9
4	19	1.6	113	10.0	194	17.3	330	29.5	440	39.7	569	51.7
5	37	6.7	225	40.6	387	69.9	660	119.5	886	160.6	1,153	209.4
6	39	4.7	236	28.6	406	49.3	692	84.3	927	113.3	1,203	147.7
7	22	3.0	134	18.1	230	31.1	392	53.2	526	71.6	683	93.3
8	16	1.1	100	6.9	172	11.8	290	20.2	386	27.1	496	35.3
9	16	1.4	95	8.4	163	14.5	277	24.8	370	33.4	478	43.5
10	32	7.0	196	42.4	338	72.9	577	124.7	774	167.7	1,008	218.5

Mussetter Engineering, Inc.

Subbasin	2-Year Peak Discharge (cfs)	2-Year Runoff Volume (ac-ft)	5-Year Peak Discharge (cfs)	5-Year Runoff Volume (ac-ft)	10-Year Peak Discharge (cfs)	10-Year Runoff Volume (ac-ft)	25-Year Peak Discharge (cfs)	25-Year Runoff Volume (ac-ft)	50-Year Peak Discharge (cfs)	50-Year Runoff Volume (ac-ft)	100-Year Peak Discharge (cfs)	100-Year Runoff Volume (ac-ft)
Table D.8. Computed peak flows and runoff volumes for Arroyo de Alamillo for the 2-, 5-, 10-, 25-, 50- and 100-year return intervals.												
1	14	1.7	350	43.7	659	82.3	1,123	140.8	1,524	191.6	2,000	252.8
2	6	0.8	147	21.3	276	40.1	472	68.6	640	93.4	842	123.2
3	5	0.5	114	11.9	215	22.4	365	38.3	495	52.1	648	68.8
4	7	0.6	172	14.3	323	26.9	548	46	740	62.6	966	82.6
5	7	0.8	183	20.6	345	38.8	587	66.3	796	90.3	1,043	119.1
6	4	0.5	108	13.1	204	24.8	348	42.4	472	57.7	619	76.1
7	16	2.8	407	69.2	766	130.5	1,307	223.2	1,777	303.9	2,337	400.9
8	6	0.9	138	22.8	260	43	444	73.6	604	100.2	794	132.1
9	4	0.4	102	9.6	192	18	326	30.8	441	41.9	577	55.3
10	10	1	248	25.1	467	47.3	794	80.9	1,076	110.1	1,408	145.3
11	2	0.2	55	3.8	103	7.2	174	12.4	234	16.8	304	22.2
12	9	1.8	237	46	446	86.8	762	148.4	1,035	202	1,363	266.5

Subbasin	2-Year		5-Year		10-Year		25-Year		50-Year		100-Year	
	Peak Discharge (cfs)	Runoff Volume (ac-ft)	Peak Discharge (cfs)	Runoff Volume (ac-ft)	Peak Discharge (cfs)	Runoff Volume (ac-ft)	Peak Discharge (cfs)	Runoff Volume (ac-ft)	Peak Discharge (cfs)	Runoff Volume (ac-ft)	Peak Discharge (cfs)	Runoff Volume (ac-ft)
1	26	2.8	479	51.6	896	96.6	1,538	166.4	2,080	225.9	2,714	296.1
2	13	1.1	234	19.6	438	36.7	751	63.3	1,012	85.9	1,317	112.6
3	19	1.2	352	22.5	656	42.2	1,120	72.6	1,506	98.6	1,954	129.3
4	11	1.7	192	30.4	359	57	617	98.1	836	133.2	1,093	174.6
5	5	1.2	91	21.2	171	39.7	294	68.4	399	92.9	522	121.8
6	14	1.4	261	24.5	487	45.8	835	78.9	1,128	107.2	1,469	140.5
7	7	0.6	120	10.1	225	18.9	385	32.5	519	44.1	676	57.8
8	4	0.5	69	9.9	129	18.6	221	32	300	43.5	392	57
9	0	0.1	7	1	13	1.9	22	3.2	30	4.4	40	5.7
10	15	1.6	269	29.3	504	54.9	865	94.5	1,169	128.3	1,525	168.3
11	2	0.3	44	6.1	82	11.3	140	19.5	190	26.5	249	34.8
12	4	0.4	64	7.6	120	14.3	207	24.6	279	33.3	365	43.7
13	74	1.6	1,347	29.8	2,433	55.7	3,991	96	5,145	130.3	6,418	170.8

Table D.9.   Computed peak flows and runoff volumes for Arroyo de la Parida for the 2-, 5-, 10-, 25-, 50- and 100-year return intervals.

Mussetter Engineering, Inc.

Subbasin	2-Year Peak Discharge (cfs)	2-Year Runoff Volume (ac-ft)	5-Year Peak Discharge (cfs)	5-Year Runoff Volume (ac-ft)	10-Year Peak Discharge (cfs)	10-Year Runoff Volume (ac-ft)	25-Year Peak Discharge (cfs)	25-Year Runoff Volume (ac-ft)	50-Year Peak Discharge (cfs)	50-Year Runoff Volume (ac-ft)	100-Year Peak Discharge (cfs)	100-Year Runoff Volume (ac-ft)
1	7	0.3	180	18.7	346	36.1	632	66.0	890	93.5	1,226	130
2	1	0.2	71	9.9	136	19.1	249	34.9	352	49.4	486	68.6
3	5	0.5	206	26.7	397	51.6	726	94.4	1,025	133.8	1,417	185.7
4	5	0.6	227	31.1	438	60.0	801	109.9	1,132	155.7	1,564	216.1
5	5	0.6	243	30.2	468	58.3	855	106.7	1,207	151.2	1,666	209.9
6	2	0.2	105	11.9	202	23.1	369	42.2	521	59.8	718	83.0
7	3	0.3	116	17.6	225	33.9	410	62.0	580	87.9	803	122.0
8	3	0.3	94	18.7	181	36.0	331	65.9	469	93.5	649	129.7
9	5	0.3	138	17.8	265	34.3	485	62.8	685	89.0	945	123.6
10	1	0.2	88	9.7	169	18.7	309	34.2	436	48.5	601	67.3
11	0	0.0	31	0.8	59	1.6	103	3.0	139	4.3	183	5.9
12	1	0.1	69	3.6	132	6.9	238	12.6	332	17.9	450	24.9
13	3	0.3	120	16.8	232	32.5	424	59.4	599	84.2	828	116.9
14	0	0.1	46	4.8	89	9.2	162	16.9	228	24.0	314	33.2
15	4	0.5	226	24.6	435	47.5	793	87.0	1,118	123.3	1,541	171.1
16	10	0.3	128	15.1	246	29.2	450	53.5	635	75.8	875	105.2
17	1	0.1	58	7.0	111	13.5	203	24.7	287	35.0	396	48.6
18	2	0.3	103	15.1	199	29.1	364	53.3	515	75.6	712	104.9
19	1	0.1	62	4.2	118	8.1	215	14.9	301	21.1	412	29.3

Table D.10.   Computed peak flows and runoff volumes for San Pedro Arroyo for the 2-, 5-, 10-, 25-, 50- and 100-year return intervals.

Mussetter Engineering, Inc.

APPENDIX E
Hydrographs for Tributary Basins
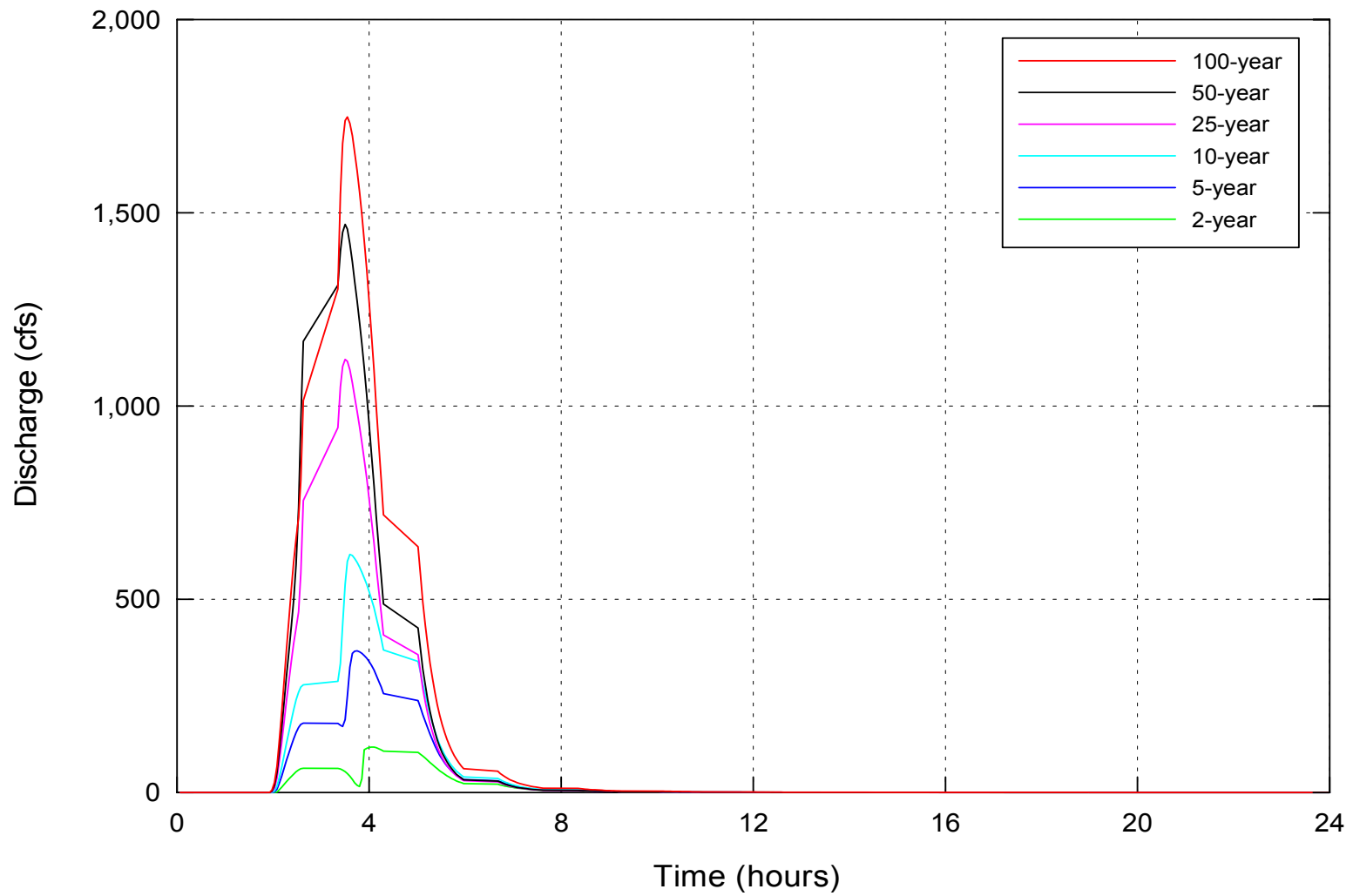
Figure E.1.   Computed hydrographs at Arroyo Sevilleta for the 2-, 5-, 10-, 25-, 50-, and 100-year events.

E.1
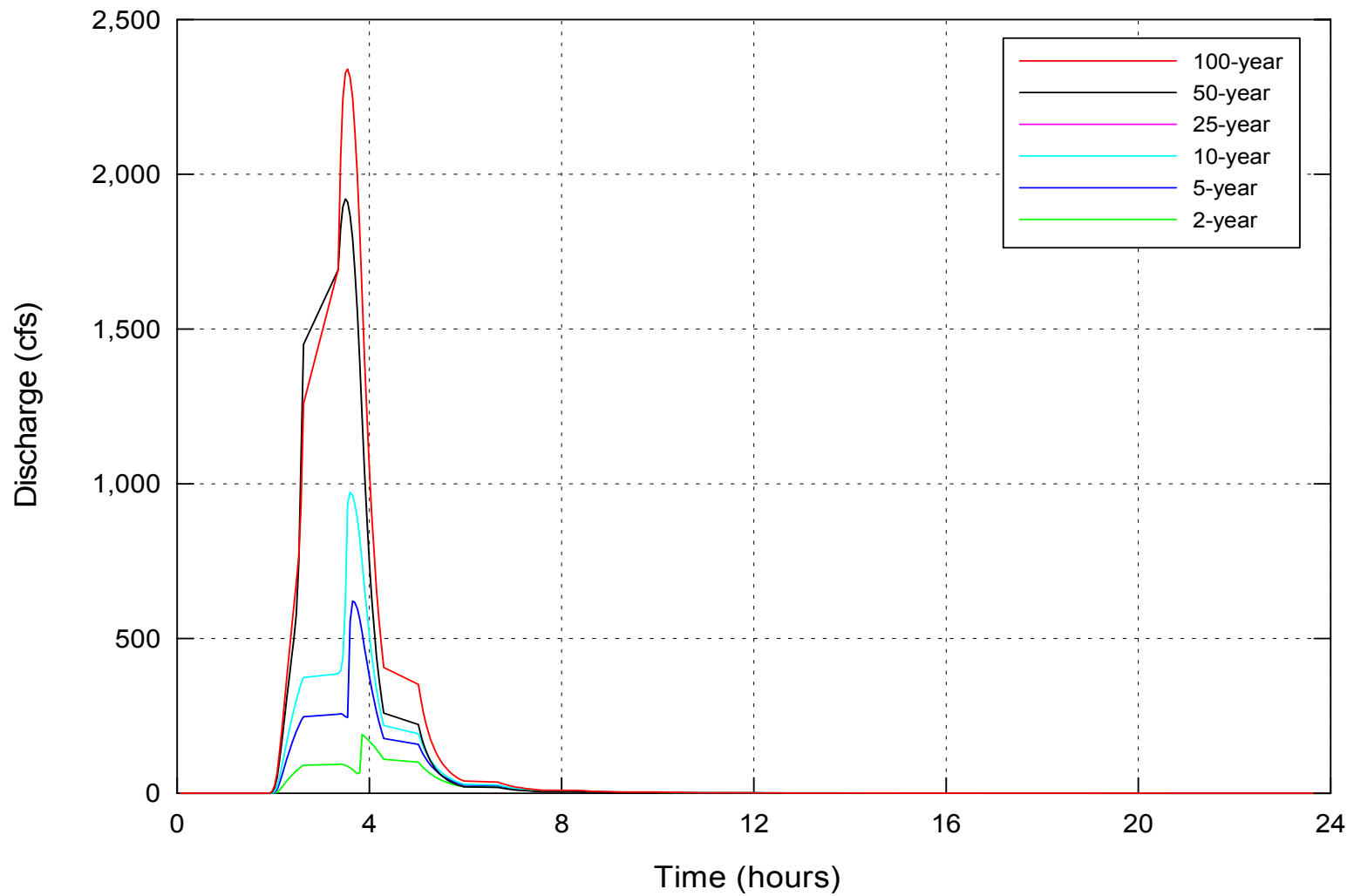
Figure E.2.   Computed hydrographs at Arroyo de Tio Bartolo for the 2-, 5-, 10-, 25-, 50-, and 100-year events.

Mussetter Engineering, Inc.
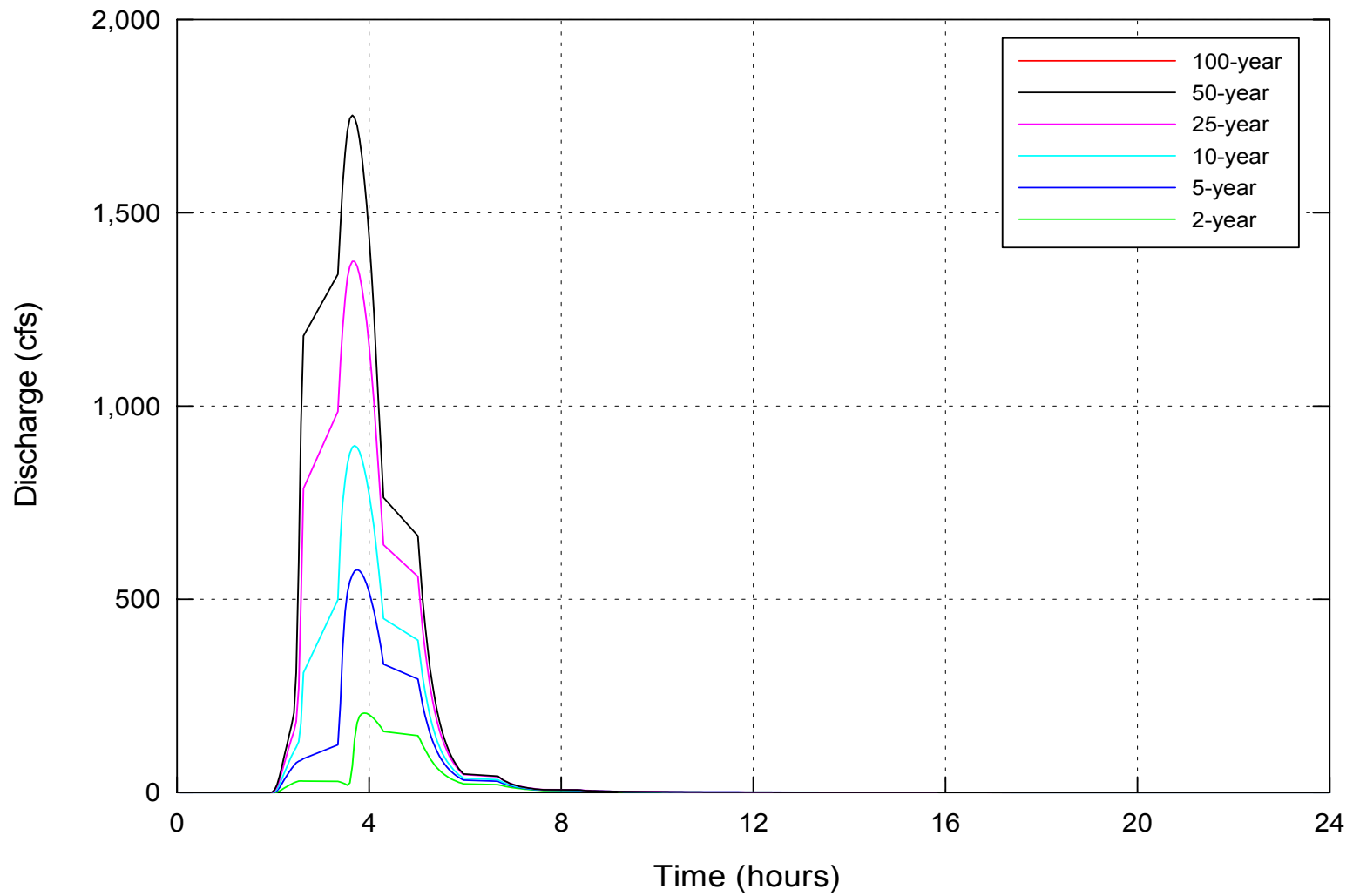
Figure E.3.   Computed hydrographs at Arroyo del Coyote for the 2-, 5-, 10-, 25-, 50-, and 100-year events.

E.3
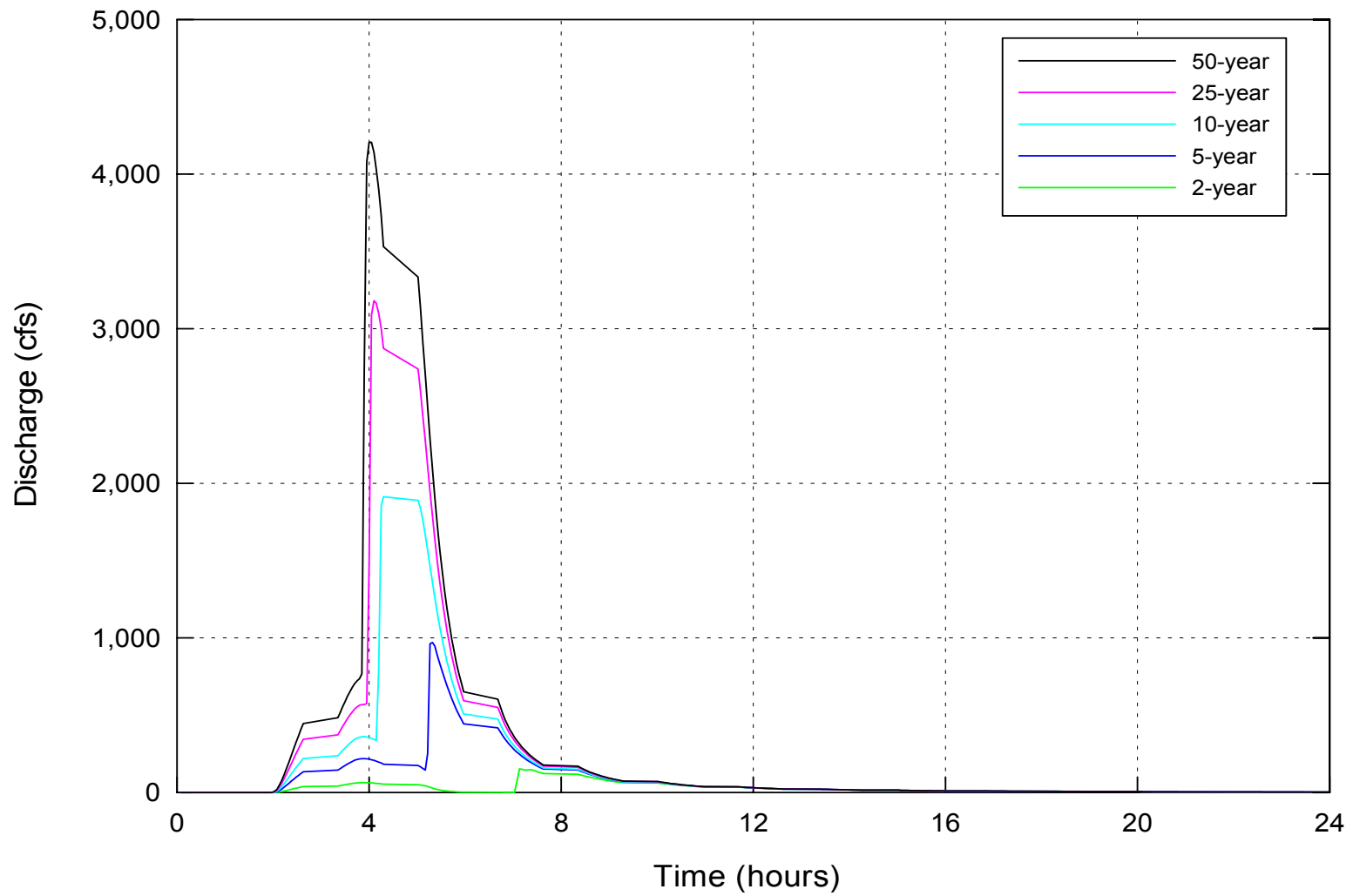
Figure E.4.   Computed hydrographs at Arroyo del Tajo for the 2-, 5-, 10-, 25-, 50-, and 100-year events.

Mussetter Engineering, Inc.
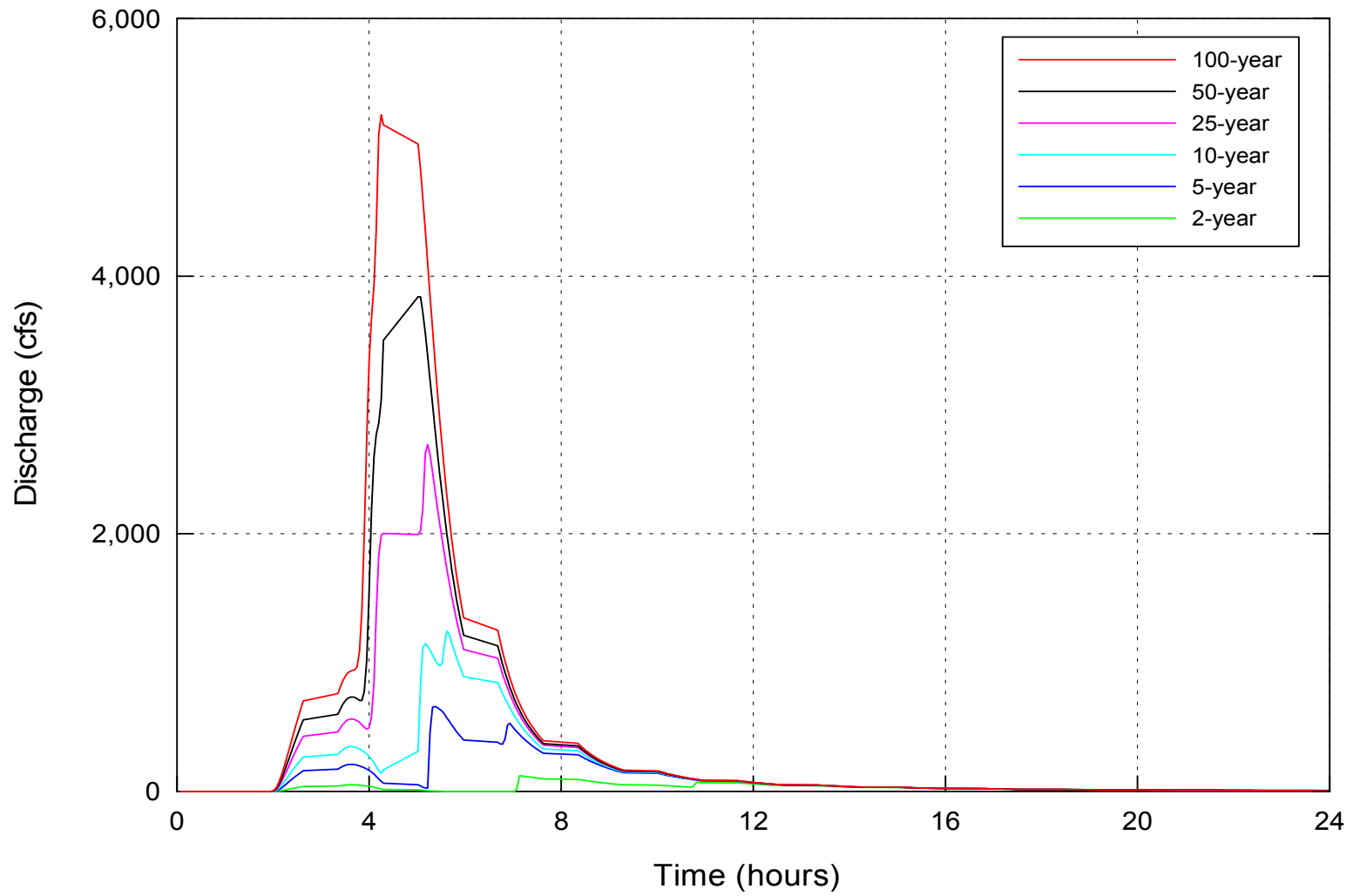
Figure E.5. Computed hydrographs at Arroyo de los Pinos for the 2-, 5-, 10-, 25-, 50-, and 100-year events.

Mussetter Engineering, Inc.
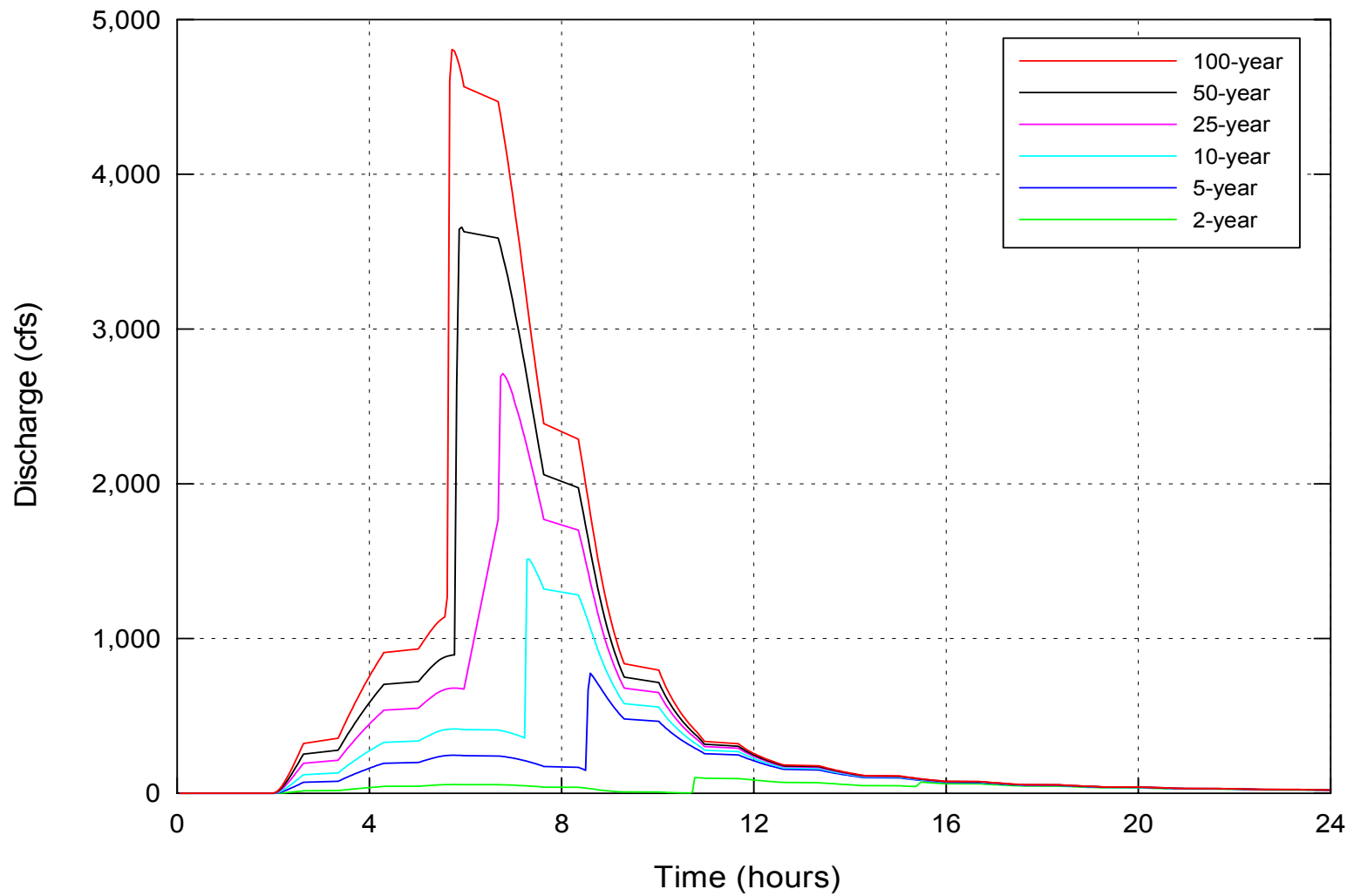
Figure E.6.   Computed hydrographs at Arroyo de la Presilla for the 2-, 5-, 10-, 25-, 50-, and 100-year events.

Mussetter Engineering, Inc.
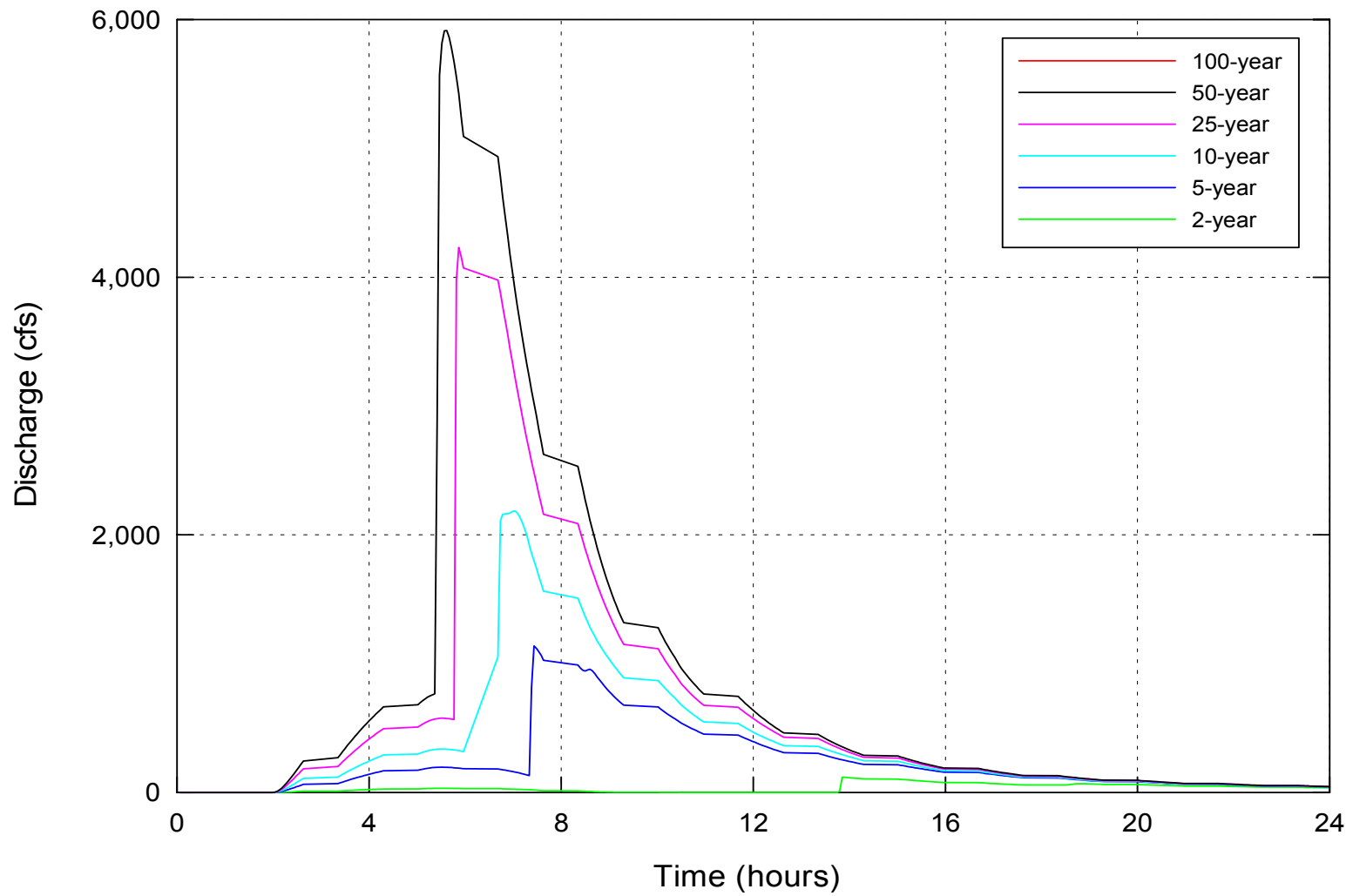
Figure E.7.   Computed hydrographs at Arroyo de las Canas for the 2-, 5-, 10-, 25-, 50-, and 100-year events.

Mussetter Engineering, Inc.
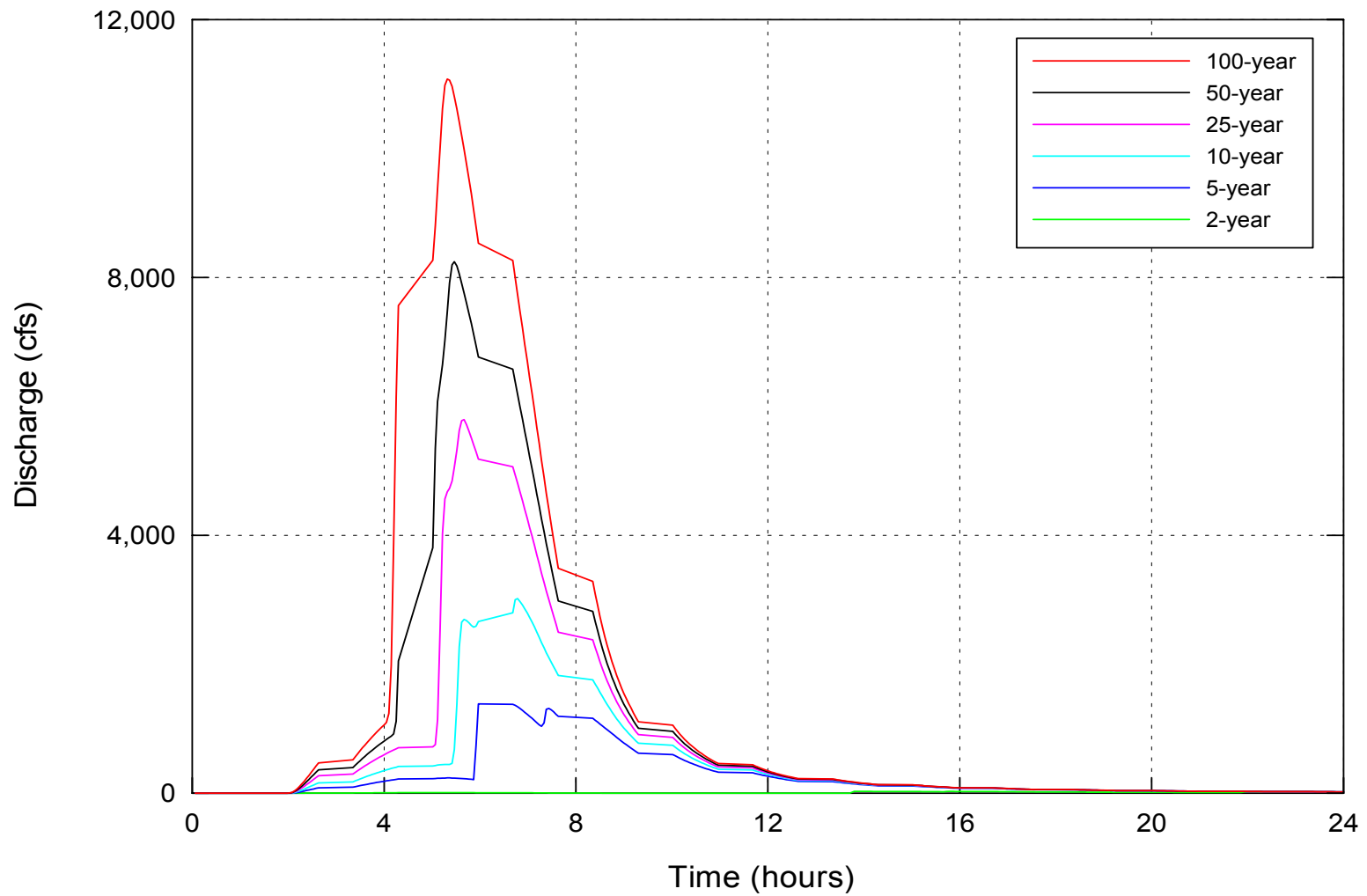
Figure E.8.   Computed hydrographs at Arroyo de Alamillo for the 2-, 5-, 10-, 25-, 50-, and 100-year events.

Mussetter Engineering, Inc.
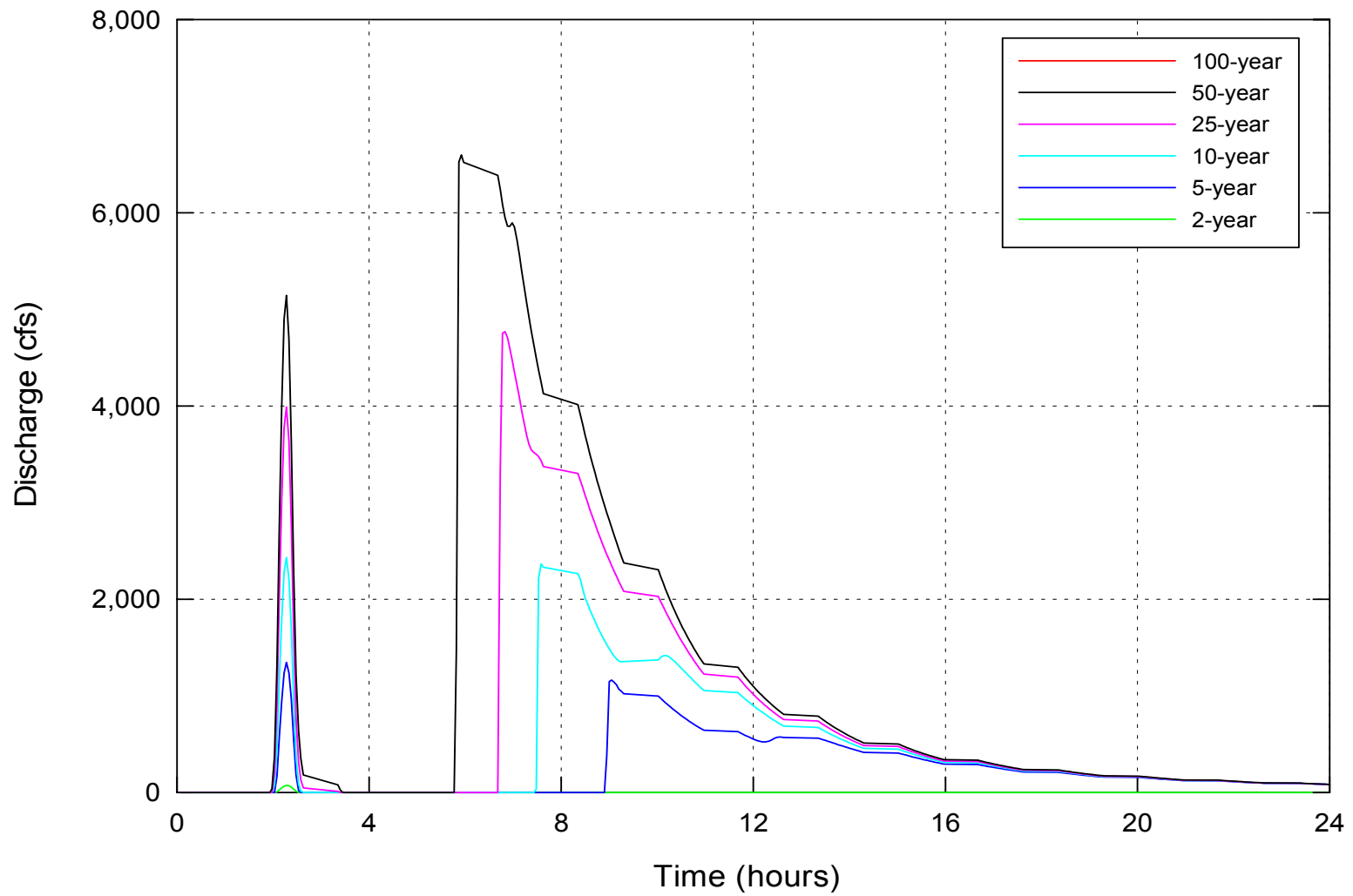
Figure E.9.   Computed hydrographs at Arroyo de la Parida for the 2-, 5-, 10-, 25-, 50-, and 100-year events.

E.9
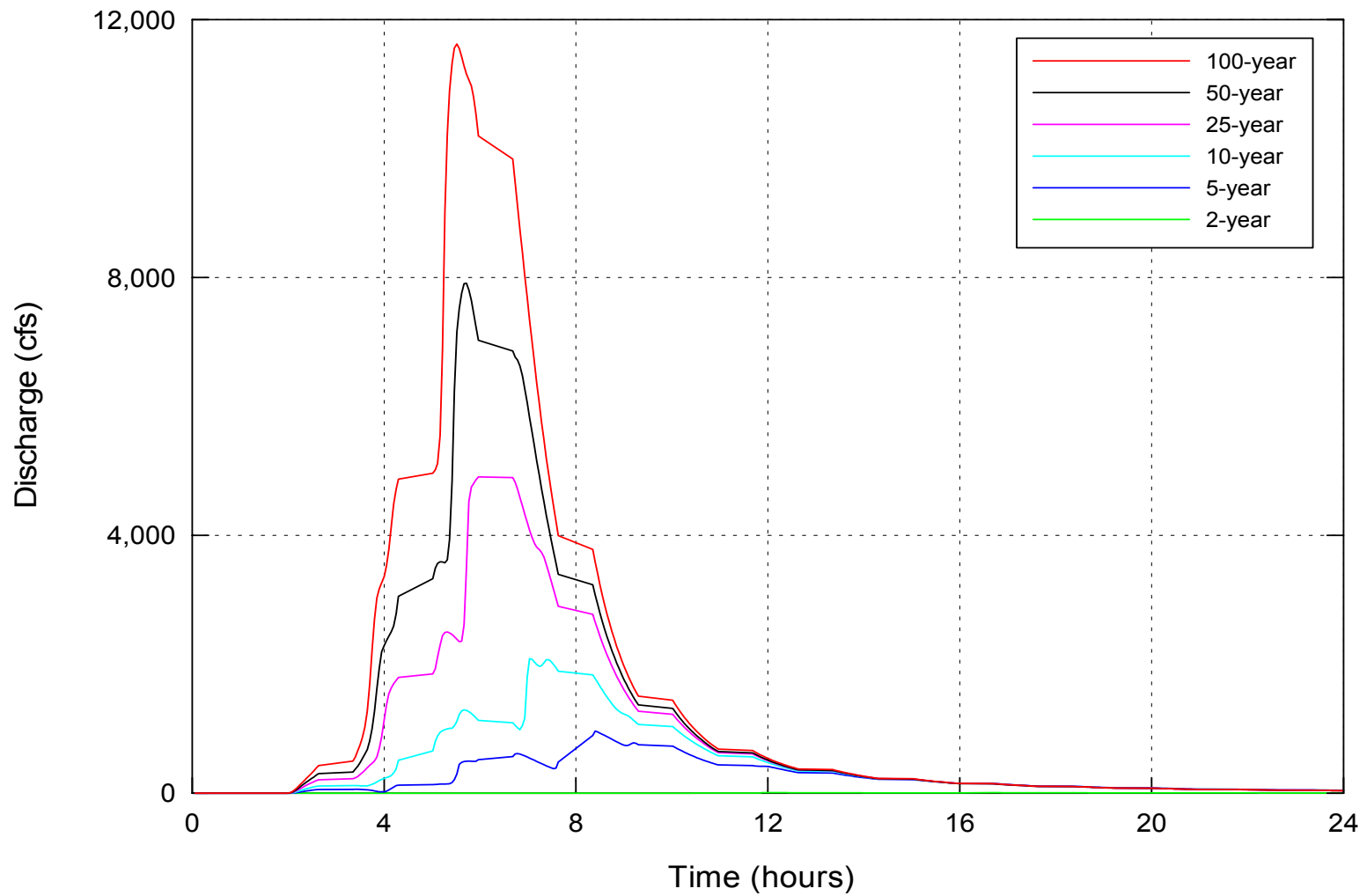
Figure E.10.   Computed hydrographs at San Pedro Arroyo for the 2-, 5-, 10-, 25-, 50-, and 100-year events.

Mussetter Engineering, Inc.

APPENDIX F
MUSLE Parameters for the Tributary Basins

Mussetter Engineering, Inc.

Table F.1.				Summary of MUSLE parameters Arroyo de Tio Bartolo.				
Subbasin	K	S (%)	n	L (ft)	LS	C	P	Percent Silt/ Clay (<#200 Sieve)
1	0.11	16.59	0.5	200	4.32	0.20	1.00	0.23
2	0.11	13.97	0.5	200	3.26	0.20	1.00	0.23
3	0.11	12.83	0.5	200	2.84	0.20	1.00	0.23

Table F.2.				Summary of MUSLE parameters Arroyo Sevilleta.				
Subbasin	K	S (%)	n	L (ft)	LS	C	P	Percent Silt/ Clay (<#200 Sieve)
1	0.17	5.32	0.5	210	0.83	0.20	1.00	0.10
2	0.17	5.06	0.5	210	0.78	0.20	1.00	0.10
3	0.17	7.00	0.5	210	1.19	0.20	1.00	0.10

Table F.3.				Summary of MUSLE parameters Arroyo del Coyote.				
Subbasin	K	S (%)	n	L (ft)	LS	C	P	Percent Silt/ Clay (<#200 Sieve)
1	0.11	14.06	0.5	180	3.12	0.20	1.00	0.22
2	0.11	13.48	0.5	180	2.92	0.20	1.00	0.22
3	0.11	8.53	0.5	100	0.00	0.20	1.00	0.22

Table F.4.				Summary of MUSLE parameters Arroyo del Tajo.				
Subbasin	K	S (%)	n	L (ft)	LS	C	P	Percent Silt/ Clay (<#200 Sieve)
1	0.12	22.40	0.5	170	6.63	0.20	1.00	0.23
2	0.14	19.45	0.5	180	5.35	0.20	1.00	0.23
3	0.10	15.80	0.5	200	3.98	0.20	1.00	0.38
4	0.13	15.16	0.5	200	3.72	0.20	1.00	0.26
5	0.10	20.03	0.5	200	5.93	0.20	1.00	0.31
6	0.10	19.21	0.5	180	5.24	0.20	1.00	0.23
7	0.10	13.96	0.5	180	3.09	0.20	1.00	0.24
8	0.11	10.03	0.5	210	1.99	0.20	1.00	0.17

Mussetter Engineering, Inc.

Table F.5.	Summary of MUSLE parameters Arroyo de la Presilla.							
Subbasin	K	S (%)	n	L (ft)	LS	C	P	Percent Silt/ Clay (<#200 Sieve)
1	0.11	15.65	0.5	190	3.82	0.20	1.00	0.26
2	0.11	14.31	0.5	215	3.51	0.20	1.00	0.26
3	0.11	17.55	0.5	210	4.86	0.20	1.00	0.26
4	0.11	15.33	0.5	200	3.79	0.20	1.00	0.26

Table F.6.	Summary of MUSLE parameters Arroyo de las Canas.							
Subbasin	K	S %)	n	L (ft)	LS	C	P	Percent Silt/ Clay (<#200 Sieve)
1	0.13	21.04	0.5	200	6.46	0.20	1.00	0.27
2	0.13	20.64	0.5	190	6.09	0.20	1.00	0.28
3	0.25	11.70	0.5	210	2.52	0.20	1.00	0.36
4	0.14	12.80	0.5	210	2.90	0.20	1.00	0.25
5	0.16	10.81	0.5	190	2.12	0.20	1.00	0.42
6	0.14	10.53	0.5	200	2.09	0.20	1.00	0.28
7	0.15	22.21	0.5	200	7.09	0.20	1.00	0.27
8	0.10	37.99	0.5	220	19.42	0.20	1.00	0.24
9	0.12	16.41	0.5	180	4.02	0.20	1.00	0.21

Table F.7.	Summary of MUSLE parameters Arroyo de las Pinos.							
Subbasin	K	S (%)	n	L (ft)	LS	C	P	Percent Silt/ Clay (<#200 Sieve)
1	0.10	16.84	0.5	190	4.31	0.20	1.00	0.29
2	0.10	16.84	0.5	190	4.31	0.20	1.00	0.29
3	0.10	16.84	0.5	200	4.43	0.20	1.00	0.29
4	0.10	16.84	0.5	200	4.43	0.20	1.00	0.29
5	0.10	16.84	0.5	200	4.43	0.20	1.00	0.29
6	0.10	16.84	0.5	200	4.43	0.20	1.00	0.29
7	0.10	16.84	0.5	200	4.43	0.20	1.00	0.29
8	0.10	16.84	0.5	160	3.96	0.20	1.00	0.29
9	0.10	16.84	0.5	190	4.31	0.20	1.00	0.29
10	0.10	16.84	0.5	190	4.31	0.20	1.00	0.29
11	0.10	16.84	0.5	180	4.20	0.20	1.00	0.29

Mussetter Engineering, Inc.

Table F.8.			Summary of MUSLE parameters Arroyo de Alamillo.					
Subbasin	K	S (%)	n	L (ft)	LS	C	P	Percent Silt/Clay (<#200 Sieve)
1	0.19	10.63	0.5	200	2.12	0.2	1	0.31
2	0.19	11.62	0.5	180	2.31	0.2	1	0.31
3	0.19	15.67	0.5	180	3.73	0.2	1	0.31
4	0.19	10.99	0.5	200	2.23	0.2	1	0.31
5	0.19	11.13	0.5	200	2.28	0.2	1	0.31
6	0.19	7.69	0.5	200	1.32	0.2	1	0.31
7	0.19	5.33	0.5	210	0.83	0.2	1	0.31
8	0.19	6.14	0.5	210	1	0.2	1	0.31
9	0.19	5.33	0.5	200	0.81	0.2	1	0.31
10	0.19	6.7	0.5	210	1.12	0.2	1	0.31
11	0.19	10.12	0.5	210	2.02	0.2	1	0.31
12	0.19	5.03	0.5	200	0.76	0.2	1	0.31

Table F.9.			Summary of MUSLE parameters Arroyo de la Parida.					
Subbasin	K	S (%)	n	L (ft)	LS	C	P	Percent Silt/Clay (<#200 Sieve)
1	0.12	19.75	0.5	200	5.79	0.2	1	0.35
2	0.12	20.95	0.5	180	6.08	0.2	1	0.35
3	0.12	20.95	0.5	200	6.41	0.2	1	0.35
4	0.12	14.61	0.5	200	3.5	0.2	1	0.35
5	0.12	14.92	0.5	200	3.62	0.2	1	0.35
6	0.12	11.71	0.5	180	2.34	0.2	1	0.35
7	0.12	13.79	0.5	200	3.19	0.2	1	0.35
8	0.12	16.53	0.5	190	4.18	0.2	1	0.35
9	0.12	12.65	0.5	200	2.78	0.2	1	0.35
10	0.12	7.43	0.5	200	1.26	0.2	1	0.35
11	0.12	15.99	0.5	200	4.06	0.2	1	0.35
12	0.12	7.43	0.5	200	1.26	0.2	1	0.35
13	0.12	15.93	0.5	180	3.83	0.2	1	0.35

Mussetter Engineering, Inc.

Subbasin	K	S (%)	n	L (ft)	LS	C	P	Percent Silt/ Clay (<#200 Sieve)
1	0.14	15.01	0.5	180	3.47	0.20	1.00	0.30
2	0.14	7.28	0.5	185	1.18	0.20	1.00	0.30
3	0.14	10.55	0.5	180	1.99	0.20	1.00	0.30
4	0.14	13.99	0.5	200	3.26	0.20	1.00	0.30
5	0.14	7.01	0.5	200	1.16	0.20	1.00	0.30
6	0.14	12.32	0.5	100	1.88	0.20	1.00	0.30
7	0.14	9.63	0.5	185	1.76	0.20	1.00	0.30
8	0.14	3.34	0.5	190	0.47	0.20	1.00	0.30
9	0.14	10.30	0.5	210	2.07	0.20	1.00	0.30
10	0.14	13.98	0.5	200	3.26	0.20	1.00	0.30
11	0.14	6.62	0.5	210	1.10	0.20	1.00	0.30
12	0.14	6.41	0.5	200	1.03	0.20	1.00	0.30
13	0.14	6.53	0.5	180	1.00	0.20	1.00	0.30
14	0.14	6.80	0.5	180	1.06	0.20	1.00	0.30
15	0.14	22.27	0.5	180	6.76	0.20	1.00	0.30
16	0.14	10.35	0.5	210	2.09	0.20	1.00	0.30
17	0.14	19.09	0.5	210	5.60	0.20	1.00	0.30
18	0.14	3.40	0.5	210	0.50	0.20	1.00	0.30
19	0.14	5.52	0.5	190	0.83	0.20	1.00	0.30

Table F.10.   Summary of MUSLE parameters San Pedro Arroyo.

Mussetter Engineering, Inc.

APPENDIX G
Cross-Section Location and Geometric Data for the Tributary Basins

Mussetter Engineering, Inc.
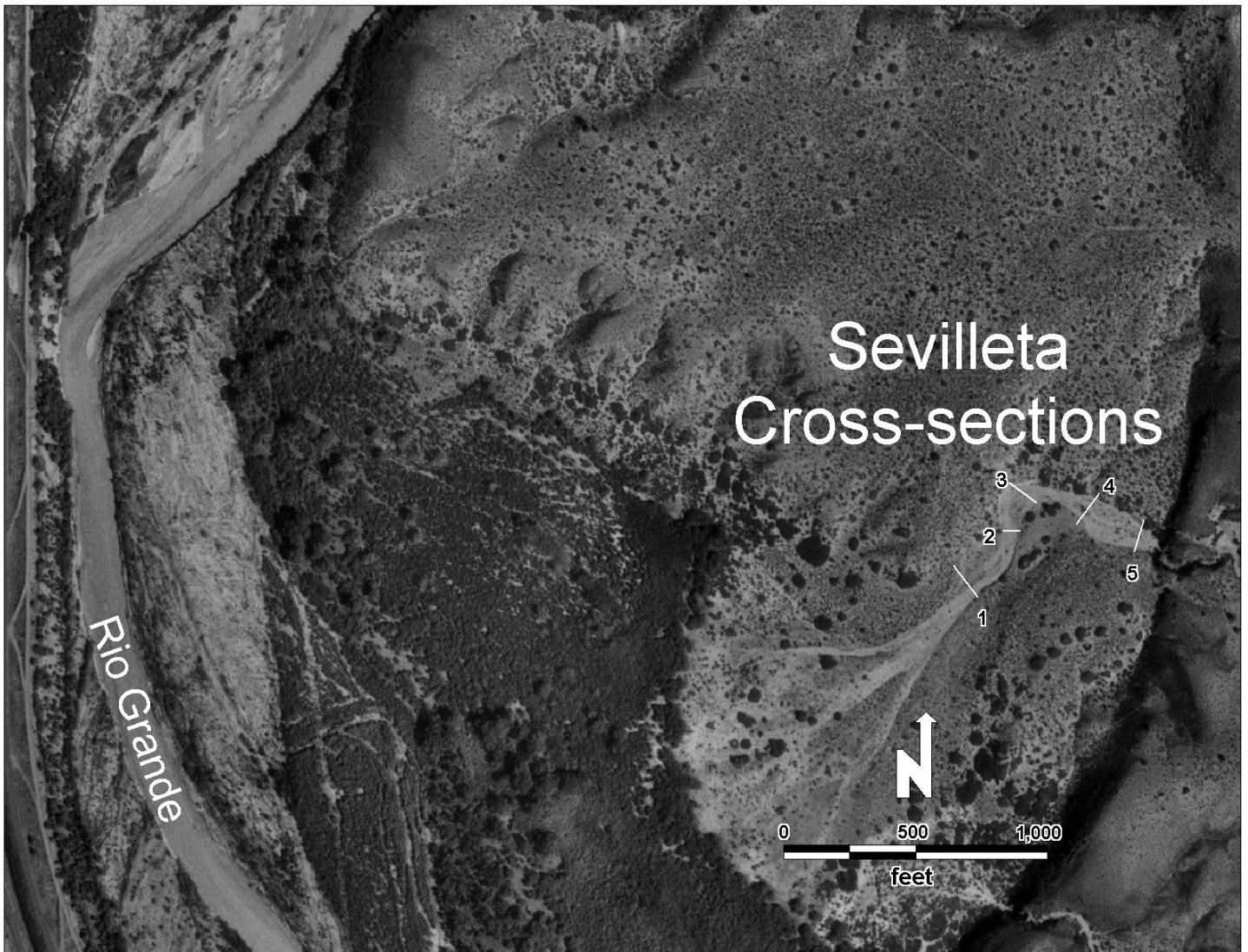
Figure G.1a.   Location of surveyed cross sections at Arroyo Sevilleta.

*M*ussetter *E*ngineering, *I*nc.
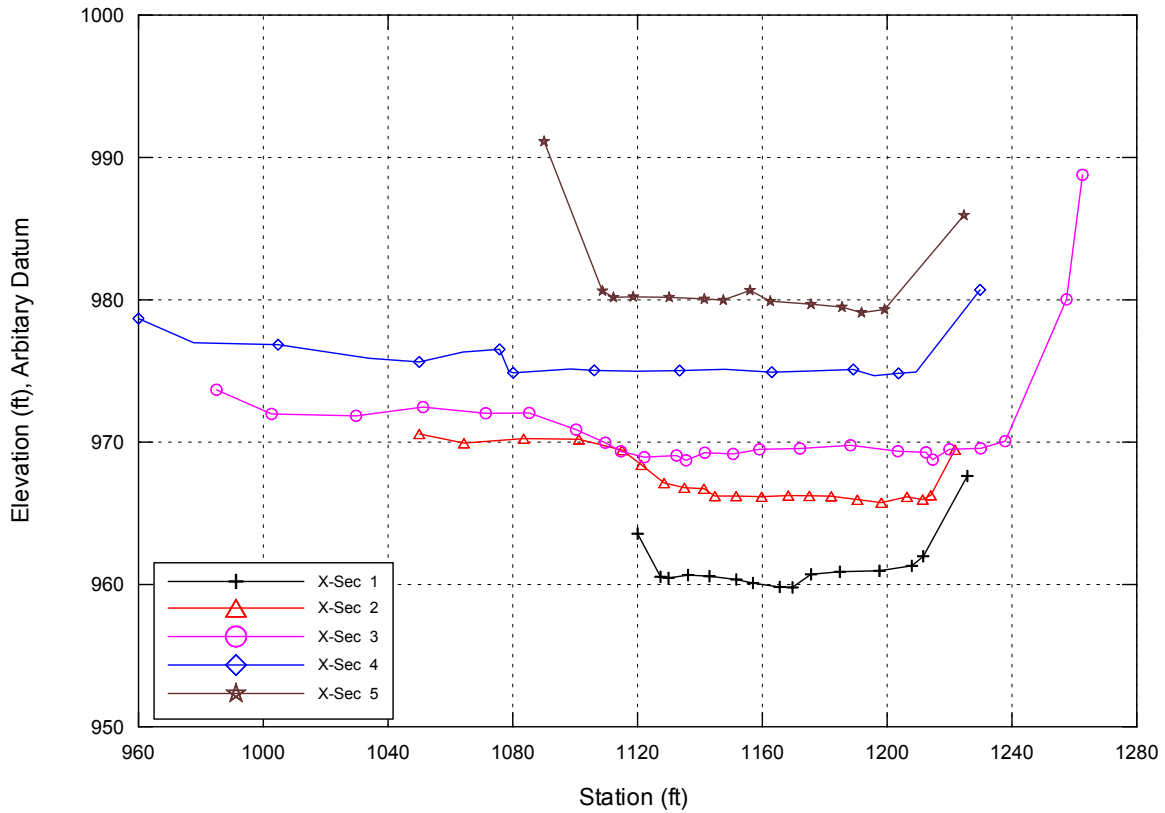
Figure G.1b.   Surveyed cross sections at Arroyo Sevilleta.
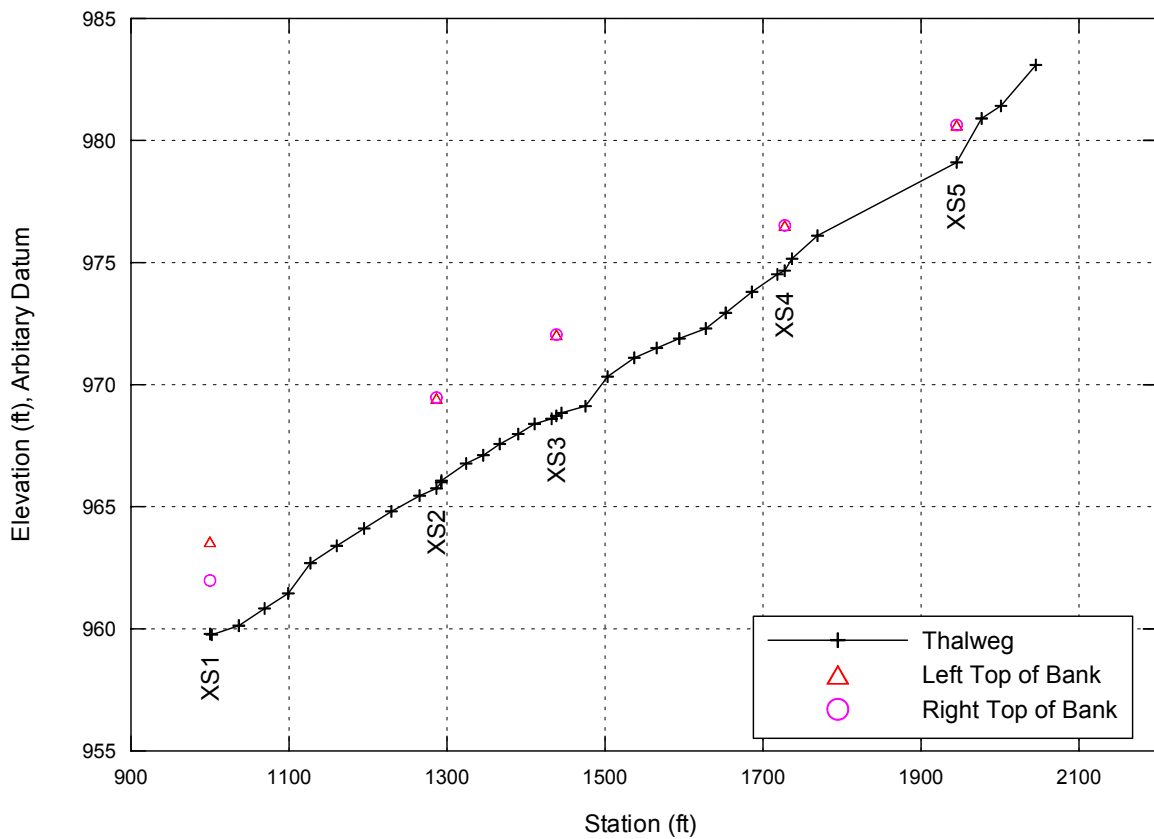
Figure G.1c.   Surveyed thalweg profile at Arroyo Sevilleta with cross-section locations.
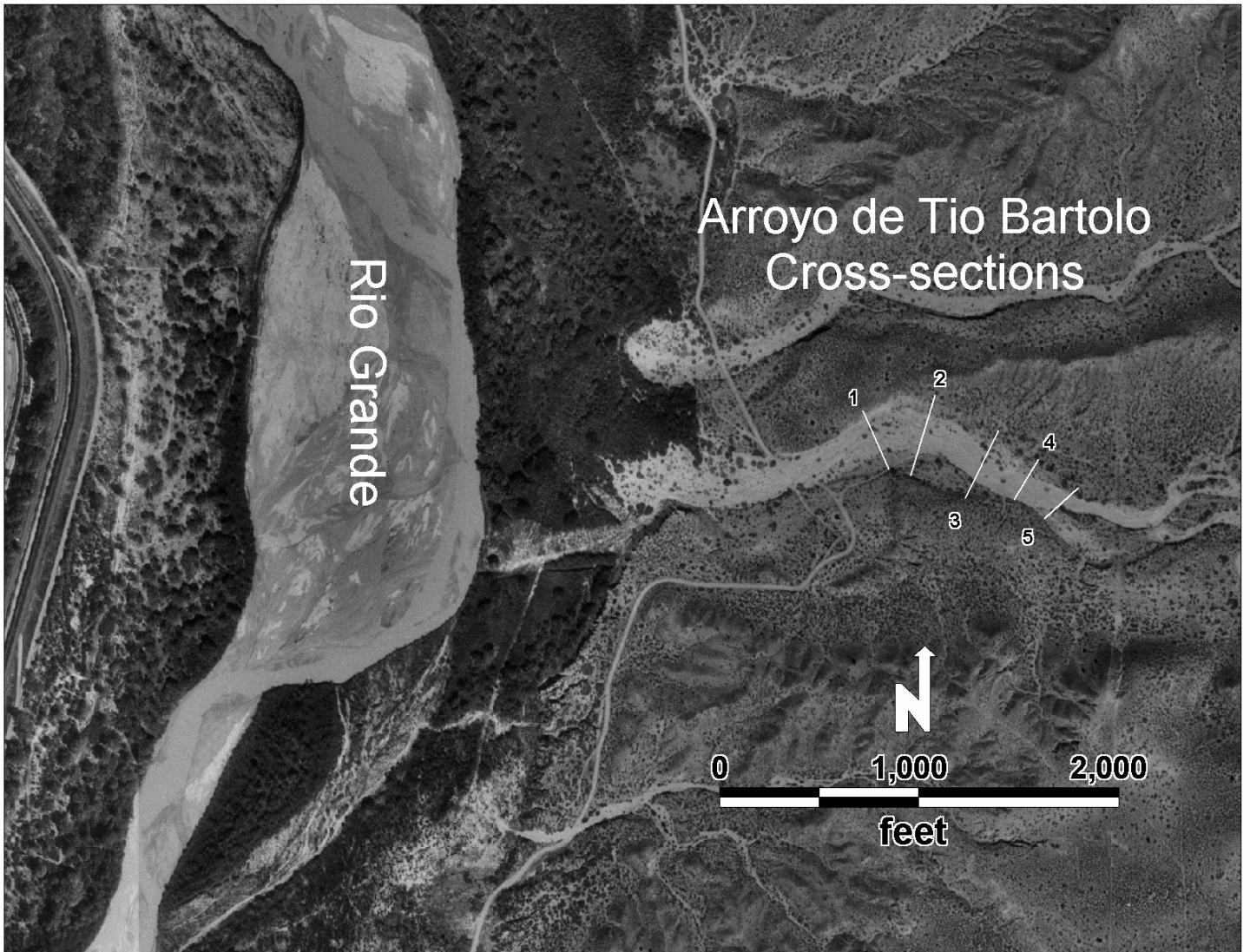
Figure G.2a.   Location of surveyed cross sections at Arroyo de Tio Bartalo.

Mussetter Engineering, Inc.
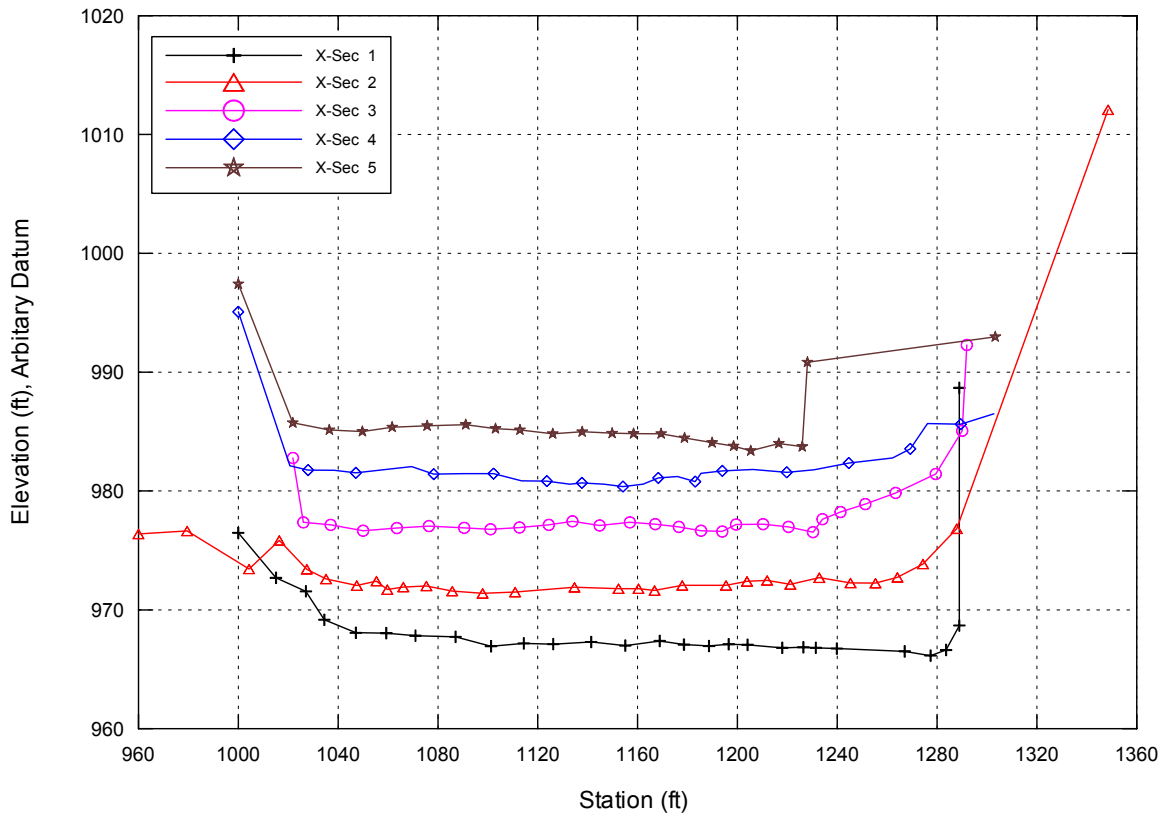
Figure G.2b.   Surveyed cross sections at Arroyo de Tio Bartalo.
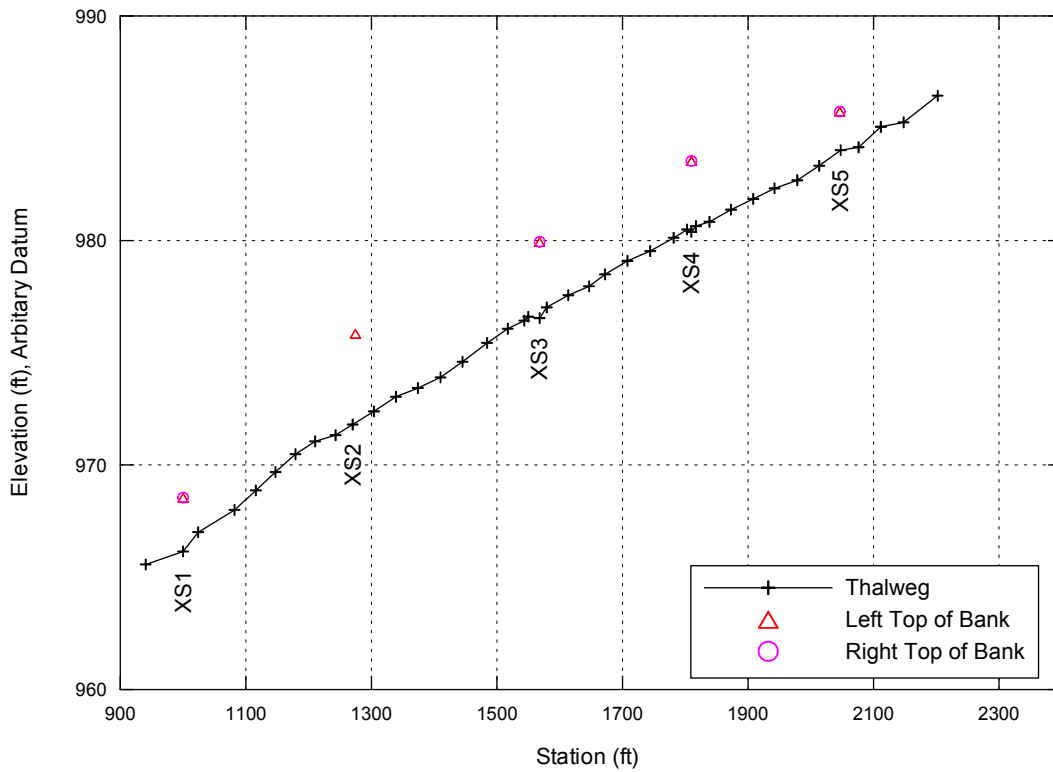
Figure G.2c.   Surveyed thalweg profile at Arroyo de Tio Bartalo with cross-section locations.

Mussetter Engineering, Inc.
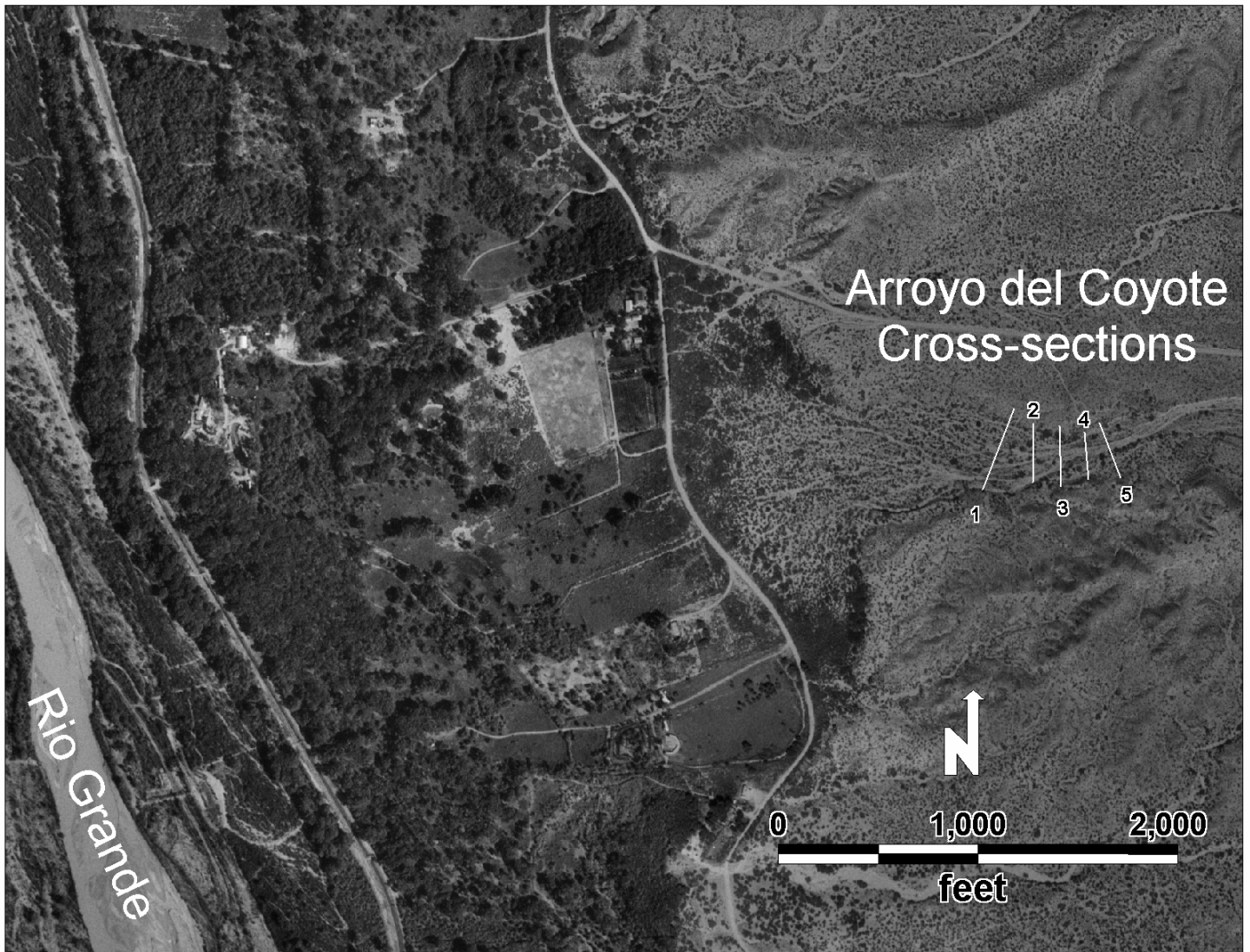
Figure G.3a.   Location of surveyed cross sections at Arroyo del Coyote.

Mussetter Engineering, Inc.
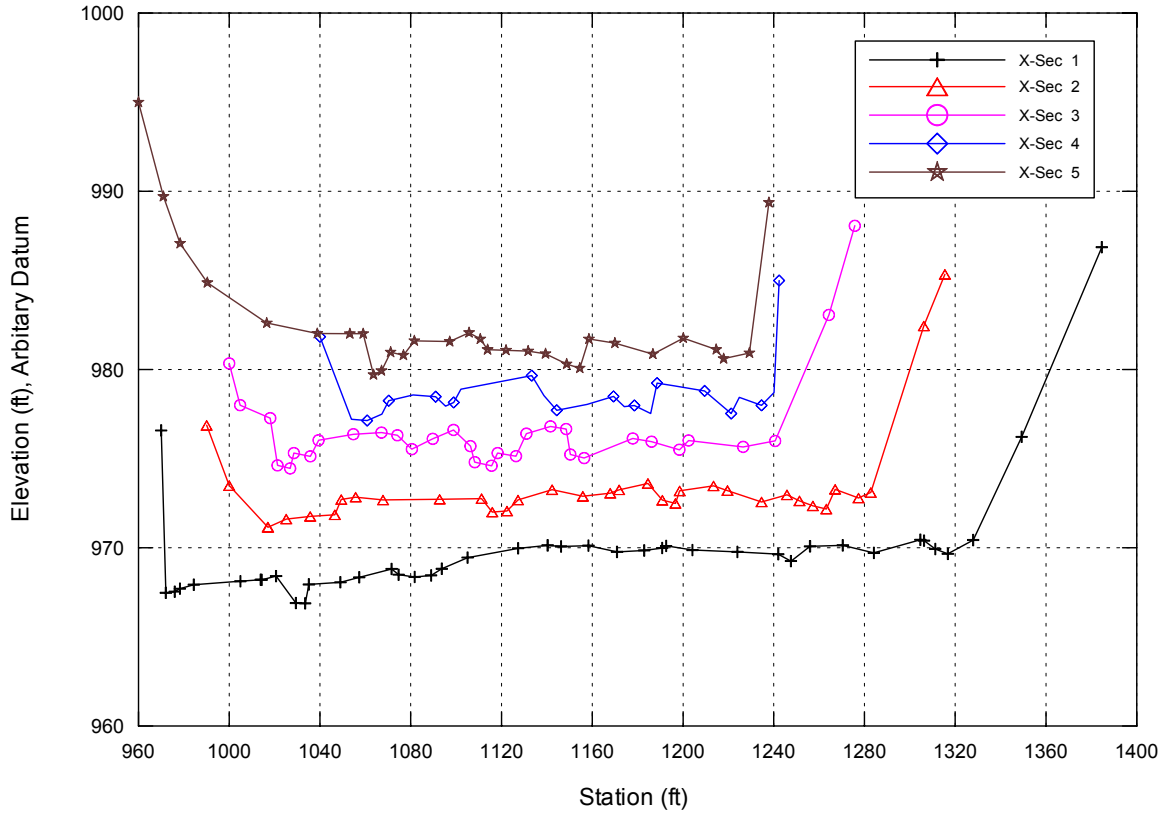
Figure G.3b. Surveyed cross sections at Arroyo del Coyote.
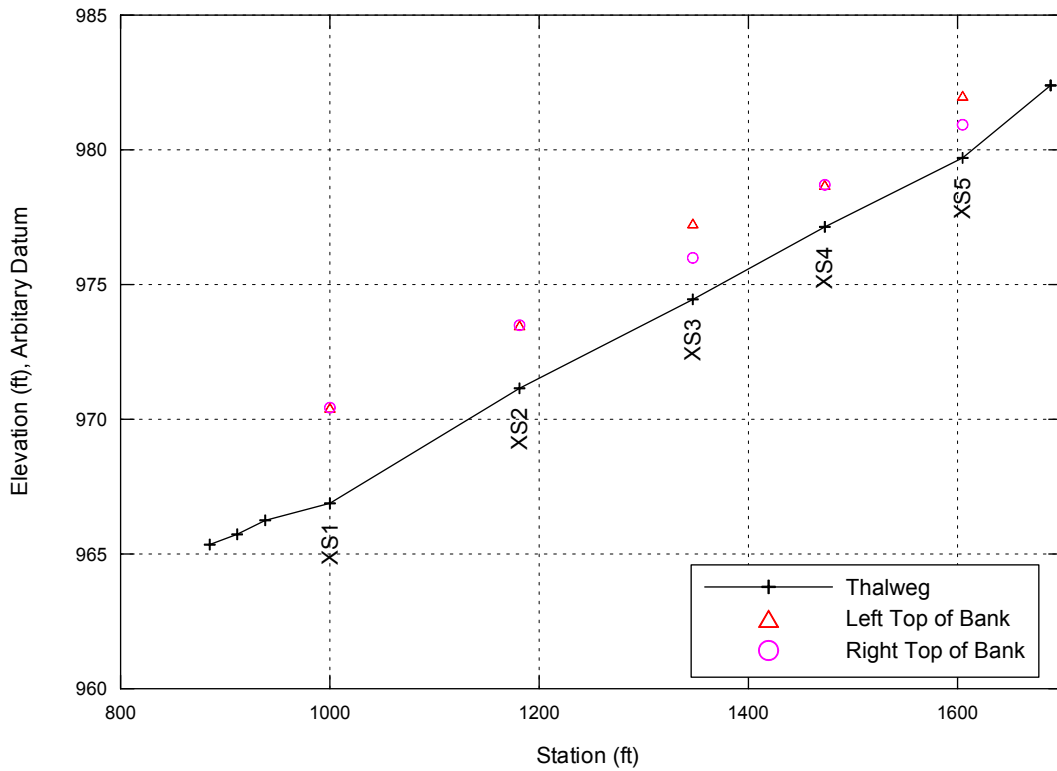
Figure G.3c.   Surveyed thalweg profile at Arroyo del Coyote with cross-section locations.

Mussetter Engineering, Inc.
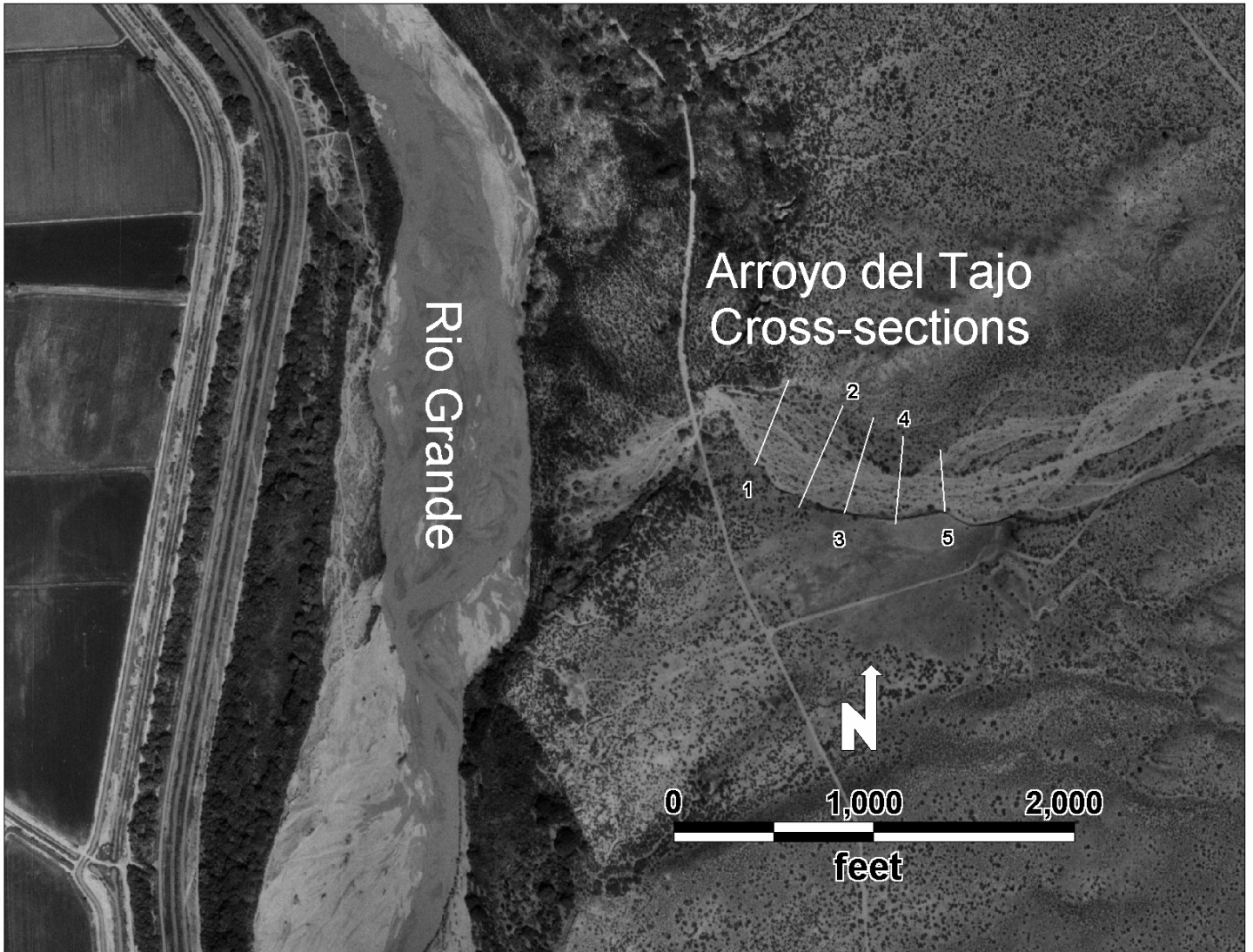
Figure G.4a.   Location of surveyed cross sections at Arroyo del Tajo.

Mussetter Engineering, Inc.
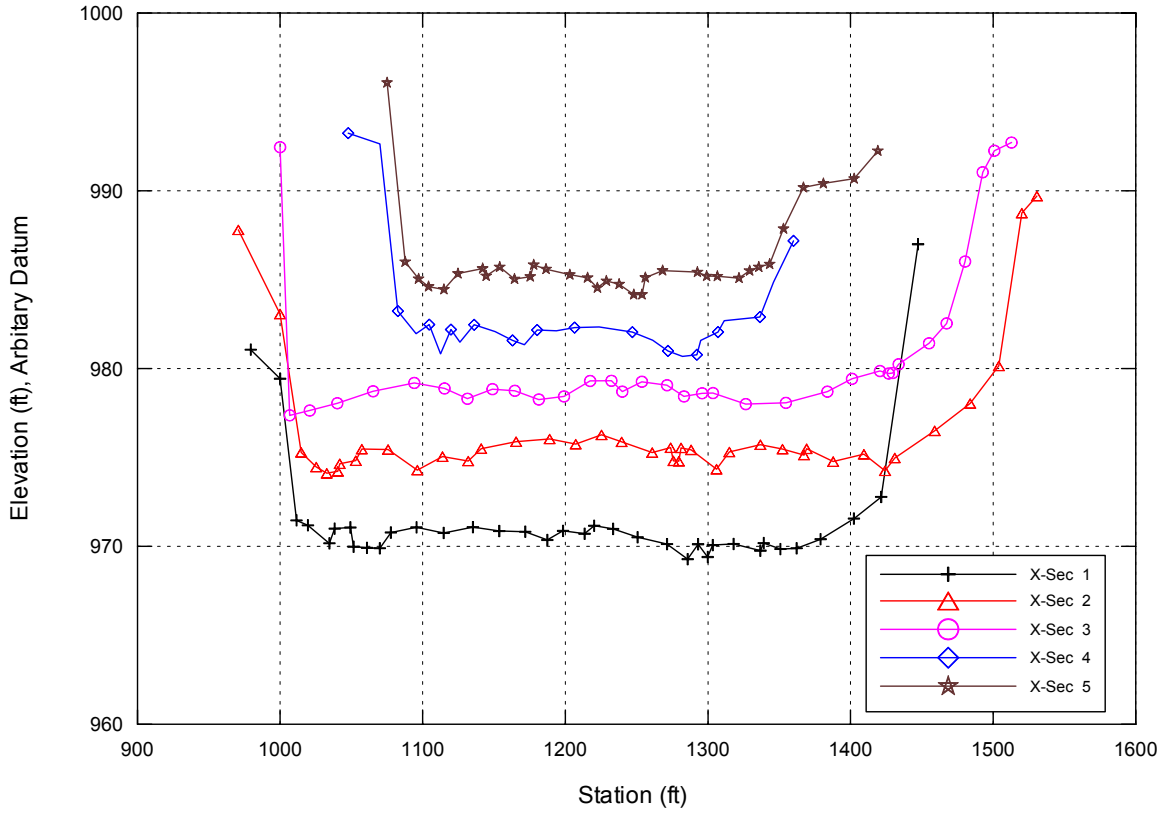
Figure G.4b.   Surveyed cross sections at Arroyo del Tajo.
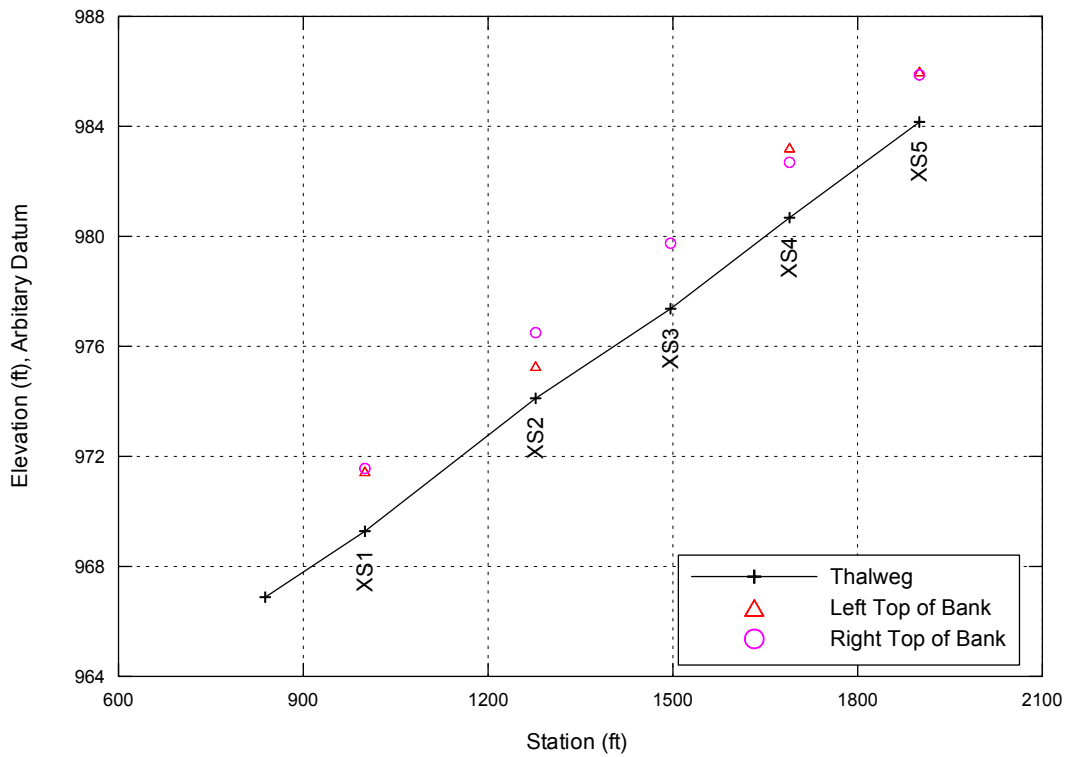
Figure G.4c.   Surveyed thalweg profile at Arroyo del Tajo with cross-section locations.

Mussetter Engineering, Inc.

Figure G.5a. Location of surveyed cross sections at Arroyo de los Pinos.

Mussetter Engineering, Inc.
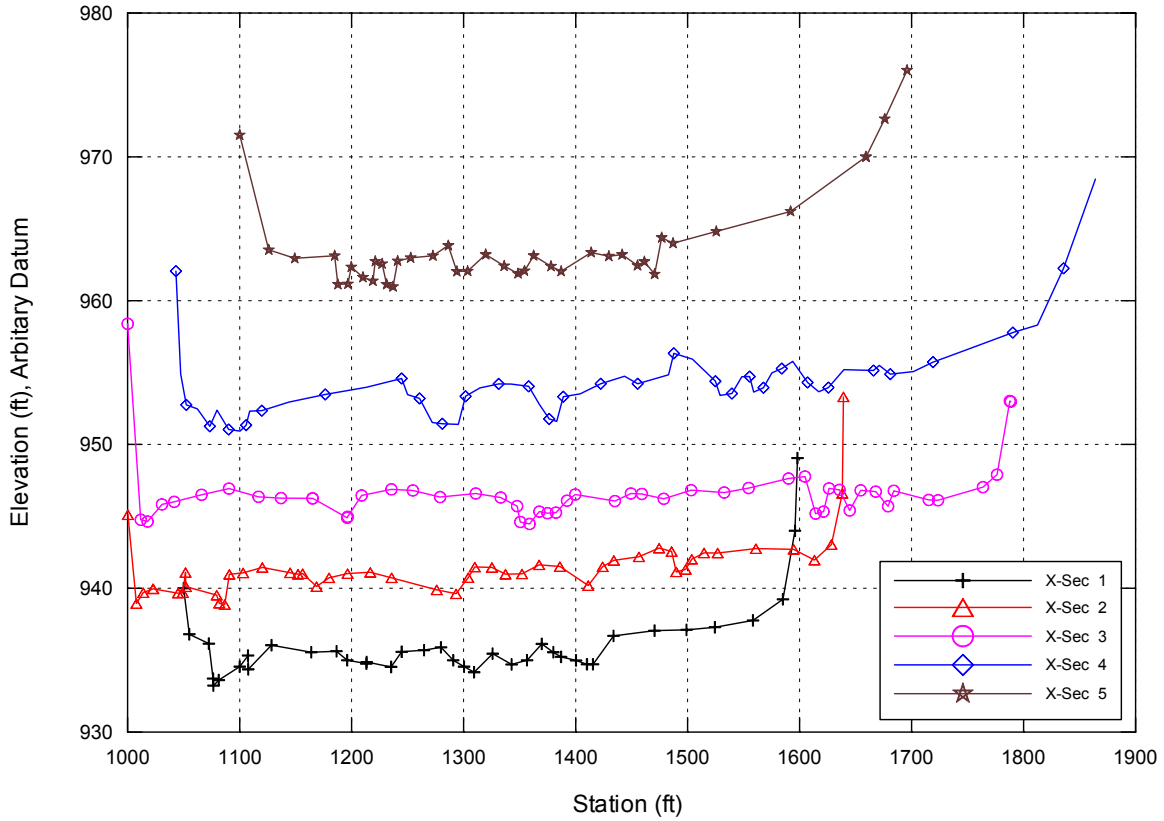
Figure G.5b.   Surveyed cross sections at Arroyo de los Pinos.
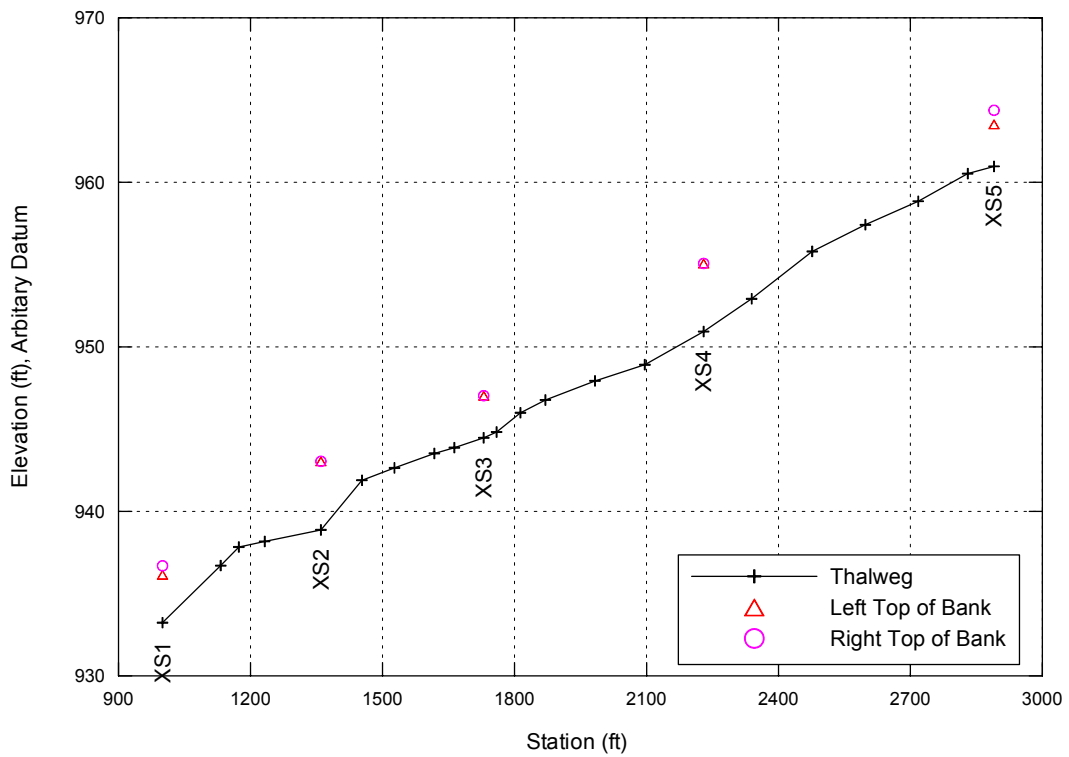
Figure G.5c.   Surveyed thalweg profile at Arroyo de los Pinos with cross-section locations.

Mussetter Engineering, Inc.
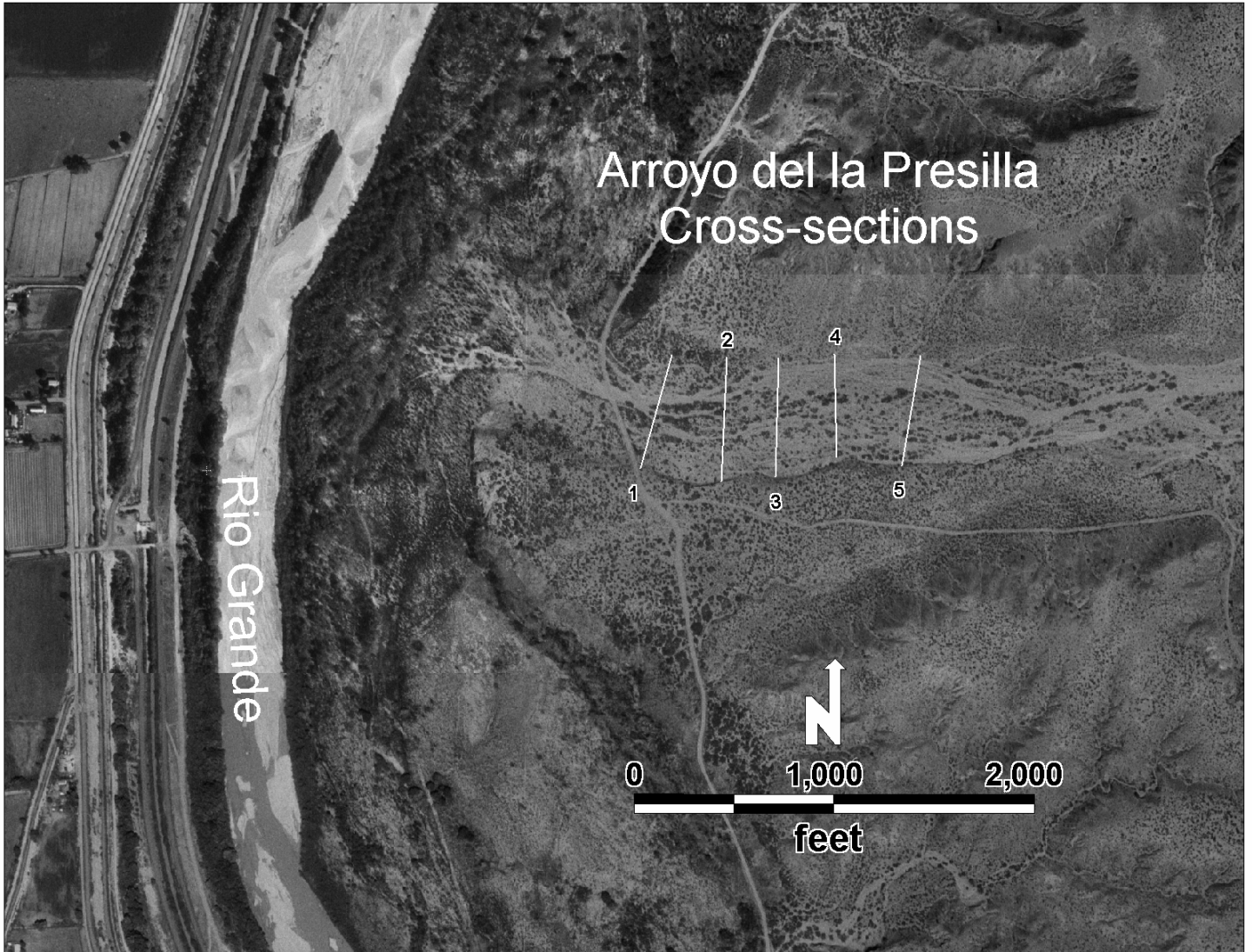
Figure G.6a.   Location of surveyed cross sections at Arroyo de la Presilla.

Mussetter Engineering, Inc.
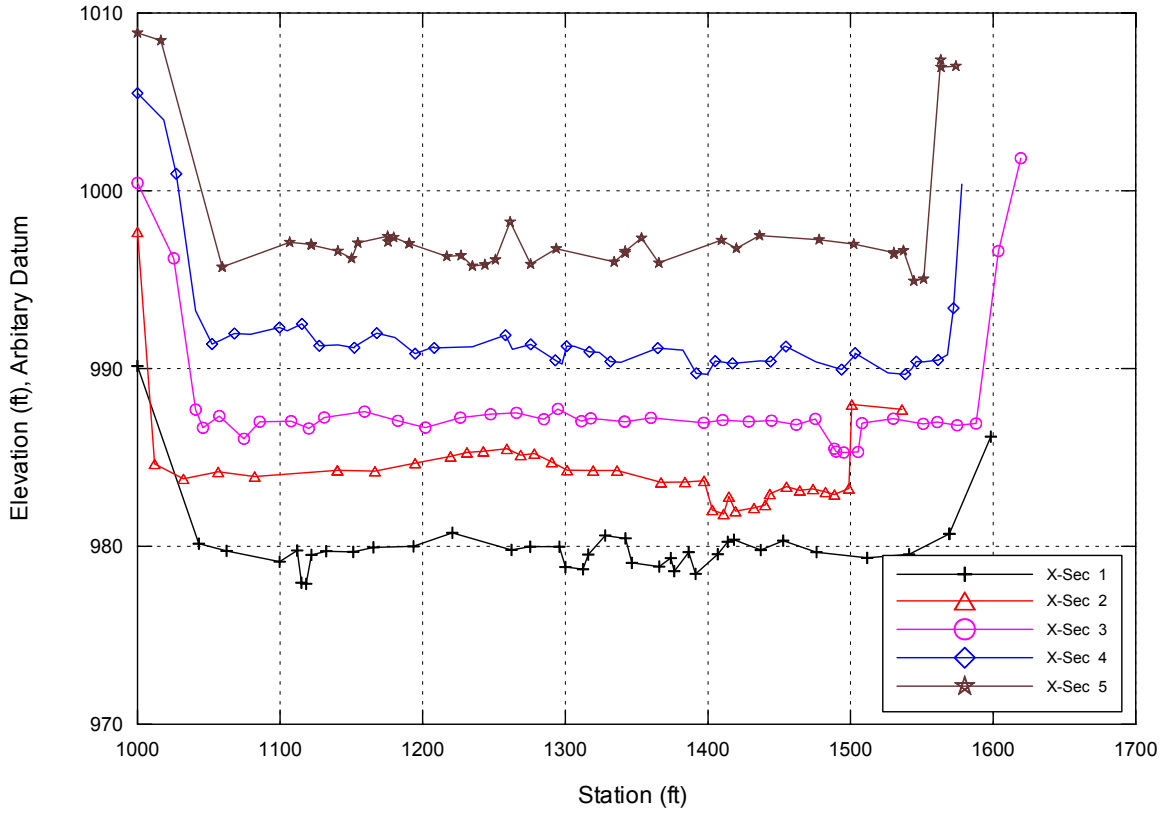
Figure G.6b. Surveyed cross sections at Arroyo del la Presilla.
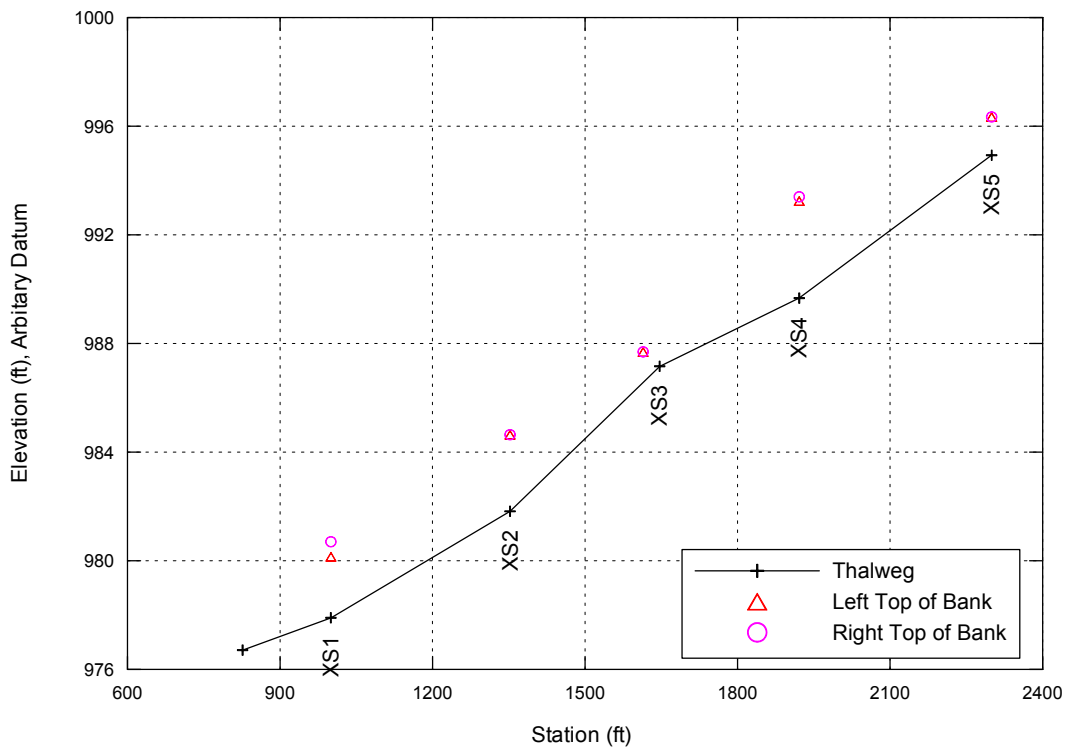
Figure G.6c.   Surveyed thalweg profile at Arroyo del la Presilla with cross-section locations.
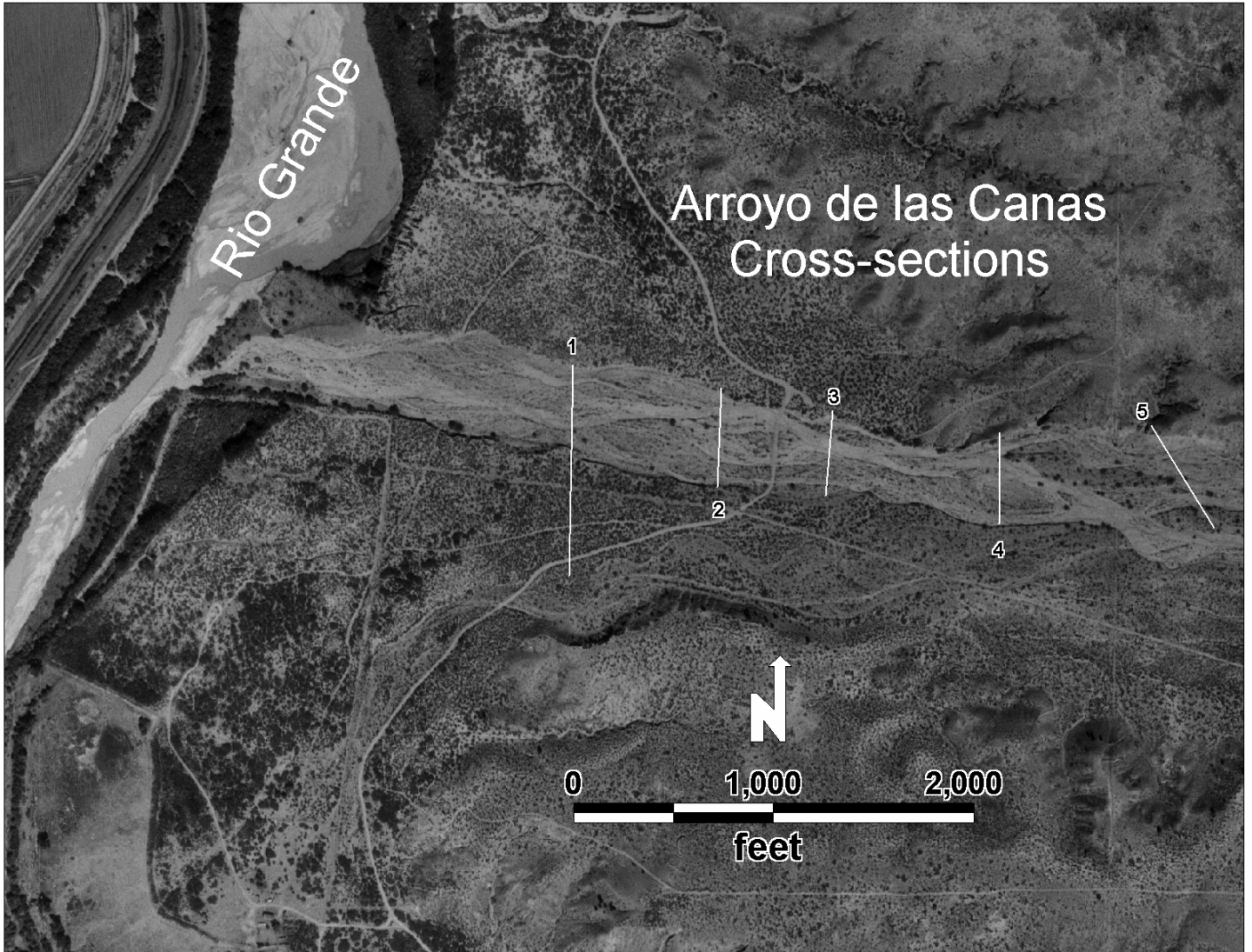
Figure G.7a.   Location of surveyed cross sections at Arroyo de las Canas.

Mussetter Engineering, Inc.
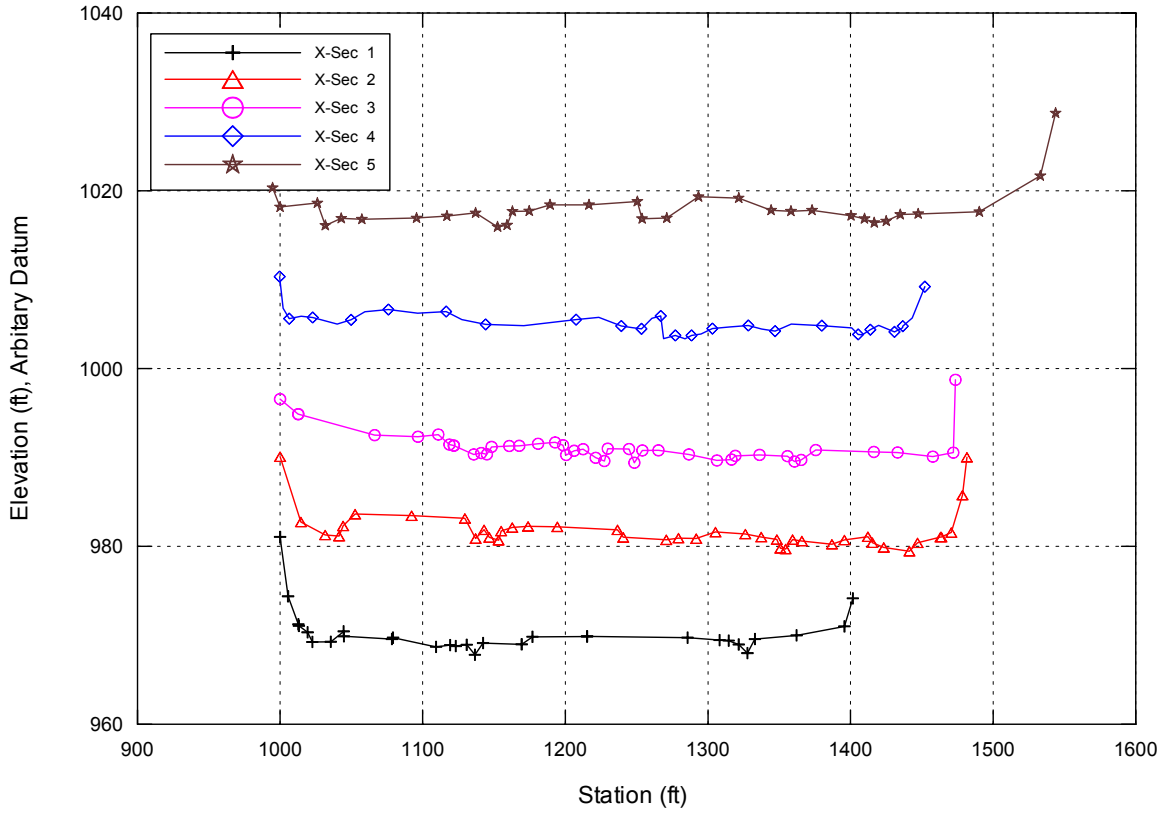
Figure G.7b. Surveyed cross sections at Arroyo del las Canas.
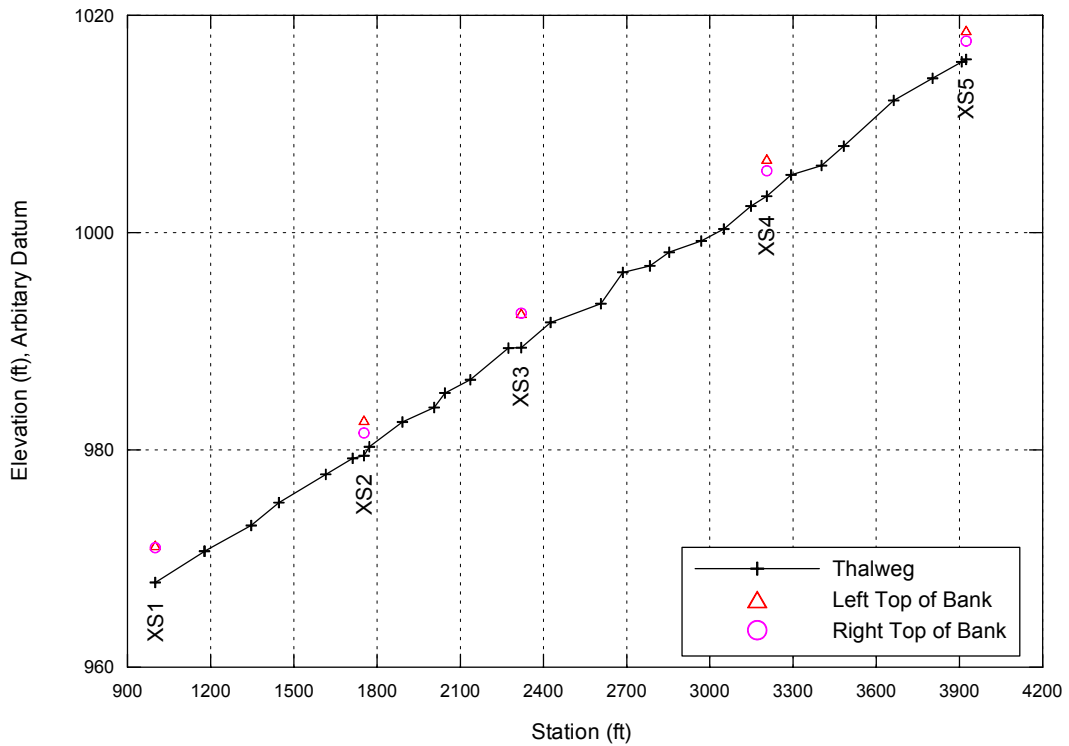
Figure G.7c. Surveyed thalweg profile at Arroyo del las Canas with cross-section locations.

G.14
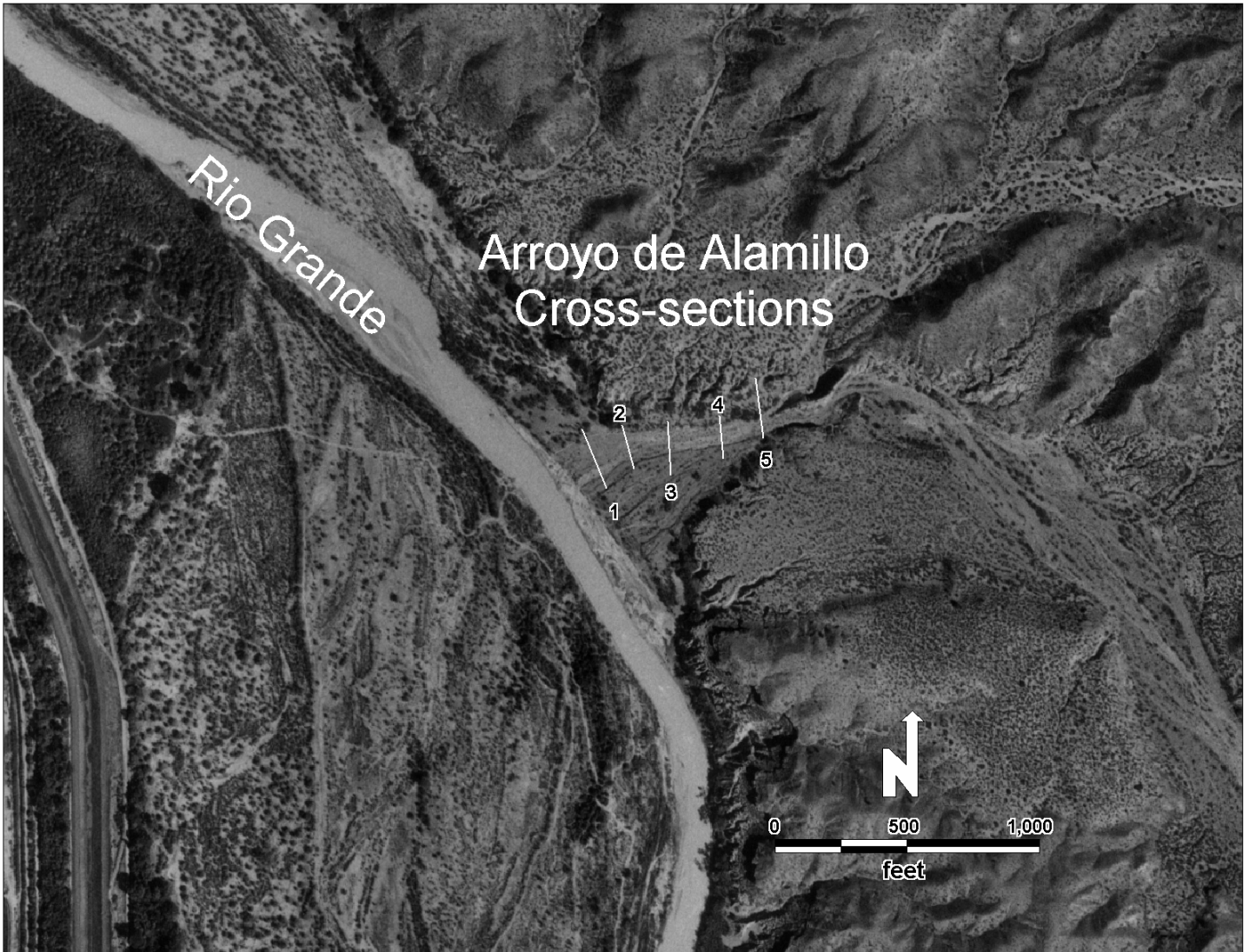
Figure G.8a.   Location of surveyed cross sections at Arroyo de Alamillo.

Mussetter Engineering, Inc.
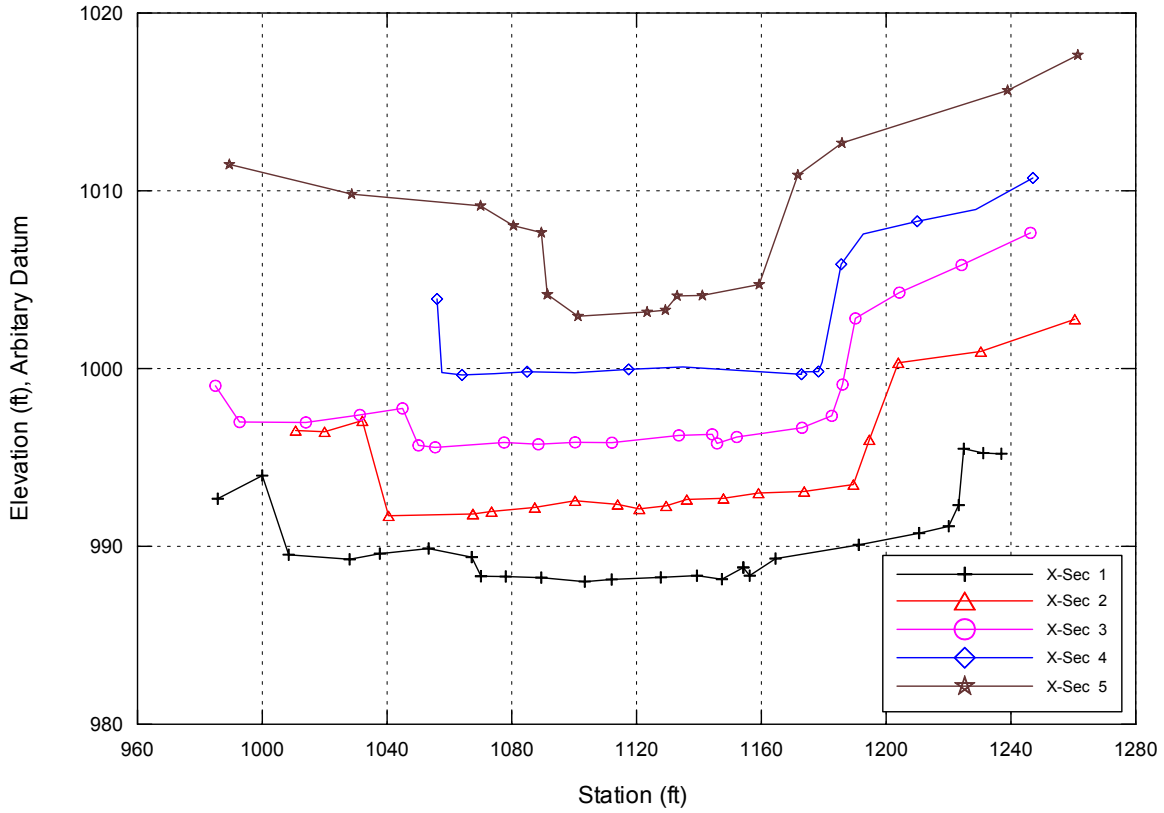
Figure G.8b.   Surveyed cross sections at Arroyo de Alamillo.
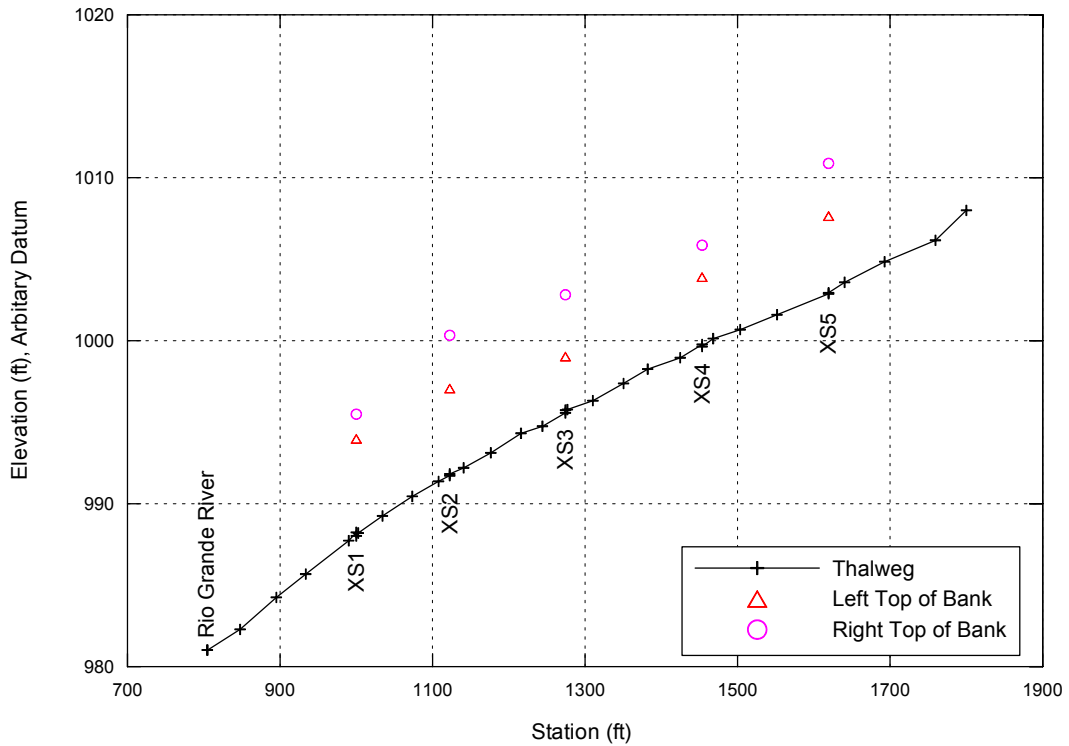
Figure G.8c.   Surveyed thalweg profile at Arroyo del Alamillo with cross-section locations.

G.16
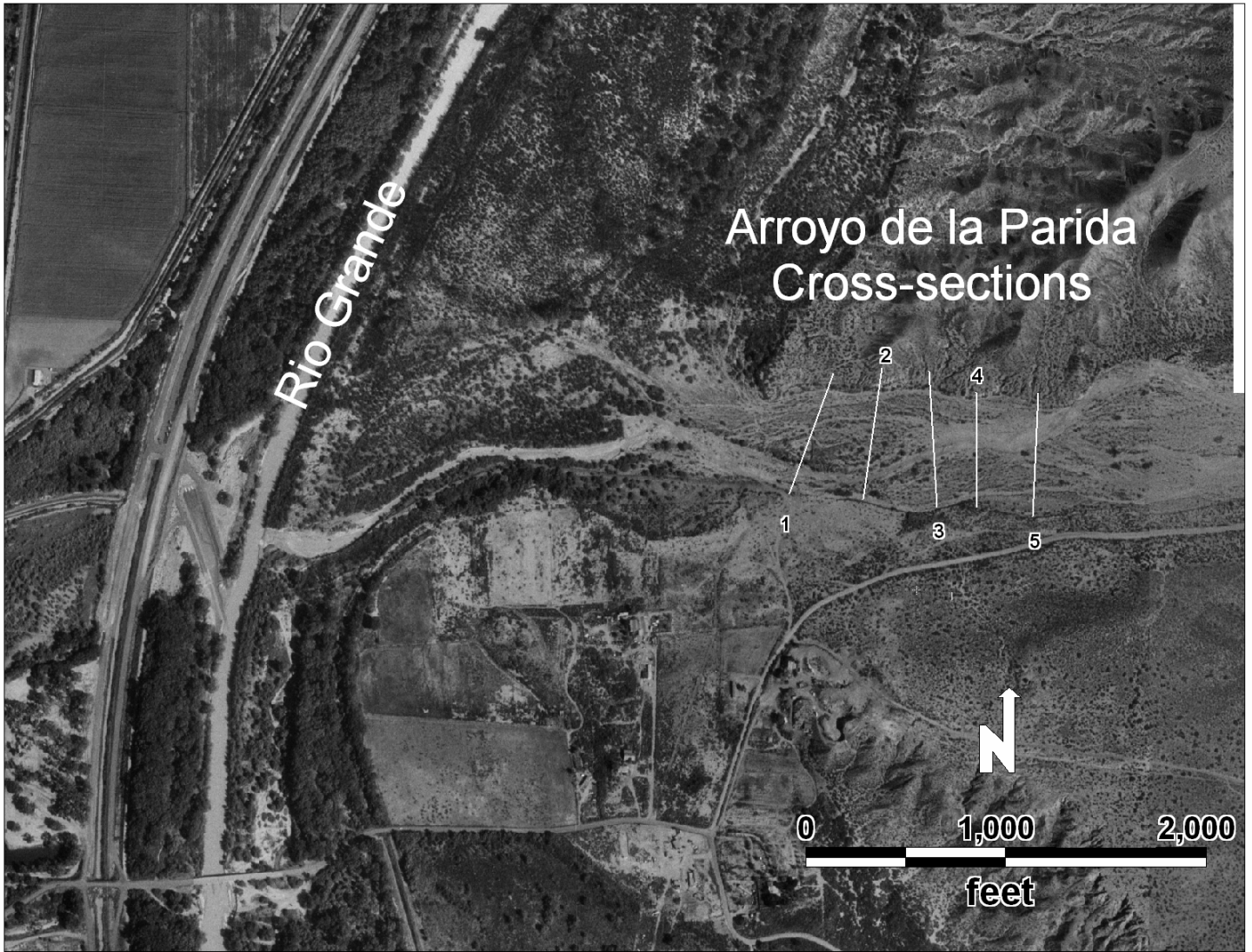
Figure G.9a.   Location of surveyed cross sections at Arroyo de la Parida.

Mussetter Engineering, Inc.
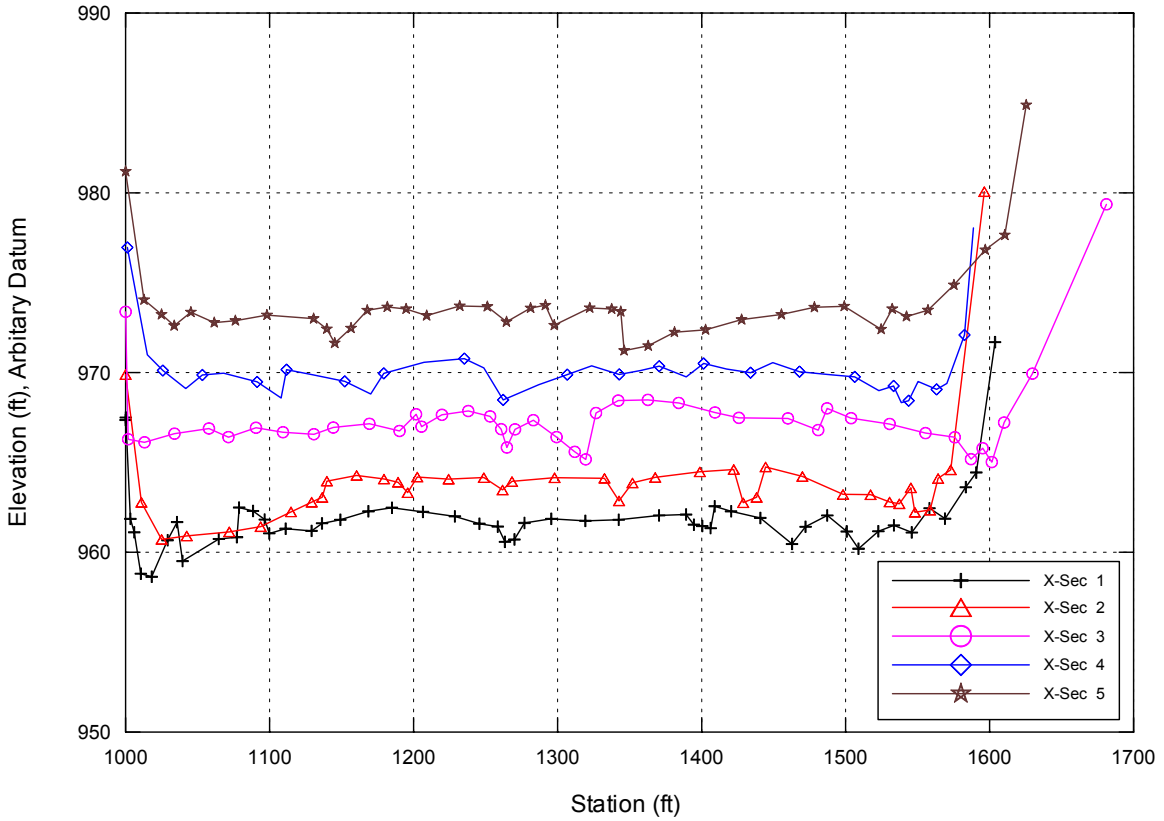
Figure G.9b.   Surveyed cross sections at Arroyo de la Parida.
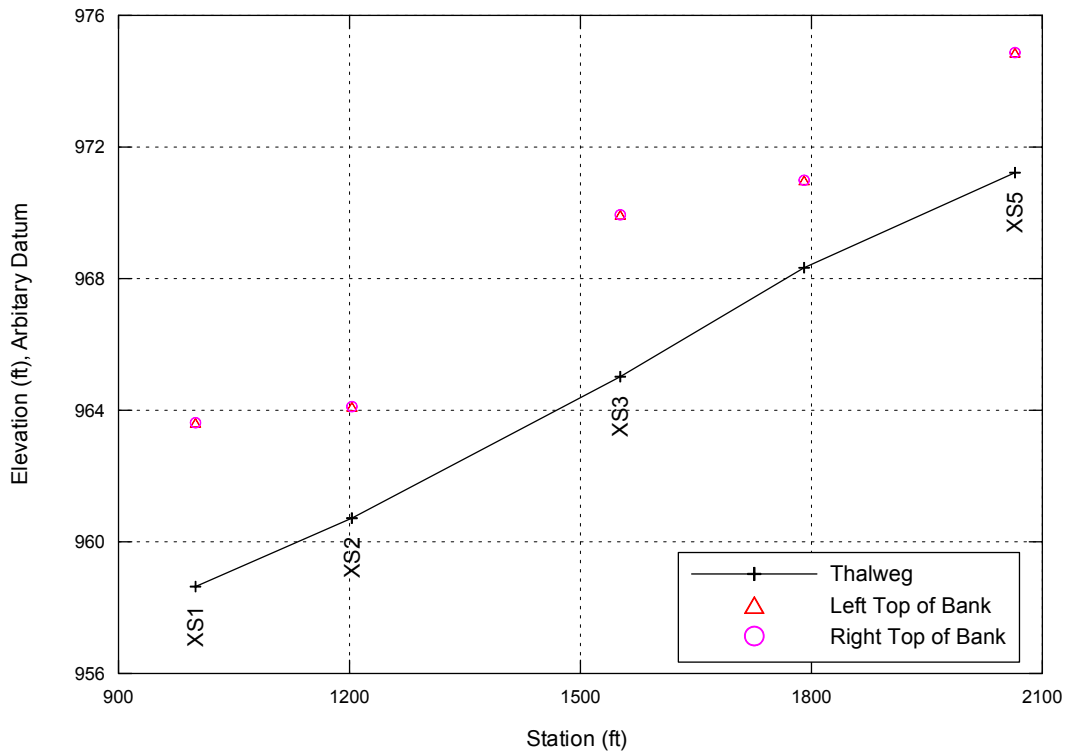
Figure G.9c.   Surveyed thalweg profile at Arroyo de la Parida with cross-section locations.

Figure G.10a. Location of surveyed cross sections at San Pedro Arroyo.

Mussetter Engineering, Inc.
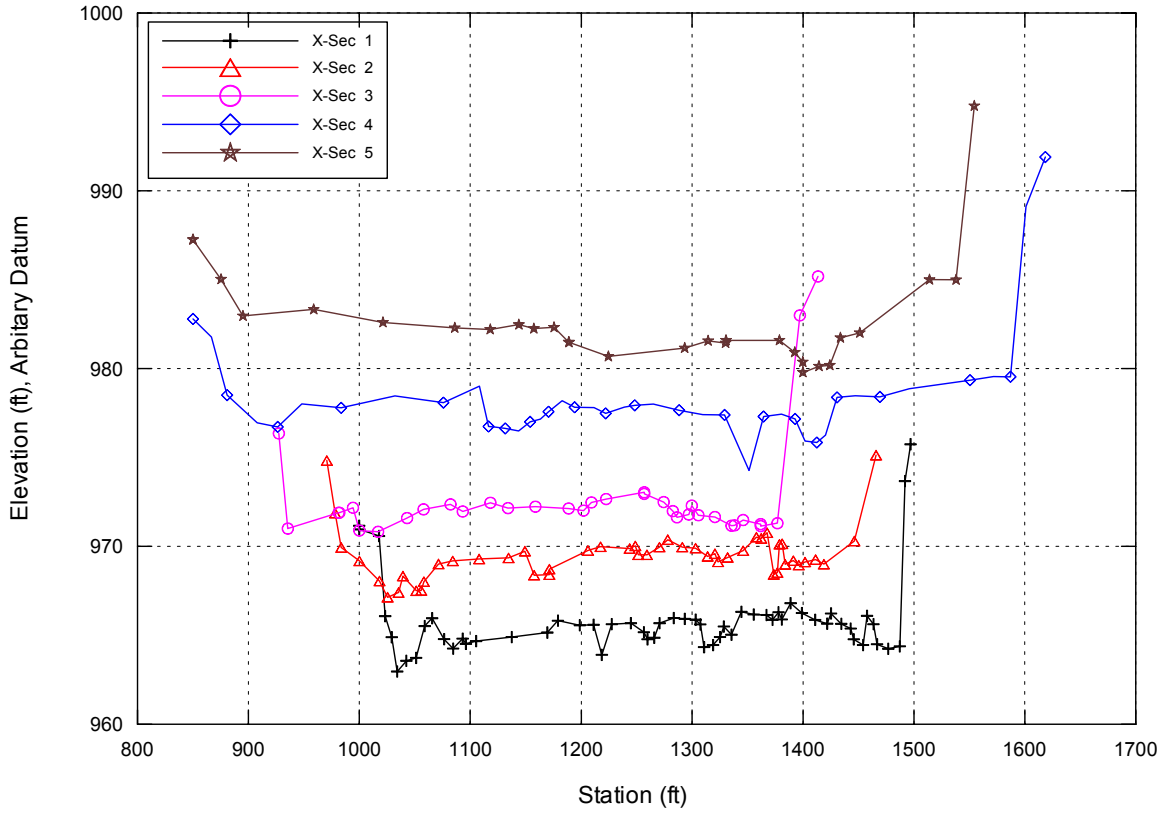
Figure G.10b. Surveyed cross sections at San Pedro Arroyo.
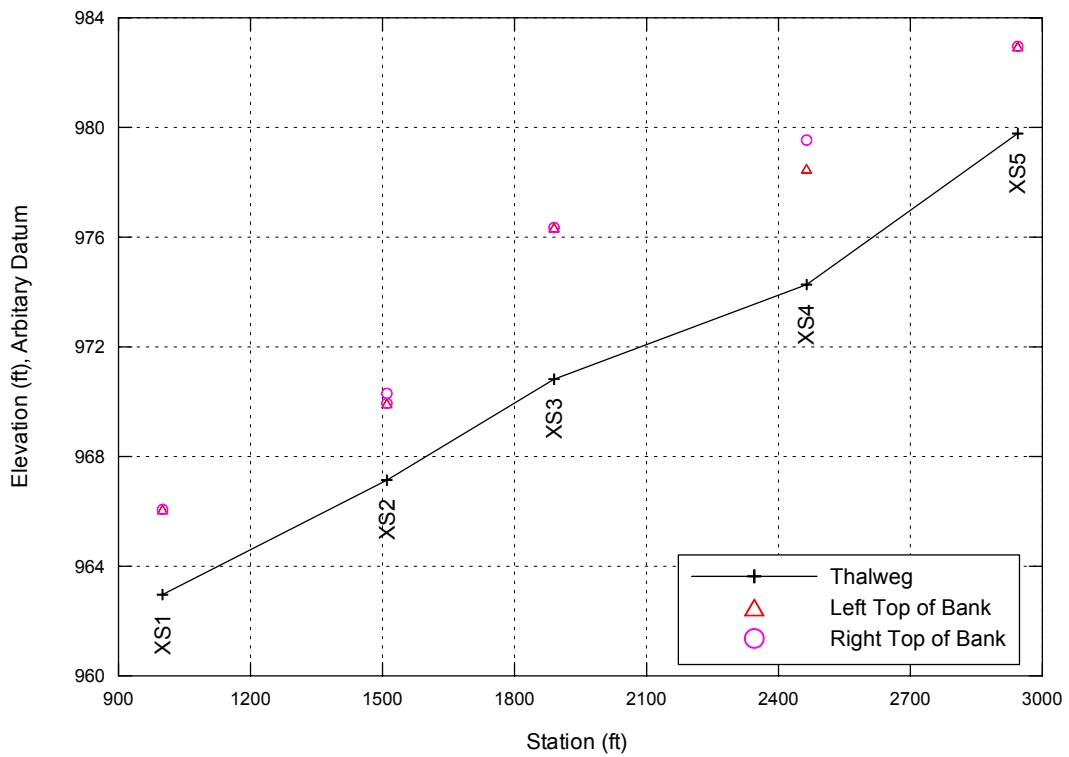
Figure G.10c. Surveyed thalweg profile at San Pedro Arroyo with cross-section locations.